AD-A013 397

HANDBOOK FOR THE DIRECT STATISTICAL ANALYSIS OF
MISSILE GUIDANCE SYSTEMS VIA CADET^{TM} (COVARIANCE
ANALYSIS DESCRIBING FUNCTION TECHNIQUE)

James H. Taylor

Analytic Sciences Corporation

Prepared for:

Office of Naval Research

31 May 1975

ADA013397
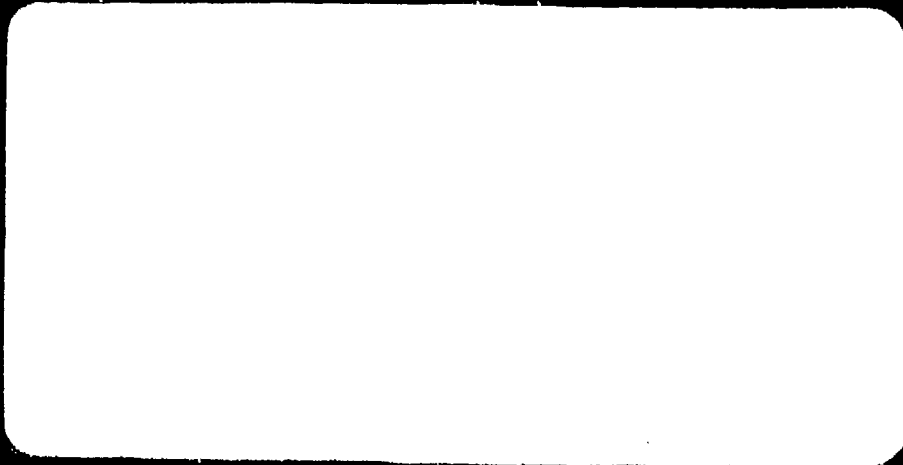
2311...

TASC

SECURITY CLASSIFICATION OF THIS PAGE (When Data Entered)

REPORT DOCUMENTATION PAGE		READ INSTRUCTIONS BEFORE COMPLETING FORM
1. REPORT NUMBER TR-385-2	2. GOVT ACCESSION NO.	3. RECIPIENT'S CATALOG NUMBER
4. TITLE (and Subtitle) HANDBOOK FOR THE DIRECT STATISTICAL ANALYSIS OF MISSILE GUIDANCE SYSTEMS VIA CADET™		5. TYPE OF REPORT & PERIOD COVERED Technical Report, 1 March 1974 - 31 Dec. 1974
		6. PERFORMING ORG. REPORT NUMBER TR-385-2
7. AUTHOR(s) James H. Taylor		8. CONTRACT OR GRANT NUMBER(s) N00014-73-C-0213
9. PERFORMING ORGANIZATION NAME AND ADDRESS The Analytic Sciences Corporation 6 Jacob Way Reading, Massachusetts 01867		10. PROGRAM ELEMENT, PROJECT, TASK AREA & WORK UNIT NUMBERS ONR Task No. NR-215-214
11. CONTROLLING OFFICE NAME AND ADDRESS THE OFFICE OF NAVAL RESEARCH Vehicle Technology Program Code 211 Arlington, Virginia 22217		12. REPORT DATE 31 May 1975
		13. NUMBER OF PAGES 218
14. MONITORING AGENCY NAME & ADDRESS(if different from Controlling Office)		15. SECURITY CLASS. (of this report) UNCLASSIFIED
		15a. DECLASSIFICATION/DOWNGRADING SCHEDULE

16. DISTRIBUTION STATEMENT (of this Report)

Distribution of this Report is Unlimited.

17. DISTRIBUTION STATEMENT (of the abstract entered in Block 20, if different from Report)

18. SUPPLEMENTARY NOTES

19. KEY WORDS (Continue on reverse side if necessary and identify by block number)

Missile Guidance Systems
Covariance Analysis
Nonlinear Systems (Continuous/Discrete)
Describing Functions (Random Input)

20. ABSTRACT (Continue on reverse side if necessary and identify by block number)

This Handbook presents detailed instructions for the application of the Covariance Analysis DEscribing Function Technique (CADET™) to the evaluation of tactical missile guidance systems (both analog and digital). Its contents include: CADET theory, simple illustrative examples (with flowcharts), model development for the missile-target

DD ₁ ᶠᴼᴿᴹ₇₃ 1473   EDITION OF 1 NOV 68 IS OBSOLETE

20. ABSTRACT (continued)

intercept problem, statistical linearization theory, discussions of the capabilities, limitations, and application philosophy of CADET, and an extensive catalog of pertinent random input describing functions. A detailed discussion of monte carlo analysis is appended, both to permit a comparison with CADET and to provide a background for the monte carlo procedures used to verify CADET.

TR-385-2

HANDBOOK FOR THE DIRECT STATISTICAL ANALYSIS OF MISSILE GUIDANCE SYSTEMS VIA CADET ™

31 May 1975

Prepared Under:

Contract No. N00014-73-C-0213
(ONR Task No. NR-215-214)

for

A

Prepared by:

James H. Taylor

Approved by:

Charles F. Price
Arthur A. Sutherland, Jr.

FOREWORD

This handbook is the culmination of research performed on the Covariance Analysis DEscribing Function Technique (CADET™) during a two-year period under Contract N00014-73-C-0213, for the Office of Naval Research. The Scientific Officer who monitored and encouraged this investigation was Mr. David Siegel.

ABSTRACT

The Covariance Analysis DEscribing Function
Technique (CADET™) -- a technique conceived
and developed at TASC for the efficient direct
statistical analysis of nonlinear systems with
random inputs -- has been proven to provide
accurate tactical missile performance projec-
tions with a small fraction of the computer
time expenditure required for a comparably
reliable monte carlo analysis. This handbook
is a self-contained, detailed exposition of
the application of CADET to the missile-target
intercept problem. The broad scope of this
document is intended to permit the direct analy-
sis of a wide variety of nonlinear and random
effects in missile guidance systems, and to
facilitate and encourage the study of other non-
linear systems via CADET.

)

TABLE OF CONTENTS

TABLE OF CONTENTS (Continued)

LIST OF FIGURES

LIST OF FIGURES (Continued)

THE ANALYTIC SCIENCES CORPORATION

LIST OF FIGURES (Continued)

LIST OF TABLES

PROLOGUE AND READER'S GUIDE

The development of a complex weapon system with stringent performance specifications, such as a tactical missile, generally requires several phases, including preliminary design and feasibility studies, decisions concerning implementation of various system functions, and compensation or design modification to obtain the best possible system performance under realistic constraints. In the later stages of development, the mathematical system model used as a basis for generating system performance projections inevitably contains nonlinear effects and random inputs. Nonlinearity is generally associated with nonlinear relations inherent to the laws of physics, unavoidable hardware nonlinearities, and essential design nonlinearities; random effects may include noise (e.g., thermal effects), sensor measurement errors, random inputs that contain information required by the system, and random initial conditions. When random effects are significant, some statistical measure of system performance is required; for example, the root-mean-square (rms) miss distance achieved at the time of target interception may be of interest in assessing the capability of a tactical missile.

The traditional approach used for the statistical analysis of the performance of systems with significant nonlinearities has been the monte carlo method. In this technique, a large number of computer simulations (trials) are made using the required nonlinear model with different, randomly chosen, initial conditions and random forcing functions generated according to given statistics. The resulting ensemble of simulations provides the basis for making estimates of the true system variable statistics. Associated with the monte carlo method is the problem that a large

number of trials is required to provide confidence in the accuracy of the results; an ensemble comprising as many as 1000 trials may be needed to obtain an accurate statistical analysis for a nonlinear system. Thus, while the monte carlo method may be useful for obtaining a few evaluations of a system's performance, it is not a very satisfactory tool for conducting extensive sensitivity and tradeoff studies for different values of the important system parameters, or for conducting detailed studies of nonlinear effects on system performance, due to the large expenditure in computer time required.

The limitations of the monte carlo approach for obtaining performance projections for realistic nonlinear models of tactical missiles strongly motivated the development of a more efficient analytic technique. The resulting methodology, conceived by the technical staff at TASC, has proven to be an exceptionally powerful means for directly evaluating the statistical behavior of nonlinear systems with random inputs (Refs. 1 to 4). For reasons that will become obvious, this method is referred to as the Covariance Analysis Describing function Technique (CADET^{TM}). The purpose of this handbook is to present detailed instructions to facilitate the application of CADET in studies of weapon systems performance.

The scope and intent of this presentation is as follows: Chapter 1 gives the theoretical development of the basic equations of CADET, both for continuous-time and mixed continuous/ discrete-time systems. Chapter 2 provides a step-by-step exposition of the CADET procedure, accompanied with computer flow-charts. Chapter 3 is a comprehensive discussion of modeling nonlinear effects in the missile-target intercept problem; the purpose of this material is threefold: to provide the basis for the examples treated herein, to expedite future use of CADET in analyzing tactical missile performance, and to provide some guidance in

modeling analogous phenomena that may occur in studying other systems having similar nonlinearities. The theory and practical application of quasi-linearization is treated in Chapter 4; exact and approximate methods for calculating random input describing functions are presented, accuracy of the quasi-linear approximation is considered, and some sensitivity issues are discussed. Chapter 5 (blue pages) provides a broad overview of the application of CADET to general problems -- touching upon philosophy of application, assessments of the strong points and limitations of CADET, and a comparison of the computational efficiency of CADET versus the monte carlo method. Finally, three appendices are included to facilitate the use and evaluation of the CADET methodology: a catalog of random input describing functions, a presentation of extensions of CADET that permit the analysis of some unusual nonlinear effects that cannot be treated accurately by the standard CADET methodology presented in Chapter 1, and a detailed discussion of the application and reliability of the monte carlo method.

The prerequisites for understanding this document are introductory modern control theory (including the state-space formulation of system models in terms of first-order vector differential or differential/difference equations, and the associated vector-matrix calculus), and elementary random process theory. The contents of this handbook have been chosen to satisfy the requirements of a somewhat diverse audience. For this reason, readers of differing backgrounds and interests will find that some sections are of greater utility than others. In the simplest case, i.e., the application of CADET to the missile-target intercept problem treating only those effects discussed in Chapter 3, the illustrative examples of Chapter 2 and the random input describing function catalog of Appendix A may suffice. For those interested in the theory of quasi-linearization and CADET, Chapters 1 and 4 should prove to be valuable adjuncts. In treating situations that require the quasi-linearization of nonlinearities

not listed in Appendix A, the examples and principles given in Chapter 4 establish the necessary starting point. Finally, Appendix C on the monte carlo method provides discussions of the theory and application cf the technique (and of its potential pitfalls in the analysis of nonlinear systems), and establishes the context for comparisons between monte carlo simulation results and CADET.

While the primary thrust of CADET development thus far has been the extension and refinement of an efficient tool for the statistical evaluation of the performance of missile guidance systems, the overall scope of CADET is evidently much more general. The system model based on a nonlinear state vector differential/ difference equation with random inputs is of broad generality, being descriptive of many continuous and discrete-time systems with random disturbances. The specific nonlinear effects discussed herein are by no means restricted in occurrence to the missile-target intercept problem. It is hoped that the success of the research presented here and in Refs. 1 to 4 will encourage other applications of the CADET concept.

1. THE COVARIANCE ANALYSIS DESCRIBING FUNCTION TECHNIQUE (CADET)

The $\underline{C}$ovariance $\underline{A}$nalysis $\underline{DE}$scribing function $\underline{T}$echnique (CADET^{TM}) is a method for directl; determining the statistical properties of solutions of nonlinear system with random inputs, recently conceived and developed at The Analytic Sciences Corporation (Refs. 1 to 4). The principal advantage of this technique is that it greatly reduces the need for monte carlo simulation, thereby achieving substantial sa ings in computer processing time. We first motivate the discussion by reviewing the covariance analysis method for linear systems; then we develop an analogous procedure (CADET) for the nonlinear case.

1.1 COVARIANCE ANALYSIS FOR LINEAR SYSTEMS

The dynamics of a linear continuous-time stochastic system can be represented by a first-order vector differential equation in which $\underline{x}(t)$ is the system state vector and $\underline{w}(t)$ is a forcing function vector,

$$\underline{\dot{x}}(t) = F(t) \, \underline{x}(t) + G(t) \, \underline{w}(t) \qquad (1.1\text{-}1)$$

where we assume that $F(t)$ and $G(t)$ are continuous with respect to t; Fig. 1.1-1 illustrates the equation. The state vector is composed of any set of variables sufficient to describe the behavior of the system completely. The forcing function vector $\underline{w}(t)$ represents disturbances as well as control inputs that may act upon the system. In what follows, the forcing function $\underline{w}(t)$ is
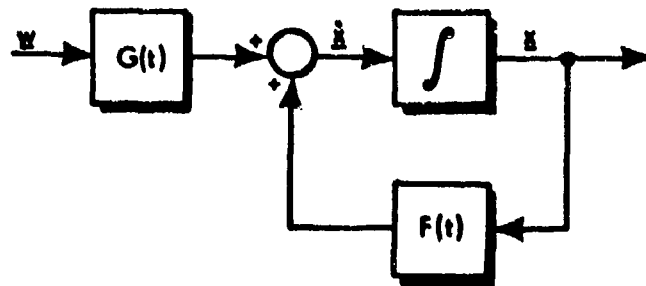
Figure 1.1-1   Representation of the Continuous-Time
                    Linear Dynamic System Equations

assumed to be composed of a mean or deterministic value $\underline{b}(t)$ and a random component $\underline{u}(t)$, the latter being comprised of elements which are uncorrelated in time; that is, $\underline{u}(t)$ is a "white noise" process having the spectral density matrix $Q(t)$. Thus $\underline{w}(t)$ is specified by*

$$\underline{w}(t) = \underline{b}(t) + \underline{u}(t)$$

$$E\left[\underline{w}(t)\right] = \underline{b}(t) \qquad\qquad (1.1\text{-}2)$$

$$E\left[\underline{u}(t)\ \underline{u}^T(\tau)\right] = Q(t)\ \delta(t\text{-}\tau)$$

Similarly, the state vector has a deterministic component $\underline{m}(t)$ and a random part $\underline{r}(t)$; for simplicity $\underline{m}(t)$ will generally be called the mean vector. The state vector $\underline{x}(t)$, then, is described statistically by its mean vector and covariance matrix,

$$\underline{x}(t) = \underline{m}(t) + \underline{r}(t)$$
$$\qquad\qquad (1.1\text{-}3)$$
$$\underline{m}(t) = E\left[\underline{x}(t)\right]$$

---

*E denotes ensemble expectation, or average value; a super-
script T denotes the transpose of a vector or matrix; $\delta(t\text{-}\tau)$
is the Dirac delta function.

$$P(t) = E\left[\underline{r}(t)\ \underline{r}^T(t)\right] \qquad\qquad (1.1\text{-}3)(\text{Cont})$$

Henceforth, the time dependence of the variables $\underline{w}$, $\underline{b}$, $\underline{u}$, Q, $\underline{x}$, $\underline{m}$, $\underline{r}$ and P will not be explicitly denoted by (t), unless required for clarity.

The differential equations that govern the propagation of the mean vector and covariance matrix for the system described by Eq. (1.1-1) can be derived directly, as demonstrated in Ref. 5, to be

$$\underline{\dot{m}} = F(t)\ \underline{m} + G(t)\ \underline{b}$$

$$\dot{P} = F(t)\ P + PF^T(t) + G(t)\ QG^T(t) \qquad\qquad (1.1\text{-}4)$$

The first and second moments of the system response are completely determined by integrating the above vector and matrix differential equations, Eq. (1.1-4), when the initial conditions, $\underline{m}(0)$ and $P(0)^*$, are specified. The elements of $\underline{m}$ represent the effects of deterministic initial conditions and biases due to deterministic system inputs ($\underline{b} \neq 0$). The diagonal elements of P are the mean square values of the random components of the state variables, and the off-diagonal elements represent the degree of correlation between the random components of the various state variables.

Equation (1.1-4) provides a <u>direct method</u> for analyzing the statistical properties of $\underline{x}$. This is to be contrasted with the <u>monte carlo method</u>, where many sample trajectories of $\underline{x}$ are calculated from computer-generated random noise and initial conditions, using Eq. (1.1-1). The moments $\underline{m}$ and P are then estimated by averaging over the ensemble of trajectories generated in the monte carlo procedure. Note that Eq. (1.1-4) leads to exact

---

*The initial time can be taken to be $t = 0$ with no loss in generality.

solutions for $\underline{m}$ and P, to within computer integration accuracy, whereas the monte carlo method yields approximate solutions for any finite number of simulations. Furthermore, the mean and co-variance equations need be solved only once over the time interval of interest, whereas Eq. (1.1-1) must be solved repeatedly using the monte carlo technique; consequently the direct analytical method is not only exact, but is also generally the most efficient technique for analyzing linear systems. With this observation as motivation, we proceed to describe a methodology whereby the sta-tistics of a nonlinear system can be computed approximately using recursive relationships similar in form to those of linear co-variance analysis, Eq. (1.1-4); the monte carlo method is treated in greater depth in Appendix C.

1.2   COVARIANCE ANALYSIS FOR NONLINEAR SYSTEMS

The nonlinear counterpart of Eq. (1.1-1) treated in this presentation is

$$\underline{\dot{x}} = \underline{f}(\underline{x},t) + G(t)\,\underline{w} \tag{1.2-1}$$

Figure 1.2-1 depicts this equation. The input and state vectors are again characterized by the quantities $\underline{b}$, Q and $\underline{m}$, P, respec-tively, given in Eqs. (1.1-2) and (1.1-3).

R-11802
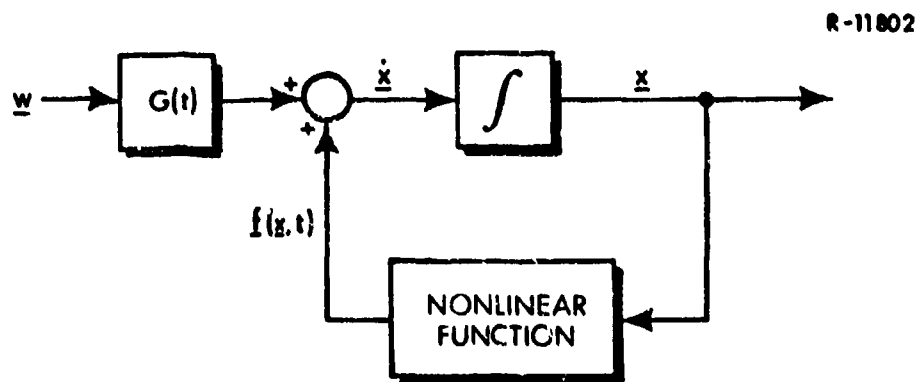
Figure 1.2-1   Nonlinear System Block Diagram

1-4

It may seem restrictive to have the random inputs enter the system differential equation linearly as in Eq. (1.2-1). However, if a system is of the form

$$\dot{\underline{x}} = \underline{f}(\underline{x}, \underline{y}, t) \tag{1.2-2}$$

and $\underline{y}$ is a correlated random process that can be represented as a random vector satisfying

$$\dot{\underline{y}} = \underline{f}_n(\underline{y}, t) + G_n(t)\, \underline{w} \tag{1.2-3}$$

where $\underline{w}$ is the sum of suitable vectors of deterministic variables, $\underline{b}$, and white noise processes, $\underline{u}$, we can rewrite Eq. (1.2-2) using the augmented state vector $\underline{x}_a$,

$$\underline{x}_a \triangleq \left[\begin{array}{c} \underline{x} \\ \hline \underline{y} \end{array} \right]$$

as

$$\dot{\underline{x}}_a = \left[\begin{array}{c} \underline{f}(\underline{x}_a, t) \\ \hline \underline{f}_n(\underline{y}, t) \end{array} \right] + \left[\begin{array}{c} 0 \\ \hline G_n(t) \end{array} \right] \underline{w} \tag{1.2-4}$$

Observe that $\underline{y}$ is thus considered to be a component of the state vector, comprised of "noise states". This procedure places the apparently more general problem of Eqs. (1.2-2) and (1.2-3) in the format given in Eq. (1.2-1); since all physically realizable random processes are correlated, the assumption that $\underline{y}$ is described by Eq. (1.2-3) is not particularly restrictive. For convenience we thus consider Eq. (1.2-1) to be the basic system model, with no significant loss in generality.

The statistical differential equations that correspond to Eq. (1.1-4) can be shown to be (Ref. 5)

$$\underline{\dot{m}} = E\left[\dot{}\ \underline{f}(\underline{x},t)\right] + G(t)\underline{b}$$

$$\triangleq \hat{\underline{f}} + G(t)\underline{b} \tag{1.2-5}$$

$$\dot{P} = E\left[\underline{f}\ \underline{r}^T\right] + E\left[\underline{r}\ \underline{f}^T\right] + G(t)QG^T(t)$$

The first equation is the direct analog of the mean differential equation of Eq. (1.1-4), since we observe that $\hat{\underline{f}}$ is simply $F(t)\underline{m}$ in the linear case. The nonlinear covariance equation can be represented in the same format as indicated in Eq. (1.1-4) by defining the auxiliary matrix N,

$$NP \triangleq E\left[\underline{f}(\underline{x},t)\ \underline{r}^T\right] \tag{1.2-6}$$

Then Eq. (1.2-5) may be written as

$$\underline{\dot{m}} = \hat{\underline{f}} + G(t)\underline{b}$$

$$\dot{P} = NP + PN^T + G(t)QG^T(t) \tag{1.2-7}$$

The relation in Eq. (1.2-6) generally provides an explicit definition of N,

$$N = E\left[\underline{f}(\underline{x},t)\ \underline{r}^T\right]P^{-1} \tag{1.2-8}$$

since P is usually positive definite* and thus a unique P^{-1} exists.

    The derivation of Eq. (1.2-5) is based directly on the principles of covariance analysis, Ref. 5. We observe, however,

---

*Often the initial condition P(0) is only positive semi-definite, in which case the pseudoinverse of P(0) could be used in Eq.(1.2-8). As shall be shown subsequently, Eq. (1.2-8) is only formal, in the sense that it is almost never used to evaluate N (refer to Eq. (1.2-10) and Section 4.1).

that the vector $\hat{f}$ and matrix N defined in Eqs. (1.2-5) and (1.2-6) are identical to the quantities which provide a minimum mean square error quasi-linear approximation to the nonlinearity $\underline{f}(\underline{x},t)$. It can be shown (refer to Section 4.1) that the approximation

$$\underline{f}(\underline{x},t) \approx \hat{\underline{f}} + N(\underline{x} - \underline{m})$$

with $\hat{\underline{f}}$ and N specified by Eqs. (1.2-5) and (1.2-6) yields the best linear approximation in the sense that

$$\underline{e} \triangleq \underline{f}(\underline{x},t) - \hat{\underline{f}} - N(\underline{x} - \underline{m})$$

satisfies the condition

$$E\left[\underline{e}^T S\underline{e}\right] = \text{minimum}$$

for any positive semi-definite matrix S. The intimate relation between the well-established describing function theory (Ref. 6) and Eq. (1.2-6) has permitted the rapid development of an approximate nonlinear covariance analysis technique based on Eq. (1.2-7) called CADET -- the Covariance Analysis DEscribing Function Technique. Henceforth, we shall refer to $\hat{f}$ as the expectation vector and N as the quasi-linear system dynamics matrix.

The quantities $\hat{\underline{f}}$ and N defined in Eqs. (1.2-5) and (1.2-6) must be determined before we can proceed to solve Eq. (1.2-7). Evaluating the indicated expected values requires knowledge of the joint probability density function (joint pdf) of the state variables. While it is possible, in principle, to evolve the n-dimensional joint pdf $p(\underline{x},t)$ for a nonlinear system with random inputs by solving a set of partial differential equations known as the Fokker-Planck equation or the forward equation of Kolmogorov (Ref. 5), this procedure is generally not practically feasible. The fact that $p(\underline{x},t)$ is not available precludes the exact solution of Eq. (1.2-7).

One procedure for obtaining an approximate solution to
Eq. (1.2-7) is to assume the form of the joint probability den-
sity function of the state variables in order to evaluate $\hat{f}$ and N
according to Eqs. (1.2-5) and (1.2-6). Although it is possible
to use any joint pdf, all of CADET development to date has been
based on the assumption that the state variables are jointly
normal; this choice was made because it is both reasonable and
convenient.

While the above assumption is strictly true only for
linear systems driven by gaussian inputs, it is often approxi-
mately valid in nonlinear systems with nongaussian inputs. Al-
though the output of a nonlinearity with a gaussian input is
generally nongaussian, it is known from the central limit theorem
that random processes tend to be made gaussian when passed through
low-pass linear dynamics ("filtered"). Thus, we rely on the
linear part of the system to insure that nongaussian nonlinearity
outputs result in nearly gaussian system variables as signals
propagate through the system. By the same token, if there are
nongaussian system inputs which are passed through low-pass linear
dynamics, the central limit theorem can again be invoked to jus-
tify the assumption that the state variables are approximately
jointly normal. The validity of the gaussian assumption for non-
linear systems with gaussian inputs has been extensively studied
and verified; nongaussian random inputs have not been considered.

From a pragmatic viewpoint, the gaussian hypothesis serves
to simplify the mechanization of CADET significantly by permitting
each scalar nonlinear relation in $\underline{f}(\underline{x},t)$ to be treated in isola-
tion, with $\hat{\underline{f}}$ and N formed from the individual random input describ-
ing functions (ridf's) for each nonlinearity. Since ridf's have
been catalogued in Ref. 6 for several classes of nonlinearities
encountered in a broad spectrum of practical problems, the

Implementation of CADET is a straightforward procedure for the analysis of many nonlinear systems. We also note that, under the gaussian assumption, the random input describing functions can be calculated directly from the mean vector, $\underline{m}$, and the covariance matrix, P, of the system state vector. Thus, we write $\hat{\underline{f}}$ and N in the form

$$\hat{\underline{f}} = \hat{\underline{f}}(\underline{m}, P, t)$$

$$N = N(\underline{m}, P, t) \qquad (1.2-9)$$

As a corollary to the above observations, we have the result (Ref. 7) that

$$N(\underline{m}, P, t) = \frac{d}{d\underline{m}} \hat{\underline{f}} \qquad (1.2-10)$$

Since calculating $\hat{\underline{f}}$ is required for the propagation of the mean (Eq. (1.2-7)), it is generally much easier to employ Eq. (1.2-10) than to evaluate N directly using Eq.(1.2-6). Quasi-linearization and the random input describing function are treated in some detail in Chapter 4.

Relations of the form indicated in Eq. (1.2-9) permit the direct evaluation of $\hat{\underline{f}}$ and N at each integration step in the propagation of $\underline{m}$ and P, as illustrated in Fig. 1.2-2. We note that the dependence of $\hat{\underline{f}}$ and N on the statistics of the state vector is due to the existence of nonlinearities in the system. Without nonlinear effects, the propagation of the mean and covariance is "uncoupled," as in Eq. (1.1-4).

To demonstrate the ease with which CADET can be mechanized under the gaussian assumption, we consider a low-order system model for the missile-target intercept problem having a single nonlinearity in Section 2.2. All of the steps involved in performing statistical analysis via CADET are illustrated in detail.

ห 16231
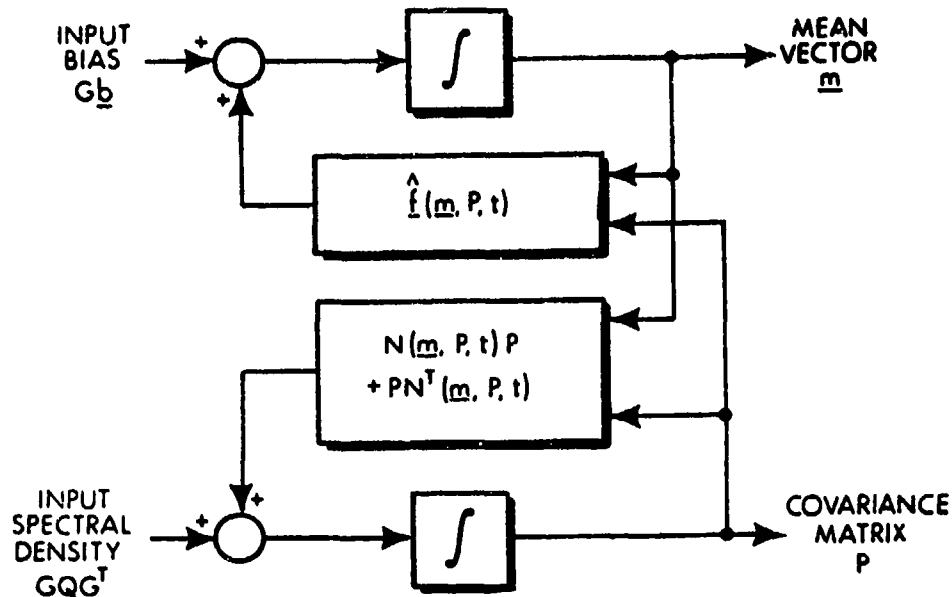
Figure 1.2-2   Nonlinear Covariance Analysis -- CADET

A comparison of quasi-linearization with the classical
Taylor series or small-signal linearization technique provides a
great deal of insight into the success of the $\widehat{\text{ri}}f$ in capturing
the essence of nonlinear effects. Small-signal linearization for
a scalar nonlinear element $f(x)$ is based on the identification of
a nominal operating point (in this context, the mean value of x,
denoted m_x) and the evaluation of the slope of the nonlinearity
at that value; then the approximation is made that

$$f(x) \cong f(m_x) + f'(m_x)(x - m_x) \qquad (1.2-11)$$

which represents the first two terms of a Taylor series expan-
sion about the given operating point, as illustrated in Fig. 1.2-3
for the example, $y = x^3$. While this is a useful approach if excur-
sions from the nominal are small, the validity of the Taylor series
approximation is questionable when x is a random variable which can
exhibit large variations about its mean value.

1-10
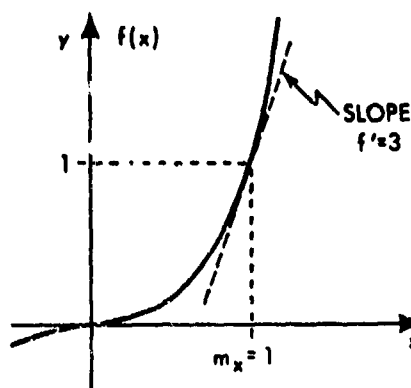
Figure 1.2-3   Taylor Series Linearization of $y = x^3$ about $m_x = 1$

By contrast, the quasi-linear representation of a non-linearity is sensitive to the input amplitude in some sense; in the case of random inputs, the statistics $m_x = E[x]$ and $p_x = E[(x-m_x)^2]$ provide the measure of input amplitude. For the example $y = x^3$, where x is a gaussian random process, we calculate the describing functions in Section 4.3 (Eq. (4.3-7)) to be

$$\hat{f} = \left(3p_x + m_x^2\right) m_x$$

$$n = 3\left(p_x + m_x^2\right)$$

so the nonlinearity is approximated by

$$x^3 \cong \left(3p_x + m_x^2\right) m_x + 3\left(p_x + m_x^2\right)(x - m_x) \qquad (1.2-12)$$

Comparing Eqs. (1.2-11) and (1.2-12), we see that the describing function gains* depend on both the mean and variance of x, as indicated in Fig. 1.2-4, while the coefficients in the Taylor series approximation do not.

---

*In treating single-input nonlinearities, it is sometimes convenient to consider $\hat{f}/m_x$ to be the mean component "gain".

R-11804

(a) Mean Component Gain

(b) Random Component Gain
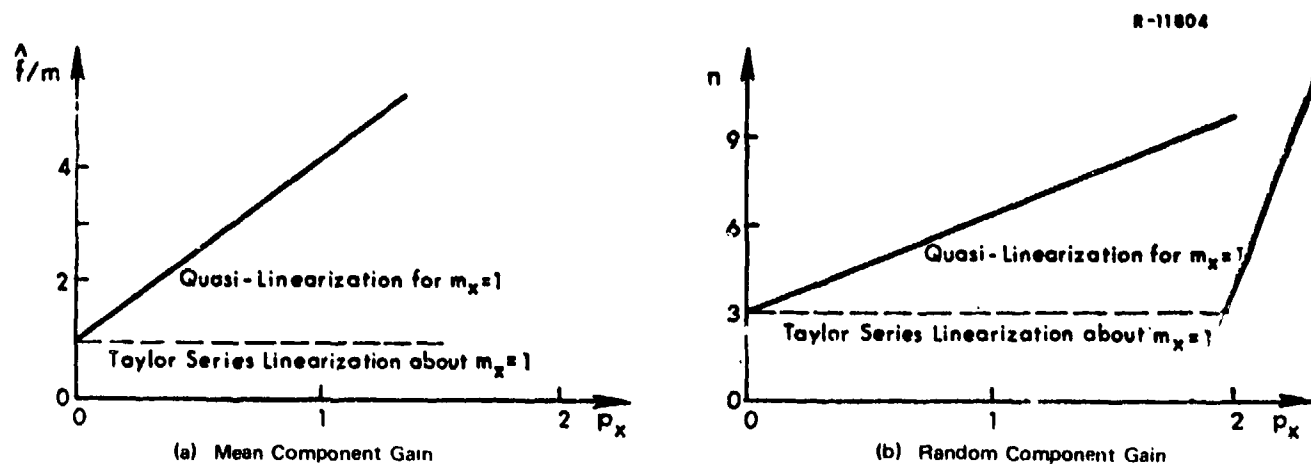
Figure 1.2-4   Quasi-Linearization of $y = x^3$ for Unity Input Mean

1.3 CONTINUOUS/DISCRETE-TIME SYSTEMS

Preceding sections of this chapter have treated continuous-time nonlinear systems; i.e., those that are governed by differential equations. However, in many practical applications, the system may include a digital computer whose operations are expressed in terms of difference equations, as illustrated in Fig. 1.3-1. Such a structure arises in missile guidance systems when digital control laws are used to generate acceleration commands, for example. In this section, equations are briefly developed for propagating the mean and covariance of a nonlinear, mixed continuous/discrete system. Systems which are wholly discrete can be treated as special cases of the following discussion.

The equations of motion for a system of the type shown in Fig. 1.3-1 are expressed in mixed differential/difference equation format. In the continuous-time phase (between sampling instants, t_k, $k = 1,2,...$) the digital computer is inactive, and the state variables of the system satisfy an equation of the form
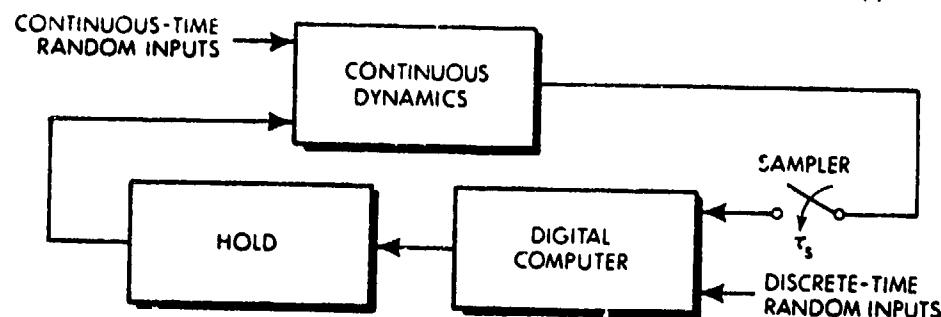
Figure 1.3-1   An Example of a Mixed Continuous/
Discrete System

$$\underline{\dot{x}} \triangleq \begin{bmatrix} \underline{\dot{x}}_c \\ \hline \underline{\dot{x}}_d \end{bmatrix} = \begin{bmatrix} \underline{f}_c(\underline{x},t) + G_c(t)\,\underline{w}_c(t) \\ \hline \underline{0} \end{bmatrix}, \quad t_k < t \le t_{k+1}$$

$$(1.3-1)$$

where $\underline{x}_c(t)$ refers to the continuously-varying states in the system, and $\underline{x}_d(t)$ is a collection of discrete-time states (e.g., states in the digital computer) which remain unchanged between the sampling times. Under the assumption that the state variables are jointly normal, the statistics between sampling instants can be propagated using a straightforward extension of the standard CADET equations (Eq. (1.2-7)) as follows:

$$\underline{\dot{m}} = \begin{bmatrix} \underline{\hat{f}}_c(\underline{m},P,t) \\ \hline \underline{0} \end{bmatrix} + \begin{bmatrix} G_c(t)\,\underline{b}_c \\ \hline \underline{0} \end{bmatrix}$$

$$(1.3-2)$$

$$\dot{P} = \begin{bmatrix} N_c(\underline{m},P,t) \\ \hline 0 \end{bmatrix} P + P \begin{bmatrix} N_c^T(\underline{m},P,t) & \vdots & 0 \end{bmatrix} + \begin{bmatrix} G_c Q_c G_c^T & \vdots & 0 \\ \hline 0 & \vdots & 0 \end{bmatrix},$$

$$t_k < t \le t_{k+1}$$

1-13

where N_c is the quasi-linear system dynamics matrix for the continuous-time state variables, defined by

$$N_c \triangleq E\left[\underline{f}_c(\underline{x},t)\,\underline{r}^T\right]$$

which is of dimension $(n_c \times n)$; n is the total number of state variables and n_c is the number of continuously-varying states. The continuous-time vector of white noise processes $\underline{w}_c(t)$ is described statistically by the mean vector $\underline{b}_c$ and spectral density matrix Q_c as before (refer to Eq. (1.1-2)).

Observe that describing functions for a nonlinear time-invariant function of gaussian discrete-time states alone need not be evaluated continuously since the statistics of the discrete-time states are constant in the interval $t_k < t \le t_{k+1}$. As a special case, if

$$\underline{f}_c(\underline{x},t) = \underline{f}_{1_c}(\underline{x}_c,t) + \underline{f}_{2_c}(\underline{x}_d) \qquad (1.3\text{-}3)$$

then N_c may be partitioned into two parts,

$$N_c(\underline{m},P,t) = \left[N_{c_1}(\underline{m}_c,P_{cc},t) \,\vdots\, N_{c_2}(\underline{m}_d,P_{dd})\right] \qquad (1.3\text{-}4)$$

where $\underline{m}$ and P are correspondingly partitioned into

$$\underline{m} = \begin{bmatrix} \underline{m}_c \\ \hline \underline{m}_d \end{bmatrix}, \qquad P = \begin{bmatrix} P_{cc} & \vdots & P_{cd} \\ \hline P_{cd}^T & \vdots & P_{dd} \end{bmatrix} \qquad (1.3\text{-}5)$$

Since $\underline{m}_d$ and P_{dd} are constant during the continuous-time phase, the matrix N_{c_2} is also constant.

At a sampling time, t_{k+1}, the digital computer performs a calculation which can be represented as a difference equation,

$$
\begin{bmatrix} \underline{x}_c(t_{k+1}^+) \\ \hline \underline{x}_d(t_{k+1}^+) \end{bmatrix} = \begin{bmatrix} \underline{x}_c(t_{k+1}) \\ \hline \underline{f}_d(\underline{x}(t_{k+1}),t_{k+1}) \end{bmatrix} + \begin{bmatrix} 0 \\ \hline G_{k+1}\underline{w}_{k+1} \end{bmatrix} \qquad (1.3\text{-}6)
$$

where the superscript (+) denotes the new values of the state variables just after a sampling instant.* The vector $\underline{w}_{k+1}$ represents a discrete-time random quantity that can enter the digital calculation as a result of sensor measurement noise, quantization, etc. It is assumed that $\underline{w}_{k+1}$ has a mean of $\underline{b}_{k+1}$ and a covariance matrix Q_{k+1}. Observe that in Eq. (1.3-6) $\underline{x}_c$ remains unchanged, since variables that satisfy differential equations cannot change instantaneously in time. Situations where it is reasonable to assume that a continuous-time variable can change "almost instantaneously" as a result of a digital operation can be treated by decomposing that variable into components that are strictly continuous (an element of $\underline{x}_c$) and digital (an element of $\underline{x}_d$), so the condition that $\underline{x}_c(t_{k+1}^+) = \underline{x}_c(t_{x+1}^+)$ represents no loss in generality.

Because the mean and covariance of $\underline{x}_c$ and $\underline{x}_d$ at t_{k+1} are known from Eq. (1.3-2), the expectation vector $\hat{\underline{f}}_d$ and quasi-linear system dynamics matrix N_d corresponding to $\underline{f}_d$ in Eq. (1.3-5) can be evaluated. Thus we can rewrite the discrete-time part of Eq. (1.3-6) approximately as

$$
\underline{x}_d(t_{k+1}^+) \cong \hat{\underline{f}}_d + N_d\left[\underline{x}(t_{k+1}) - \underline{m}(t_{k+1})\right] + G_{k+1}\underline{w}_{k+1} \qquad (1.3\text{-}7)
$$

From Eq.(1.3-7) it follows that the mean and covariance of the system states just after the discrete-time calculation are given by

---

*The discrete-time operation actually takes place between t_{k+1} and $t_{k+1} + \epsilon$. In this discussion it is assumed that ϵ is negligible in comparison with the time-scale of the continuous-time dynamics, although finite computational delays can be treated in a straightforward manner.

$$\underline{m}_c(t_{k+1}^+) = \underline{m}_c(t_{k+1})$$

$$\underline{m}_d(t_{k+1}^+) = \hat{\underline{f}}_d$$

$$P(t_{k+1}^+) = \left[\begin{array}{c:c} I & 0 \\ \hdashline & N_d \end{array}\right] P(t_{k+1}) \left[\begin{array}{c:c} I & \\ \hdashline & N_d^T \\ 0 & \end{array}\right] + \left[\begin{array}{c:c} 0 & 0 \\ \hdashline 0 & G_{k+1}Q_{k+1}G_{k+1}^T \end{array}\right]$$

$$(1.3-8)$$

After evaluating Eq. (1.3-8), $\underline{m}(t_{k+1}^+)$ and $P(t_{k+1}^+)$ are the initial conditions for propagating the mean vector and covariance matrix over the next continuous-time phase using Eq. (1.3-2). Thus by alternately implementing the continuous-time and digital mean vector and covariance matrix propagation equations, Eqs. (1.3-2) and (1.3-8), the performance of a nonlinear system described by a mixed differential/difference equation can be evaluated.

The developments discussed in this chapter provide the necessary tools for analyzing the performance of a broad class of nonlinear systems with random inputs. The efficiency realized by CADET has made it an attractive technique for performing sensitivity studies and investigations of the impact of nonlinear effects on the accuracy of tactical missile guidance systems; it is anticipated that CADET will prove to be equally powerful in treating other nonlinear systems.

2. <u>CADET APPLICATION: SIMPLE ILLUSTRATIONS</u>

In this chapter we demonstrate many of the details that are involved in the application of CADET to a practical problem involving the statistical evaluation of the performance of a nonlinear system with random inputs. Simplified formulations of the missile-target intercept problem are treated, with guidance modules that are either analog or digital; the corresponding CADET equations are obtained; and their solution -- to establish the evolution of the system variable statistics during a given scenario -- is outlined in computer flow-chart format.

2.1 MISSILE-TARGET EQUATIONS OF MOTION

This section treats the basic differential equations describing the motion of a tactical missile and a target to be intercepted. In subsequent sections, examples of two types of guidance modules are considered -- continuous-time (analog) and discrete-time (digital) -- to provide the basis for detailing the CADET methodology, both for systems represented entirely by differential equations and for systems described by mixed differential/ difference equations. In order to obtain a system model which is simple enough to permit a clear presentation of the step-by-step procedure entailed in the use of CADET, we reduce the planar missile-target intercept problem to its bare essentials. Chapter 3 provides a more detailed discussion on modeling the missile-target intercept problem; here we present only a summary of the required dynamic equations.

The coordinate frame and the basic variables are portrayed in Fig. 2.1-1. Here we consider variations about a head-on
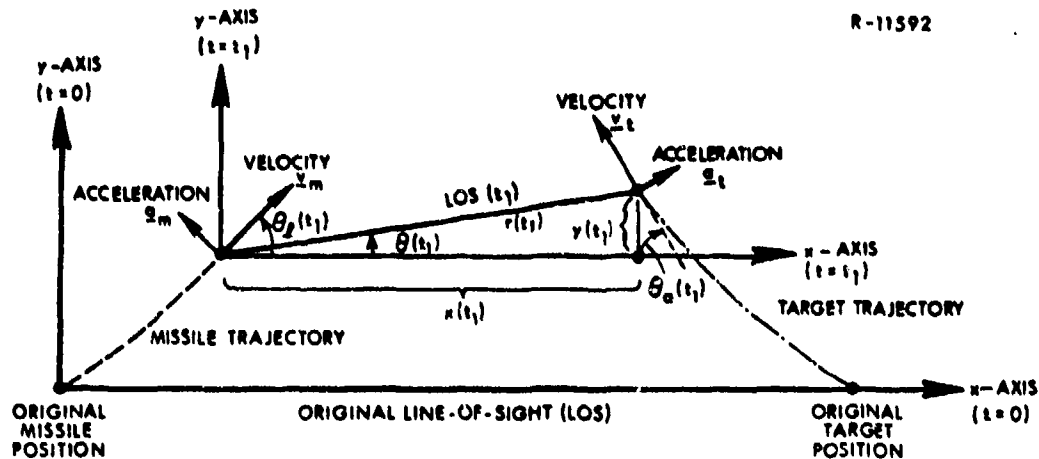
Figure 2.1-1   Missile-Target Planar Intercept Geometry

intercept, i.e., the missile lead angle, θ_ℓ, and target aspect angle, θ_a, are assumed to be small. For the purpose of illustrating the mechanization of CADET, we make the following approximations based on small-angle assumptions:

- The down-range separation, x, and missile-target range, r, are deterministic, given approximately by

$$x(t) \approx r(t) \approx (v_m + v_t)(T-t)$$

$$\triangleq (v_m + v_t)\, t_{go}$$

(2.1-1)

  where T is the nominal terminal time (time of intercept), t_{go} is the time-to-go, and v_m and v_t are the constant missile and target velocity magnitudes, respectively.

- The lateral or cross-range separation, y, is determined by the missile and target lateral accelerations, a_m and a_t respectively, as in Eq. (3.5-14)

$$\ddot{y} \approx a_t - a_m$$

(2.1-2)

- The autopilot and airframe dynamics are represented by a linear plant, modeled by a transfer function with a single dominant pole at $s = -1/\tau$,

followed by an ideal limiter, to model the airframe saturation effect. Thus the unlimited missile lateral acceleration $\tilde{a}_m$ satisfies the differential equation

$$\dot{\tilde{a}}_m + \frac{1}{\tau}\,\tilde{a}_m = \frac{1}{\tau}\,a_c \qquad (2.1\text{-}3)$$

where a_c is the acceleration command generated by the guidance module, and the limited value, a_m, is given by

$$a_m = f(\tilde{a}_m) = \begin{cases} \tilde{a}_m & , \quad |\tilde{a}_m| \le a_{max} \\[2ex] a_{max}\,\text{sign}(\tilde{a}_m), & \quad |\tilde{a}_m| > a_{max} \end{cases} \qquad (2.1\text{-}4)$$

● The target acceleration, a_t, is the sum of a deterministic variable and a band-limited gaussian process satisfying

$$\dot{a}_t + \omega_t\,a_t = w(t) \qquad (2.1\text{-}5)$$

where ω_t is the target maneuver bandwidth. The random input w is described by

$$E\left[w(t)\right] = b(t)$$
$$\qquad (2.1\text{-}6)$$
$$E\left[(w(t)-b(t))(w(\tau)-b(\tau))\right] = q(t)\,\delta(t-\tau)$$

where b is the deterministic component of the input and q is the spectral density of the white noise process, $w - b$.

Given the preceding simplified equations of motion, we complete the missile-target intercept model by considering simple examples of the two basic classes of guidance modules: continuous-time and digital.

2.2   THE CONTINUOUS-TIME CASE: PROPORTIONAL GUIDANCE

The acceleration command dictated by the classical proportional guidance law (refer to Section 3.5.1) is given by

$$a_c = n'\,v_c\,\dot{\theta} \qquad (2.2\text{-}1)$$

where n' is the navigation ratio (a constant, here taken to be 3), v_c is the closing velocity, which in the present scenario is approximately given by the sum of the missile and target velocities,

$$v_c \triangleq r(t)/t_{go} \approx v_m + v_t \qquad (2.2\text{-}2)$$

and $\dot{\theta}$ is the angular rate of the line-of-sight (LOS)(Fig. 2.1-1). Using the assumptions made in Section 2.1, Eq. (2.2-1) can be reformulated to yield the approximation

$$\frac{1}{\tau} a_c \approx \frac{n'}{t_{go}\tau} \left(\dot{y} + \frac{y}{t_{go}} \right) \triangleq \beta \left(\dot{y} + \frac{y}{t_{go}} \right) \qquad (2.2\text{-}3)$$

where β denotes $n'/\tau t_{go}$ for notational simplicity. The complete system model based on the foregoing assumptions and development is portrayed in Fig. 2.2-1.

R-15234
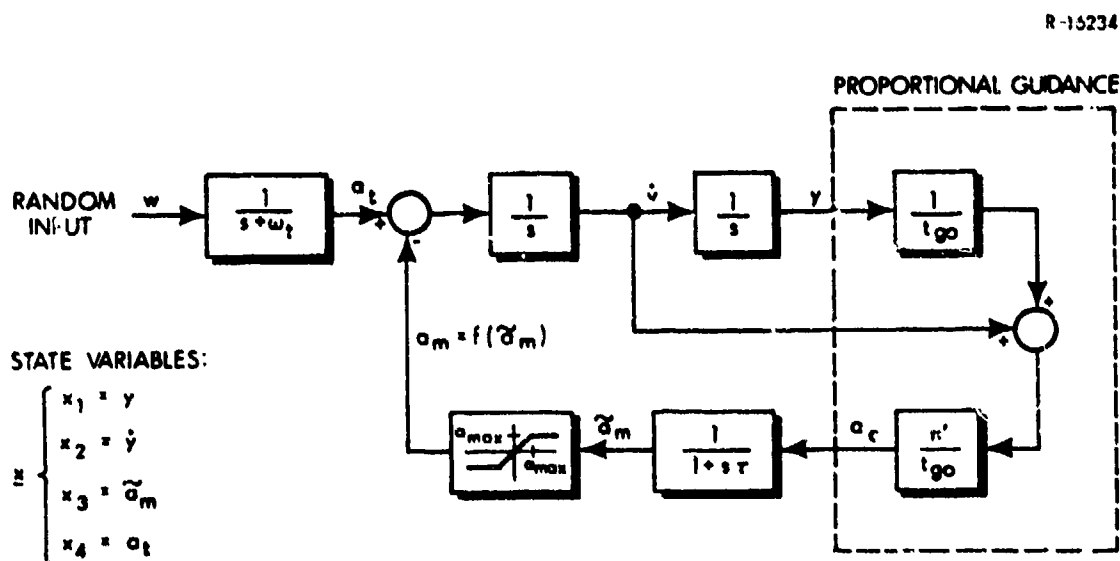
Figure 2.2-1   Simplified Missile-Target Intercept Model With Continuous-Time Guidance

The state vector differential equation associated with Fig. 2.2-1 is given by

$$\underline{\dot{x}} = \begin{bmatrix} \dot{x}_1 \\ \dot{x}_2 \\ \dot{x}_3 \\ \dot{x}_4 \end{bmatrix} = \begin{bmatrix} 0 & 1 & 0 & 0 \\ 0 & 0 & 0 & +1 \\ \beta/t_{go} & \beta & -1/\tau & 0 \\ 0 & 0 & 0 & -\omega_t \end{bmatrix} \underline{x} + \begin{bmatrix} 0 \\ -1 \\ 0 \\ 0 \end{bmatrix} f(x_3) + \begin{bmatrix} 0 \\ 0 \\ 0 \\ 1 \end{bmatrix} w(t)$$

$$\triangleq F\underline{x} + \underline{d}f(x_3) + \underline{g}\,w(t) \qquad\qquad (2.2\text{-}4)$$

From the statistics of the input to the limiter,

$$m_3 = E\left[x_3\right]$$

$$r_3 = x_3 - m_3 \qquad\qquad (2.2\text{-}5)$$

$$\sigma_3^2 = E\left[r_3^2\right]$$

we can directly evaluate the scalar random input describing functions (ridf's) used in the quasi-linear representation for the limiter $f(x_3)$,

$$f(x_3) \approx \hat{f} + nr_3 \qquad\qquad (2.2\text{-}6)$$

as derived in Example 3 of Section 4.3:

$$n = PI\left(\frac{a_{max}+m_3}{\sigma_3}\right) + PI\left(\frac{a_{max}-m_3}{\sigma_3}\right) - 1$$

$$\hat{f} = \sigma_3\left[G\left(\frac{a_{max}+m_3}{\sigma_3}\right) - G\left(\frac{a_{max}-m_3}{\sigma_3}\right)\right] - m_3 \qquad\qquad (2.2\text{-}7)$$

The functions $G(v)$ and $PI(v)$ are defined in Eq. (4.3-13); they are the standard functions used in quasi-linearizing piecewise-linear elements (Ref. 6). Many computer scientific subroutine

packages have available the subroutine "ERF(v)", in which case

$$PI(v) = \frac{1}{2} \left(1 + ERF \left(\frac{v}{\sqrt{2}} \right) \right)$$

$$G(v) = vPI(v) + \frac{1}{\sqrt{2\pi}} e^{-\frac{1}{2} v^2}$$

(2.2-8)

permits direct calculation of $\hat{f}$ and n. Given the two constituents of the quasi-linear representation of the limiter indicated in Eqs. (2.2-6) and (2.2-7), we substitute into Eq. (2.2-4) to get

$$\hat{\underline{f}} = F\underline{m} + \underline{d}\hat{f}$$

$$N = \begin{bmatrix} 0 & 1 & 0 & 0 \\ 0 & 0 & -n & 1 \\ \beta/t_{go} & \beta & -1/\tau & 0 \\ 0 & 0 & 0 & -\omega_t \end{bmatrix}$$

(2.2-9)

Finally, from the input statistics, b and q, the differential equations and initial conditions that approximately govern the propagation of the state vector deterministic component ("mean") and covariance matrix are given by Eq.(1.2-7):

$$\dot{\underline{m}} = \hat{\underline{f}} + \underline{g} \, b; \qquad \underline{m}(0) = \underline{m}_0$$

$$\dot{P} = NP + PN^T + \underline{g} \, \underline{g}^T q; \qquad P(0) = P_0$$

(2.2-10)

The CADET methodology utilizes the preceding relations to determine the time histories of the mean vector, $\underline{m}$, and covariance matrix, P, over the duration of an ensemble of engagements $(0 \le t \le T)$. Any standard numerical integration technique may then be used to solve Eq. (2.2-10). The structure of a computer

program to carry out the CADET analysis of tactical missile performance is indicated in Fig. 2.2-2.

The results of a CADET and monte carlo statistical analysis of the performance of the preceding missile guidance system (obtained from Ref. 1) are depicted in Fig. 2.2-3. Since the rms lateral separation between the missile and target is of primary importance in assessing the ability of the missile to intercept the target, only that variable is portrayed. The white noise input spectral density, q, was chosen to be a constant yielding an rms target lateral acceleration of 160 ft/sec^2, the bandwidth ω_t was assumed to be 1 rad/sec, and the autopilot time constant τ was taken to be 1 sec. All initial conditions ($\underline{m}_0$ and P_0) were zero.

This missile performance study considered three levels of airframe saturation. In Fig. 2.2-3a, the linear case corresponding to an infinite acceleration command limit is shown; here, CADET reduces to the standard linear covariance analysis (Section 1.1) which is exact, and the 200-trial monte carlo analysis provides an adequate approximation to this result. For the study of Fig. 2.2-3b, the restriction that the missile lateral acceleration cannot exceed 322 ft/sec^2 leads to a five-fold increase in σ_y at the terminal time, here taken to be 10 sec; the CADET and monte carlo approximate solutions are in good agreement. Even in the case where the missile lateral acceleration constraint is very severe ($a_{max} = 32.2$ ft/sec^2), causing a further large decrease in missile capability as shown in Fig. 2.2-3c, the CADET solution is verified by the monte carlo analysis.

Thus we observe that the direct statistical analysis via CADET, implemented according to Fig. 2.2-2, quite accurately captures the effect of a significant nonlinearity in the missile-target intercept problem. This investigation is performed with an expenditure of computer time that is a small fraction

R-16257

```
┌─────────────┐
│   INITIAL   │
│ CONDITIONS  │
└─────────────┘
       │
  m₀, P₀, t₀
       │
┌─────────────┐
│  CALCULATE  │
│  =SCRIBING  │
│  JNCTIONS   │
│ Eq. (2.2-7) │
└─────────────┘
       │
┌─────────────┐
│  EVALUATE   │
│ f̂(m,P), N(m,P) │
│ Eq. (2.2-9) │
└─────────────┘
       │
┌─────────────┐
│  EVALUATE   │
│   ṁ, Ṗ      │
│ Eq. (2.2-10)│
└─────────────┘
       │
┌─────────────┐
│ PROPAGATE:  │
│ m(t) → m(t+Δt) │
│ P(t) → P(t+Δt) │
│ BY NUMERICAL│
│ INTEGRATION │
└─────────────┘
       │
    ◇ t + Δt = T? ◇ ── NO ──┐
       │                    │
      YES           ┌──────────────┐
       │            │    UPDATE    │
┌─────────────┐     │  t = t + Δt  │
│     END     │     └──────────────┘
└─────────────┘
```

$$\underline{m}_0, P_0, t_0$$

CALCULATE
ESCRIBING
JNCTIONS
Eq. (2.2-7)

EVALUATE
$\hat{\underline{f}}(\underline{m}, P), N(\underline{m}, P)$
Eq. (2.2-9)

EVALUATE
$\dot{\underline{m}}, \dot{P}$
Eq. (2.2-10)

PROPAGATE:
$\underline{m}(t) \rightarrow \underline{m}(t + \Delta t)$
$P(t) \rightarrow P(t + \Delta t)$
BY NUMERICAL
INTEGRATION

$t + \Delta t = T?$

UPDATE
$t = t + \Delta t$

END
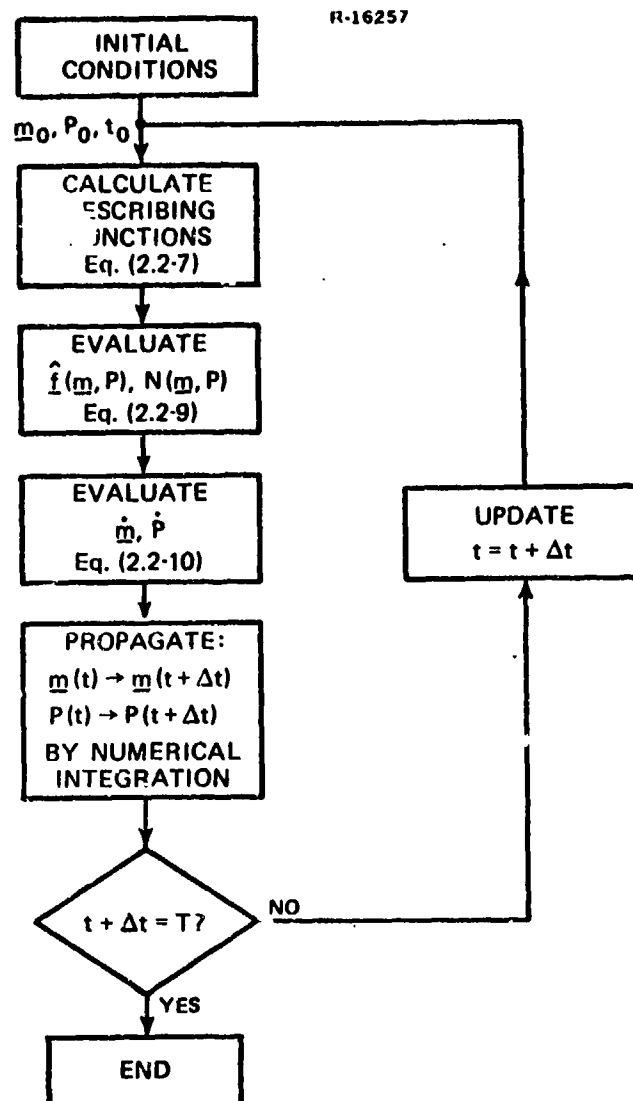
Figure 2.2-2   Flow Chart for the Direct
                Statistical Analysis of a
                Continuous-Time System
                via CADET

2-8

R-16244

(a) Linear Case, $a_{max} = \infty$

(b) Moderate Limiting, $a_{max} = 322$ ft/sec^2

(c) Severe Limiting, $a_{max} = 32.2$ ft/sec^2
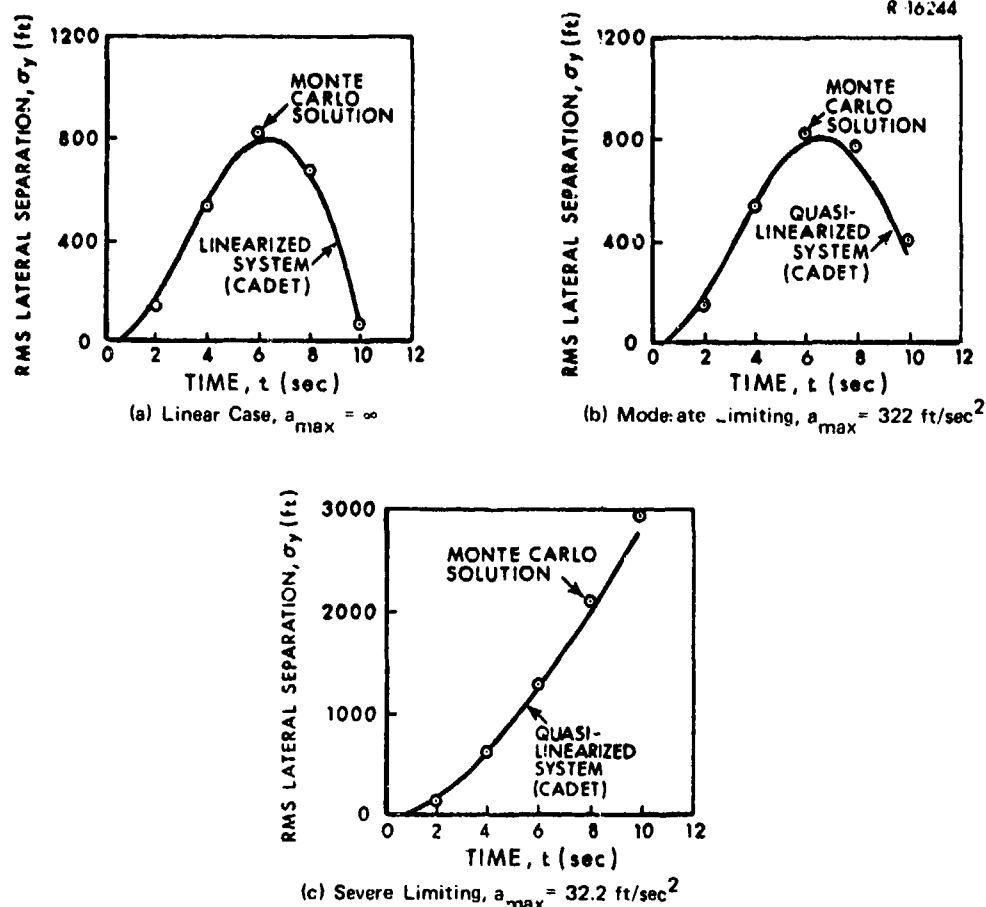
Figure 2.2-3   Performance Projections for Various Levels
of Airframe Acceleration Saturation

(approximately 1/100) of that required for an accurate monte carlo
study. Furthermore, the effect of decreasing missile performance
caused by airframe saturation is completely beyond the scope of
linear covariance analysis, which requires the small-signal line-
arization of the saturation nonlinearity, i.e., replacing $f(x_3)$
by a unity linear gain, regardless of the saturation level. Con-
sequently the small-signal linearization approach completely ob-
scures the nonlinear effect and leads to a quite over-optimistic
prediction of missile performance when compared to a more realistic
assumption -- e.g., that a_m cannot exceed 322 ft/sec^2, as evident
in Figs. 2.2-3a and 2.2-3b.

2.3 GUIDANCE SYSTEMS WITH DIGITAL DATA PROCESSING

In some guidance systems, discrete-time measurements of certain system variables are made available to a computer for data processing purposes; acceleration commands are then calculated (in an on-line mode by use of a suitable algorithm) which are used to control the missile. In this presentation, we assume that the available signal is a noisy sampled measurement of LOS angle, θ, so we have the sequence of values given by

$$z_k = \theta_k + v_k, \qquad k = 1,2,\ldots \qquad (2.3\text{-}1)$$

at the sampling instants, $t_k = k\tau_s$, where τ_s is the sampling period. The zero-mean white noise sequence, v_k, is quantified by its variance

$$\sigma_v^2 = E\left[v_k^2\right] \qquad (2.3\text{-}2)$$

Generally, the random effects modeled by this sequence include external inputs (e.g., jamming) and measurement error. In light of the small angle conditions, we use the approximation

$$\theta \cong y/r \overset{\Delta}{=} x_1/r \qquad (2.3\text{-}3)$$

where r is deterministic, given by Eq. (2.1-1), and x_1 is the state variable representing y, Fig. 2.2-1.

Based on the information provided by the measurement sequence z_k, the computer algorithm is often of the form

$$\underline{x}_d(t_k^+) = F_{d,k}\,\underline{x}_d(t_k) + \underline{k}_k z_k \qquad (2.3\text{-}4)$$

(cf. Section 3.5.2 for the design of a guidance module based on the Kalman filter and optimal control theory) where $\underline{x}_d$ is the vector of digital states, comprised of variables which are stored in memory and up-dated according to Eq. (2.3-4) as each new measurement z_k is made and processed. The matrix $F_{d,k}$ and vector $\underline{k}_k$, which may vary from one digital operation to the next, are specified by the filter algorithm. The difference equation, Eq. (2.3-4), in combination with the initial condition $\underline{x}_{d0}$ determines the time-histories of $\underline{x}_d$.

A typical control law (again, refer to Section 3.5.2) then specifies an acceleration command, a_c given in Eq. (2.1-3), that is a linear combination of the digital states,

$$a_c = \underline{c}_k^T \underline{x}_d(t_k^+), \qquad t_k^+ \leq t \leq t_{k+1} \qquad (2.3\text{-}5)$$

This relation completes the description of the overall system model, depicted in Fig. 2.3-1.

R-16229
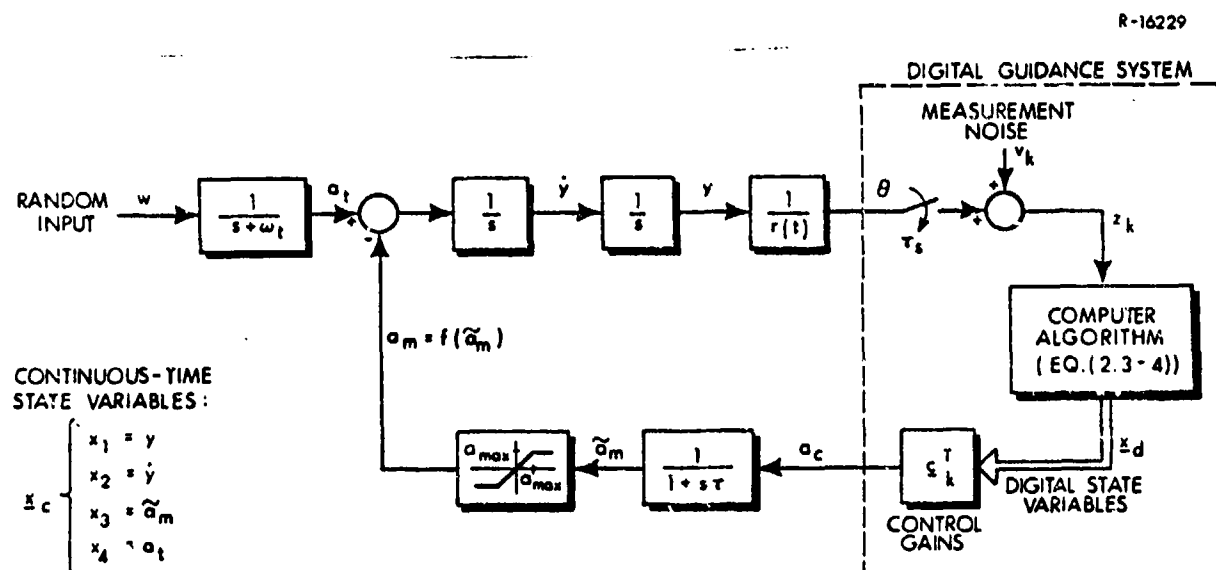
Figure 2.3-1   Simplified Missile-Target Intercept Model With Digital Guidance

The mixed continuous/discrete-time system depicted in Fig. 2.3-1 and represented by the total state vector

$$\underline{x}^T = \begin{bmatrix} \underline{x}_c^T & \vdots & \underline{x}_d^T \end{bmatrix} \qquad (2.3-6)$$

satisfies a differential/difference equation of the form treated in Section 1.3. Corresponding to this division of state variables into continuous-time and digital states, we have

$$\underline{m} = \begin{bmatrix} \underline{m}_c \\ ---- \\ \underline{m}_d \end{bmatrix} , \qquad P = \begin{bmatrix} P_{cc} & \vdots & P_{cd} \\ ---- & \vdots & ---- \\ P_{cd}^T & \vdots & P_{dd} \end{bmatrix} \qquad (2.3-7)$$

The nonlinearity $f(\hat{a}_m)$ given in Eq. (2.1-4) falls in the continuous-time dynamics; its argument is a continuous state variable, x_3. Thus quasi-linearization proceeds as in Eqs.(2.2-6) through (2.2-8). We can then determine the matrix N_c and vector $\hat{\underline{f}}_c$ required for the propagation of $\underline{m}$ and P during the continuous-time phase (Eq. (1.3-2)):

$$N_c = \begin{bmatrix} 0 & 1 & 0 & 0 & \vdots & \underline{0}^T \\ 0 & 0 & -n & 1 & \vdots & \underline{0}^T \\ 0 & 0 & -1/\tau & 0 & \vdots & \frac{1}{\tau}\underline{c}_k^T \\ 0 & 0 & 0 & -\omega_t & \vdots & \underline{0}^T \end{bmatrix}$$

$$\qquad (2.3-8)$$

$$\hat{\underline{f}}_c = \begin{bmatrix} m_2 \\ (m_4 - \hat{f}) \\ (-m_3 + \underline{c}_k^T \underline{m}_d)/\tau \\ -\omega_t m_4 \end{bmatrix}$$

These quantities are all that are required for the propagation of $\underline{m}$ and P between sample times according to Eq. (1.3-2),

$$\dot{\underline{m}} = \left[\frac{\underline{r}_c}{\underline{0}}\right] + \left[\frac{\underline{g}}{\underline{0}}\right] b$$

$$(2.3\text{-}9)$$

$$\dot{P} = \left[\frac{N_c}{0}\right] P + P \left[N^T \mid 0\right] + \left[\frac{\underline{g}\,\underline{g}^T \mid 0}{0 \mid 0}\right] q$$

where b and q are the deterministic component and the spectral density of the random component of the random input, respectively, as defined in Eq. (2.1-6), and $\underline{g}$ is given in Eq. (2.2-4).

In the present example, the digital operation taking place in the infinitesimal interval (t_k, t_k^+) has been formulated as a single linear time-varying difference equation, Eq. (2.3-4). Recalling that

$$z_k = x_1(t_k)/r(t_k) + v_k \tag{2.3-10}$$

we obtain

$$\underline{x}_d(t_k^+) = \left[\frac{1}{r(t_k)}\,\underline{k}_k \mid \underline{0} \mid \underline{0} \mid \underline{0} \mid F_{d,k}\right]\left[\frac{\underline{x}_c(t_k)}{\underline{x}_d(t_k)}\right] + \underline{k}_k v_k$$

$$(2.3\text{-}11)$$

$$\triangleq N_{d,k}\,\underline{x}(t_k) + \underline{k}_k v_k$$

The change in $\underline{m}$ and P during the digital phase of operation (as given in Eq. (1.3-8)) is then

$$\underline{m}(t_k^+) = \left[\frac{I \mid 0}{N_{d,k}}\right]\underline{m}(t_k) \triangleq N_k \underline{m}(t_k)$$

$$(2.3\text{-}12)$$

$$P(t_k^+) = N_k P(t_k)\,N_k^T + \left[\frac{0 \mid 0}{0 \mid \sigma_v^2 \underline{k}_k \underline{k}_k^T}\right]$$

Implementation of the CADET equations given above (Eqs. (2.3-9) and (2.3-12)) is portrayed in computer flow-chart format in Fig. 2.3-2.

We observe that the difference equation satisfied by the digital states is linear time-varying, so the matrix N_d (Eq. (2.3-11)) contains no describing functions. If it is necessary to include nonlinear effects in the discrete-time portion of the system model, one must evaluate appropriate random input describing functions to be substituted in the vector $\hat{f}_d$ and matrix N_d (Eq. (1.3-7)); some added complexity is entailed in this case.

The examples given in Sections 2.2 and 2.3 illustrate the fundamentals involved in the application of CADET to provide assessments of the performance of a tactical missile represented by a simple low-order system model with one significant nonlinear effect. CADET has been successfully applied to system models of considerably higher order and complexity (refer, for example, to Table 5.1-1). The flow charts shown in Figs. 2.2-2 and 2.3-2 accurately reflect the methodology used in the more complex problems.
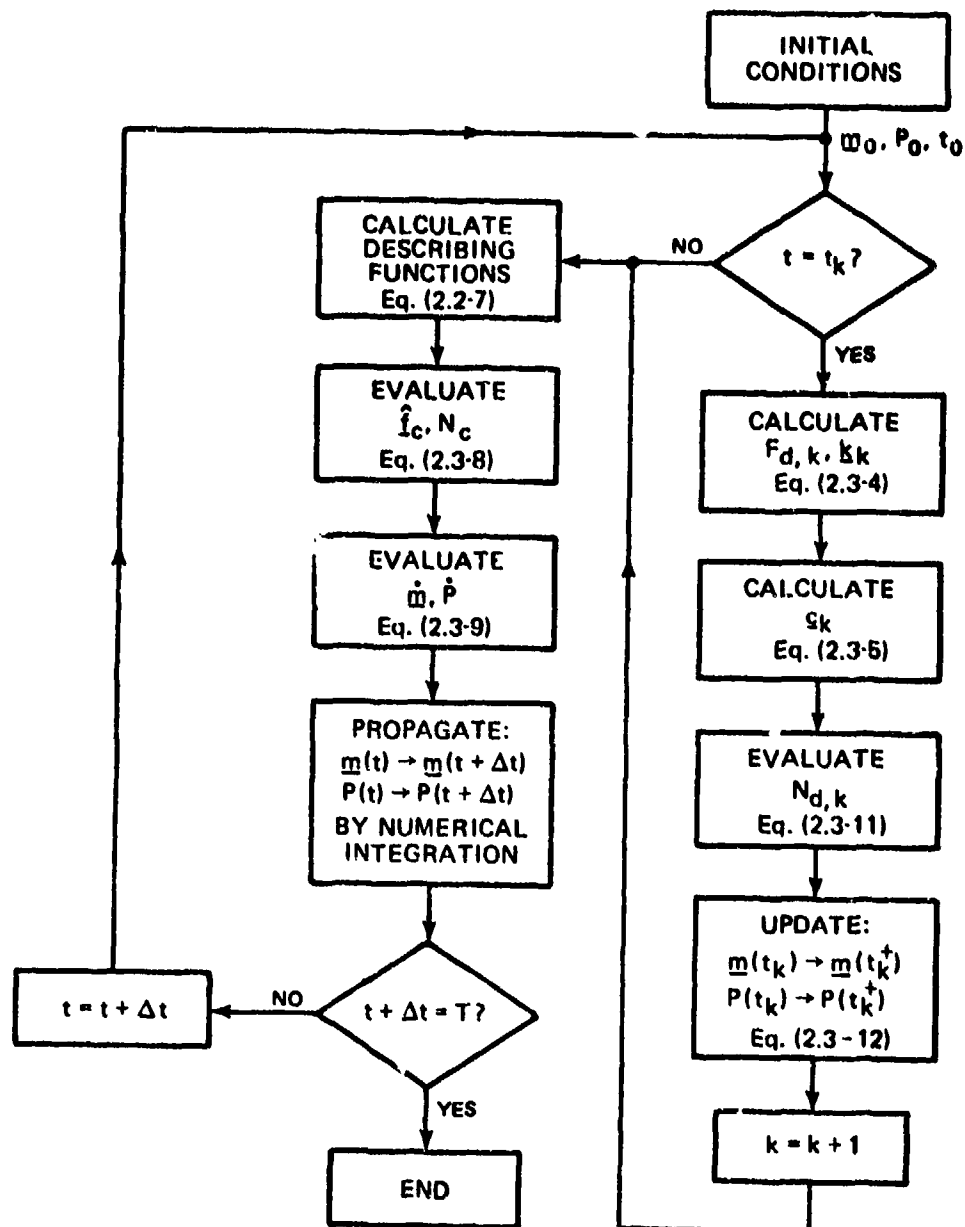
Figure 2.   Flow Chart for the Direct
              Statistical Analysis of a Mixed
              Continuous/Discrete-Time System
              via CADET

3. MODEL DEVELOPMENT FOR THE
MISSILE-TARGET INTERCEPT PROBLEM

This chapter presents mathematical models which describe various subsystems required in treating the general missile-target intercept problem. The material included here summarizes the nonlinear effects that have been treated in past CADET applications (Refs. 1 to 4). The aims of this presentation are to aid future users of CADET in analyzing tactical missile performance, and to provide some guidance in modeling analogous phenomena that may occur in the simulation of other nonlinear systems with random inputs.

3.1 ELEMENTS OF THE MODEL

The overall interconnection of the subsystems which comprise the missile-target intercept model is indicated in Fig. 3.1-1. The principal variables are shown as outputs of the appropriate blocks, and random disturbances are denoted w_i. Detailed models underlying each input-output relationship are given in subsequent sections of the chapter. Observe that the models developed here are of considerably greater realism than those used in the illustrative examples of Chapter 2, although the basic closed-loop guidance system is of the same structure.

3.2 THE MISSILE-TARGET KINEMATICS MODEL

The missile-target engagement presented here is restricted to the terminal homing phase in a planar intercept configuration.
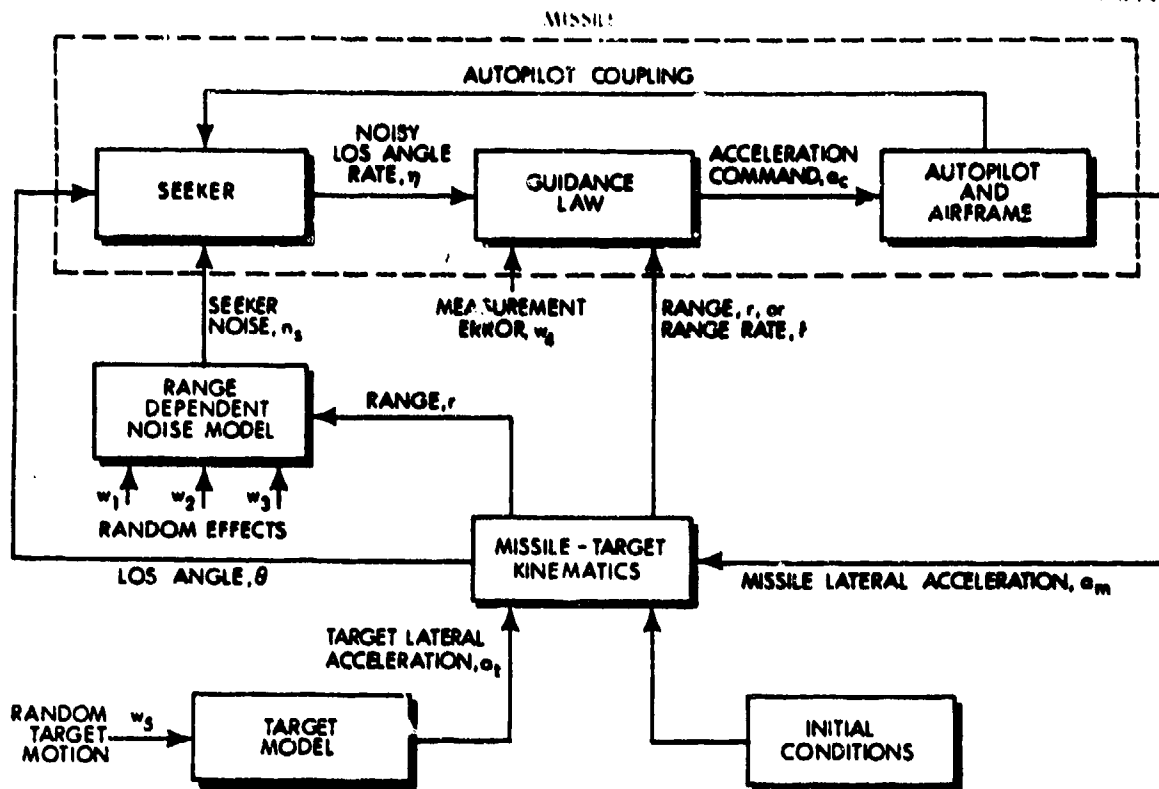
Figure 3.1-1   Basic System Block Diagram

An inertial coordinate system is defined by the positions of the missile and target at the initiation of the terminal homing phase (taken to occur at t = 0); the missile is at the origin and the line-of-sight (LOS) to the target defines the x-axis at t = 0 (see Fig. 3.2-1). The coordinate frame moves with the missile, without rotation; by definition, we designate x and y, respectively, to be the instantaneous down-range and cross-range missile-target separation. Expressing the separation in polar coordinates, the relations

$$r = \sqrt{x^2 + y^2}$$

$$\theta = \tan^{-1}(y/x)$$

define the instantaneous range and LOS angle of the target. The angles θ_ℓ (missile lead angle) and θ_a (target aspect angle) specify the orientation of the missile and target velocity vectors with respect to the x-axis, and θ_{va} defines the direction of the missile acceleration vector with respect to the velocity vector; by convention, θ_ℓ, θ_a and θ_{va} are positive in the directions defined in Fig. 3.2-1.

R-11592a
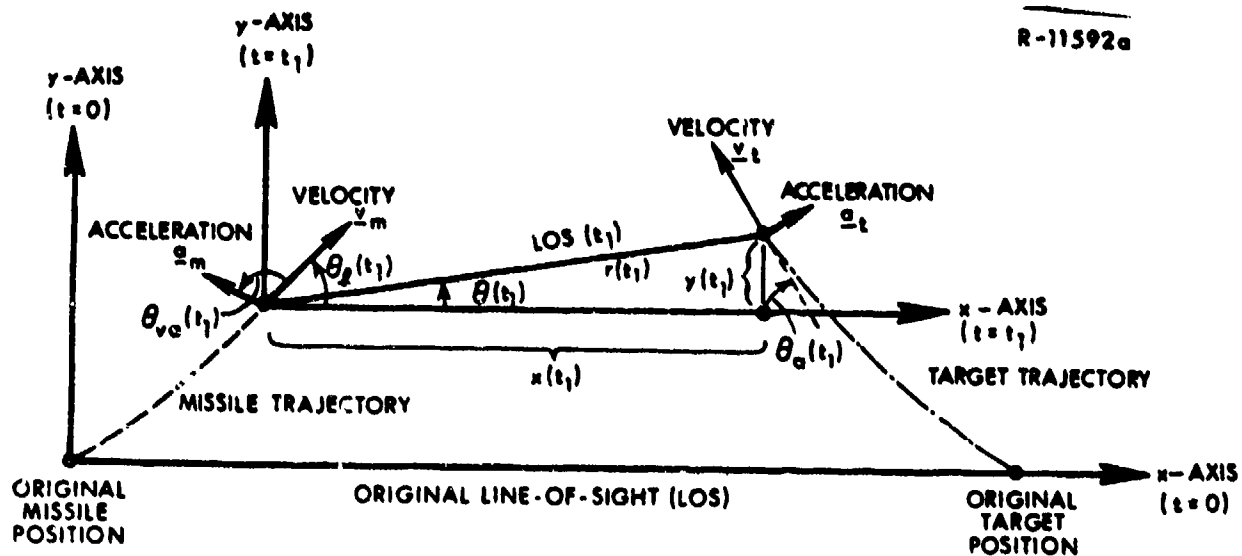
Figure 3.2-1   Target-Missile Planar
Intercept Geometry

        In deriving the equations of motion, it can often be assumed that the missile and target velocity vector magnitudes are constant, or, equivalently, that the missile and target acceleration vectors are normal to the velocity vectors (e.g., θ_{va} is 90 degrees in Fig. 3.2-1). This condition, which neglects the effect of drag, is representative of many missile-target engagement situations during the critical last few seconds. Under this assumption, the lateral acceleration of either vehicle

produces a rotation of the corresponding velocity vector, given by

$$\dot{\theta}_\ell = \frac{1}{v_m} \, a_m$$

$$\dot{\theta}_a = \frac{1}{v_t} \, a_t \qquad\qquad (3.2\text{-}1)$$

The equations describing the relative motion of the target are determined by projecting the velocity vectors onto the axes shown in Fig. 3.2-1; in terms of the velocity magnitudes v_m and v_t,

$$\dot{x} = -v_m \cos(\theta_\ell) - v_t \cos(\theta_a)$$

$$\dot{y} = -v_m \sin(\theta_\ell) + v_t \sin(\theta_a) \qquad\qquad (3.2\text{-}2)$$

Equation (3.2-2) represents the essential nonlinearities inherent to the missile-target kinematic relationship; the overall kinematic equations are portrayed in block diagram form in Fig.3.2-2.
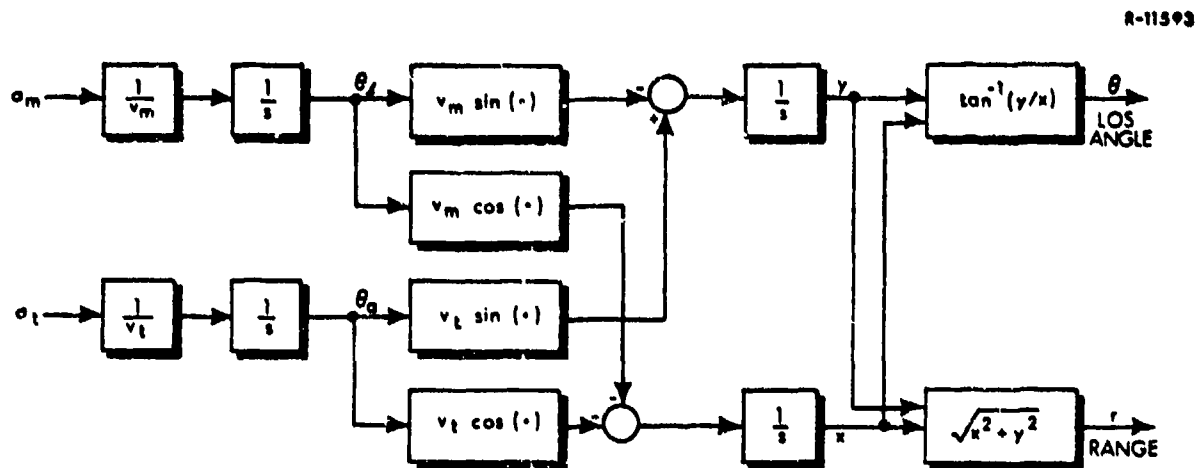
Figure 3.2-2   Block Diagram Formulation of Missile-Target Kinematics

In situations where drag effects are not negligible, the missile velocity vector magnitude will vary with time (according to a nonlinear differential equation) due to the fact that $\underline{a}_m$ is not normal to $\underline{v}_m$ ($\theta_{va} \neq 90$ deg). Thus v_m must be treated as a state variable and the velocity vector rotation is given by the nonlinear relation

$$\dot{\theta}_\ell = \frac{a_m}{v_m} \sin (\theta_{va}) \tag{3.2-3}$$

This case is discussed in greater detail in Section 3.4.

3.3 THE TARGET MODEL

The model representing the target behavior is based on the assumption that the target velocity has constant magnitude with a direction described by the aspect angle, θ_a, shown in Fig. 3.2-1. The aspect angle is determined by the target lateral acceleration, a_t, as indicated in Eq. (3.2-1). A commonly-used target maneuver model represents target lateral acceleration as a correlated gaussian process derived from a gaussian white noise input by one stage of low-pass filtering. In differential equation formulation, we have*

$$\dot{a}_t = -\omega_t a_t + w_5 \tag{3.3-1}$$

This relation and the equivalent low-pass filter representation are depicted in Fig. 3.3-1

By adjusting the values of target maneuver bandwidth, ω_t, and rms level, σ_{a_t}, a wide range of target maneuver characteristics can be represented. The instantaneous target maneuver

---

*The five white noise inputs to the system are simply denoted w_j, $j = 1,2,\ldots,5$, to correspond with Fig. 3.1-1.

R-11887
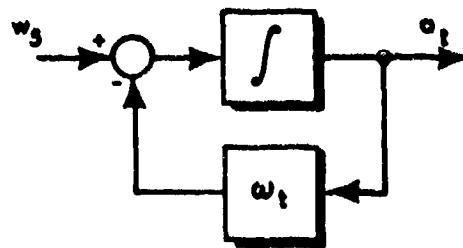
(a) Differential Equation Representation

(b) Transfer Function Formulation

Figure 3.3-1   Band-Limited Gaussian Noise Model
                      for Target Lateral Acceleration

rms level is determined by the spectral density, q_5, of the random input w_5 and the initial condition on σ_{a_t}; for example, if q_5 is constant and

$$E\left[a_t(0)^2\right] = \frac{q_5}{2\omega_t} \qquad (3.3-2)$$

then the rms level of the target acceleration is constant throughout the engagement,

$$\sigma_{a_t} \equiv \sqrt{q_5/2\omega_t} \qquad (3.3-3)$$

It is important to note that the autocorrelation function and the corresponding power spectral density for a poisson square wave -- i.e., a square wave that switches between $\pm\sigma_{a_t}$ ft/sec^2 with random poisson-distributed switching times having an average of $\omega_t/2$ zero-crossings per second (Ref. 8) -- are identical to those of the above gaussian process, although the associated probability density functions are quite different. The poisson model

is often used to represent target evasive or "jinking" maneuvers.
The poisson square wave can only take on values of $\pm \sigma_{a_t}$, so at
any given time its probability density function (pdf) consists of
impulses with a weighting of 0.5 at plus and minus σ_{a_t}, whereas
the above markov process is assumed to have a gaussian amplitude
distribution. Therefore, the response of an amplitude dependent
nonlinear operator could be quite different when driven by each
of these two signal forms. However, if the random square wave is
passed through a narrow-band filter or integrator, its pdf would
experience broadening due to the filter's finite bandwidth. In
the case of an integrator, for example, the resulting wave shape
would be a series of linear segments of constant slope. By appli-
cation of the central limit theorem, as discussed in Ref. 8, the
distribution of the output of a linear subsystem approaches the
gaussian density function as the number of stages of filtering it
represents increases. In this case, the relative target position,
given by x and y in Fig. 3.2-2, are of particular interest in
assessing the performance of a tactical missile; these variables
are two integrations removed from a_t. Thus, although the poisson
square wave may in some situations be a more realistic target
maneuver model, we take advantage of the statistical similarity
of the gaussian process and the poisson square wave and the exis-
tance of kinematic dynamics to justify representing this random
effect by a band-limited gaussian process, which simplifies
CADET analysis.

3.4   THE AUTOPILOT-AIRFRAME MODEL

In accordance with the assumption that the missile and
target trajectories are confined to a plane, we describe the
missile airframe orientation by the variables depicted in Fig.
3.4-1. This figure establishes the sign convention of each quan-
tity; each variable is positive as shown. Note that we are

particularizing the airframe model at this point by discussing the
tail-controlled tactical missile; this is done to provide a con-
crete model for consideration, not to exclude other configura-
tions. The primary airframe variables are:

- Angle of attack, α
- Control surface deflection, δ
- Missile body angle, θ_m
- Missile velocity vector, $\underline{v}_m$
- Missile acceleration vector, $\underline{a}_m$

The velocity vector is specified by its normal and longitudinal
components, v_n and v_ℓ respectively, or by its magnitude, v_m, and
angular relation to the original line-of-sight (missile lead angle),
θ_ℓ. Similarly, the acceleration vector is defined in terms of its
normal and longitudinal components, a_n and a_ℓ respectively, or by
its magnitude, a_m, and angular relation to the velocity vector,
θ_{va}. We neglect gravity effects, tacitly assuming that the
intercept plane is horizontal or that the missile has perfect
gravity compensation.

R-16238
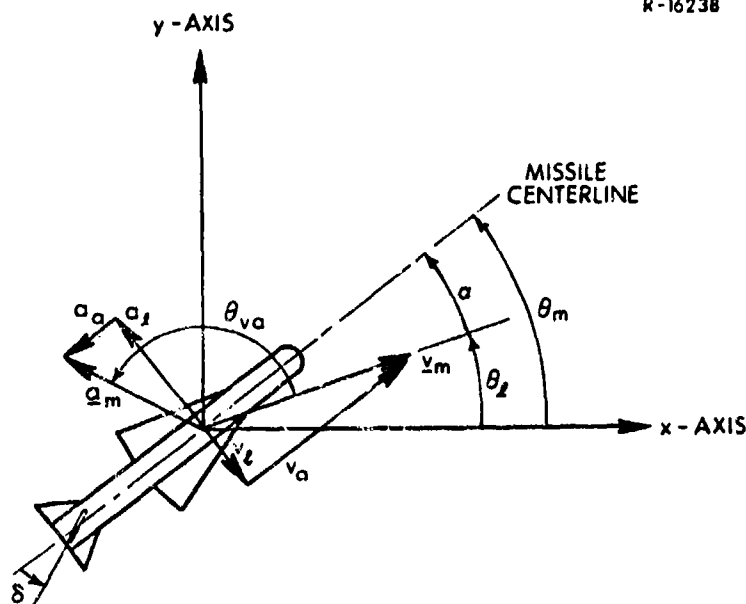
Figure 3.4-1   Geometric Definition of Intercept-
                    Plane System Variables

3.4.1 Linear Airframe Dynamics

In a general situation, the differential equations expressing the airframe dynamics are nonlinear and time-varying due to the dependence of the airframe parameters on variations in altitude, angle of attack, Mach number and other factors. However, we first consider a linearized model of the airframe dynamic equations,

$$\ddot{\theta}_m = M_q \dot{\theta}_m + M_\alpha \alpha + M_\delta \delta$$

$$\dot{\alpha} = \dot{\theta}_m - L_\alpha \alpha - L_\delta \delta \tag{3.4-1}$$

where the constants M_q, M_α, M_δ, L_α and L_δ represent the airframe stability derivatives. The latter are obtained from the nonlinear airframe parameters by making the following assumptions:

- Missile velocity is constant (drag effects are negligible over the period of time considered; a_m is normal to v_m or $\theta_{va} = 90$ deg).

- Altitude remains nearly constant.

- The center of pressure, mass and inertia of the missile are constant.

- Lift force and moments are linearly related to changes in angle of attack about some trim condition and to control fin deflection.

- Fin effectiveness is independent of angle of attack.

The output of the airframe model is the missile lateral acceleration magnitude, which is given by

$$a_m = v_m \dot{\theta}_\ell = v_m (\dot{\theta}_m - \dot{\alpha})$$

$$= v_m (L_\alpha \alpha + L_\delta \delta) \tag{3.4-2}$$

where v_m is the magnitude of the missile velocity vector. The physical basis of the linear airframe dynamic equations is treated in more detail in Section 3.4-2 (refer to Eq. (3.4-16)).

The missile treated here is steered by control fin deflection. Assuming that the actuator dynamics are linear and of first order, we have

$$\dot{\delta} = -\mu\delta + \mu u(t) \tag{3.4-3}$$

where $u(t)$ represents a commanded fin deflection and $1/\mu$ is the actuator time constant. For typical values of the stability derivatives in Eq. (3.4-1), the missile airframe will exhibit an underdamped or even an unstable response to a commanded fin deflection. Acceptable control is achieved by introducing feedback compensation in the fin deflection command,

$$u(t) = -\left[k_c a_c - k_a(a_m/v_m) - k_b\dot{\theta}_m\right] \tag{3.4-4}$$

where a_c is the commanded acceleration provided by the guidance module (see Section 3.5). The parameter k_c is chosen to give unity steady state gain from a_c to a_m, and k_b and k_a are chosen to give the desired transient response. A complete block diagram of the compensated linear missile dynamic equations is shown in Fig. 3.4-2.

For ready assessment of the compensated missile airframe dynamics in the linear case, it is convenient to use a transfer function formulation of the model. Given two outputs, a_m and $\dot{\theta}_m$, we desire to obtain $g_1(s)$ and $g_2(s)$ to provide the input-output relations indicated in Fig. 3.4-3. Utilization of standard block diagram reduction techniques shows that the dynamics indicated in Fig. 3.4-2 are equivalent to the transfer function formulation depicted in Fig. 3.4-3, where

R-11597

Figure 3.4-2   Compensated Missile Airframe Dynamics

R-11598

Figure 3.4-3   Transfer Function Definition
of the Compensated Missile
Airframe Dynamics

$$g_1(s) = \frac{e_3 s^2 + e_2 s + e_1}{s^3 + c_3 s^2 + c_2 s + c_1} \qquad (3.4\text{-}5)$$

$$g_2(s) = \frac{d_2 s + d_1}{s^3 + c_3 s^2 + c_2 s + c_1} \qquad (3.4\text{-}6)$$

The indicated transfer function coefficients are given by

$$c_1 = \mu \left[(k_a + k_b)(L_\delta M_\alpha - L_\alpha M_\delta) - M_\alpha - L_\alpha M_q \right] \qquad (3.4\text{-}7)$$

$$c_2 = \mu(L_\alpha + L_\delta M_q k_a - M_q - M_\delta k_b) - (M_\alpha + L_\alpha M_q)$$

$$c_3 = \mu(1 - L_\delta k_a) + L_\alpha - M_q$$

$$d_1 = \mu k_c (L_\delta M_\alpha - L_\alpha M_\delta)$$

$$d_2 = -\mu M_\delta k_c$$

$$e_1 = \mu v_m k_c (L_\delta M_\alpha - L_\alpha M_\delta)$$

$$e_2 = \mu v_m L_\delta M_q k_c$$

$$e_3 = -\mu v_m L_\delta k_c$$

(3.4-7)(Cont.)

The aerodynamic coefficients used in any given study are chosen to correspond to the specified intercept conditions. For example, if the engagement occurs at 35,000 ft., with a missile velocity magnitude v_m = 3000 ft/sec, airframe data taken from Ref. 10, Vol. II, Appendix H serves as a typical case. The compensating gains k_a, k_b and k_c (Eq. (3.4-4)) are set to achieve a suitable damped airframe response. These parameters and the corresponding transfer function coefficients are given in Table 3.4-1. The fact that e_1, e_2 and e_3 do not all have the same algebraic sign demonstrates that $g_1(s)$ has a right half plane zero, which is characteristic of the tail-controlled missile configuration depicted in Fig. 3.4-1.

3.4.2 Nonlinear Airframe Dynamics

In scenarios requiring significant missile maneuvers, nonlinear aerodynamic effects can have a considerable impact on homing guidance system performance. In the most general case, the differential equations of motion contain expressions that

TABLE 3.4-1

EXAMPLE OF COMPENSATED LINEAR MISSILE
AIRFRAME DATA IN THE TERMINAL HOMING PHASE

Parameter	Symbol	Value
Actuator Lag Time Constant	$1/\mu$	0.0533 sec
Aerodynamic Coefficients	M_q	-0.462 sec^{-1}
	M_α	-5.81 sec^{-2}
	M_δ	-72.0 sec^{-2}
	L_α	0.379 sec^{-1}
	L_δ	0.070 sec^{-1}
Compensating Gains	k_a	1.02 sec
	k_b	0.188 sec
	k_c	0.476×10^{-3} sec^2/ft
Transfer Function Coefficients	c_1	720.0 sec^{-3}
	c_2	275.3 sec^{-2}
	c_3	18.3 sec^{-1}
	d_1	0.240 sec^{-2} ft^{-1}
	d_2	0.642 sec^{-1} ft^{-1}
	e_1	720.0 sec^{-3}
	e_2	-0.865 sec^{-2}
	e_3	-1.87 sec^{-1}
Transfer Function Poles	s_1	-3.16 sec^{-1}
	s_2	$-7.56 + 13.0j$ sec^{-1}
	s_3	$-7.56 - 13.0j$ sec^{-1}

involve nonlinear functions of the following fundamental param-
eters:

- angle of attack
- missile velocity and Mach number
- control surface deflection
- air density
- center of pressure for missile body
- missile mass
- missile moment of inertia
- missile center of gravity location

The development of a nonlinear aerodynamic model requires a somewhat greater degree of specificity than that needed for the general discussion of the linear case given above. For this reason, we confine our attention to a missile modeling problem that is similar to that detailed in Ref. 3. The resulting nonlinear model is typical of tail-controlled cruciform missile airframe dynamics under the conditions noted below.

During the terminal intercept phase, the missile is assumed to be in a glide mode of operation, corresponding to a thrust force of zero. Consequently, missile mass, moment of inertia, and center of gravity are constant and need not be considered as variables in the airframe equations. The assumption that the intercept plane is nearly horizontal in the last few seconds of an engagement implies that the free stream air density, ρ_∞, and the speed of sound, v_s, are constants. The latter condition allows us to use missile velocity, v_m, and Mach number, v_m/v_s, interchangeably. The variables of the required nonlinear airframe equations of motion are then defined in Fig. 3.4-1.

The lateral component of missile acceleration, a_ℓ, results from the lateral aerodynamic force which is assumed to be separable into contributions $F_{\ell_{aot}}$ and $F_{\ell_{fd}}$ due to nonzero angle of attack and fin deflection, respectively. Similarly, the axial component of missile acceleration, a_a, is due to the axial force contributions $F_{a_{aot}}$ and $F_{a_{fd}}$ due to α and δ. The positive sense of a_ℓ is chosen to correspond to the sense of the lateral forces produced by positive α and δ, respectively, and the positive sense of a_a corresponds to positive drag. Letting m denote the mass of the missile during the terminal intercept phase, the acceleration components a_ℓ and a_a can be expressed in terms of these force components as

$$a_\ell = \left(F_{\ell_{aot}} + F_{\ell_{fd}}\right)\Big/m$$

$$a_a = \left(F_{a_{aot}} + F_{a_{fd}}\right)\Big/m$$

(3.4-8)

It is then a simple derivation (Ref. 3) to show that

$$\dot{\alpha} = \dot{\theta}_m + \frac{1}{mv_m}\left[\left(F_{a_{aot}} + F_{a_{fd}}\right)\sin\alpha - \left(F_{\ell_{aot}} + F_{\ell_{fd}}\right)\cos\alpha\right]$$

$$(3.4-9)$$

The differential equation for body angular rate, $\dot{\theta}_m$, is obtained from the summation of the moments acting about the body principal axis. The body lateral force $F_{\ell_{aot}}$ acting on the airframe at the body center of pressure, and the control surface lateral force $F_{\ell_{fd}}$ acting at the center of pressure for the tail are primary contributions to the moment equation. Other aerodynamic moments may also be significant; for example, rotation of the missile body produces a moment m_q that is sometimes not negligible. Letting I_b denote the missile moment of inertia about the body axis and letting d_α and d_δ denote the respective moment arms through which the forces $F_{\ell_{aot}}$ and $F_{\ell_{fd}}$ act, the expression for the missile body angular acceleration is

$$\ddot{\theta}_m = -\frac{1}{I_b}\left(F_{\ell_{aot}}d_\alpha + F_{\ell_{fd}}d_\delta + m_q\right) \qquad (3.4-10)$$

The rate of change of the magnitude of the velocity vector can be obtained from the projection of the body acceleration components onto the velocity vector. This procedure, followed by the substitution of Eq. (3.4-8), yields

$$\dot{v}_m = -\frac{1}{m_o}\left[\left(F_{a_{aot}} + F_{a_{fd}}\right)\cos\alpha + \left(F_{\ell_{aot}} + F_{\ell_{fd}}\right)\sin\alpha\right]$$

$$(3.4-11)$$

The above lateral and axial forces are in themselves a source of nonlinearity. For example, they are proportional to the dynamic pressure, q_∞, given by

$$q_\infty = \frac{1}{2} \rho_\infty v_m^2 \tag{3.4-12}$$

The dependency of the forces on α and δ is also nonlinear; how the relations are modeled would depend on the particular missile under consideration and the range of α and δ of interest. The study in Ref. 3 obtained realistic results with the following truncated double-power-series expansion formulation:

$$F_{\ell_{aot}} = k_1 v_m \left(1 + k_{11}\alpha^2\right)\left(1 + k_{12}v_m\right)\alpha$$

$$F_{\ell_{fd}} = k_2 v_m \left(1 + k_{21}\alpha^2\right)\left(1 + k_{22}v_m\right)\delta$$

$$F_{a_{aot}} = k_3 v_m \left(1 + k_{31}\alpha^2\right)\left(1 + k_{32}v_m\right) \tag{3.4-13}$$

$$F_{a_{fd}} = k_4 v_m \left(1 + k_{41}v_m + k_{42}v_m^2\right)\delta^2$$

These relations can be directly substituted into Eqs. (3.4-9) and (3.4-11). The moment equation, Eq. (3.4-10), requires further consideration because while the moment arm d_δ may be considered constant (since the variation in the fin center of pressure is small in comparison to its nominal magnitude), the moment arm d_α is generally a function of α and v_m; the combined nonlinear moment term $F_{\ell_{aot}}d_\alpha$ can be realistically modeled by (Ref. 3)

$$F_{\ell_{aot}}d_\alpha = k_5\left(1 + k_{51}v_m\right)\alpha + k_6\left(1 + k_{61}v_m\right)\alpha^3 \tag{3.4-14}$$

The body rate moment contribution to Eq. (3.4-10), m_q, is generally small with respect to the force components, so it can often be adequately represented by a linear term,

$$m_q = -I_b M_q \dot{\theta}_m \tag{3.4-15}$$

where M_q then corresponds to the stability derivative defined in the body rate term in Eq. (3.4-1).

3-16

A further simplification of the basic aerodynamic dif-
ferential equations, Eqs. (3.4-9) to (3.4-11), can be achieved
by making suitable small-angle approximations to the trigonometric
functions involved; this entails truncating the series

$$\sin \alpha = \alpha + \frac{1}{6} \alpha^3 + \ldots$$

$$\cos \alpha = 1 - \frac{1}{2} \alpha^2 + \ldots$$

at a point consistant with the range of α and the accuracy of the
nonlinear representation of the normal and longitudinal forces,
Eq. (3.4-13). The basic equations then contain only terms of the
form $\alpha^k \delta^\ell v_m^m$ for which quasi-linear gains may be derived directly
using Cases 1 to 3 of Section 4.3.2; many results of this form
are given in Appendix A.

To relate the nonlinear model to the linear case given
in Eq. (3.4-1), we observe that the linear terms of Eqs. (3.4-9)
to (3.4-14) with v_m taken to be constant are equivalent if

$$L_\alpha = \frac{1}{m} \left[k_1 (1 + k_{12} v_m) - k_3 (1 + k_{32} v_m) \right]$$

$$L_\delta = \frac{k_2}{m} (1 + k_{22} v_m)$$

$$(3.4-16)$$

$$M_\alpha = - \frac{k_5}{I_b} (1 + k_{51} v_m)$$

$$M_\delta = - \frac{k_2}{I_b} (1 + k_{22} v_m) d_\delta$$

The nonlinear model of the autopilot-airframe module is
completed by deriving a formulation of the control fin actuator

dynamics and compensation. A simple linear model for this function is given in Eqs. (3.4-3) and (3.4-4), viz.

$$\dot{\delta} = -\mu\delta + \mu u(t)$$

$$(3.4-17)$$

$$u = -\left[k_c a_c - k_a a_\ell - k_b \dot{\theta}_m \right]$$

with typical parameter values given in Table 3.4-1. If there are significant nonlinear effects to be modeled, such as actuator saturation, hysteresis, nonlinear friction or the like, then it may be necessary to develop a much more detailed representation. An example of a complete autopilot/airframe model in which control fin actuator saturation is included is depicted in Fig. 3.4-4.

3.5 THE GUIDANCE SUBSYSTEM MODEL

The operation of the guidance module may be separated into two cascaded functions: filtering of the signals obtained from the seeker in order to reduce the effect of measurement noise, and control of the missile lateral acceleration on the basis of the filtered measurements. There are a number of filtering and control schemes that can be used in tactical missile design, as reported in Refs. 9 and 10. The systems that result may be divided into analog guidance modules in which the missile acceleration command is obtained by standard analog techniques which may be modeled using continuous-time dynamic equations, and digital guidance modules in which filtering is accomplished using discrete-time data processing techniques, including sophisticated algorithms based on modern estimation theory (extended Kalman filters), and the control function may be based on optimal control theory. In this section, we treat the classical proportional guidance law as an example of the first category, and discuss several alternative digital guidance systems based on the use of a Kalman filter.

Figure 3.4-4   Typical Nonlinear Representation of the Autopilot/Airframe Module

3.5.1 Proportional Guidance

The guidance signal available from the seeker (η in Fig. 3.1-1) is typically a variable proportional to LOS angle rate, $\dot\theta$, corrupted by measurement noise. This signal is passed through a single-stage low-pass noise filter, the output of which is thus a filtered estimate of LOS angle rate, $\hat\theta \approx \dot\theta$. The proportional guidance law is then implemented, which calls for the component of missile lateral acceleration that is normal to the line-of-sight (LOS) to be proportional to the closing velocity times the estimated LOS angle rate.

This guidance law is based on the concept of the <u>missile-target collision triangle</u>. In a simplified scenario in which the target is following a straight line trajectory, with constant aspect angle θ_a^* and velocity vector magnitude v_t, the most efficient intercept path for the missile (assuming its velocity, v_m, is also constant) is a straight line specified by a constant lead angle θ_ℓ^*, chosen such that the cross-range components of the missile and target velocity vectors are equal:

$$v_m \sin \theta_\ell^* = v_t \sin \theta_a^* \qquad (3.5\text{-}1)$$

If the missile lead angle is not equal to θ_ℓ^*, then there is a nonzero heading error, θ_{HE}, given by

$$\theta_{HE} \triangleq \theta_\ell^* - \theta_\ell \qquad (3.5\text{-}2)$$

We observe that flight along the collision triangle (along the vector $\underline{v}_m^*$, Fig. 3.5-1) results in a nonrotating LOS, i.e., $\dot\theta \equiv 0$. Thus $\dot\theta$ can be considered the error signal for this guidance strategy.

For the purpose at hand, we assume that the missile acceleration vector $\underline{a}_m$ is normal to the velocity vector (θ_{va} is
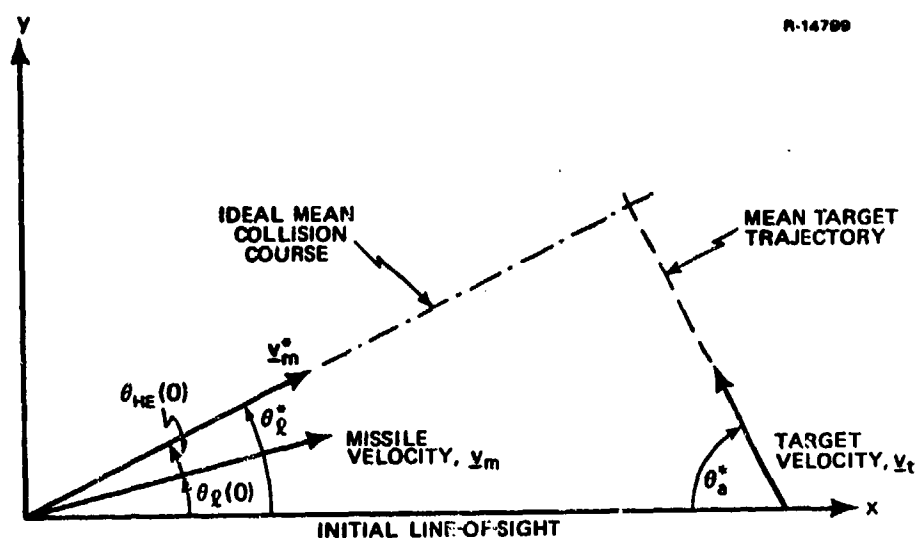
Figure 3.5-1   Deviation from the Collision Course Triangle

90 degrees in Fig. 3.2-1); thus we desire to generate an acceleration command to cause a_m to satisfy

$$a_m \cos (\theta_\ell - \theta) = n'v_c\hat{\dot{\theta}} \tag{3.5-3}$$

where the parameter n' is called the navigation ratio. The closing velocity is obtained by projecting the missile and target velocity vectors onto the instantaneous line of sight; as shown in Fig. 3.2-1,

$$v_c = v_m \cos (\theta_\ell - \theta) + v_t \cos (\theta_a + \theta) \tag{3.5-4}$$

In order to achieve a response that obeys Eq. (3.5-3), the ideal acceleration command a_c' should be chosen to satisfy

$$a_c' = \frac{n'v_c\hat{\dot{\theta}}}{\cos (\theta_\ell - \theta)} \tag{3.5-5}$$

where the incorporation of the factor $1/\cos (\theta_\ell - \theta)$ as dictated by Eq. (3.5-3) is known as secant compensation.

In mechanizing the guidance law, the value of the closing velocity is never known exactly. If a radar homing seeker is used, then a reasonable estimate of v_c can be obtained by doppler measurements or by differencing range measurements. An infrared seeker system generally does not yield a good estimate of range, in which case v_c may be taken to be a prespecified constant. Any uncertainty in the closing velocity is modeled by introducing a variable e_v into Eq. (3.5-5) which represents either a band limited noise, obtained by a single-stage low-pass filter with white noise input, or a bias, denoted simply e_{vb}. Thus, for example,

$$ a_c' = n' \, \hat{\dot{\theta}} \left[v_m + \frac{v_t \cos(\theta_a + \theta) + e_v}{\cos(\theta_\ell - \theta)} \right] \qquad (3.5\text{-}6) $$

provides the final acceleration command used in Ref. 4, where e_v is modeled by one of the differential equations

Random Uncertainty: $\dot{e}_v = -\omega_4 e_v + w_4$, $E\left[e_v(0)\right] = 0$

$$ \qquad (3.5\text{-}7) $$

Bias Uncertainty: $\dot{e}_v = 0$, $e_v(0) = e_{vb}$

and w_4 is white noise with spectral density q_4. With this model we can study either the effect of the noisy estimation of v_c or of a constant error in the assumed value of v_c.

Finally, the guidance law must account for an important nonlinear constraint on missile operation -- acceleration command limiting. The actual acceleration command a_c that determines the input to the fin deflection actuator in Figs. 3.4-2 or 3.4-4 must not exceed the structural capacity of the airframe and must not be so large as to cause the missile to stall. Thus the above idealized acceleration command a_c' must be limited in order to prevent excessive lateral acceleration command levels or angle of attack; the limiting procedure is represented by the saturation nonlinearity

$$a_c = f(a_c') \triangleq \begin{cases} a_c' & , \quad |a_c'| \leq a_{max} \\ a_{max} \text{ sign } (a_c'), & |a_c'| > a_{max} \end{cases} \quad (3.5\text{-}8)$$

The guidance law features described above are incorporated in the system model illustrated in block diagram form in Fig.3.5-2.
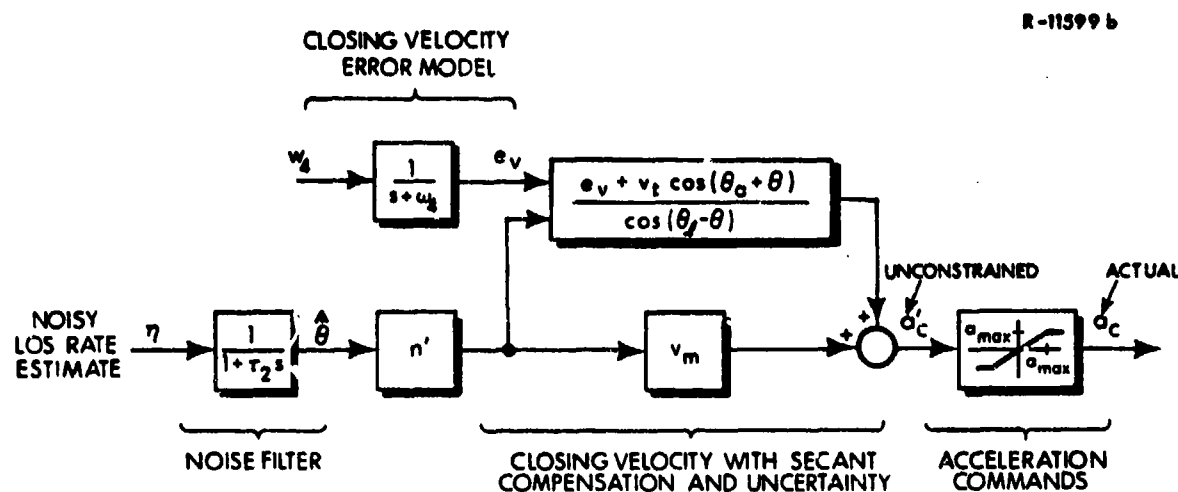
Figure 3.5-2   Proportional Guidance Law Model

3.5.2 Modern Digital Guidance Systems

Recently-proposed high-accuracy guidance systems for tactical missiles have been designed using digital data processing and optimal estimation and control theory. The resulting combination of Kalman filter and optimal control law that comprises the digital guidance module is generally based on a linear system representation ("filter model") that is significantly less detailed than the simulation model ("truth model") which strives to represent all important dynamic effects. Quantities that can be assumed to be available to the filter without measurement noise are treated as deterministic inputs to the filter and thus need not be considered in the model (Ref. 11). To obtain a filter model that is linear in

the variables of interest, all nonlinearities that occur in the truth model are replaced by constant or time-varying gains derived by small-signal or Taylor series linearization.

Kalman Filter Model — A basic 3-state Kalman filter can be designed for the missile-target intercept problem using the model depicted in Fig. 3.5-3. It is assumed that noisy measurements of LOS angle, θ, are available to the filter in conjunction with noise-free measurements of missile lateral acceleration and missile-target range. The range information is required in the filtering procedure because the LOS angle is assumed to be related to the cross-range separation, y, by the time-varying gain 1/r, and the measurement noise sequence v_k (Fig. 3.5-3) is range dependent, as detailed below; the Kalman filter algorithm makes use of knowledge of these dependencies in generating estimated values of the filter state variables, denoted $\underline{\hat{x}}_f$.

In state-space formulation, the filter model is given by the vector differential equation

$$\underline{\dot{x}}_f = F_f \underline{x}_f(t) + \underline{g}_f w_5(t) + \underline{d}_f a_m(t) \tag{3.5-9}$$

where

$$\underline{x}_f = \begin{bmatrix} y \\ \dot{y} \\ a_t \end{bmatrix}, \quad F_f = \begin{bmatrix} 0 & 1 & 0 \\ 0 & 0 & 1 \\ 0 & 0 & -\omega_t \end{bmatrix}, \underline{g}_f = \begin{bmatrix} 0 \\ 0 \\ 1 \end{bmatrix}, \quad \underline{d}_f = \begin{bmatrix} 0 \\ -1 \\ 0 \end{bmatrix} \tag{3.5-10}$$

and w_5 is the white noise process which is the input to the target acceleration model (Section 3.3). The white noise process w_5 is specified by its mean and spectral density,

$$E\left[w_5(t)\right] = 0$$

$$E\left[w_5(t)\, w_5(\tau)\right] = q_5 \delta(t-\tau) \tag{3.5-11}$$

R-16228
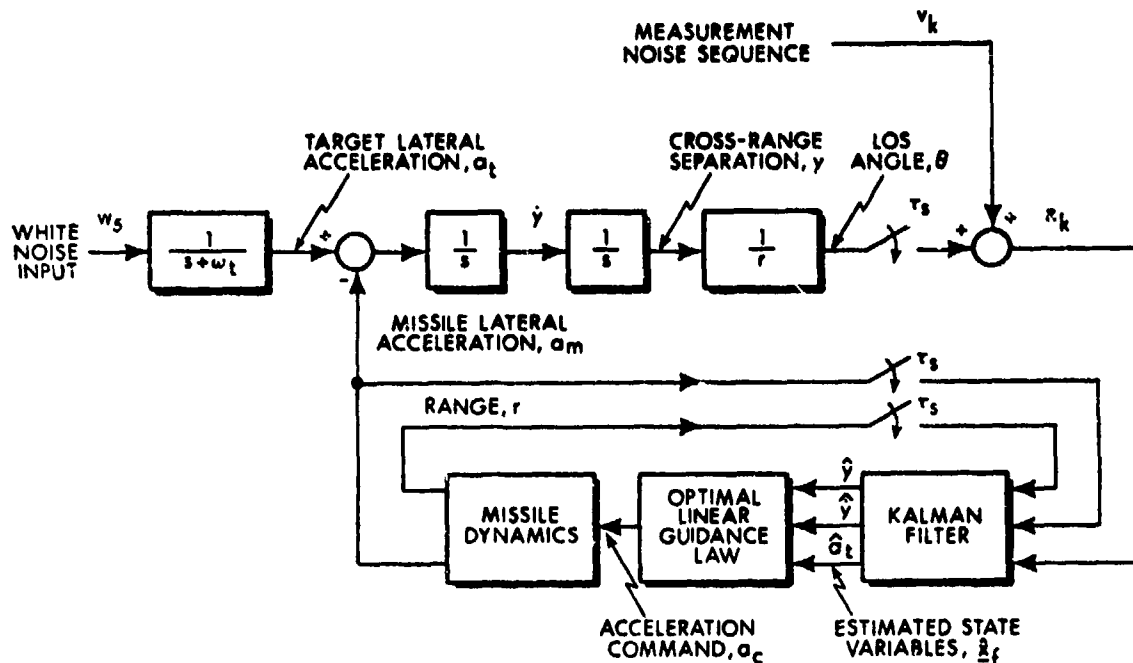
Figure 3.5-3   Missile-Target Intercept Model for the
                      Derivation of the Digital Guidance Module

The vector $\underline{x}_f$ is initially specified by the mean vector $\underline{m}_f(0)$ and covariance matrix $P_f(0)$; observe that these may or may not be directly related to the statistical initial conditions on the truth model state vector, since the filter model variables are not necessarily a subset of these states. In the kinematics subsystem model, for example, $\dot{y}$ is generally not a state variable; rather the time derivative of the state y is a nonlinear function of the states θ_ℓ (missile lead angle) and θ_a (target aspect angle) as given in Eq. (3.2-2),

$$\dot{y} = -v_m \sin \theta_\ell + v_t \sin \theta_a$$

3-25

in which case

$$m_{f_2}(0) = E\left[\dot{y}(0)\right] = -v_m E\left[\sin\theta_\ell(0)\right] + v_t E\left[\sin\theta_a(0)\right]$$

$$= -v_m e^{-\frac{1}{2}p_{\theta_\ell}}\sin m_{\theta_\ell} + v_t e^{-\frac{1}{2}p_{\theta_a}}\sin m_{\theta_a} \qquad (3.5\text{-}12)$$

where m_{θ_ℓ} and p_{θ_ℓ} are the mean and variance of θ_ℓ, respectively, m_{θ_a} and p_{θ_a} refer to the same statistics of θ_a, and use has been made of the result

$$E\left[\sin x\right] = e^{-\frac{1}{2}p_x}\sin m_x$$

(Ref. 3; see also Eq. (4.3-10)). The variance of $\dot{y}(0)$ can be calculated from the statistics of $\theta_a(0)$ and $\theta_\ell(0)$ in a similar manner. It is also possible to choose $\underline{m}_f(0)$ and $P_f(0)$ to be inconsistent with the truth model state initial statistics, to determine the performance of the filter when its initialization is in error.

The model shown in Fig. 3.5-3 can be derived directly from the results given in other sections of this chapter under the simplifying assumptions that

- Missile and target acceleration vectors (Fig. 3.2-1) are normal to the respective velocity vectors (velocity vector magnitudes are constant).

- Kinematic nonlinearities (Fig. 3.2-2) are negligible.

- The target maneuver is represented by a band-limited gaussian process (Fig. 3.3-1).

- Seeker dynamics (Section 3.6) are negligible.

We then obtain the results

$$\theta = \sin^{-1}(y/r)$$

$$\approx y/r \qquad\qquad (3.5\text{-}13)$$

from Fig. 3.2-1, and

$$\frac{d}{dt}(\dot{y}) = v_t \, \dot{\theta}_a \, \cos \theta_a - v_m \, \dot{\theta}_\ell \, \cos \theta_\ell$$

$$= a_t \, \cos \theta_a - a_m \, \cos \theta_\ell$$

$$\approx a_t - a_m \qquad\qquad (3.5\text{-}14)$$

from Eqs. (3.2-1) and (3.2-2). These relations in combination with Eq. (3.3-1) complete the derivation of the dynamic equations depicted in Fig. 3.5-3.

The measurement to be processed by the Kalman filter is the sampled LOS angle, θ_k, corrupted by additive independent samples of noise v_k. The latter have zero mean and range-dependent variance given by

$$E\left[v_k^2 \right] = \left(\frac{\sigma_1}{r(t_k)} \right)^2 + (\sigma_2 r(t_k))^2 + \sigma_3^2$$

$$\triangleq \sigma_v^2(r(t_k)) \qquad\qquad (3.5\text{-}15)$$

where σ_1, σ_2 and σ_3 represent the constant rms levels of noise components defined in Section 3.6.1. In terms of the state vector $\underline{x}_f$ in Eq. (3.5-9) and the approximation indicated in Eq. (3.5-13), the LOS angle measurement is expressed as

$$z_k = \underline{h}^T(t_k) \, \underline{x}_f(t_k) + v_k$$

$$\underline{h}^T(t_k) = \left[\frac{1}{r(t_k)} \quad 0 \quad 0 \right] \qquad\qquad (3.5\text{-}16)$$

The discrete Kalman filter provides an estimate, $\hat{\underline{x}}_f$, of the reduced-order state vector $\underline{x}_f$ utilizing mechanization equations (Ref. 11) of the form

$$\dot{\hat{\underline{x}}}_f(t) = F_f \hat{\underline{x}}_f(t) + \underline{d}_f a_m(t), \qquad t_{k-1} < t \le t_k \qquad (3.5\text{-}17)$$

$$\hat{\underline{x}}_f(t_k^+) = \hat{\underline{x}}_f(t_k) + \underline{k}_k(\underline{z}_k - \underline{h}^T(t_k)\hat{\underline{x}}_f), \quad t_k < t \le t_k + \epsilon \triangleq t_k^+ \qquad (3.5\text{-}18)$$

where $\hat{\underline{x}}_f(t_k)$ denotes the solution to Eq. (3.5-17) just before a measurement is processed, and $\hat{\underline{x}}_f(t_k^+)$ represents the state vector estimate after the measurement and update take place*. The gain vector $\underline{k}_k$ is obtained recursively from the matrix covariance equation associated with the Kalman filter; the sequence of operations is given by: (i) <u>propagation of the filter covariance matrix</u> according to

$$P_k = \Phi P_{k-1}^+ \Phi^T + Q \qquad (3.5\text{-}19)$$

where P_{k-1}^+ is the value of the filter covariance matrix after the previous update, Φ, given by

$$\Phi \triangleq \exp(F_f \tau_s) \qquad (3.5\text{-}20)$$

is the transition matrix expressed in the usual matrix exponential form, $\tau_s = t_k - t_{k-1}$ is the time interval between samples, and

$$Q \triangleq q_5 \int_0^{\tau_s} e^{F_f(\tau_s - t)} \underline{g}_f \underline{g}_f^T e^{F_f^T(\tau_s - t)} \, dt \qquad (3.5\text{-}21)$$

---

*Refer to the footnote on page 1-15.

is the noise covariance matrix; (ii) <u>calculation of the Kalman gain vector</u>,

$$\underline{k}_k = P_k \underline{h}_k \left(\underline{h}_k^T P_k \underline{h}_k + \sigma_v^2(r(t_k)) \right)^{-1}$$
(3.5-22)

(iii) <u>updating the filter covariance matrix</u> (to represent the effect of updating the state vector estimate)

$$P_k^+ = P_k - \underline{k}_k \left(\underline{h}_k^T P_k \underline{h}_k + \sigma_v^2 \right) \underline{k}_k^T$$
(3.5-23)

It is likely that the range-dependent gain vector in this example can be precomputed and stored as a function of range if range information is available in the guidance module. Otherwise, the implementation of Eqs. (3.5-22) and (3.5-23) would be responsible for most of the digital computational capability required by this guidance system.

Equations (3.5-17) to (3.5-23) are a set of typical Kalman filter mechanization equations based on a simplified design model. The filter state estimates $\hat{y}$, $\hat{\dot{y}}$ and $\hat{a}_t$ provide the basis for the missile guidance law which generates the commanded missile lateral acceleration, denoted a_c in Fig. 3.4-2. An optimal control approach to developing a guidance law is described below.

<u>Control Law Model</u> — An optimal control policy is derived by selecting the commanded acceleration time history to minimize an appropriate performance index. An index that is found useful for the missile guidance problem is the so-called quadratic index,

$$J = E \left[y^2(t_f) + \gamma \int_0^{t_f} a_c'(t)^2 \, dt \right]$$
(3.5-24)

which effectively minimizes the expected value of the square of the miss distance while imposing a penalty on the control level. The quantities $y(t_f)$ and γ are the terminal miss distance at

intercept time t_f and the weighting on control effort, respec-
tively. The value of J is constrained by the equations of motion
given in Eqs. (3.5-9) and (3.5-10) and the form of the autopilot
dynamics. The compensated missile airframe dynamics can be
modeled by the first order transfer function

$$\frac{a_m}{a_c'} = \frac{\omega_m}{s + \omega_m} \qquad (3.5-25)$$

where we note that the higher-order autopilot dynamics, Eq.(3.4-5),
and airframe saturation are neglected in Eq. (3.5-25).

The solution to the above minimization problem is called
an <u>optimal guidance law</u>. By invoking the separation principle
(Ref. 12), it is known that the control is of the form

$$a_c' = c_1 \mathring{y} + c_2 \hat{y} + c_3 \hat{a}_t + c_4 a_m \qquad (3.5-26)$$

The indicated control gains, c_i, have been determined by Willems*
(Ref. 13) to be functions of t_{go}, the time until intercept:

$$c_1 = \frac{n'}{t_{go}^2}$$

$$c_2 = \frac{n'}{t_{go}}$$

$$c_3 = n' \left[\frac{e^{-\omega_t t_{go}} + \omega_t t_{go} - 1}{\omega_t^2 t_{go}^2} \right] \qquad (3.5-27)$$

$$c_4 = -n' \left[\frac{e^{-\omega_m t_{go}} + \omega_m t_{go} - 1}{\omega_m^2 t_{go}^2} \right]$$

---

*The derivation cited above is based on the assumption of con-
tinuous control -- i.e., the sampled and held nature of the
control law is neglected.

The time-to-intercept, t_{go}, and optimal navigation ratio, n', are given by

$$t_{go} = t_f - t \triangleq \left.\frac{r}{v_c}\right|_{t=0} - t \qquad (3.5\text{-}28)$$

where v_c is the closing velocity, Eq. (3.5-4), and

$$n' = \frac{3t_{go}^2 \left[t_{go} - \left(1-e^{-\omega_m t_{go}}\right)/\omega_m\right]}{3\gamma + \frac{3}{2\omega_m^3}\left(1-e^{-2\omega_m t_{go}}\right) + \frac{3t_{go}}{\omega_m^2}\left(1-2e^{-\omega_m t_{go}}\right) + t_{go}^2\left(t_{go} - \frac{3}{\omega_m}\right)} \qquad (3.5\text{-}29)$$

The expression for n' is considerably simplified if the compensated airframe dynamics are neglected entirely; from Eq. (3.5-25), $a_m = a_c'$ if we permit ω_m to approach infinity, in which case

$$\left.n'\right|_{\omega_m \to \infty} = \frac{3}{1 + 3\gamma/t_{go}^3} \qquad (3.5\text{-}30)$$

If there is no constraint on acceleration, γ is equal to zero and the resulting navigation ratio from Eq. (3.5-30) is constant.

Finally, in implementing the control given in Eq. (3.5-26), it is often advantageous to use an alternative formulation for t_{go}:

$$t_{go} = \frac{r}{v_c} = -\frac{r}{\dot{r}} \qquad (3.5\text{-}31)$$

Using the instantaneous value of range divided by closing velocity is equivalent to Eq. (3.5-28) when range is nearly deterministic. This expression is conveniently evaluated in the digital guidance module using a discrete approximation to the derivative; at each sampling instant

$$t_{go,k} = \frac{\tau_s r_k}{r_{k-1} - r_k} \qquad (3.5\text{-}32)$$

Given the above set of optimal linear control gains, various suboptimal approximations can be made to simplify the computational requirements. If γ, $1/\omega_m$, c_3 and c_4 are taken to be zero, for example, a digital version of classical proportional guidance (based on optimal estimation theory) with $n' = 3$ is the resulting control policy. Another common simplified guidance law is obtained by including a component of target acceleration in the formulation of the autopilot command by permitting c_3 to be nonzero. A complete digital guidance module having the latter form is depicted in Fig. 3.5-4.
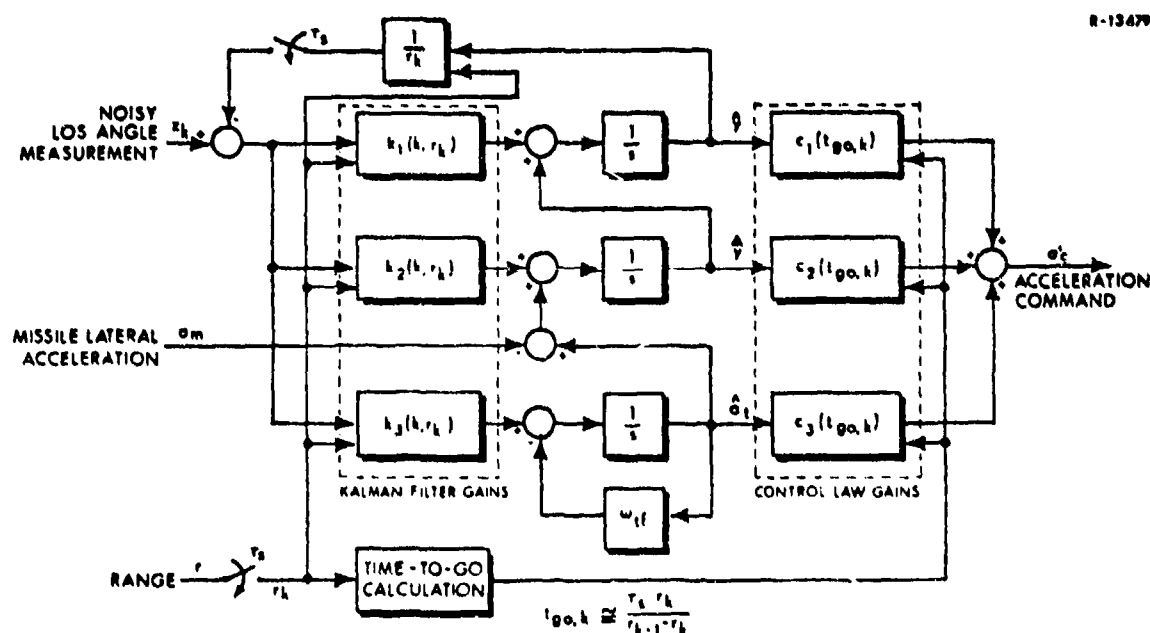
Figure 3.5-4   Digital Guidance Module Based on Optimal Estimation and Control

The digital guidance module must be correctly interfaced with the overall truth model to permit simulation of the missile-target intercept problem. At the input to the guidance subsystem, noisy measurements of LOS angle must be made available to the

Kalman filter. How this signal is obtained is generally determined by the specific seeker design and hardware considerations. A variable which is often readily available as the seeker output is η, shown in Fig. 3.6-9, which is an approximate noisy measure of line-of-sight angular rate; to be more precise, it is demonstrated in Section 3.6.3 that η is related to the LOS angle θ by dynamics that can be approximately represented in transfer function form as

$$\frac{\eta(s)}{\theta(s)} = \frac{s}{1 + \tau_d s} \qquad (3.5\text{-}33)$$

where τ_d represents the dominant time constant of the overall seeker track loop. Thus a direct method for obtaining the required filter input signal from the seeker output η is to interpose a prefilter of the form

$$h_f(s) = \tau_d + \frac{1}{s} \qquad (3.5\text{-}34)$$

to provide effective compensation for the dominant pole in the seeker dynamic model.

Another factor in implementing the guidance law is that the ideal acceleration command a_c' given in Eq. (3.5-26) is based on the assumption that missile acceleration is normal to the LOS. As in the previous section (cf. Eq. (3.5-3)), the fact that a_m is actually nearly normal to the velocity vector requires secant compensation (division by $\cos(\theta_\ell - \theta)$) to guarantee that the acceleration command leads to a suitable acceleration component normal to the LOS.

The guidance module design is completed by incorporating an ideal limiter to prevent excessive acceleration command levels. An overview of a typical digital guidance module based on the foregoing discussion is shown in Fig. 3.5-5.
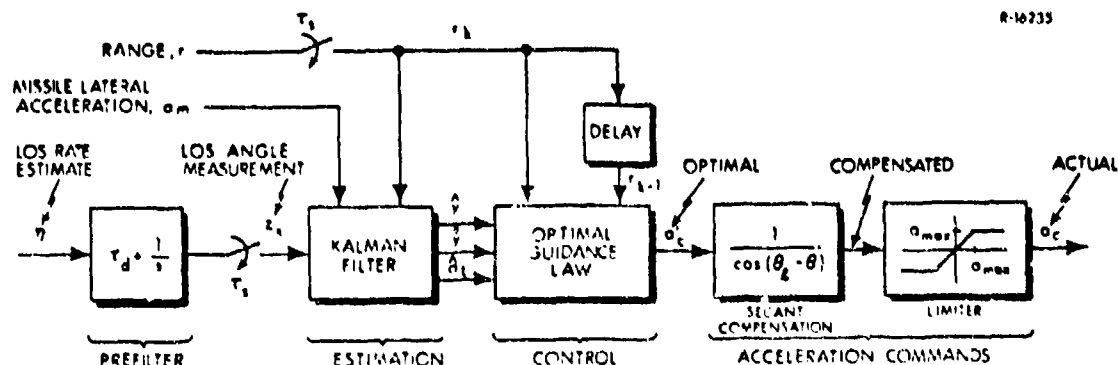
Figure 3.5-5   Complete Digital Guidance Module Structure

3.6 THE SEEKER SUBSYSTEM MODEL

There are several effects inherent to the seeker which can have a marked influence on overall missile performance. These include

- Boresight error distortion sources

       Noise
       Aberration
       Receiver and signal processing characteristics

- Disturbance torque sources

       Seeker mass imbalance
       Seeker gimbal friction
       Spring restoring forces on the seeker head

3.6.1 Boresight Error Distortion

A fundamental variable in the seeker subsystem is the true boresight error, ε_{true}, defined by the angle between the antenna centerline and the instantaneous line-of-sight (LOS) to the target; referring to Fig. 3.6-1,

$$\varepsilon_{true} = \theta - \theta_h - \theta_m = \theta - \phi \tag{3.6-1}$$
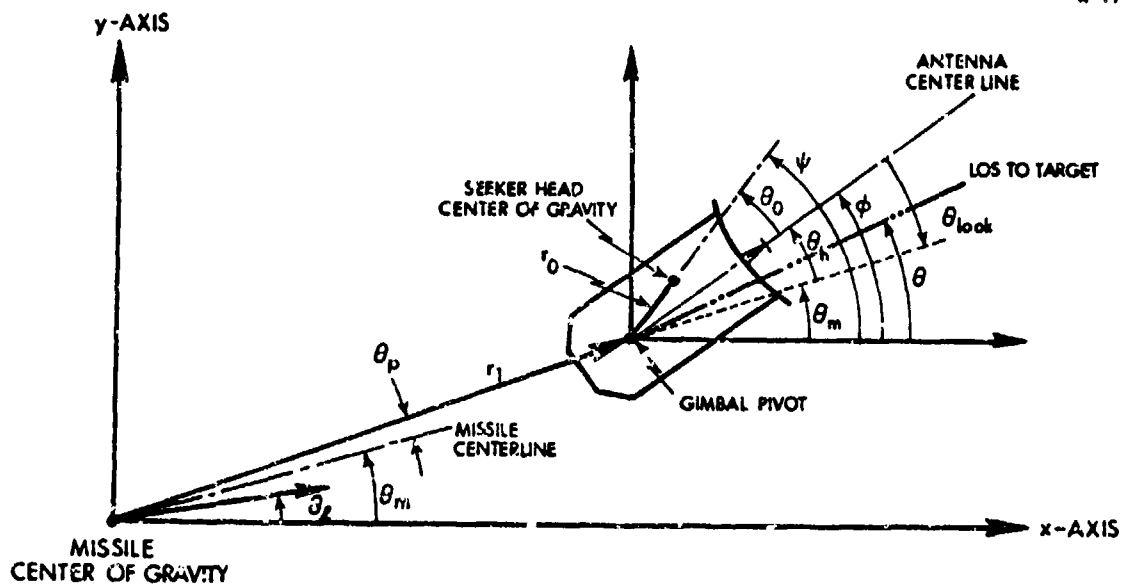
Figure 3.6-1   Seeker System Configuration

The estimated or measured value of the boresight error will differ from ε_{true} due to several factors; among the more important of these are aberration, noise, and nonlinear receiver characteristics.

The effect of <u>aberration</u> is very highly dependent upon the geometry of the seeker-detector cover, the frequency and polarization of the incident energy, and other factors; furthermore, it is variable due to manufacturing tolerances, possible erosion during flight, and changes in environmental parameters. This phenomenon can often be represented by a nonlinear and possibly time-varying operation on the look angle, $\theta_{look} = \theta - \theta_m$, so that an effective boresight error, ε_{eff}, is obtained in the form

$$\varepsilon_{eff} = \theta_{look} + \theta_{ab} - \theta_h \qquad (3.6-2)$$

where the aberration angle θ_{ab} is a nonlinear function of θ_{look}, as depicted in Fig. 3.6-2. A tactical missile with a radar tracking system that exhibits nonlinear aberration (caused by a protective radome) is treated in Ref. 3. In that study, the radome aberration characteristic was modeled as a piecewise-linear relation with odd symmetry and 5 linear segments, as depicted in Fig. 3.6-3.

R-16242
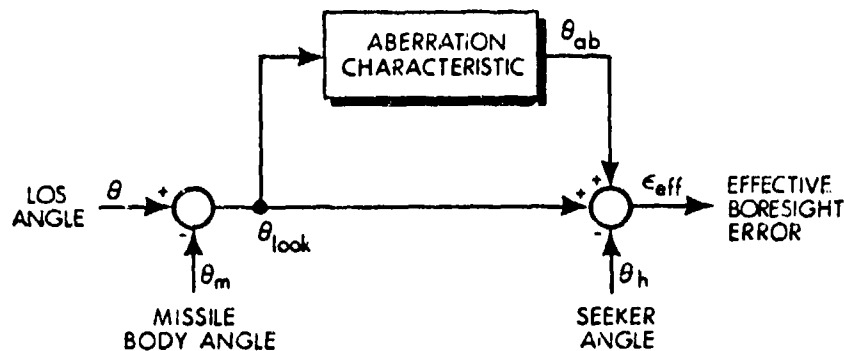
Figure 3.6-2   Boresight Aberration Model
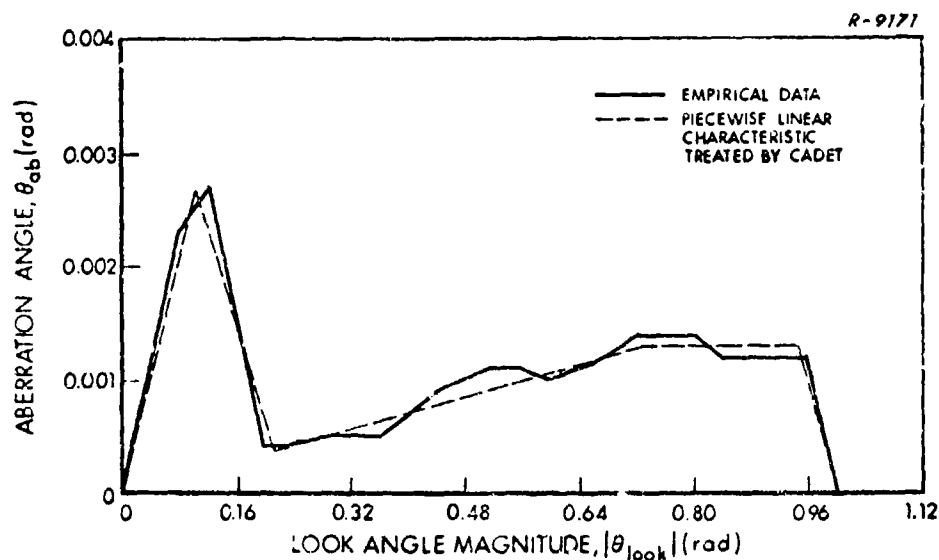
Figure 3.6-3   Nonlinear Angular Aberration Characteristic Investigated in Ref. 3

In considering the degrading effects of <u>noise</u>, we include three fundamental categories of effects. <u>Inverse range proportional noise</u>, which has an effective rms level of the form

$$\sigma_a(r) = \frac{\sigma_1}{r} \qquad\qquad (3.6-4)$$

where σ_1 is a constant, is representative of a noise source that increases in effect as range approaches zero. Target angular scintillation (caused by the apparent motion of the target due to the change in position of the target controid of radiation) is a phenomenon of this sort. This effect can be modeled as a **wide-band noise** state,* x_1, with constant rms level, σ_1, multiplied by a gain $1/r$. Range proportional noise includes any noise source that yields an effective noise level that decreases as the missile approaches the target, i.e., as range approaches zero. This type of random disturbance may be represented by an equivalent noise with an rms level of the form

$$\sigma_b(r) = \sigma_2 \qquad \qquad (3.6\text{-}5)$$

which in turn can be modeled by a wide-band noise state x_2 with a constant rms level of σ_2 passing through a gain r. Noise sources that exhibit this property are the distant stand-off jammer and receiver noise (generally due to thermal effects). Range independent noise represents noise sources that have a constant effect on the signal-to-noise ratio; target amplitude scintillation (due to time-varying effective target cross section, for example) and seeker servo noise are typical examples of noise sources that can be modeled by a noise state x_3 of constant variance σ_3^2. The complete noise model is shown in Fig. 3.6-4 where w_1, w_2, and w_3 are gaussian white noise processes.

All three types of noise described above have been treated in previous studies (Refs. 2 to 4), in two forms. The most elementary implementations of this model may be taken to be linear time-varying; i.e., $r(t)$ is assumed to be deterministic in the noise model. In a more recent treatment, Ref. 4, the nonlinear relation indicated in Fig. 3.6-4 is rigorously implemented by

---

*Where no conventional state variable nomenclature is suggested, arbitrary state numbers are assigned for convenient reference.

R-11602
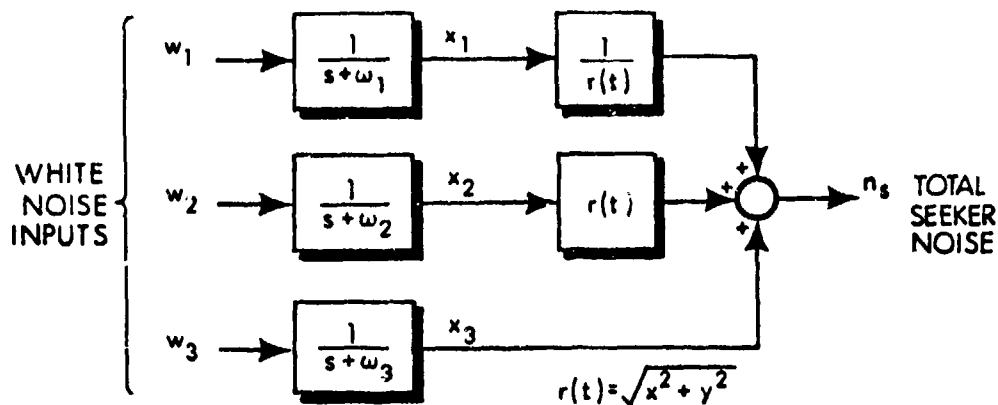
Figure 3.6-4   Seeker Noise Model

$$n_s = \frac{x_1}{\sqrt{x^2+y^2}} + x_2 \sqrt{x^2+y^2} + x_3 \qquad (3.6\text{-}6)$$

where x_1, x_2 and x_3 are the wide-band noise states mentioned above and x and y are the cartesian components of missile-target separation, respectively (see Fig. 3.2-1). The linear time-varying formulation may be adequate in situations where range has a negligible random component (as is sometimes the case for the head-on intercept where the mean missile lead angle and mean target aspect angle are both zero), but Eq. (3.6-6) is generally significantly more accurate when the range is appreciably nondeterministic.

The receiver characteristic is a potentially complicated effect, highly dependent upon the specific antenna design, type of detector, and signal processing scheme. In order to avoid a very specialized discussion based on a particular tactical missile, we confine our attention to one basic phenomenon: the attenuation of the received signal which occurs when the effective boresight error, ε_{eff}, becomes large, i.e., when ε_{eff} approaches ε_{max} in Fig.3.6-5a. The detector alone will have an output which is very nearly proportional to its input for small values; however, as the effective boresight error magnitude approaches ε_{max}, we note in Fig. 3.6-5b

R-11603
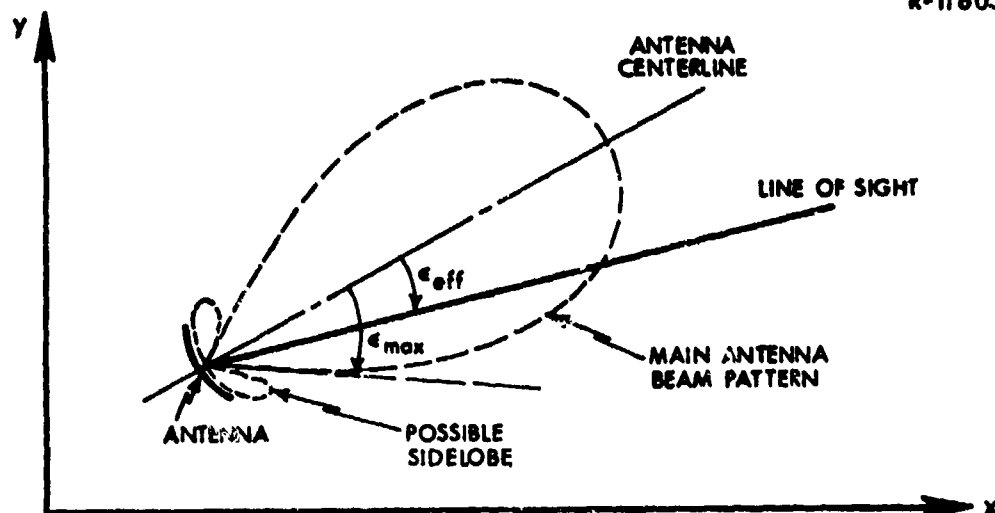
(a) Antenna Beam Pattern
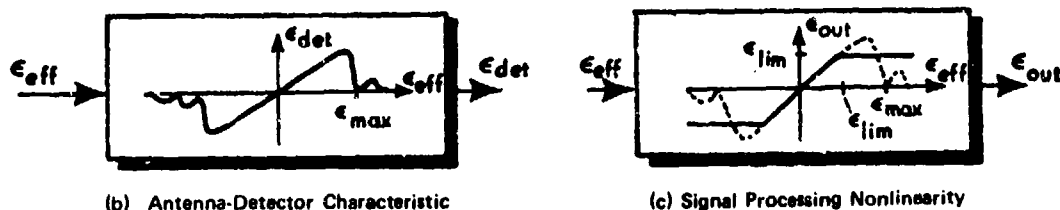
(b) Antenna-Detector Characteristic

(c) Signal Processing Nonlinearity

Figure 3.6-5   Receiver Boresight Error Distortion Effects

that the signal strength decreases to a null. If the antenna pattern
has appreciable sidelobe sensitivity, there may also be some response
for values of ε_{eff} greater than ε_{max}. The upper limit on the bore-
sight error, $\bar{\varepsilon}$, such that the detector characteristic is nearly
linear for $|\varepsilon_{eff}|$ less than $\bar{\varepsilon}$, is quite variable, depending on the
type of target tracking system under consideration. For monopulse
radar or infrared detectors, $\bar{\varepsilon}$ could be as small as a fraction of a
degree (Ref. 14).

The undesirable detector null and possible spurious side-
lobe response can be circumvented in the signal processing scheme.

As an example, some value $\varepsilon_{lim} \leq \bar{\varepsilon}$ may be chosen; a nonlinearity is then introduced such that whenever the effective boresight error magnitude exceeds ε_{lim}, the output of the signal processor is held at $\pm \varepsilon_{lim}$. This provides a simple model, depicted in Fig. 3.6-5c, which will capture the effect of a narrow antenna beamwidth and a reasonable signal processing nonlinearity.

The combined effects of aberration, noise, and receiver/ signal processing characteristic are illustrated in the general boresight error model shown in Fig. 3.6-6. We mention in passing that a more exact noise model might divide noise sources into external, predetection and postdetection effects, i.e., noise sources entering the boresight error model before aberration takes place, and before, as well as after, the receiver characteristic. For the present discussion, this categorization is excessively detailed.

R-16237
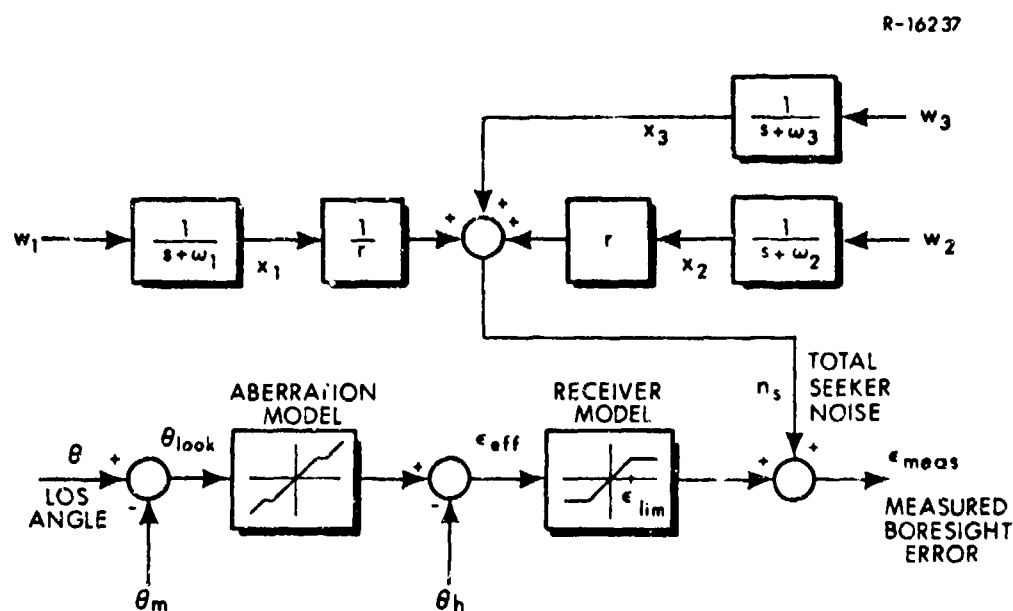
Figure 3.6-6   Final Boresight Error Measurement Model

3.6.2 Disturbance and Control Torques

The seeker model is completed by developing a suitable tracking and stabilization control system including several important

sources of disturbance torque inputs. In terms of the inertially-referenced angles ϕ and ψ shown in Fig. 3.6-1, we can derive a relation of the form

$$I_p\ddot{\phi} = I_p\ddot{\psi} = T_c - T_d \qquad (3.6-7)$$

where I_p is the moment of inertia of the seeker head about the gimbal pivot, T_c is the external control torque (derived from an electric servo motor, for example), and T_d is the total disturbance torque.* For the present discussion, consider three components,

$$T_d = T_m + T_f + T_r \qquad (3.6-8)$$

where T_m is an effective torque due to <u>seeker head mass imbalance</u>, and we include two external torque components, T_f due to <u>nonlinear friction in the gimbal</u> and T_r due to <u>nonlinear restoring torques</u>. Since the seeker head center of gravity is generally displaced from the pivot point, as shown in Fig. 3.6-1 and specified by the parameters r_0 and θ_0, the moment of inertia I_p is related to the corresponding moment of inertia referred to the center of gravity by

$$I_p = I_0 + mr_0^2 \qquad (3.6-9)$$

where m is the mass of the seeker head.

The external torques due to spring and friction effects are modeled by the relations

Restoring Torque: $\quad T_r = f_1(\theta_h)$

$$\qquad (3.6-10)$$

Friction Torque: $\quad T_f = f_2(\dot{\theta}_h)$

where θ_h is the angle between the seeker and missile center lines. Often restoring torques are linear for small angle deflections,

*The use of hydraulic actuators for mechanizing the seeker tracking function generally leads to a quite different model of the seeker dynamics; we do not consider this case here.

becoming nonlinear only as θ_h increases in magnitude, as illustrated in Fig. 3.6-7a. This behavior corresponds to the symmetric "hard spring" case (Ref. 15) where the elastic limit of a spring is exceeded and Hooke's law for linear spring behavior becomes invalid; often the nonlinear term is taken to be a power law relation,

$$f_1(\theta_h) = k_1 \theta_h + k_\kappa \left| \frac{\theta_h}{\theta_{lim}} \right|^\kappa \text{sign} (\theta_h) \qquad (3.6\text{-}11)$$

where κ is an integer greater than one, so that T_r exhibits a distinct departure from linearity as $|\theta_h|$ exceeds θ_{lim}, as is typical of a symmetric nonlinear spring characteristic. A common type of nonlinear friction is the dry or Coulomb effect depicted in Fig. 3.6-7b (Ref. 15), where

$$f_2(\dot{\theta}_h) = k_2 \text{ sign} (\dot{\theta}_h) \qquad (3.6\text{-}12)$$

i.e., the friction term of the disturbance torque has constant magnitude with the algebraic sign of the gimbal angle rate.

R-11604

(a) Nonlinear Restoring Torque, $f_1(\theta_h)$

(b) Nonlinear Friction Effect, $f_2(\dot{\theta}_h)$
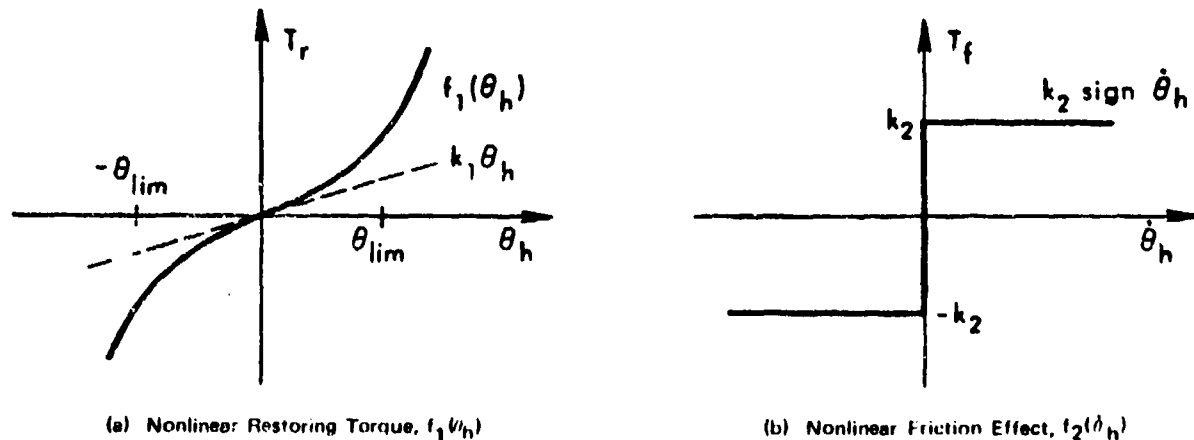
Figure 3.6-7   External Disturbance Torque Models

The effective disturbance torque component due to seeker mass imbalance can readily be determined by application of the basic

principles of mechanics (Ref. 16); the details are given in Ref. 1. Combining the seeker mass imbalance term with the friction and spring disturbance torque components, we obtain the complete disturbance torque contribution,

$$T_d = f_1(\theta_h) + f_2(\dot{\theta}_h) + mr_G \left[r_1 \ddot{\theta}_m \cos (\psi - \theta_m) \right.$$
$$\left. + r_1 (\dot{\theta}_m)^2 \sin (\psi - \theta_m) + v_m \dot{\theta}_\ell \cos (\psi - \theta_\ell) \right]$$

(3.6-13)

The control torque T_c in Eq. (3.6-7) is chosen to make the seeker track the target, i.e., to maintain the measured boresight error at a small value. The nominal seeker is designed under the assumption that there is no friction and that spring effects are negligible; thus, it is necessary to include rate feedback in the torque command (a feedback term proportional to ϕ which is measured by a rate gyro) to provide suitable damping. Thus we write the nominal control torque as

$$T_{cn} = k_s \left[\frac{\epsilon}{\tau_1} - k_g (\dot{\theta}_m + \dot{\theta}_h) \right]$$

(3.6-14)

where τ_1 is the track loop time constant, k_g is the rate gyro gain, and k_s is the torque servo gain. The implementation of this control is depicted in Fig. 3.6-8.

While the implementation of the seeker control function depicted in Fig. 3.6-8 will provide an adequate response under ideal conditions, it can be shown (cf. Section 3.6.3) that the dynamic response of the seeker is quite sensitive to steady-state disturbance torque inputs. Since, as we have already indicated, disturbance torques generally have a significant impact on the effectiveness of the seeker, compensation must be included to achieve satisfactory performance. A simple and effective compensation

3-43

R-16230

MISSILE BODY
ANGULAR ACCELERATION
$\ddot{\theta}_m$
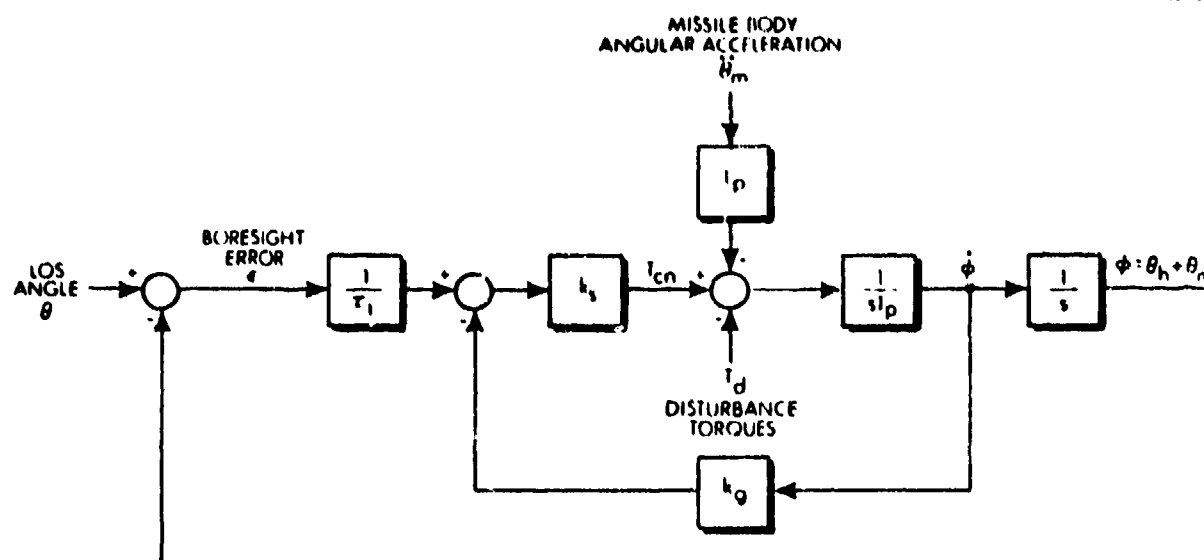
Figure 3.6-8   Nominal Seeker Track Loop (Neglect-
ing All Nonlinear Effects)

procedure is to insert proportional plus integral cascade compen-
sation before the torque summing junction in Fig. 3.6-8. That is,
we specify the compensated control torque by

$$T_{cc} = \left(1 + \frac{k_0}{s}\right) T_{cn} \tag{3.6-15}$$

The complete seeker simulation model, representing the
synthesis of the dynamic equations derived in this section, is
shown in Fig. 3.6-9.

3.6.3 Transfer Function Representation of the Equivalent Linear Seeker

For a subsystem of the complexity of the seeker as modeled
in Fig. 3.6-9, it is often helpful to derive the transfer function
formulation of the linear system obtained by neglecting all non-
linearities. Several assertions made in the previous section in
simplifying the seeker model are based on this representation, and
the procedure used for the purpose of designing the compensation
network (choice of k_0) can best be treated in this way. More de-
tails may be found in Ref. 4.
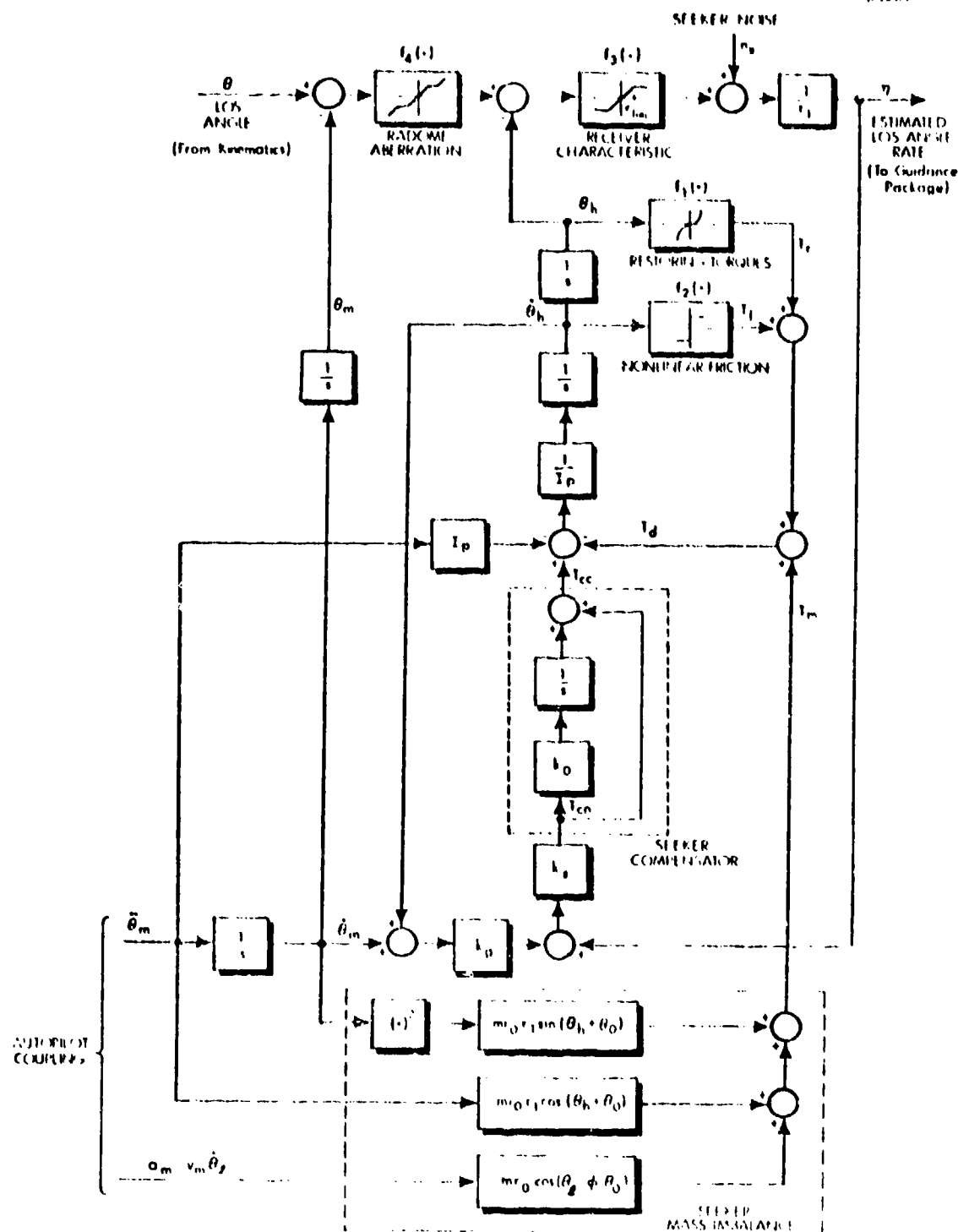
Figure 3.6-9   Complete Seeker Model

We define four inputs (refer to Fig. 3.6-10),

$$u_1 = 0$$

$$u_2 = \ddot{\theta}_m$$

$$u_3 = n_s(t) \tag{3.6-17}$$

$$u_4 = T_m$$

The transfer functions $d_1(s)$ to $d_4(s)$ for the equivalent block diagram representation depicted in Fig. 3.6-11 can be shown to be

$$d_1(s) = \frac{k_3}{\tau_1} \frac{s\left[s^2 + q_3 s + p_1\right]}{s^3 + q_3 s^2 + q_2 s + q_1}$$

$$d_2(s) = \frac{-k_3}{I_p \tau_1} \frac{k_2 s + k_1}{s\left[s^3 + q_3 s^2 + q_2 s + q_1\right]} \tag{3.6-18}$$

$$d_3(s) = \frac{1}{k_3} \; d_1(s)$$

$$d_4(s) = \frac{k_3}{I_p \tau_1} \frac{s}{s^3 + q_3 s^2 + q_2 s + q_1}$$

where the numerator and denominator coefficients are given by

$$p_1 = \frac{k_1 + k_s k_g k_0}{I_p} \qquad\qquad q_2 = p_1 + \frac{k_s}{I_p} \frac{k_3}{\tau_1}$$

$$\tag{3.6-19}$$

$$q_1 = \frac{k_s k_0 k_3}{I_p \tau_1} \qquad\qquad q_3 = \frac{k_2 + k_s k_g}{I_p}$$

The nominal seeker is defined by a choice of parameters that leads to acceptable dynamic behavior in the absence of

R-11609
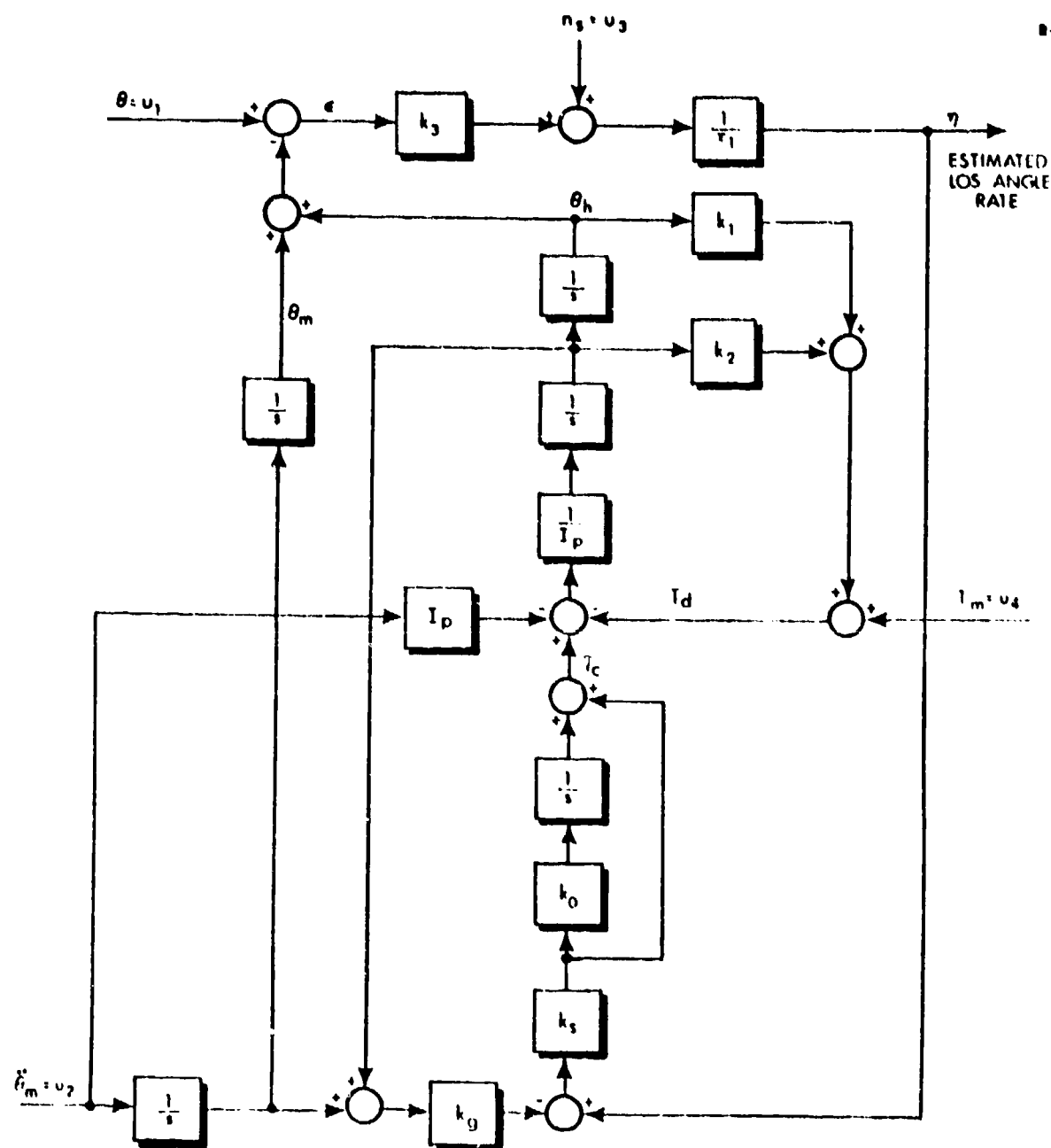
Figure 3.6-10   Linear Seeker Model

R-11610
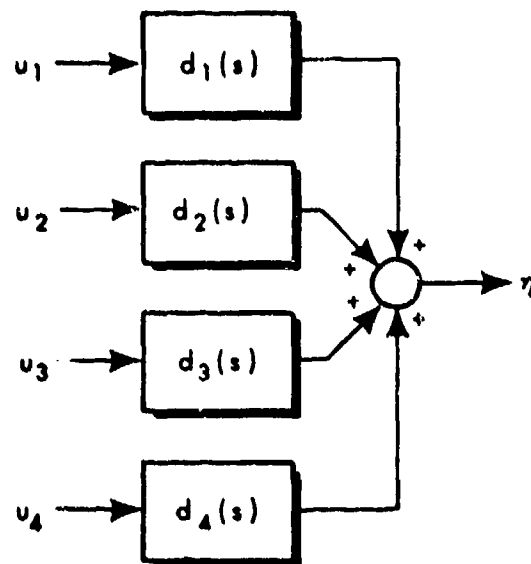
Figure 3.6-11   Linear Seeker Model in
                   Transfer Function Form

disturbance torques; example data and transfer functions are given in Table 3.6-1. A second case is the nominal compensated seeker, which has been designed to exhibit a significantly better performance in the presence of disturbance torques; the design by root locus techniques is indicated in Ref. 4 and the transfer functions are summarized in Table 3.6-2.

In both the nominal and the nominal compensated seeker, we note that $d_2(s) = 0$. This demonstrates that with no linear friction or spring restoring torques, the seeker has perfect stabilization, i.e., the measured boresight error is unaffected by rotation of the missile body.

For frequencies considerably less than 10 rad/sec, we have $d_{n1} = d_{c1} = s$, which is the transfer function of a differentiator. Hence, the assertion that η is an estimate of the LOS angular rate ($\dot{\sigma}$) holds at low frequencies.

The seeker compensation removes steady state disturbance torque sensitivity, due to the zero of $d_{c1}(s)$ at $s = 0$, as discussed in Ref. 4.

TABLE 3.6-1

TYPICAL NOMINAL SEEKER SPECIFICATIONS

Parameters	Transfer Functions
$k_0 = k_1 = k_2 = 0$	
$k_3 = 1$	$d_{n1}(s) = \dfrac{100}{12} \dfrac{s(s+60)}{(s+10)(s+50)}$
$k_g = 1$	$d_{n2}(s) \equiv 0$
$k_s = 6 \dfrac{\text{in-oz-sec}}{\text{rad}}$	$d_{n3}(s) = d_{n1}(s)$
$I_p = 0.1$ in-oz-sec^2	$d_{n4}(s) = \dfrac{1000}{12} \dfrac{1}{(s+10)(s+50)}$
$\tau_1 = 0.12$ sec	

TABLE 3.6-2

TYPICAL NOMINAL COMPENSATED SEEKER SPECIFICATIONS

Parameters	Transfer Functions
$k_1 = k_2 = 0$	$d_{c1}(s) = \dfrac{100s(s^2+60s+1200)}{12(s^3+60s^2+1700s+10,000)}$
$k_3 = k_g = 1$	
$k_0 = 20$ sec^{-1}	$d_{c2}(s) \equiv 0$
$k_s = 6 \dfrac{\text{in-oz-sec}}{\text{rad}}$	$d_{c3}(s) = d_{c1}(s)$
$I_p = 0.1$ in-oz-sec^2	
$\tau_1 = 0.12$ sec	$d_{c4}(s) = \dfrac{1000s}{12(s^3+60s^2+1700s+10,000)}$
Poles at $s = -7.71$, $s = -16.1 \pm 24.8j$	

3.7   SYSTEM MODEL SUMMARY

An example of a complete missile-target intercept model is portrayed in Fig. 3.7-1 with representations of all of the subsystems described in the previous sections appropriately interconnected. This particular system model was extensively analysed in an investigation of the accuracy and efficacy of CADET in evaluating the impact of various random and nonlinear effects on the performance of missile guidance systems in Ref. 4. As indicated in previous sections, there are many assumptions behind this formulation; the system depicted in Fig. 3.7-1 is intended to be demonstrative of the large class of problems that may be considered in this realm, and not to be all inclusive.

All of the state variables are depicted except angle of attack, α, control fin deflection, δ, and the seeker state required to implement proportional plus integral compensation, Eq. (3.6-31); these states are encompassed in the linear dynamics represented by the transfer functions $g_1(s)$, $g_2(s)$ (Fig. 3.4-3), and $(1+k_0/s)$. For convenient reference, we list the nonlinearities incorporated in this particular system model and indicate their form:

- Seeker head restoring torque

$$f_1(\theta_h) = k_1 \left| \frac{\theta_h}{\theta_{lim}} \right|^\kappa \quad \text{sign} \ (\theta_h)$$

- Seeker gimbal friction

$$f_2(\dot{\theta}_h) = k_2 \ \text{sign} \ (\dot{\theta}_h)$$

- Receiver/signal processing characteristic

$$f_3(\epsilon) = \begin{cases} \epsilon & , \ |\epsilon| \leq \epsilon_{lim} \\ \epsilon_{lim} \text{sign}(\epsilon) & , \ |\epsilon| > \epsilon_{lim} \end{cases}$$
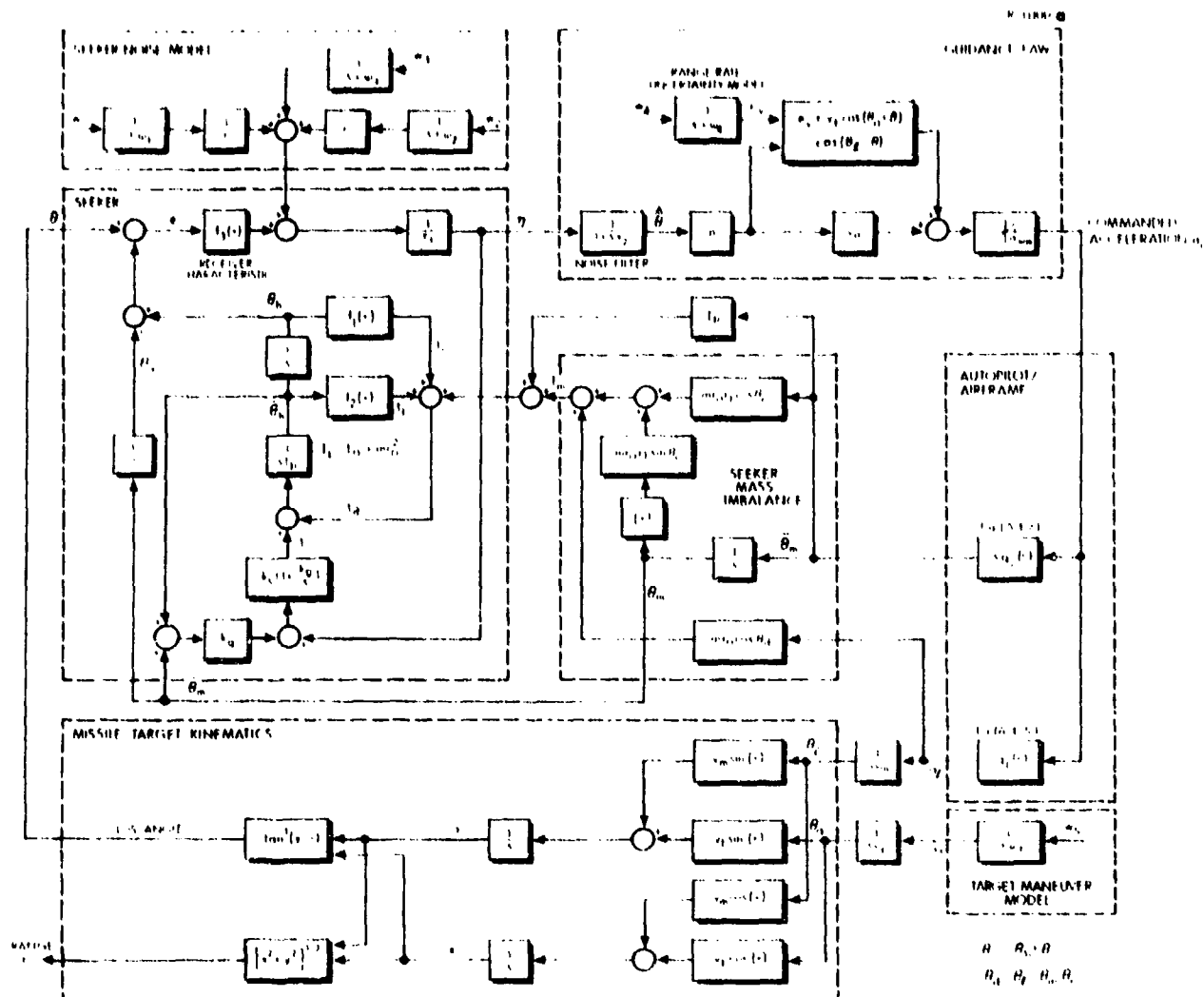
Figure 3.7-1   A Complete Missile-Target Intercept Model

- Range dependent noises

$$n_s = \frac{x_1}{\sqrt{x^2+y^2}} + x_2 \sqrt{x^2+y^2} + x_3$$

- Seeker mass imbalance torque

$$T_m = mr_0 \left[r_1 \ddot{\theta}_m \cos(\theta_h+\theta_0) + r_1 (\dot{\theta}_m)^2 \sin(\theta_h+\theta_0) \right.$$

$$\left. + v_m \dot{\theta}_\ell \cos(\theta_\ell-\theta_m-\theta_h-\theta_0) \right]$$

3-51

- LOS angle calculation

$$\theta = \tan^{-1}(y/x)$$

- Range calculation

$$r = \sqrt{x^2 + y^2}$$

- Velocity resolution

$$\dot{x} = -v_m \cos(\theta_\ell) - v_t \cos(\theta_a)$$

$$\dot{y} = -v_m \sin(\theta_\ell) + v_t \sin(\theta_a)$$

- Acceleration command limiting

$$a_c = \begin{cases} a_c' \, , & |a_c'| \leq a_{max} \\ a_{max}\,\text{sign}(a_c'), & |a_c'| > a_{max} \end{cases}$$

- Proportional guidance law with secant compensation and closing velocity error model

$$a_c' = n'\hat{\dot{\theta}} \left[v_m + \frac{v_t \cos(\theta_a + \theta) + e_v}{\cos(\theta_\ell - \theta)} \right]$$

This chapter presents an overview of modeling tasks that arise in considering the missile-target intercept problem. Realistic representations for a variety of nonlinear effects have been given, both to provide a ready reference for future studies of tactical missile performance and to facilitate model development in other areas. The material is intended to guide the user in developing mathematical models appropriate for analyzing missile systems using CADET.

4. QUASI-LINEARIZATION: PRINCIPLES AND PROCEDURES

4.1 CADET AND STATISTICAL LINEARIZATION

To review the fundamental equations of CADET derived in Section 1.2, Eqs. (1.2-6) and (1.2-7), the differential equations

$$\dot{\underline{m}} = \hat{\underline{f}} + G\underline{b}$$

$$\dot{P} = NP + PN^T + GQG^T \tag{4.1-1}$$

govern the approximate evolution of the mean vector and covariance matrix of the state variables,

$$\underline{m} = E\left[\underline{x}\right]$$

$$P = E\left[(\underline{x}-\underline{m})(\underline{x}-\underline{m})^T\right] \tag{4.1-2}$$

where the state vector differential equation is nonlinear and time-varying,

$$\underline{\dot{x}} = \underline{f}(\underline{x},t) + G(t)\underline{w} \tag{4.1-3}$$

Equation (4.1-1) involves the vector $\hat{\underline{f}}$ and matrix N which are defined by

$$\hat{\underline{f}} = E\left[\underline{f}(\underline{x},t)\right]$$

$$N = E\left[\underline{f}(\underline{x},t)(\underline{x}-\underline{m})^T\right]P^{-1} \tag{4.1-4}$$

Analytic expressions for $\hat{\underline{f}}$ and N in Eq.(4.1-4) can be determined only if the form of the joint probability density function

of the state variables is known or assumed. For many problems
(the present one included; cf. Section 1.2) it is appropriate to
assume that the states are jointly normal, or nearly so. A power-
ful corollary to the gaussian assumption is that each scalar non-
linear relation embedded in the state variable differential equa-
tions may be treated in isolation; this fact greatly facilitates
the evaluation of $\hat{f}$ and N in the application of CADET. Another
direct result of the normality assumption is that f and N are func-
tions of $\underline{m}$, P and t alone and are not dependent upon higher-order
moments.

It was mentioned in Section 1.2 that f and N defined in
Eq. (4.1-4) have also been derived in the context of applying sta-
tistical linearization to arrive at a quasi-linear approximation
to the vector nonlinearity $\underline{f}(\underline{x},t)$. The form obtained is

$$\underline{f}(\underline{x},t) \cong \hat{\underline{f}} + N\underline{r} \tag{4.1-5}$$

where

$$\underline{r} = \underline{x} - \underline{m} \tag{4.1-6}$$

is the random component of the state vector $\underline{x}$. Since the theory
of random input describing functions under the gaussian assump-
tion is well developed (Ref. 6) and of direct utility in CADET
analysis, it behooves us to consider quasi-linearization in some
detail.

In Section 4.2 we outline the overall context of describ-
ing function theory, the derivation of basic results, and basic
limitations of the technique. Sections 4.3 and 4.4 treat some
specific examples of ridf calculation, giving a few general results
and some useful approximation techniques (including discussions of
suitability and accuracy). In Section 4.5 we consider the sensi-
tivity of ridf calculation to departures from the gaussian assump-
tion. The above sections treat a single nonlinearity, in accordance

with the assertion that each nonlinear relation can be treated independently, as mentioned in Section 1.2. For a proof of the validity of this procedure, see Refs. 7 and 11.

4.2 PRINCIPLES OF QUASI-LINEARIZATION

In the discussion that follows, we consider the quasi-linearization of the single nonlinearity, $f(\underline{x})$. In some instances, the nonlinearity may be a single function of one or two states, as in the example treated in Chapter 2 where $f(x_3)$ represents the ideal limiter characteristic acting on the missile lateral acceleration, x_3 (Fig. 2.2-1). In other cases, the nonlinearity may be a complicated function of a number of states; as an example, combining Eq. (3.4-2) and the last term of Eq. (3.6-13) with $\dot{\theta}_0 = 0$ leads to a seeker mass imbalance torque term of the form

$$mr_0v_m\dot{\theta}_\ell \cos(\psi-\theta_\ell) = mr_0v_m(L_\alpha\alpha+L_\delta\delta) \cos(\theta_h+\theta_m-\theta_\ell)$$

which involves the variables $\alpha, \delta, \theta_h, \theta_m, \theta_\ell$ which may, for example, be state variables x_1 to x_5, respectively. The complexity of this formulation tends to obscure the basic form of the nonlinearity, i.e., $v_1 \cos v_2$, where v_1 and v_2 are simply linear combinations of the indicated state variables,

$$\underline{v} \triangleq \begin{bmatrix} v_1 \\ v_2 \end{bmatrix} = \begin{bmatrix} mr_0v_mL_\alpha & mr_0v_mL_\delta & 0 & 0 & 0 \\ 0 & 0 & 1 & 1 & -1 \end{bmatrix} \underline{x}$$

$$\triangleq H\underline{x} \tag{4.2-1}$$

Since the input variable statistics are immediately obtainable from the state statistics, Eq. (4.1-2),

$$\begin{aligned} \underline{m}_v &= H\underline{m} \\ P_v &= HPH^T \end{aligned} \tag{4.2-2}$$

we simply treat nonlinearities as functions of one or several _input variables_, v or $\underline{v}$, where the statistics of $\underline{v}$ are given by Eq. (4.2-2). From this point on, we omit the subscript "v" to simplify our notation; $\underline{m}$ and P always refer to the nonlinearity input statistics, and $\underline{r}$ denotes the random component of $\underline{v}$. The fact that only a few input variables need to be considered simplifies the subsequent development.

The essence underlying all quasi-linear analysis is the substitution of one or more approximate, input-amplitude-sensitive linear gain(s) for each system nonlinearity. The analytic form of the resulting quasi-linear gains (describing functions) is determined by three factors:

- The _nonlinearity_

- The assumed nonlinearity input _form_

- The _error criterion_ used (the measure
  of approximation error to be minimized)

The number of describing functions required to represent each nonlinearity is determined by the number of _input variables_ and the number of _input signal components_ specified by the assumed input form; each input variable component has its own independent measure of amplitude and requires a quasi-linear gain.

Given a nonlinearity and an assumed input variable form, hereafter taken to be the sum of a gaussian random variable and a deterministic signal ("mean"), we desire to express the nonlinearity output as a linear combination of each input signal component plus an error or distortion term. Considering the general case of a nonlinearity with k inputs, we have

$$z = f(v_1, v_2, \ldots, v_k, t) \tag{4.2-3}$$

4-4

for which we seek an approximation of the form

$$z = z_0 + \underline{b}^T \underline{r} \qquad\qquad (4.2-4)$$

where z_0 and $\underline{b}$ (a vector of dimension k) are to be determined.*

Based on the desired form of the quasi-linear approximation, Eq. (4.2-4), we consider the mean square error,

$$\hat{\epsilon}^2 = E\left[\left\{z - z_0 - \sum_{j=1}^{k} b_j r_j\right\}^2\right] \qquad\qquad (4.2-5)$$

Setting the partial derivatives of the mean square approximation error with respect to z_0 and b_j equal to zero gives us the set of necessary conditions for minimization,

$$\frac{\partial \hat{\epsilon}^2}{\partial z_0} = 2E\left[\left\{f - z_0 - \sum_{j=1}^{k} b_j r_j\right\}(-1)\right] = 0$$

$$\frac{\partial \hat{\epsilon}^2}{\partial b_j} = 2E\left[\left\{f - z_0 - \sum_{j=1}^{k} b_j r_j\right\}(-r_j)\right] = 0, \qquad j = 1, 2, \ldots, k$$

$$(4.2-6)$$

Taking the indicated expected values term-by-term reduces Eq. (4.2-6) to

$$z_0 = E[f]$$

$$\underline{b}^T P = E\left[f\,\underline{r}^T\right] \qquad\qquad (4.2-7)$$

---

*The first term in Eq. (4.2-4) could be expressed as $\underline{a}^T \underline{m}$, i.e., a linear combination of the means; however, we note that the elements of $\underline{a}$ can only rarely be found explicitly, as can be appreciated in the example of Eq. (4.3-34).

where we have expressed the results in their more compact vector-matrix form.

Comparing Eqs. (4.2-2) and (4.2-7), we have

$$f(\underline{v},t) = E\left[f\right] + E\left[f\ \underline{r}^T\right]P^{-1}\underline{r}$$

$$\triangleq \hat{f} + \underline{n}^T\ \underline{r} \tag{4.2-8}$$

which is identical to the scalar case of Eqs. (4.1-4) and (4.1-5).

To see that the above solutions do indeed lead to minimum mean square error, we observe that

$$\frac{\partial^2\hat{\epsilon}^2}{\partial z_o^2} = 2 > 0$$

$$\frac{\partial^2\hat{\epsilon}^2}{\partial b_j^2} = 2\ F\left[r_j^2\right] > 0, \qquad j = 1,2,\ldots,k$$

which are sufficient conditions for the existence of a local minimum.

In evaluating the expected values needed in Eq. (4.2-8) we invoke the assumption of joint normality to write (Ref. 11)

$$p(\underline{v}) = \left[(2\pi)^k|P|\right]^{-\frac{1}{2}}\exp\left\{-\frac{1}{2}\ \underline{r}^T\ P^{-1}\underline{r}\right\} \tag{4.2-9}$$

By definition, then

$$\hat{f} \triangleq \left[(2\pi)^k|P|\right]^{-\frac{1}{2}}\int_{-\infty}^{\infty}\cdots\int_{-\infty}^{\infty} f(\underline{v},t)\ \exp\left\{-\frac{1}{2}\ (\underline{v}-\underline{m})^TP^{-1}(\underline{v}-\underline{m})\right\}$$

$$dv_1\ dv_2\ \ldots\ dv_k \tag{4.2-10}$$

To aid in evaluating $\underline{m}$, we form

$$\left(\frac{\partial \hat{f}}{\partial \underline{m}}\right)^T \triangleq \begin{bmatrix} \frac{\partial \hat{f}}{\partial m_1} \\ \frac{\partial \hat{f}}{\partial m_2} \\ \cdot \\ \cdot \\ \cdot \\ \frac{\partial \hat{f}}{\partial m_k} \end{bmatrix} = \left[(2\pi)^k |P|\right]^{-\frac{1}{2}} \int_{-\infty}^{\infty} \cdots \int_{-\infty}^{\infty} f(\underline{v},t) \exp\left\{-\frac{1}{2}\underline{r}^T P^{-1}\underline{r}\right\} P^{-1}\underline{r}$$

$$dv_1 dv_2 \cdots dv_k$$

$$= P^{-1} E\left[f(\underline{v},t)\,\underline{r}\right] \qquad\qquad (4.2-11)$$

which demonstrates that the second relation in Eq. (4.2-7) under the gaussian assumption is identical to*

$$\underline{n}^T = \frac{\partial \hat{f}}{\partial \underline{m}} \qquad\qquad\qquad (4.2-12)$$

which is the scalar version of Eq. (1.2-10). After $\hat{f}$ is calculated according to Eq. (4.2-10) for utilization in Eq. (4.2-8), the random component describing function vector $\underline{n}$ usually may be obtained much more easily using Eq. (4.2-11), than by direct solution of Eq. (4.2-8).

From the development outlined above, we note that the use of describing functions provides an approximation to nonlinear phenomena that retains input-amplitude sensitivity through the dependence of $\hat{f}$ and $\underline{n}$ on $\underline{m}$ and P. In CADET, the usefulness of the quasi-linear approximation, Eq. (4.2-8), depends on the validity of the gaussian assumption on $\underline{x}$. The accuracy question is a very complex issue -- probably, an unresolvable one in a general,

---

*Note that by convention the derivative of a scalar by a column vector is a row vector, and, by extension, the derivative of a column vector by a column vector is a matrix.

rigorous sense. The following paragraphs provide some insight into the problem, however.

An important factor is that <u>it is generally beneficial to have a system of the form indicated in Fig. 4.2-1 where there is a significant preponderance of linear dynamics over nonlinea. elements -- especially if the linear parts</u>, represented in transfer function form by $W_j(s)$, <u>are "low-pass"</u>, in which case the central limit theorem indicates that the outputs v_j are quite nearly gaussian, despite nongaussian inputs u_j. We observe, however, that this condition is not in itself completely decisive, since the CADET equations are based on the assumption that <u>all</u> states must be nearly jointly normal. The examples considered in Appendix B are situations in which the nonlinearity inputs are given to be gaussian, yet the nongaussian nature of state variables after the nonlinearity leads to inaccurate CADET results.

R-16243
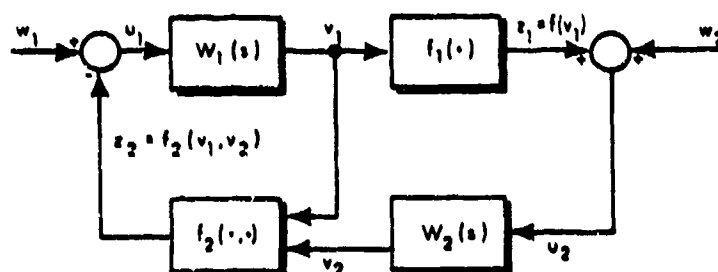
Figure 4.2-1   Example of a Nonlinear System With
                      Desirable Separation of Nonlineari-
                      ties by Linear Dynamics

Another issue that may have considerable impact on the accuracy of quasi-linearization is <u>the nature of each nonlinearity with regard to being odd of even in its input variables with respect to the input mean</u>. To illustrate this terminology, a function $f(v_1, v_2)$ is odd in v_1 with respect to m_1 and even in v_2 with respect to m_2 if

$$f(m_1 - r_1, v_2) = f(m_1 + r_1, v_2) \text{ for all } r_1$$

$$f(v_1, m_2 - r_2) = f(v_1, m_2 + r_2) \text{ for all } r_2$$

For the rest of this discussion, we consider the zero-mean case, and refer only to oddness and evenness since the extension to non-zero means is obvious.

It is beneficial to have single-input nonlinearities which are odd functions of their inputs. (Section A.1 contains a comprehensive catalogue of rīdf's for this basic type of non-linearity.) In contrast, even nonlinearities must be considered with caution. It is simple to demonstrate that the random component gain, n, is identically equal to zero when $f(v)$ is an even function of a zero-mean input v; this condition generally provides an inadequate approximation.

In treating multiple-input nonlinearities, the situation becomes more complicated. Let us consider a few examples: first, we inspect

$$f(v_1, v_2) = v_1 v_1 \cong \hat{f} + n_1 r_1 + n_2 r_2$$

$$\hat{f} = m_1 m_2 + p_{22}$$

$$n_1 = m_2$$

$$n_2 = m_1$$

where the indicated quasi-linear approximation has been derived in Ref. 3. In a zero-mean situation, the quasi-linear representation degenerates to a single mean component* given by p_{12}, the cross correlation of v_1 and v_2. By extension, any two-input relation of the form

$$f(v_1, v_2) = f_{1,odd}(v_1) \ f_{2,odd}(v_2)$$

will have zero random component describing functions when v_1 and v_2 have zero means, which will generally lead to unsatisfactory results. Next, we consider

$$f(v_1, v_2) = v_1 v_2^2 \cong \hat{f} + n_1 r_1 + n_2 r_2$$

---

*We observe that the quasi-linear approximation, Eq. (4.2-8), always conveys the mean input-output relation correctly.

$$\hat{f} = \left[m_1(m_2^2 + p_{22}) + 2m_2 p_{12}) \right]$$

$$n_1 = m_2^2 + p_{22}$$

$$n_2 = 2(m_1 m_2 + p_{12})$$

which can be derived using the general result given in Eqs.(4.3-22), (4.3-32), and (4.3-33). Here, in the zero-mean input case, we have no output mean and non-zero random component gains for both r_1 and r_2, provided p_{12} and p_{22} are non-zero. Thus in general it would seem that two-input relations of the form

$$f(v_1, v_2) = f_{1,odd}(v_1)\, f_{2,even}(v_2)$$

are advantageous from the point of view of describing function approximation accuracy in the zero mean case. Finally, using the result in Eqs. (4.3-39) and (4.3-40),

$$f(v_1, v_2) = v_1^2\, v_2^2 \doteq \hat{f} + n_1 r_1 + n_2 r_2$$

$$\hat{f} = (m_1^2 + p_{11})(m_2^2 + p_{22}) + 2p_{12}(p_{12} + 2m_1 m_2)$$

$$n_1 = 2m_1(m_2^2 + p_{22}) + 4m_2 p_{12}$$

$$n_2 = 2m_2(m_1^2 + p_{11}) + 4m_1 p_{12}$$

Again, there is no random-component transmission ($n_1 = n_2 = 0$) in the zero mean case, so the nonlinearity form

$$f(v_1, v_2) = f_{1,even}(v_1)\, f_{2,even}(v_2)$$

is apt to give poor results in this situation. As in the discussion of single-input nonlinearities, these comments may be directly extended to the non-zero mean case.

The preceding paragraphs consider the accuracy of quasi-linear approximation for a number of nonlinearity types. The problem that often arises is "zero transmission" of one or more random component(s); the basis of this phenomenon is that the random input describing function n in the quasi-linear approximation, Eq. (4.2-8), only captures that random component of the nonlinearity output, z, which is correlated with the input variables, in the sense that

$$E\left[r_j z\right] \neq 0$$

How serious this effect is on the overall accuracy of CADET is highly dependent upon the complete system model; it may be that the random effect which is neglected by the quasi-linearization procedure is truly insignificant, in the sense that other linear or nonlinear dynamics may dominate. In this eventuality, the usefulness of CADET is unimpaired. On the other hand, it is a straightforward exercise to fabricate simple examples where a CADET analysis would be totally incorrect -- cf. Appendix B. A loose but useful analogy can be drawn between the relation of describing function accuracy to the validity of the complete quasi-linear system model (in particular, to the accuracy of CADET analysis) and the parameter sensitivity problem in linear systems theory (in particular, the relation between the accuracy of standard covariance analysis, Section 1.1, and imprecision in knowledge of the linear gains of the system model). In the parameter sensitivity problem, an inaccurate value for a specific gain in the model of a system may have virtually no effect on the overall system performance (in the low sensitivity case), or it may make the model behave in a completely different manner than the system (in the high sensitivity case), rendering the model meaningless. Thus in assessing the usefulness of CADET in a given situation, one must use insight and experience in order to evaluate the approximate accuracy of the describing functions used and the relative importance of their inaccuracy.

The preceding comments on the significance of oddness and evenness should provide some useful guidelines in estimating the accuracy of various ridf's. The results outlined in Section 4.4 also provide a good qualitative "feel" for the inaccuracy in describing function calculations that arise from the departure of the nonlinearity input from the gaussian assumption. We emphasize that, because CADET is an approximate technique, it should be compared with monte carlo simulations in a few selected cases, to verify that CADET accurately captures the nonlinear effects under consideration (refer to Fig. 5.2-2).

4.3 RANDOM INPUT DESCRIBING FUNCTION CALCULATIONS

4.3.1 Single-Input Nonlinearities

In obtaining a quasi-linear representation of a nonlinear function of one variable (v) under the gaussian assumption, we have

$$f(v) \cong \hat{f} + nr \tag{4.3-1}$$

where

$$m = E\left[v\right]$$

$$r = v - m$$

$$p = \sigma^2 = E\left[r^2\right]$$

$$\hat{f} = \frac{1}{\sqrt{2\pi}\sigma} \int_{-\infty}^{\infty} f(v) \; e^{-\frac{1}{2}\left(\frac{v-m}{\sigma}\right)^2} dv \tag{4.3-2}$$

$$n = \frac{\partial \hat{f}}{\partial m} = \frac{1}{\sqrt{2\pi}\sigma^3} \int_{-\infty}^{\infty} (v-m) \; f(v) \; e^{-\frac{1}{2}\left(\frac{v-m}{\sigma}\right)^2} dv$$

Since the catalog of random input describing functions (ridf's) provided in Appendix A is not exhaustive, the following detailed examples will provide future users of CADET with some useful insights into the development of describing functions for other non-linearities.

As a general observation, it is often advantageous to use a linear transformation to simplify the exponential function in Eq. (4.3-2); the change of variable

$$u = \frac{v - m}{\sigma}$$

yields

$$\hat{f} = \frac{1}{\sqrt{2\pi}} \int_{-\infty}^{\infty} f(\sigma u + m) e^{-\frac{1}{2} u^2} du \qquad (4.3\text{-}3)$$

Further simplification may result by eliminating all terms in f that are odd in u; for example

$$\int_{-\infty}^{\infty} \left[a_0 + a_1 u + a_2 u^2 + \cdots \right] e^{-\frac{1}{2} u^2} du = \int_{-\infty}^{\infty} \left[a_0 + a_2 u^2 + a_4 u^4 + \cdots \right] e^{-\frac{1}{2} u^2} du$$

In general,

$$\int_{-\infty}^{\infty} f(\sigma u + m) e^{-\frac{1}{2} u^2} du = \int_{-\infty}^{\infty} f_{ev}(\sigma u + m) e^{-\frac{1}{2} u^2} du \qquad (4.3\text{-}4)$$

where the even part is given by

$$f_{ev}(\sigma u + m) = \frac{1}{2} \left[f(\sigma u + m) + f(-\sigma u + m) \right] \qquad (4.3\text{-}5)$$

After this procedure has been carried out, the following integral evaluations often prove to be useful:

$$\frac{1}{\sqrt{2\pi}} \int_{-\infty}^{\infty} e^{-\frac{1}{2} u^2} du = 1$$

$$\frac{1}{\sqrt{2\pi}} \int_{-\infty}^{\infty} u^2 e^{-\frac{1}{2} u^2} du = 1$$

$$\frac{1}{\sqrt{2\pi}} \int_{-\infty}^{\infty} u^4 e^{-\frac{1}{2} u^2} du = 3 \qquad (4.3\text{-}6)$$

$$\vdots$$

$$\frac{1}{\sqrt{2\pi}} \int_{-\infty}^{\infty} u^{2k} e^{-\frac{1}{2} u^2} du = (1)(3)(5)\cdots(2k-1), \quad k \geq 1$$

These results and others involving the integrand factor $e^{-\frac{1}{2}u^2}$ may be found in any complete tables of definite integrals; cf. Ref. 16.

Example 1: Using the above relations, we can obtain the quasi-linear representation of the nonlinearity v^3 by inspection. From Eq. (4.3-3)

$$\hat{f} = E\left[v^3\right] = \frac{1}{\sqrt{2\pi}} \int_{-\infty}^{\infty} (\sigma u + m)^3 e^{-\frac{1}{2}u^2} du$$

Dropping terms that are odd in u yields

$$\hat{f} = \frac{1}{\sqrt{2\pi}} \int_{-\infty}^{\infty} \left[m^3 + 3m\sigma^2 u^2\right] e^{-\frac{1}{2}u^2} du$$

so application of Eqs. (4.3-6) and (4.3-2) results in

$$\hat{f} = m^3 + 3m\sigma^2$$

$$n = \frac{\partial \hat{f}}{\partial m} = 3(m^2 + \sigma^2) \tag{4.3-7}$$

Example 2: Trigonometric nonlinearities may be treated conveniently using the above techniques in conjunction with complex variable notation: recall that the complex function e^{iv} is of the form

$$f(v) = e^{iv}$$

$$= \cos v + i \sin v \tag{4.3-8}$$

so we have

$$\hat{f} = \frac{1}{\sqrt{2\pi}\sigma} \int_{-\infty}^{\infty} \exp\left\{-\frac{1}{2}\left(\frac{v-m}{\sigma}\right)^2 + iv\right\} dv$$

Adding and subtracting $(-\frac{1}{2}\sigma^2 + im)$ in the argument of the exponential function permits us to complete a square;

$$\hat{f} = \frac{e^{-\frac{1}{2}\sigma^2 + im}}{\sqrt{2\pi}\sigma} \int_{-\infty}^{\infty} \exp\left\{ -\frac{1}{2}\left(\frac{v-m-i\sigma^2}{\sigma}\right)^2 \right\} dv$$

The final result is obtained by transforming as in Eq. (4.3-3);

$$\hat{f} = e^{-\frac{1}{2}\sigma^2 + im}$$

$$= e^{-\frac{1}{2}\sigma^2}(\cos m + i \sin m) \qquad (4.3\text{-}9)$$

Taking the real and imaginary parts of Eq. (4.3-9) yields the mean component of the quasi-linear approximations of cos v and sin v, respectively; the random component ridf is obtained by taking the partial derivative with respect to the mean. We thus obtain

$$\cos v \cong E\left[\cos v\right] + (v - m)$$

$$= e^{-\frac{1}{2}\sigma^2}\left[\cos m - (\sin m)\, r\right]$$

$$\qquad (4.3\text{-}10)$$

$$\sin v \cong E\left[\sin v\right] + n(v - m)$$

$$= e^{-\frac{1}{2}\sigma^2}\left[\sin m + (\cos m)r\right]$$

Example 3: Piecewise-linear characteristics commonly occur in models of systems with saturation, quantization, dead-zone, and other similar phenomena. Consider the ideal limiter (saturation element):

$$f(v) = \begin{cases} v & , \quad |v| \le v_{max} \\ v_{max}\text{sign}(v), & \quad |v| > v_{max} \end{cases} \qquad (4.3\text{-}11)$$

Direct application of Eq. (4.3-3) leads to

$$\hat{f} = -\frac{v_{max}}{\sqrt{2\pi}} \int_{-\infty}^{a_1} e^{-\frac{1}{2}u^2} du + \frac{1}{\sqrt{2\pi}} \int_{a_1}^{a_2} (\sigma u + m) e^{-\frac{1}{2}u^2} du$$

$$+ \frac{v_{max}}{\sqrt{2\pi}} \int_{a_2}^{\infty} e^{-\frac{1}{2}u^2} du \qquad (4.3\text{-}12)$$

where

$$a_1 = -\frac{v_{max} + m}{\sigma}$$

$$a_2 = \frac{v_{max} - m}{\sigma}$$

Since some of the limits of these integrals are finite, the direct evaluation of $\hat{f}$ in terms of elementary functions is not possible. We require two auxiliary functions based on the normal density function, here denoted PF(w):

$$PF(w) \stackrel{\Delta}{=} \frac{1}{\sqrt{2\pi}} e^{-\frac{1}{2}w^2}$$

$$PI(w) \stackrel{\Delta}{=} \int_{-\infty}^{w} PF(\omega)\ d\omega$$

$$\qquad (4.3\text{-}13)$$

$$G(w) \stackrel{\Delta}{=} \int_{-\infty}^{w} PI(\omega)\ d\omega$$

$$= w\ PI(w) + PF(w)$$

Some useful properties of these functions are

$$PF(-w) = PF(w)$$

$$PI(-w) = 1 - PI(w) \qquad (4.3\text{-}14)$$

$$G(-w) = G(w) - w$$

$$\lim_{w \to \pm\infty} PF(w) = 0$$

$$\lim_{w \to -\infty} PI(w) = 0, \qquad \lim_{w \to \infty} PI(w) = 1 \qquad (4.3\text{-}15)$$

$$\lim_{w \to -\infty} G(w) = 0, \qquad \lim_{w \to \infty} G(w) = \lim_{w \to \infty} w = \infty$$

The mean ridf term $\hat{f}$ (Eq. (4.3-12)) can be manipulated directly to obtain

$$\hat{f} = \sigma\left[G\left(\frac{v_{max}+m}{\sigma}\right) - G\left(\frac{v_{max}-m}{\sigma}\right) \right] - m \qquad (4.3\text{-}16)$$

From Eq. (4.3-13) we have that

$$\frac{dG}{dw} = PI(w)$$

so by inspection the random component gain is

$$n = \frac{\partial \hat{f}}{\partial m} = PI\left(\frac{v_{max}+m}{\sigma}\right) + PI\left(\frac{v_{max}-m}{\sigma}\right) - 1 \qquad (4.3\text{-}17)$$

The functions in Eqs. (4.3-13), (4.3-16) and (4.3-17) are standard in several works (cf. Refs. 6 and 18). Other references (cf. Refs. 15, 17) use the error function,

$$erf(w) \triangleq \frac{2}{\sqrt{\pi}} \int_0^w e^{-\omega^2} d\omega \qquad (4.3\text{-}18)$$

which is related to the probability integral $PI(w)$ by

$$erf(w) = 2PI(\sqrt{2}w) - 1 \qquad (4.3\text{-}19)$$

Since the error function is available in some computer scientific subroutine packages, it may be advantageous to use

$$n = \frac{1}{2}\left[\, \text{erf}\left(\frac{v_{max}+m}{\sqrt{2}\sigma}\right) + \text{erf}\left(\frac{v_{max}-m}{\sqrt{2}\sigma}\right)\,\right] \qquad (4.3\text{-}20)$$

This result and many other describing function representations for a variety of piecewise-linear functions may be found in Ref. 6; basic examples are given in Appendix A.

4.3.2 Multiple-Input Nonlinearities

As might be anticipated, the describing function derivation for functions with multiple inputs becomes more involved than for the single-input case. In general, for two variables we seek

$$f(v_1,v_2) \cong \hat{f} + n_1 r_1 + n_2 r_2 \triangleq \hat{f} + \underline{n}^T \underline{r}$$

where

$$\underline{m} = E\left[\underline{v}\right]$$

$$\underline{r} = \underline{v} - \underline{m}$$

$$P = E\left[\underline{r}\,\underline{r}^T\right] = \begin{bmatrix} \sigma_1^2 & \rho\sigma_1\sigma_2 \\ \rho\sigma_1\sigma_2 & \sigma_2^2 \end{bmatrix}$$

$$\hat{f} = \frac{1}{2\pi|P|^{1/2}} \int_{-\infty}^{\infty}\int_{-\infty}^{\infty} f(v_1,v_2)\, e^{-\frac{1}{2}\underline{r}^T P^{-1}\underline{r}}\, dv_1 dv_2$$

$$n_1 = \frac{\partial \hat{f}}{\partial m_1} \qquad\qquad (4.3\text{-}21)$$

$$n_2 = \frac{\partial \hat{f}}{\partial m_2}$$

To demonstrate evaluation of integrals of this form, we consider the following general form of two-input nonlinearity for which we derive a useful new result:

Case 1: For a nonlinearity that has a linear factor in one variable,

$$f(v_1, v_2) = v_1 g(v_2) \qquad (4.3\text{-}22)$$

we write Eq. (4.3-21) out fully to obtain

$$\hat{f} = \frac{1}{2\pi\sigma_1\sigma_2\sqrt{1-\rho^2}} \int_{-\infty}^{\infty} \int_{-\infty}^{\infty} v_1 g(v_2) \exp\left\{ -\frac{1}{2(1-\rho^2)} \left[\left(\frac{v_1-m_1}{\sigma_1}\right)^2 \right.\right.$$

$$\left.\left. -2\rho\left(\frac{v_1-m_1}{\sigma_1}\right)\left(\frac{v_2-m_2}{\sigma_2}\right) + \left(\frac{v_2-m_2}{\sigma_2}\right)^2 \right]\right\} dv_1 dv_2 \qquad (4.3\text{-}23)$$

It would be possible to integrate this equation with respect to v_1 directly, making use of the relation

$$\int_{-\infty}^{\infty} u \exp(-\mu u^2 + 2\nu u)\, du = \sqrt{\frac{\pi}{\mu}}\, e^{\frac{\nu^2}{\mu}}\, \frac{\nu}{\mu} \qquad (4.3\text{-}24)$$

(Ref. 17). However, a more systematic approach, explained below, reduces the possibility of error in the manipulations and algebra involved in evaluating $\hat{f}$. (The same technique is indispensable for three or more variables.)

Consider the argument of the exponential factor, $\underline{r}^T P^{-1} \underline{r}$; we seek a linear transformation $\underline{w} = R^{-1}\underline{r}$ which simplifies the integrations of Eq. (4.3-23). Choose the matrix R to be

$$R \triangleq \begin{bmatrix} \sigma_1\sqrt{1-\rho^2} & \sigma_1\rho \\ 0 & \sigma_2 \end{bmatrix} \qquad (4.3\text{-}25)$$

so by definition

$$P = RR^T \qquad (4.3\text{-}26)$$

Defining $\underline{w}$ to be given by

$$\underline{w} = R^{-1}(\underline{v}-\underline{m})$$

$$= \begin{bmatrix} \dfrac{v_1-m_1}{\sigma_1\sqrt{1-\rho^2}} - \rho\,\dfrac{v_2-m_2}{\sigma_2\sqrt{1-\rho^2}} \\[3mm] \dfrac{v_2-m_2}{\sigma_2} \end{bmatrix} \qquad (4.3\text{-}27)$$

we obtain

$$(\underline{v}-\underline{m})^T\, P^{-1}\,(\underline{v}-\underline{m}) = \underline{w}^T\underline{w} \qquad (4.3\text{-}28)$$

This change of variables in Eq. (4.3-23) leads to

$$\hat{f} = \frac{1}{2\pi}\int_{-\infty}^{\infty}\int_{-\infty}^{\infty}\left\{m_1+\sigma_1\left(\sqrt{1-\rho^2}\,w_1+\rho w_2\right)\right\}\, g\,(\sigma_2 w_2+m_2)\,e^{-\frac{1}{2}(w_1^2+w_2^2)}\,dw_1 dw_2$$

$$(4.3\text{-}29)$$

The matrix R in Eq. (4.3-25) is specifically chosen to be <u>lower triangular</u>, i.e., zero below the diagonal, in order to make v_2 a linear function of w_2 alone, so that integration with respect to w_1 can be carried out irrespective of the form of g. Discarding the odd terms in w_1, we use Eq. (4.3-6) to arrive at

$$\hat{f} = \frac{1}{\sqrt{2\pi}}\int_{-\infty}^{\infty}(m_1+\sigma_1\rho w_2)\; g\,(\sigma_2 w_2+m_2)\,e^{-\frac{1}{2}w_2^2}\,dw_2 \qquad (4.3\text{-}30)$$

which has reduced the evaluation of $\hat{f}$ in Eq. (4.3-23) to an integration in one variable.

The result in Eq. (4.3-30) can be further interpreted to obtain a fundamental form for nonlinearities which are linear in one variable. First, consider the ridf approximation of $g(v_2)$ alone: from Eqs. (4.3-1) to (4.3-3) we have

$$g(v_2) \approx \hat{g}(m_2, \sigma_2) + n_g(m_2, \sigma_2)(v_2 - m_2)$$

where

$$\hat{g} \triangleq \frac{1}{\sqrt{2\pi}} \int_{-\infty}^{\infty} g(\sigma_2 w_2 + m_2) e^{-\frac{1}{2} w_2^2} dw_2$$

$$n_g \triangleq \frac{1}{\sigma_2^2} \frac{1}{\sqrt{2\pi}} \int_{-\infty}^{\infty} \sigma_2 w_2 \, g(\sigma_2 w_2 + m_2) e^{-\frac{1}{2} w_2^2} dw_2$$

(4.3-31)

We then recognize that Eq. (4.3-30) is simply

$$\hat{f} = m_1 \hat{g} + \rho \sigma_1 \sigma_2 \, n_g \qquad (4.3\text{-}32)$$

and that the two random component ridf's are

$$n_1 = \frac{\partial \hat{f}}{\partial m_1} = \hat{g}(m_2, \sigma_2)$$

$$n_2 = m_1 \frac{\partial \hat{g}}{\partial m_2} + \rho \sigma_1 \sigma_2 \frac{\partial n_g}{\partial m_2} \qquad (4.3\text{-}33)$$

$$= m_1 n_g + P_{12} \frac{\partial n_g}{\partial m_2}$$

Consequently, given that the nonlinearity $g(v_2)$ is readily quasi-linearized, it is a direct matter of differentiation to evaluate ridf's for the multiple input nonlinearity $v_1 g(v_2)$.

Example 4: As a special case, for the single-input nonlinearity

$$f(v) = vg(v)$$

where $g(v)$ has the quasi-linear approximation

$$g(v) \approx \hat{g} + n_g(v - m)$$

we obtain

$$\hat{f} = m\hat{g} + \sigma^2 n_g$$

$$n = \hat{g} + mn_g + \sigma^2 \frac{\partial n_g}{\partial m}$$

This result permits the direct evaluation of ridf's for nonlinearities that are related to simpler forms $[g(v)]$ by multiplicative powers of v, provided the quasi-linear approximation of the simpler form is available.

Example 5: For the nonlinearity

$$f(v_1 \ v_2) = v_1 \cos v_2$$

we apply the relations given in Eqs. (4.3-32) and (4.3-33) to the ridf's given in Eq. (4.3-10) to obtain

$$\hat{f} = \left[m_1 \cos m_2 - p_{12} \sin m_2 \right] e^{-\frac{1}{2} p_{22}}$$

$$n_1 = e^{-\frac{1}{2} p_{22}} \cos m_2 \qquad (4.3-34)$$

$$n_2 = -\left[m_1 \sin m_2 + p_{12} \cos m_2 \right] e^{-\frac{1}{2} p_{22}}$$

This result was obtained in Ref. 3 by the more tedious direct evaluation of Eq. (4.3-21).

Case 2: By using similar transformation techniques (refer to Eqs. (4.3-25) and (4.3-26)), the three-variable case

$$f(v_1, v_2, v_3) = v_1 g(v_2, v_3) \tag{4.3-35}$$

has been proven to lead to a mean component quasi-linear term of the form

$$\hat{f} = m_1 \hat{g} + P_{12} \frac{\partial \hat{g}}{\partial m_2} + P_{13} \frac{\partial \hat{g}}{\partial m_3}$$

$$= m_1 \hat{g} + P_{12} n_{g_2} + P_{13} n_{g_3} \tag{4.3-36}$$

where $g(v_2, v_3)$ is represented in quasi-linear form by

$$g(v_2, v_3) \cong \hat{g} + n_{g_2}(v_2 - m_2) + n_{g_3}(v_3 - m_3) \tag{4.3-37}$$

This result should greatly expedite the evaluation of ridf's for three-input nonlinearities that are linear in one variable.

Case 3: Based on the above results, Eqs. (4.3-32) and (4.3-36), it is a matter of direct extension to prove a general direct quasi-linear approximation for the nonlinearity class

$$f(v_1, v_2) = v_1^k g(v_2), \qquad k = 1, 2, \ldots \tag{4.3-38}$$

First, we treat the case

$$f(v_1, v_2) = v_1^2 g_2(v_2) \tag{4.3-39}$$

as a special case of Eqs. (4.3-35) and (4.3-36) with g given by $v_1 g_2(v_2)$; applying Eq. (4.3-32), we obtain

$$\hat{f} = (m_1^2 + \sigma_1^2)\, \hat{g}_2 + 2m_1 p_{12} \frac{\partial \hat{g}_2}{\partial m_2} + p_{12}^2 \frac{\partial^2 \hat{g}_2}{\partial m_2^2} \qquad (4.3\text{-}40)$$

We can then proceed by induction to show that the general form of the mean component ridf is

$$\hat{f} = E\left[v_1^k\right]\hat{g} + kp_{12}E\left[v_1^{k-1}\right]\frac{\partial \hat{g}}{\partial m_2} + \frac{1}{2}\,k(k-1)p_{12}^2\,E\left[v_1^{k-2}\right]\frac{\partial^2 \hat{g}}{\partial m_2}$$

$$+ \cdots + kp_{12}^{k-1}\,E\left[v_1\right]\frac{\partial^{k-1}\hat{g}}{\partial m_2^{k-1}} + p_{12}^k\,\frac{\partial^k \hat{g}}{\partial m_2^k} \qquad (4.3\text{-}41)$$

or, to use the more compact binomial coefficient notation (Ref.18),

$$\binom{k}{j} \triangleq \frac{k(k-1)\ \cdots\ (k-j+1)}{j!} \qquad (4.3\text{-}42)$$

$$\hat{f} = \sum_{j=0}^{k} \binom{k}{j} p_{12}^j\,E\left[v_1^{k-j}\right]\frac{\partial^j \hat{g}}{\partial m_2^j} \qquad (4.3\text{-}43)$$

The random component ridf's are directly obtained by differentiation according to Eq. (4.2-11). This simple and powerful expression for $\hat{f}$ reduces the ridf evaluation to a relatively easy task for a broad class of two-variable functions.

Various techniques exist for manipulating nonlinearities into forms that are directly treated by the above developments. A particularly fruitful approach is the use of trigonometric identities to reformulate nonlinearities, as the following case demonstrates.

Example 6: For a nonlinear function with multiple trigonometric factors, e.g.

$$f(v_1, v_2, v_3) = v_1 \sin v_2 \cos v_3 \qquad (4.3\text{-}44)$$

we can use the sum-and-difference formulae (cf. Ref. 19) to obtain

$$g \triangleq \sin v_2 \cos v_3 = \frac{1}{2}\left[\sin(v_2+v_3) + \sin(v_2-v_3)\right]$$

and proceed as follows: From Eq. (4.3-10),

$$E\left[\sin w\right] = e^{-\frac{1}{2}\sigma_w^2}\sin(m_w)$$

where $w = v_2 \pm v_3$. In the two cases $w = v_2 \pm v_3$, Eq. (4.2-2) yields

$$w = v_2+v_3 \longrightarrow m_w = m_2+m_3, \quad \sigma_w^2 = p_{22}+p_{33}+2p_{23}$$

$$w = v_2-v_3 \longrightarrow m_w = m_2-m_3, \quad \sigma_w^2 = p_{22}+p_{33}-2p_{23}$$

Thus

$$\hat{g} = E\left[\sin v_2 \cos v_3\right]$$

$$= \frac{1}{2}e^{-\frac{1}{2}(p_{22}+p_{33})}\left[e^{-p_{23}}\sin(m_2+m_3) + e^{p_{23}}\sin(m_2-m_3)\right]$$

and the direct application of Eq. (4.3-36) leads to

$$\hat{f} = m_1\hat{g} + \frac{1}{2}e^{-\frac{1}{2}(p_{22}+p_{23})}\left[(p_{12}+p_{13})e^{-p_{23}}\cos(m_2+m_3)\right.$$

$$\left. + (p_{12}-p_{13})e^{p_{23}}\cos(m_2-m_3)\right] \qquad (4.3-45)$$

Obtaining this result by the direct application of Eq. (4.2-10) would be very tedious.

With the tools developed in this section of the handbook and the catalogue of single-variable ridf's provided in Appendix A, a broad class of nonlinearities can be treated in a straightforward manner (with little or no analysis of the sort illustrated in this chapter). Thus these contributions significantly enhance the direct usefulness of CADET.

4.4 EFFECTS OF DIFFERENT PROBABILITY DENSITY FUNCTIONS

An important issue that must be investigated in order to assess the potential accuracy of CADET is the effect of deviations from the assumed joint normality of the state variables on the evaluation of random input describing functions (ridf's). The gaussian hypothesis is the only approximation made in the application of CADET, so any inaccuracy in performance projections obtained via CADET is due to the nongaussian nature of the actual state variable joint probability density function (pdf).

In this section, we present results of an investigation of the sensitivity of quasi-linearization to changes in the pdf of the nonlinearity input (Ref. 4). We compare the ridf's corresponding to three common nonlinearities -- the limiter, the sinusoidal operator, and a power law nonlinearity -- computed for a variety of density functions. Seven probability density functions with quite different functional forms are considered. Four of these are given in Table C.2-1, viz., the exponential, gaussian, triangular, and uniform distributions. Three additional densities are special cases of the sum of two symmetrical triangular functions, defined in general by

$$p(x) \triangleq \begin{cases} \frac{1}{2\Delta} \left(1 - \frac{\big| |x| - x_o \big|}{\Delta} \right), & \big| |x| - x_o \big| \leq \Delta \\ 0, & \big| |x| - x_o \big| > \Delta \end{cases} \qquad (4.4\text{-}1)$$

which has a zero mean, a variance given by

$$\sigma^2 = x_o^2 + \frac{1}{6} \Delta^2 \qquad (4.4\text{-}2)$$

and a kurtosis (ratio of fourth moment to variance squared) of

$$\lambda \triangleq \frac{\mu_4}{\sigma^4} = \frac{x_o^4 + \Delta^2 x_o^2 + \frac{1}{15} \Delta^4}{x_o^4 + \frac{1}{3}\Delta^2 x_o^2 + \frac{1}{36} \Delta^4} \qquad (4.4\text{-}3)$$

The three cases of Eq. (4.4-1) chosen for the comparison correspond to $\Delta = \frac{1}{2} x_o$, x_o and $2x_o$; the associated pdf's are portrayed in Fig. 4.4-1. Note that two of these densities are bimodal; i.e., they have two distinct peaks.

(a) $\Delta = \frac{1}{2} x_o$ (b) $\Delta = x_o$

(c) $\Delta = 2x_o$
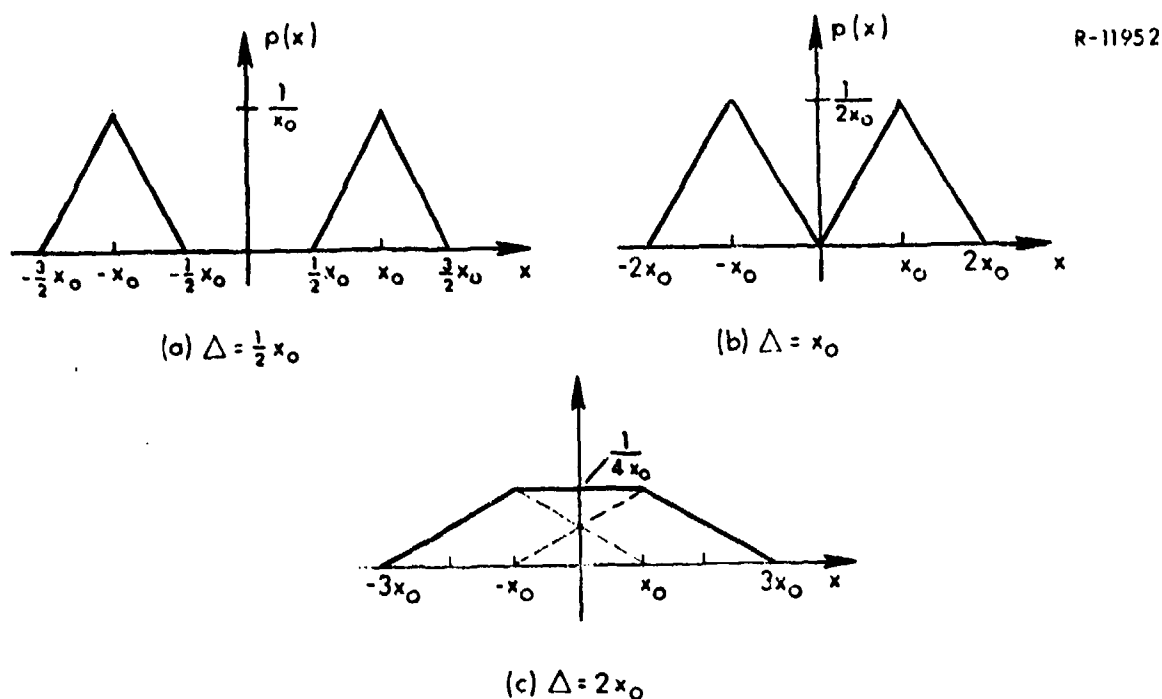
Figure 4.4-1   Three Density Functions Comprised of Two Triangles

It is shown in the discussion of confidence intervals for the estimated standard deviation obtained via the monte carlo method (Section C.2) that the kurtosis has a significant impact on the confidence we have in the accuracy of the estimate. Here it is observed that the value of the random input describing function calculated for various pdf's seems to be directly related to the kurtosis. Thus we order the seven pdf's under consideration according to the value of λ:

$$p_1(x) = \frac{1}{\sqrt{2}\sigma} \exp\left(-\frac{\sqrt{2}}{\sigma}|x|\right) ; \qquad\qquad \lambda_1 = 6 \qquad \text{(exponential)}$$

$$p_2(x) = \frac{1}{\sqrt{2\pi}\,\sigma} \exp\left(-\frac{x^2}{2\sigma^2}\right) ; \qquad\qquad \lambda_2 = 3 \qquad \text{(gaussian)}$$

$$p_3(x) = \frac{1}{\sqrt{6}\,\sigma}\left(1 - \frac{|x|}{\sqrt{6}\,\sigma}\right) , \; |x| \leq \sqrt{6}\,\sigma; \qquad \lambda_3 = 2.4 \quad \text{(triangular)}$$

$$p_4(x) = \frac{1}{4x_0}\left(1 - \frac{\left||x| - x_0\right|}{2x_0}\right) , \; \left||x| - x_0\right| \leq 2x_0 ; \quad \lambda_4 = 2.14 \quad \text{(Fig. 4.4-1c)}$$

$$p_5(x) = \frac{1}{2\sqrt{3}\,\sigma} , \quad |x| \leq \sqrt{3}\,\sigma ; \qquad\qquad \lambda_5 = 1.8 \qquad \text{(uniform)}$$

$$p_6(x) = \frac{1}{2x_0}\left(1 - \frac{\left||x| - x_0\right|}{x_0}\right) , \; \left||x| - x_0\right| \leq x_0 ; \quad \lambda_6 = 1.52 \quad \text{(Fig. 4.4-1b)}$$

$$p_7(x) = \frac{1}{x_0}\left(1 - \frac{2\left||x| - x_0\right|}{x_0}\right) , \; \left||x| - x_0\right| \leq \tfrac{1}{2} x_0; \quad \lambda_7 = 1.16 \quad \text{(Fig. 4.4-1a)}$$

$$(4.4\text{-}4)$$

While these density functions are not exhaustive in a formal sense, they do represent a variety of situations. All of the densities given in Eq. (4.4-4) have even symmetry; we note that skew densities can be disregarded in this context with no loss in generality. For a skew density $p_S(x)$ we can define its even part by

$$p_{ev}(x) = \frac{1}{2}\left(p_S(x) + p_S(-x)\right)$$

Since the three nonlinearities considered are symmetric (odd) and the mean values of their inputs are zero, only the even part of the pdf contributes to the describing function calculation.

Limiter — The ideal limiter or saturation operator,

$$
f(x) = \begin{cases} x & , \quad |x| \le \delta \\ \\ \delta \text{ sign } (x) & , \quad |x| > \delta \end{cases}
\tag{4.4-5}
$$

is a common piecewise-linear function used to model nonlinear phenomena. In Fig. 4.4-2, we portray the various describing function gains for this nonlinearity, corresponding to the pdf's defined in Eq. (4.4-4), as functions of the ratio of the input rms level, σ, to the saturation point, δ. As would be expected, all seven quasi-linear gains capture the fact that the effective gain starts to decrease from unity whenever a significant portion of the assumed input pdf lies beyond the saturation point, i.e., whenever there is a significant probability that $|x|$ is greater than δ. As has been pointed out previously, this effect is the key to the success of quasi-linearization techniques in reflecting nonlinear system behavior that is beyond the scope of small-signal (Taylor series) linearization.

It is interesting to observe that the relative positions of the curves in Fig. 4.4-2 exhibit a monotonic relation to the value of λ. The greater the difference between λ for a particular pdf and the value for the gaussian case ($\lambda = 3$), the greater the difference between that density function's ridf curve and the curve for a gaussian distribution. This behavior holds in all the cases considered here, and is indicative of the fact that the value of λ is one quantitative measure of how "close" the density function is to being gaussian. The variation of the ridf's with λ is about at its maximum (on a percentage basis) for the case $\sigma = 2\delta$; the ridf decreases 13% as λ increases from 3 to 6, and increases 28% as λ decreases from 3 to 1.16.
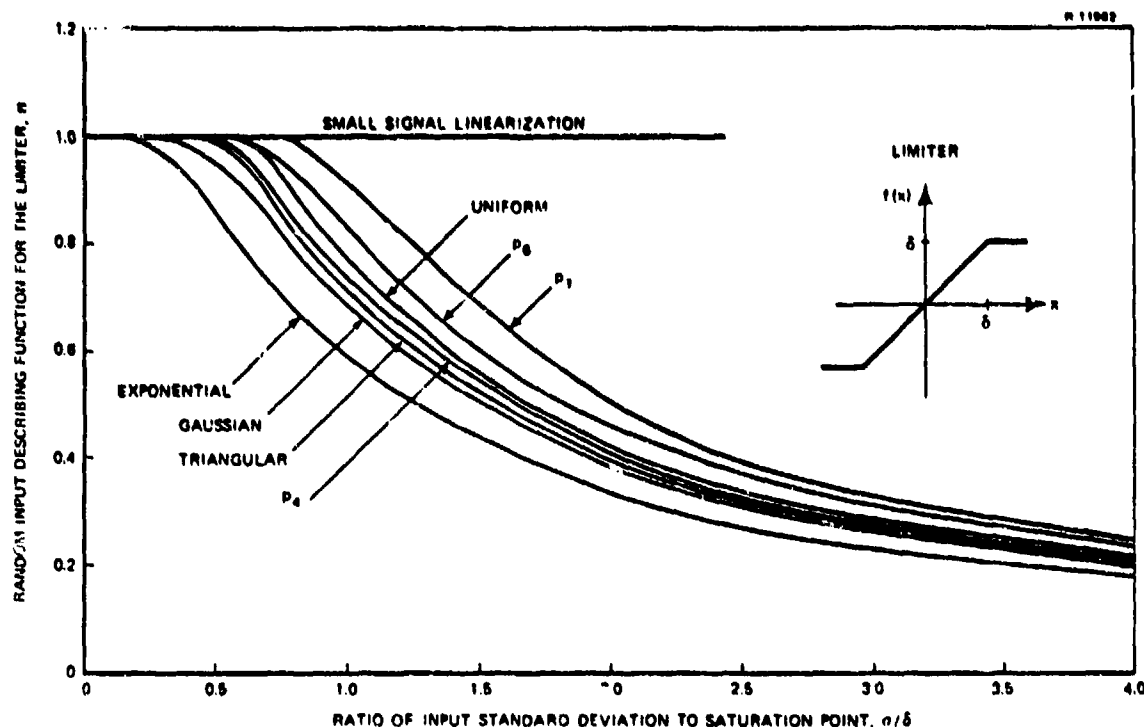
Figure 4.4-2   Random Input Describing Function
                Sensitivity for the Limiter

P_i · Law — A similar study was performed for a power-
law characte istic,

$$f(x) = x^2 \text{ sign } (x) \tag{4.4-6}$$

This type of nonlinearity is often used to model effects such as
the "hard spri.._' characteristic (Ref. 15) discussed in consider-
ing nonlinear restoring torques acting on the missile seeker head,
Section 3.6. For the power law, the ridf's calculated for the
same density functions considered previously have the form (Ref.4)

$$n_i = \mu_i \sigma \tag{4.4-7}$$

where σ is the input rms level and μ_i are coefficients determined
by the input pdf's, $p_i(x)$. Thus the describing function gain for
$f(x)$ increases linearly with the input rms level, in direct con-
trast to the small-signal linear gain which is identically equal

to zero, as shown in Fig. 4.4-3. It is again observed that there is a monotonic relation between λ_i and the ridf curves. In this case, an increase in λ leads to an increase in the describing function gain, which is contrary to the behavior shown for the limiter. This is a result of the fact that the power law output increases more rapidly with increasing input than a linear characteristic, whereas the opposite is true for saturation. For the power law nonlinearity, the ridf sensitivity is independent of σ, i.e., the ratio of ridf's calculated for $p_i(x)$ and $p_j(x)$ is simply μ_i/μ_j. For f(x) in Eq. (4.4-6), the describing function gain n varies from + 33% for the exponentially distributed case, to -34% for the pdf $p_7(x)$, compared to the gaussian input ridf, which shows that this nonlinearity is somewhat more sensitive to variations in λ than the limiter.
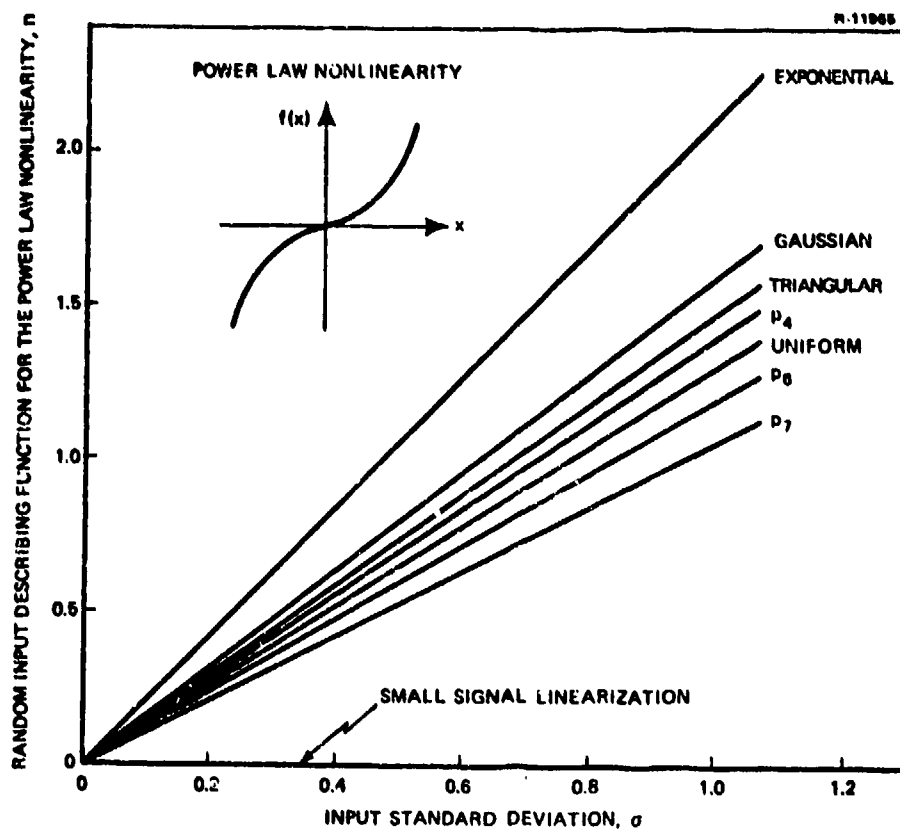
Figure 4.4-3   Random Input Describing Function Sensitivity for the Power Law Nonlinearity

Sinusoidal Operator – The third nonlinearity considered
in these sensitivity studies is the sinusoidal operator,

$$f(x) = \sin x$$

which is needed to resolve the missile and target velocity vec-
tors in the missile-target intercept model, for example. A po-
tential source of difficulty with this function is that the non-
linearity output periodically changes sign with increasing or
decreasing values of its input. This leads to quasi-linear gains
that, for large values of rms input, σ, may even differ in sign
for different input pdf's. This problem is not unique to CADET;
in many modeling and simulation studies, care must be exercised
when the input to a sinusoidal operator (or any other trigono-
metric nonlinearity) can exceed $\pm$ 90 deg ($\pm \pi/2$ rad), since in
some sense the "gain" can change sign in some situations. Bear-
ing this in mind, we have calculated the random input describing
functions for values of σ as large as 3 rad to indicate where
such effects become important, as shown in Fig. 4.4-4.

The quasi-linear gains for $\sigma < \pi/2$ rad show some simi-
larily to those obtained for the limiter; this is a reasonable
mode of behavior, since the sine function shows a definite satu-
ration effect of the range $|x| \leq \pi/2$ rad. As expected, the ridf's
are inversely related to λ for $\sigma < \pi/2$ rad, i.e., as λ increases,
n decreases. However, as the input rms level approaches 3 rad,
the describing functions for all of the pdf's except $p_1(x)$ and
$p_2(x)$ become negative, and the monotonic relationship between λ
and n appears to be lost.

The preceding studies indicate that the sensitivity of
random input describing function calculations to variations in
input probability density function is slight for small values of
input rms level; as σ approaches zero, the quasi-linear gains
approach unity for the limiter and sinusoidal operator, and zero
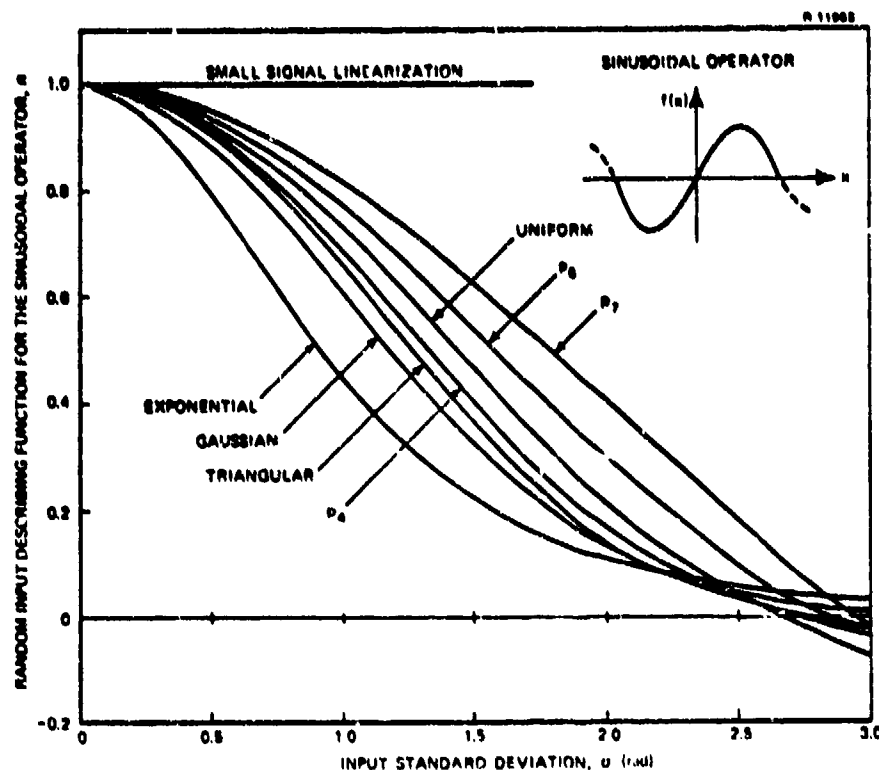
Figure 4.4-4   Random Input Describing Function
                Sensitivity for the Sinusoidal
                Operator

for the power law nonlinearity. These limiting cases are the same
values of gain that would be obtained by the traditional small-
signal linearization approach -- viz., by replacing f(x) with a
linear gain equal to the slope of the function at the origin
(Section 1.2). As a general result, it has been shown (Ref. 6)
that quasi-linearization subsumes small-signal linearization,
i.e., for small signals the two are equivalent. This, in turn,
proves that CADET provides nearly exact statistical analyses when
the random variables have a small rms value in relation to the sys-
tem nonlinearities, i.e., when most of each nonlinearity input
probability density function lies in the linear region of its non-
linearity. As the rms levels of system variables increase so that
the nonlinearities are being exercised significantly, the describ-
ing function sensitivity to the input pdf can be appreciable; then

4-33

it must be ascertained how sensitive the system performance is to variations in gain at each point in the system model where a non-linearity occurs. No general answer can be given to this question; the verification of CADET for particular applications must be accomplished by direct comparison with monte carlo results, as has been done in Chapter 4 of Ref. 4 for the missile homing guidance system.

4.5   DESCRIBING FUNCTIONS NOT EXISTING IN CLOSED FORM UNDER THE GAUSSIAN ASSUMPTION

For certain nonlinearities, random input describing functions cannot be obtained in closed form under the assumption that the inputs are jointly normal. In this section we indicate some approximate methods for computing ridf's that involve either approximations to the input probability density function, or approximations to the nonlinearity, and discuss their usefulness.

An example of interest in the missile-target intercept problem is the nonlinearity

$$f(x,y) = \sqrt{x^2 + y^2} \qquad\qquad (4.5-1)$$

which defines the missile-to-target range in terms of the cartesian components of the separation, x and y. This problem is considered in some detail to provide a focus for the discussion of several ridf approximation techniques. We compare the accuracy of each approach for the nonlinearity given in Eq. (4.5-1), and point out some pitfalls that may be encountered if care is not taken.

In order to simplify the discussion, we assume that y does not have a mean component, and x has a negligible random component. This approximation is valid in many missile-target intercept situations except at the very end of the engagement (refer to Section 4.1 of Ref. 4). With these assumptions, there

are only two ridf's, $\hat{f}$ and n_y, needed for a quasi-linear representation of the range. Thus from Eq. (4.1-4), we seek to evaluate

$$\hat{f} = E\left[\sqrt{m_x^2 + y^2}\right] = \int_{-\infty}^{\infty} p(y)\sqrt{m_x^2 + y^2}\,dy$$

$$n_y = \frac{1}{\sigma_y^2}\int_{-\infty}^{\infty} yp(y)\sqrt{m_x^2 + y^2}\,dy$$

Under the assumption that y is a gaussian random variable, the second of these integrals can be evaluated analytically; however, the first, which is of the form

$$\hat{f} = \frac{1}{\sqrt{2\pi}\sigma_y}\int_{-\infty}^{\infty}\sqrt{m_x^2 + y^2}\,\exp\left[-\frac{y^2}{2\sigma_y^2}\right]dy \qquad (4.5\text{-}2)$$

cannot generally be solved in closed form unless $m_x = 0$, in which case we have

$$\hat{f} = E\left[|y|\right] = \sqrt{\frac{2}{\pi}}\,\sigma_y \qquad (4.5\text{-}3)$$

For the more general situation given by Eq. (4.5-2) with $m_x \neq 0$, it is desirable to use some approximate technique to obtain a closed form expression for $\hat{f}$ that is convenient for use in a CADET analysis.*

A Taylor series expansion of a function of a random variable, f(y), about the mean of that variable, m, results in

$$f(y) = f(m) + \frac{df}{dy}\bigg|_{y=m} r + \frac{1}{2}\frac{d^2f}{dy^2}\bigg|_{y=m} r^2 + \dots \qquad (4.5\text{-}4)$$

---

*While $\hat{f}$ in Eq. (4.5-2) for given values of m_x and σ_y can be calculated by numerical integration, a less time-consuming approach is desired for repeated evaluation in a CADET analysis.

where $r = y-m$. We desire to determine the expected value of the above function, which is given by

$$E\left[f(y)\right] = f(m) + \frac{1}{2}\left.\frac{d^2f}{dy^2}\right|_{y=m}\sigma_y^2 + \frac{1}{6}\left.\frac{d^3f}{dy^3}\right|_{y=m}E\left[r^3\right] + \ldots$$

$$(4.5-5)$$

where use is made of the fact that $E\left[r\right]$ is zero to eliminate the second term in Eq. (4.5-4); all other odd central moment terms ($E\left[r^3\right]$ etc.) are also zero for symmetric pdf's. Truncating the series given in Eq. (4.5-5) at the second term, we obtain

$$E\left[f(y)\right] \approx f(m) + \frac{1}{2}\left.\frac{d^2f}{dy^2}\right|_{y=m}\sigma_y^2 \qquad (4.5-6)$$

which is an approximation suggested in Ref. 8. We note that this result is independent of the particular density function of y. If more terms are desired, the higher-order central moments can be evaluated using a specified pdf. If y is gaussian, all odd central moments are zero and even central moments are given by (Ref. 8)

$$\mu_{2k} \triangleq E\left[r^{2k}\right] = (1)(3)(5)\ldots(2k - 1)\sigma^{2k}$$

as can be inferred from Eq. (4.3-6). Thus the full expansion is

$$E\left[f(y)\right] \approx f(m) + \frac{1}{2}\left.\frac{d^2f}{dy^2}\right|_{y=m}\sigma^2 + \frac{(1)(3)}{4!}\left.\frac{d^4f}{dy^4}\right|_{y=m}\sigma^4+\ldots$$

$$(4.5-7)$$

The use of the first term alone in Eq. (4.5-7) corresponds to small signal linearization; taking two terms as indicated in Eq. (4.5-6) results in a quasi-linear gain that is often useful. We observe that the existence of a well-behaved (i.e.,

convergent) expansion for $f(y)$ does not guarantee that Eq. (4.5-7) exhibits the same behavior.

In the present case, the series expansion approach is effective for evaluating $\hat{f}$ only in situations where m_x is considerably larger in magnitude than σ_y, due to the singularities of the derivatives of $\sqrt{m_x^2 + y^2}$ at the origin ($m_x = 0$). To demonstrate this difficulty, we write the series expansion for the nonlinearity under consideration (Ref. 19),

$$f(y) = \sqrt{m_x^2 + y^2} = |m_x| \left[1 + \frac{1}{2} \left(\frac{y}{m_x} \right)^2 - \frac{1}{8} \left(\frac{y}{m_x} \right)^4 + \ldots \right] \quad (4.5-8)$$

from which we obtain

$$\hat{f} = |m_x| \left[1 + \frac{1}{2} \left(\frac{\sigma_y}{m_x} \right)^2 - \frac{3}{8} \left(\frac{\sigma_y}{m_x} \right)^4 + \ldots \right] \quad (4.5-9)$$

as an approximate describing function to represent the mean component of the range. For m_x considerably larger than σ_y, the first few terms of this expansion yield acceptable accuracy.* However, since m_x approaches zero as range goes to zero in the missile-target intercept problem, using Eq. (4.5-9) is generally not suitable.

A second method for approximating the integral in Eq. (4.5-2) is the substitution of a nongaussian pdf for which the integral can be obtained in closed form. As in previous sensitivity studies (Section 4.4), the best result is obtained using the triangular pdf. Substituting this distribution into

---

*We note that the expansion indicated in Eq. (4.5-9) never converges formally, i.e., for any value of σ_y/m_x, no matter how small, the series will eventually diverge as more terms are evaluated. This is a standard property of asymptotic expansions which are useful only when truncated after a finite number of terms.

Equation (4.5-1) leads to an integral that is evaluated in closed form to be

$$\hat{f} \cong \frac{|m_x|}{\nu}\left[\sqrt{1+\nu^2} +\nu^2 \log\left(\frac{1+\sqrt{1+\nu^2}}{\nu}\right) + \frac{4}{\sqrt{6}}\left(\nu^3 - (1+\nu^2)^{3/2}\right)\right]$$

(4.5-10)

where the auxiliary variable ν is given by

$$\nu \triangleq \frac{m_x}{\sqrt{6}\sigma_y}$$

(4.5-11)

The accuracy of Eq. (4.5-10) is quite good, especially when compared with the poor approximation given by the series expansion in Eq. (4.5-9) when $|m_x|$ is less than or equal to σ_y. The error between Eq. (4.5-10) and the exact result specified in Eq. (4.5-2), as shown in Fig. 4.5-1, is less than 3%, which is adequate for most applications.

We note that the conclusion that the series expansion technique is not useful for computing the ridf in the case treated above should not be taken as universally true. When series approximations for an ridf can be obtained which are accurate over the entire range of the input statistics, they will generally yield good results. Another important consideration is that the series expansion technique is generally feasible for highly complicated nonlinearities, as demonstrated in Section A.4, while evaluating $\hat{f}$ by integration with any approximate pdf p(y) may be impractical or impossible. The cases treated in Section A.4 thus illustrate the power of the series expansion technique, given in Eqs. (4.5-6) and (4.5-7), while the above presentation indicates the care that must be exercised to avoid convergence problems.

This chapter presents a detailed outline of the theory and application of statistical linearization. Guidance in

R-11973a

NORMALIZED RANDOM INPUT DESCRIBING FUNCTION FOR THE RANGE, $\hat{f}/\sigma_y$

TAYLOR SERIES EXPANSION

2 TERMS

4 TERMS

TRIANGULAR DENSITY

EXACT SOLUTION, GAUSSIAN DENSITY

NORMALIZED MEAN VALUE OF DOWNRANGE SEPARATION, m_x/σ_y
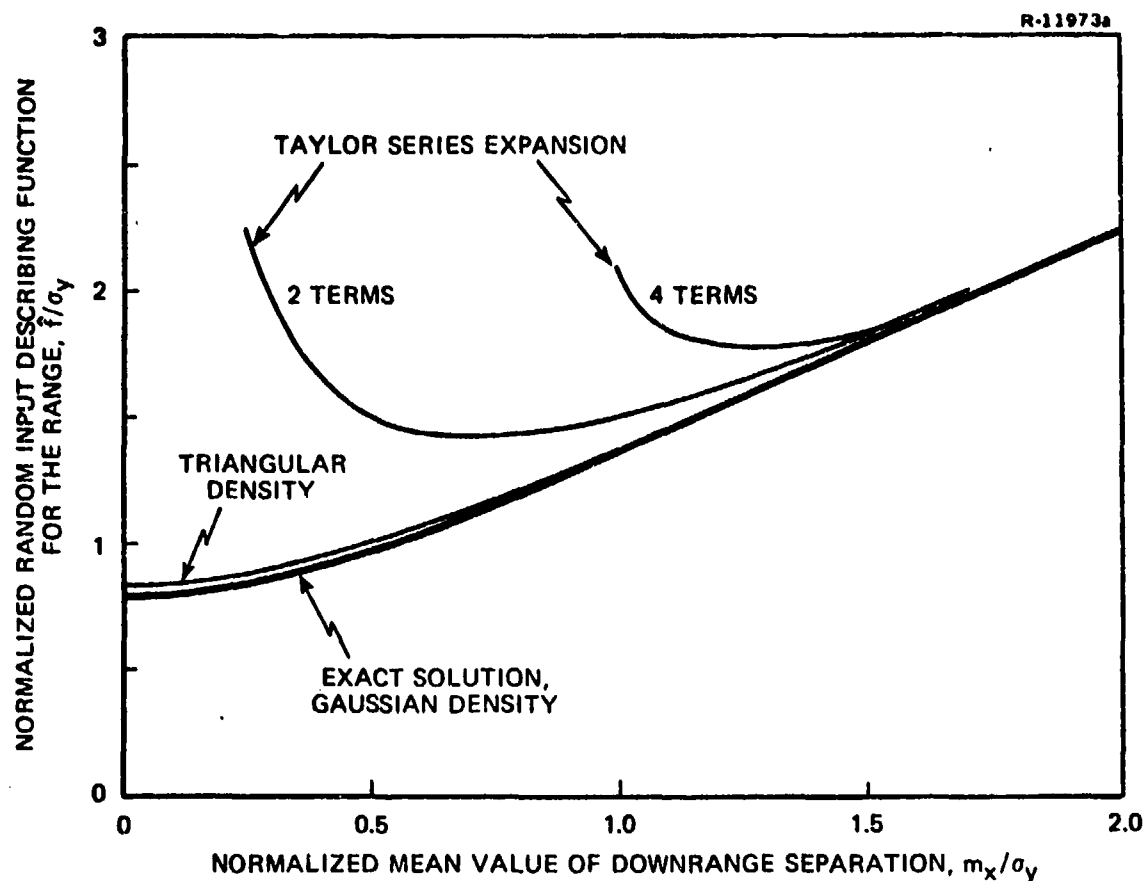
Figure 4.5-1   Comparison of Approximations for
                    the Expected Value of the Range

deriving random input describing functions is supplied in a
variety of examples, and a comprehensive discussion of the sen-
sitivity of ridf calculation to deviations from the assumption
of joint normality is provided. These contributions should aid
future users of CADET in performing statistical analyses of non-
linear systems with random inputs, and in assessing the accuracy
of their results.

5.   <u>OVERVIEW AND ASSESSMENT OF CADET</u>

5.1 DIRECT CADET-MONTE CARLO COMPARISONS

Since CADET and the monte carlo method are the only tools available for the statistical analysis of the performance of non-linear systems with random inputs, the ultimate value of CADET can only be established by comparing the relative efficacy of the two approaches. In this section, we will touch on <u>utility</u>, <u>ease of application</u>, <u>expenditure of computer time</u>, and <u>accuracy</u>. Based on these factors, and on other characteristics of the two techniques, we will outline the philosophy for the application of CADET that has been developed at TASC, and summarize the strong and weak points of this methodology. The conclusions, while based chiefly on extensive experience gained in treating the missile-target intercept problem, should provide useful guidelines for broader applications of CADET.

5.1.1 Overview and CADET Mechanization

In Chapter 1 we have derived differential equations governing the approximate evolution of the mean vector and covariance matrix of nonlinear time-varying systems with random inputs, having the form

$$\underline{\dot{x}} = \underline{f}(\underline{x},t) + G(t)\ \underline{w}(t) \tag{5.1-1}$$

where $\underline{x}(t)$ and $\underline{w}(t)$ are vectors composed of the system states and random inputs, respectively. (Refer to Section 1.2 for further details.) Before the CADET equations can be implemented, it is necessary to have the random input describing functions (ridf's) required for a quasi-linear representation of every system

nonlinearity. The ridf's for a broad set of single-input non-
linearities are directly available from Ref. 6 (see also Appen-
dix A). In addition, Chapter 4 of this handbook provides ridf's
for a number of common multiple-input nonlinearity forms. Con-
sequently, use of CADET is often a matter of direct substitution
of known ridf's in the mean and covariance equations, as demon-
strated in Chapter 2. If a matrix computer language is available
to the analyst, the construction of a computer program for apply-
ing CADET is no more difficult than the programming required for
using the monte carlo method. As an added benefit, CADET does
not necessitate use of a random number generator; a common source
of concern in the monte carlo method is the question of what con-
stitutes a "good" random number sequence and how such a sequence
can be generated.

Thus from the point of view of utility and mechaniza-
tion, the two techniques appear to be quite comparable -- there
is no clear-cut reason to state that one technique is superior
to the other based on these considerations.

5.1.2 Accuracy and Efficiency

One of the main arguments that can be advanced for the
use of CADET in obtaining projections of nonlinear system per-
formance is the significant reduction in computer central pro-
cessing unit (CPU) time achieved by using CADET instead of the
monte carlo method. In making this comparison, two issues must
be addressed: the number of monte carlo trials that must be per-
formed in order to obtai comparably accurate results, and the
practical limitation imposed by computer costs. From the stand-
point of accuracy, a decision regarding the required number of
monte carlo trials is somewhat arbitrary, because the error
mechanisms of CADET and the monte carlo method are dissimilar.

Referring to Fig. C.3-2b, we note that, in a situation where the
statistics are quite nongaussian, the CADET computation of the
rms value of a system variable appears to be at least as accurate
as the value estimated with 400 monte carlo trials, in the sense
that the 95% confidence band for 400 trials brackets the CADET re-
sult. Where the statistics are more nearly gaussian, e.g. as in
Fig. C.3-2a, it would seem that CADET accuracy is comparable to
that achieved by more than 500 monte carlo trials.* On the other
hand, a pragmatic evaluation of the efficiency of CADET should take
into account the fact that most monte carlo studies must be limited
in scope by computer budget constraints. A reasonable upper bound
is thus 256 trials since, in the gaussian case, this results in
95% confidence that an accuracy of 10% can be achieved (Section C.2);
for high-order systems, even this number of trials may require an
inordinate amount of computer time. For the present discussion,
we therefore compare the relative efficiency of the monte carlo
and CADET approaches on the basis of 256 trials, recognizing that
the estimated rms values of the system variables obtained for this
number of monte carlo experiments may be less accurate than the
CADET results.

In past studies, Refs. 1 to 4, the savings in computer
CPU time achieved by the application of CADET has always been
significant in comparison with 256-trial monte carlo studies, even
though the system treated in some cases has been of high order
(with up to 42 system states) and very nonlinear (having up to
26 nonlinearities). We discuss below how both of these factors
tend to reduce the relative efficiency of CADET.

Monte carlo simulation for a system with n states requires
the integration of an n-vector differential equation (repeated q
times where q is the number of trials), while CADET involves the

---

*Recall that CADET is exact in the linear gaussian case,
Section 1.1.

propagation of the n-element mean vector, $\underline{m}$, and the $n \times n$ symmetric covariance matrix, P -- a total of $n(n+3)/2$ elements. Thus the computational burden for CADET can increase as fast as $n^2/2$ while the CPU time for monte carlo analysis only varies as n, demonstrating that an increase in the number of states may reduce the advantage of CADET in efficiency. This factor can be mitigated to a large extent when there is little dynamic cross-coupling in the system; in the quasi-linear system model, Eq. (4.1-4), this corresponds to N having few non-zero elements (N being sparse). In many practical problems, N is sparse and a considerable increase in the computational efficiency of CADET can be realized by the application of techniques which circumvent multiplications involving zero elements, thus streamlining the evaluation of $\dot{P}$ (Eq. (1.2-7)). Such an approach has proven to be valuable in the studies presented in Ref. 3.

The number of nonlinearities may also increase the computation time required by CADET, since the calculation of a random input describing function generally requires more logical and numerical operations than evaluating the corresponding nonlinear function in the monte carlo program (refer to Appendix A, for example). The investigation treated in Ref. 4 was exceptional in having nearly as many nonlinearities as state variables; more typical applications of CADET would focus on a few principal nonlinear effects, leading to a still more favorable comparison of CADET with the monte carlo method in terms of computational burden per performance evaluation.

Using the same integration method in performing the monte carlo ensemble of simulations as was used in propagating the system mean vector and covariance matrix via CADET, and assuming that the same integration step size is required in each procedure, the results summarized in Table 5.1-1 indicate the effect of the system dimensionality (number of states) and degree of nonlinearity (number of nonlinearities) in typical studies of the missile-target

TABLE 5.1-1

COMPARISON OF CADET AND MONTE CARLO EFFICIENCY
BASED ON 256-TRIAL MONTE CARLO ANALYSIS

Study	Number of States*	Number of Nonlinearities	Ratio of Computer Time Costs: Monte Carlo/CADET
Ref. 2	10	2	30
Ref. 3	17	5	15-20
Ref. 4	22	32	10
Ref. 23	42	26	20-30**

*Continuous- and discrete-time dynamic states only; bias states omitted.

**Optimized, using fast sparse-matrix-multiplication subroutines.

intercept problem. Comparing the investigations of Refs. 2 and 4, we note a considerable decrease in relative CADET efficiency caused by increased s, omp ity; in the analysis of the system model given in 3, an intermediate degree of complexity and corresponding efficiency is noted. The study of Ref. 23, also indicated in Table 5.1-1, shows the significant improvement that can be achieved by careful CADET program optimization, using the fast sparse-matrix-multiplication subroutine approach mentioned above.

We should also point out that in some circumstances the monte carlo approach may require a reduced integration step size to avoid failure of the numerical integration technique (refer to Section 4.4 of Ref. 4, for examp . In such cases the monte carlo/CADET CPU time ratio will be even higher.

5.2 OTHER FACTORS AND PHILOSOPHY OF APPLICATION

In comparing CADET and the monte carlo method for use in obtaining performance projections for nonlinear systems with random inputs, we have observed that there are several significant similarities. Both techniques are applicable to nonlinear system models with an arbitrary number of states and nonlinearities, and we often rely on the gaussian assumption in assessing the accuracy of the performance statistics obtained (refer to Sections 1.2 and C.2). In either case, departure from normality can be compensated for to a certain extent; in CADET, nongaussian probability density functions can be used in calculating describing functions, while in monte carlo simulation the fact that the confidence band limits may increase for nongaussian random variables (Fig. C.2-2) can be counteracted by increasing the number of trials performed. The principle trade-off between the two methods is in efficiency versus versatility.

The monte carlo simulation ensemble of q representative state trajectories (Eq. (C.1-4)) can be used not only as a data base for calculating estimated performance statistics $\hat{m}(t)$ and $\hat{P}(t)$ at instants of time of interest, but also for estimating higher order moments, and for generating histograms which are approximate density functions for the variables under consideration. However, the versatility of the monte carlo method can only be exploited with a further significant increase in computer time expenditure over that indicated in Table 5.1-1; while the estimation of $\hat{m}$ and $\hat{P}$ may require several hundred trials or more, it is generally necessary to perform thousands of trials in order to obtain an accurate estimate of the pdf of a random variable (and, of course, what constitutes an "accurate estimate" is generally a subjective value judgment in a nongaussian case). In the sense that one can always obtain a better estimate of the statistics of a random variable by running more trials (computer budget permitting), the monte carlo method is a "self-checking" procedure.

CADET, on the other hand, provides approximate values for $\underline{m}(t)$ and $P(t)$ in a single numerical integration of the quasi-linear covariance equations (Eq. (1.2-7)), usually in a small fraction of the computer processing time required for an accurate monte carlo analysis.

One of the primary purposes of the statistical analysis of nonlinear system performance is the evaluation of the change in system effectiveness due to variations in random input levels, initial condition statistics, system parameter values and secondary nonlinear effects. The multiplicity of factors such as these implies that the analysis will generally be done repeatedly, and computational efficiency is thus an important consideration. This point is a strong argument in favor of CADET. On the other hand, the versatility of monte carlo simulation (with its self-check capability) permits us to assess the accuracy of the monte carlo analysis. This is a feature lacking in CADET which makes it advisable to utilize monte carlo simulation in a monitoring capacity, since it is always possible to obtain reasonably accurate performance projections by increasing the number of trials sufficiently.

The effective use of CADET and monte carlo analysis in concert can be demonstrated in a hypothetical trade-off study where two parameters, say α_1 and α_2, are to be varied over certain ranges to obtain optimal performance in some sense (to minimize rms terminal miss distance in the missile-target intercept problem, for example). As shown in Fig. 5.2-1, a few points in the parameter plane are chosen for careful CADET-monte carlo comparison (verification of CADET); then extensive performance curves are generated using CADET, from which the optimal values of α_1 and α_2 are chosen. If desired, the vicinity of the point of optimality can be studied using a few selected values of α_1 and α_2 and performing the required monte carlo simulations. Similar approaches can be used in studying sensitivity to nonlinear and random effects.
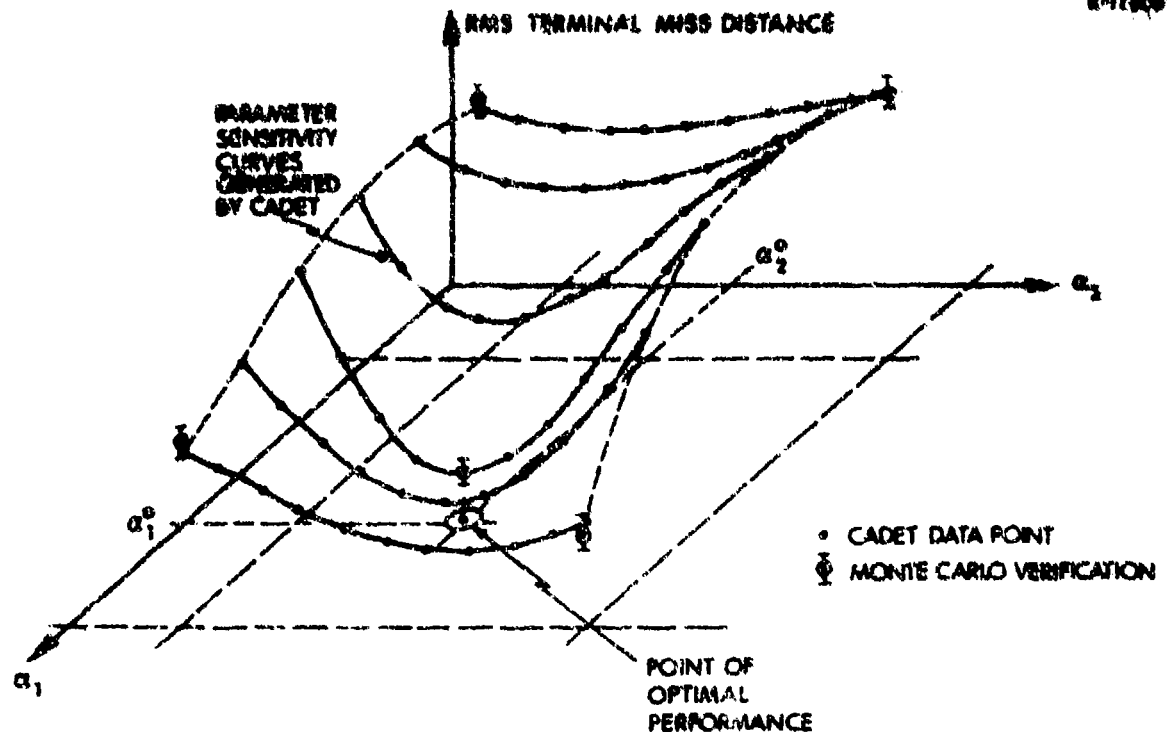
Figure 5.2-1   Illustration of CADET and Monte Carlo
Analysis in a Parameter Trade-Off Study

The overall philosophy of CADET usage, based on the str[
points of both CA ET and monte carlo simulation, is illustrated :
Fig. 5.2-2. The initial verification procedure is generally und[
taken for the "nominal system," i.e., for the system with nomina[
parameter values, and is of necessity quite meticulous. Thus
several hundred monte carlo trials may be performed, and if ther[
is reason to believe that the system is highly nonlinear -- so
that the system variables may be quite nongaussian -- it may be
necessary to investigate higher order moments or histograms to
decide whether more trials are needed in order to obtain a re-
liable statistical analysis. Once this phase has been complet[
satisfactorily, the CADET parameter sensitivity studies can then
be performed. Observe that the preliminary careful but time-
consuming monte carlo study is always required if accurate per-
formance statistics are to be obtained from monte carlo simulatio
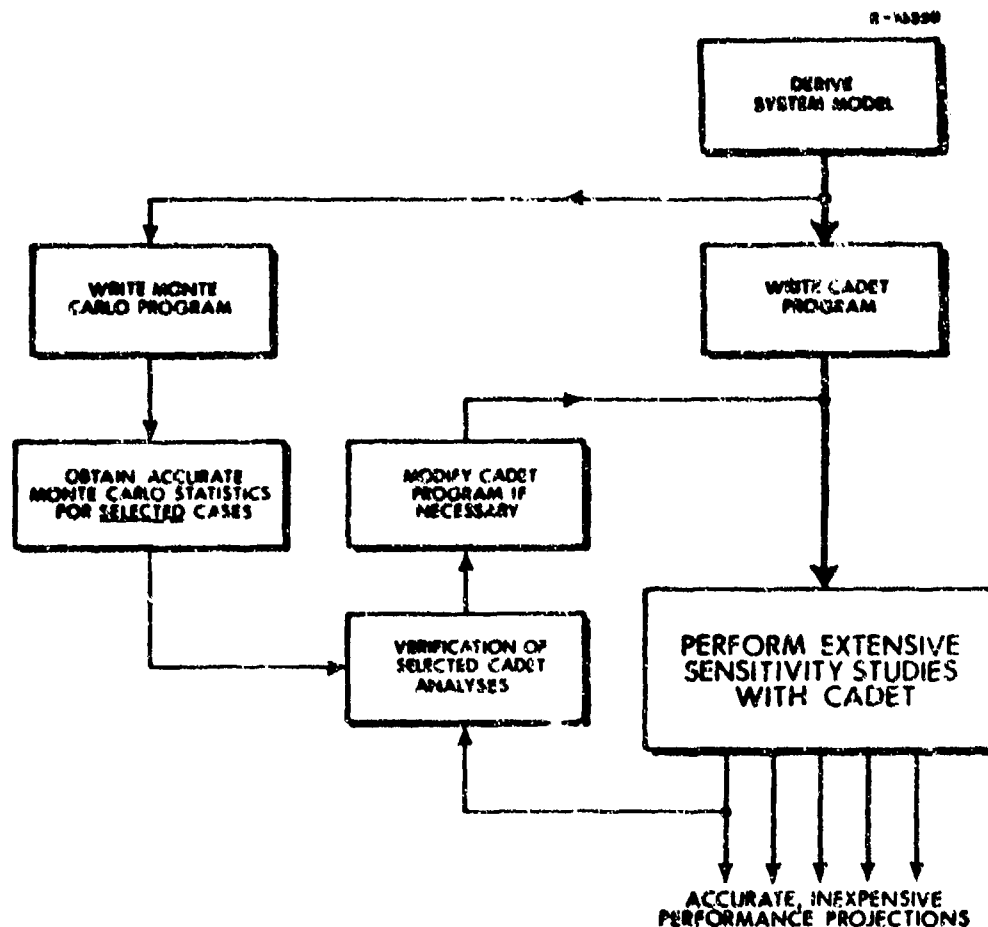
Figure 5.2-2   Philosophy of CADET Application

with high confidence. The use of these statistics to verify
CADET paves the way for efficiently performing a wide variety of
sensitivity studies. In the latter analyses, it may be advisable
to make comparisons with monte carlo results in selected cases to
reverify CADET accuracy. This approach mirrors that used in the
studies described in Refs. 1 to 4.

5.3 CADET DEVELOPMENT TO DATE: SUMMARY AND CONCLUSIONS

5.3.1 Summary

A major goal of the studies described in Refs. 1 to 4
was to extend the proven capability of the Covariance Analysis
DEscribing Function Technique -- CADET -- to provide accurate

performance projections for tactical missile guidance system models that are quite realistic -- i.e., that incorporate a number of significant nonlinear and random effects. The approach used to achieve this objective has entailed

- Verification of CADET performance projections by the use of selected monte carlo performance studies

- Investigation of the sensitivity of CADET analysis to deviation from the assumption that the state variables are jointly normal.

In these investigations, the following effects were treated:

Sources of Nonlinearity

- Guidance law
- Acceleration command limiting
- Aerodynamic effects (nonlinear airframe)
- Missile-target intercept geometry
- Coordinate transformations
- Range-dependent seeker noise sources
- Receiver/signal processing characteristics
- Seeker radome aberration
- Seeker mass imbalance
- Seeker gimbal Coulomb friction
- Seeker head restoring torques (nonlinear spring effects)

Random Effects

- Tracking sensor noise and measurement errors
- Range rate measurement error
- Target maneuvers
- Deviation of initial conditions from nominal values

Two aspects of the sensitivity problem have been considered in Chapter 4: the sensitivity of random input describing function

calculations to the probability density function of the nonlinearity input, and the calculation of approximate random input describing functions when it is inconvenient to use the exact result for the gaussian case.

5.3.2 Conclusions

The investigations described in Refs. 1 to 4 have indeed shown that CADET is an accurate and efficient tool for conducting statistical analyses of the performance of a tactical missile system including the effects of a number of significant nonlinear and random phenomena. The conclusions drawn from these studies can be summarized as follows:

- CADET has the demonstrated ability to capture the impact of all of the nonlinear effects listed above on guidance system performance. In all cases studied, CADET results are close to or within the 95% confidence limits of the monte carlo analysis for up to 500 trials. This degree of agreement was generally maintained even in the numerous instances where the nonlinearities were shown to have a marked deleterious effect on rms miss distance.

- Even in cases where the number of system states and nonlinearities is large, CADET shows a significant computational advantage over the monte carlo method: Between 10 and 30 CADET performance projections have been obtained for the same amount of computer time required by one accurate monte carlo study.

- There are certain highly nonlinear cases in which CADET analysis may be inadequate. Typically, these are situations in which a nonlinearity input is uncorrelated with its output; for a more complete discussion, refer to Section 4.2 and Appendix B. The Modified CADET methodology presented in Appendix B appears to offer a solution to this problem.

- Highly nongaussian system variables not only lead to inaccuracy in the CADET analysis, but also make the monte carlo method less reliable and reduce the meaningfulness of the basic statistical measures of system performance, the mean vector and covariance matrix.

- The value of the kurtosis, λ, (the fourth central moment of a density function divided by the variance squared) is a useful measure of the departure of the density of a random variable from the gaussian case It would thus be valuable to estimate this parameter for each nonlinearity input in the monte carlo analysis to help in appraising the accuracy of the monte carlo method and CADET.

In light of these and related findings, it is felt that confidence in the ability of CADET to provide accurate statistical analyses of complex nonlinear missile guidance systems with a number of random disturbances has been quite well established. Based on the diversity and complexity of the effects studied so far, it seems reasonable to anticipate that similar results will be obtained in applying CADET to a broad spectrum of problems modeled by nonlinear systems with random inputs. It is hoped that this handbook will facilitate the further extension of the usefulness of CADET, as well as permitting the direct application of the technique to the missile-target intercept problem.

APPENDIX A

A CATALOG OF RANDOM INPUT
DESCRIBING FUNCTIONS

In this appendix, we provide random input describing functions (ridf's) required for quasi-linear representations of a number of nonlinearities that are commonly associated with effects that may be incorporated in a realistic missile-target intercept model. The material is organized in order of increasing complexity; single-input nonlinearities are listed first, followed by two-input characteristics, and finally, selected three-input nonlinearities are considered. Two highly nonlinear guidance laws are also treated, to demonstrate results that have been successfully used in the CADET analysis of missile guidance system performance. For those results without explanatory notes, ridf's have been taken from Ref. 6 or directly obtained using the formulae given in Cases 1 to 3 of Section 4.3. The background and notation of this appendix and a number of useful examples are given in Chapter 4.

A.1 RIDF'S FOR SINGLE-INPUT NONLINEARITIES

General case: $y = f(v)$, $E\left[v\right] = m$, $E\left[(v-m)^2\right] = p = \sigma^2$

Quasi-linear representation: $y \cong \hat{f} + nr$, $r = v-m$

Definition of ridf's: $\hat{f} \triangleq E\left[f(v)\right] = \dfrac{1}{\sqrt{2\pi}\,\sigma} \int_{-\infty}^{\infty} f(v)\; e^{-\frac{1}{2}\left(\frac{v-m}{\sigma}\right)^2} \; dv$

$$n = \frac{\partial \hat{f}}{\partial m}$$

A.1.1 Simple Analytic Nonlinearities

$\underline{y = \sin(v)}$

$$\hat{f} = e^{-\frac{1}{2}p} \sin m$$

$$n = e^{-\frac{1}{2}p} \cos m \qquad (A.1\text{-}1)$$

$\underline{y = \cos(v)}$

$$\hat{f} = e^{-\frac{1}{2}p} \cos m$$

$$n = -e^{-\frac{1}{2}p} \sin m \qquad (A.1\text{-}2)$$

$\underline{y = v^2}$

$$\hat{f} = m^2 + p$$

$$n = 2m \qquad (A.1\text{-}3)$$

$\underline{y = v^3}$

$$\hat{f} = m(3p + m^2)$$

$$n = 3(p+m^2) \qquad (A.1\text{-}4)$$

$\underline{y = v^4}$

$$\hat{f} = m^4 + 6m^2 p + 3p^2$$

$$n = 4m(m^2 + 3p) \qquad (A.1\text{-}5)$$

$\underline{y = v^5}$

$$\hat{f} = m^5 + 10m^3 p + 15p^2 m$$

$$n = 5(m^4 + 6m^2 p + 3p^2) \qquad (A.1\text{-}6)$$

Results for higher powers can be obtained directly using the
relations given in Example 4 of Section 4.3.

A.1.2 **Nonlinearities Involving Sign (v) and Piecewise-Linear Characteristics**

Nonlinearities in this group require evaluations of $PF(w)$, $PI(w)$ and $G(w)$ given by

$$PF(w) = \frac{1}{\sqrt{2\pi}} \, e^{-\frac{1}{2}w^2}$$

$$PI(w) = \int_{-\infty}^{w} PF(\omega) \, d\omega \qquad\qquad (A.1\text{-}7)$$

$$G(w) = \int_{-\infty}^{w} PI(\omega) \, d\omega = wPI(w) + PF(w)$$

(For more details, see Example 3 of Section 4.3.) For convenient reference, the piecewise-linear gains listed below are depicted in Fig. A.1-1.

R-16240

(a) Ideal Relay (b) Ideal Limiter

(c) Linear Gain With Deadzone (d) Relay With Deadzone (e) Limiter With Deadzone
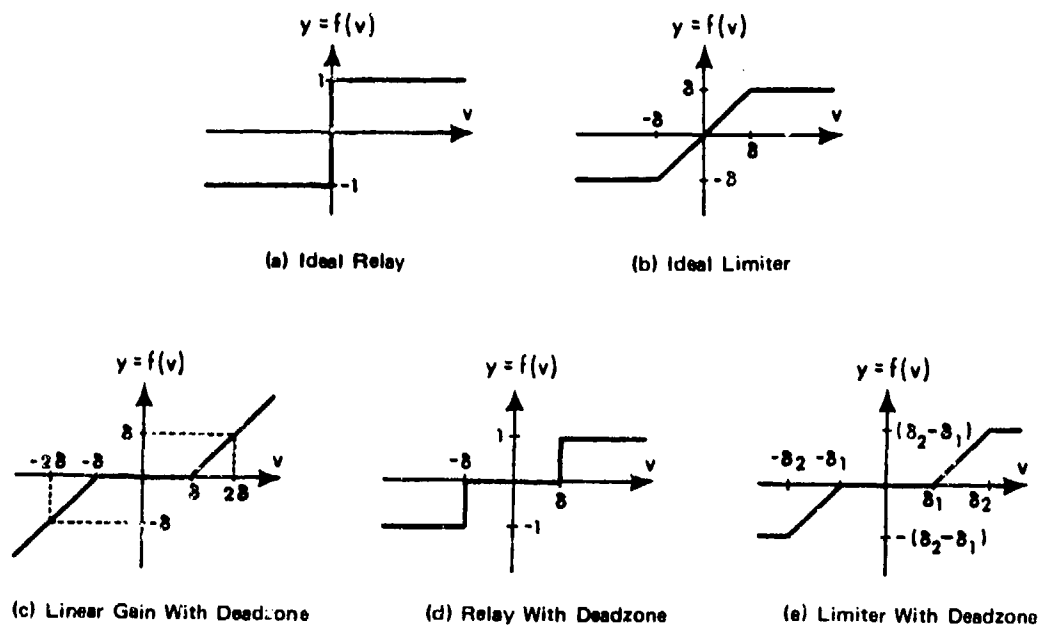
Figure A.1-1 Basic Piecewise-Linear Characteristics

Ideal Relay $\quad y = \text{sign}(v)$

$$\hat{f} = 2PI\left(\frac{m}{\sigma}\right) - 1$$

$$n = \frac{2}{\sigma} PF\left(\frac{m}{\sigma}\right)$$

$$(A.1-8)$$

Ideal Limiter

$$y = \begin{cases} v, & |v| \leq \delta \\ \delta \; \text{sign}(v), & |v| > \delta \end{cases}$$

$$\hat{f} = \sigma\left[G\left(\frac{\delta+m}{\sigma}\right) - G\left(\frac{\delta-m}{\sigma}\right)\right] - m$$

$$n = PI\left(\frac{\delta+m}{\sigma}\right) + PI\left(\frac{\delta-m}{\sigma}\right) - 1$$

$$(A.1-9)$$

Linear Gain
With Deadzone

$$y = \begin{cases} 0, & |v| \leq \delta \\ (|v|-\delta)\text{sign}(v), & |v| > \delta \end{cases}$$

$$\hat{f} = 2m - \sigma\left[G\left(\frac{\delta+m}{\sigma}\right) - G\left(\frac{\delta-m}{\sigma}\right)\right]$$

$$n = 2 - PI\left(\frac{\delta+m}{\sigma}\right) - PI\left(\frac{\delta-m}{\sigma}\right)$$

$$(A.1-10)$$

Relay With
Deadzone

$$y = \begin{cases} 0, & |v| \leq \delta \\ 1, & |v| > \delta \end{cases}$$

$$\hat{f} = PI\left(\frac{\delta+m}{\sigma}\right) - PI\left(\frac{\delta-m}{\sigma}\right)$$

$$n = \frac{1}{\sigma}\left[PF\left(\frac{\delta+m}{\sigma}\right) + PF\left(\frac{\delta-m}{\sigma}\right)\right]$$

$$(A.1-11)$$

Limiter With Deadzone

$$y = \begin{cases} 0 & , & |v| \le \delta_1 \\ (|v|-\delta_1)\,\text{sign}(v) & , & \delta_1 < |v| \le \delta_2 \\ (\delta_2-\delta_1)\,\text{sign}(v) & , & \delta_2 < |v| \end{cases}$$

$$\hat{f} = \sigma\left[\,\left(\frac{}{}\right) - G\left(\frac{\delta_2-m}{\sigma}\right)\right] - \sigma\left[G\left(\frac{\delta_1+m}{\sigma}\right) - G\left(\frac{\delta_1-m}{\sigma}\right)\right]$$

$$n = \text{PI}\left(\frac{\delta_2+m}{\sigma}\right) + \text{PI}\left(\frac{\delta_2-m}{\sigma}\right) - \text{PI}\left(\frac{\delta_1+m}{\sigma}\right) - \text{PI}\left(\frac{\delta_1-m}{\sigma}\right)$$

$$(A.1-12)$$

We observe that ridf's for a large number of more complicated piecewise-linear characteristics can be obtained by decomposing them into a linear combination of the basic nonlinearities shown in Fig. A.1-1. To cite two examples, a multi-level ideal symmetric quantizer can be expressed as the sum of several characteristics of the type portrayed in Fig. A.1-1d, and a change from unity gain to a gain of k at breakpoints $\pm\,\delta$ can be represented by a linear unity gain plus the characteristic of Fig. A.1-1c multiplied by (k-1). These procedures are demonstrated in Fig. A.1-2. From decompositions of this sort, the associated ridf's can be obtained from the results given in Eqs. (A.1-8) to (A.1-12) by simple addition; for the above examples, we obtain:

Five-level Symmetric Quantizer (Fig. A.1-2a)

$$\hat{f} = \text{PI}\left(\frac{\delta+2m}{2\sigma}\right) - \text{PI}\left(\frac{\delta-2m}{2\sigma}\right) + \text{PI}\left(\frac{3\delta+2m}{2\sigma}\right) - \text{PI}\left(\frac{3\delta-2m}{2\sigma}\right)$$

$$n = \frac{1}{\sigma}\left[\text{PF}\left(\frac{\delta+2m}{2\sigma}\right) + \text{PF}\left(\frac{\delta-2m}{2\sigma}\right) + \text{PF}\left(\frac{3\delta+2m}{2\sigma}\right) + \text{PF}\left(\frac{3\delta-2m}{2\sigma}\right)\right]$$

$$(A.1-13)$$

A-5

R-16239
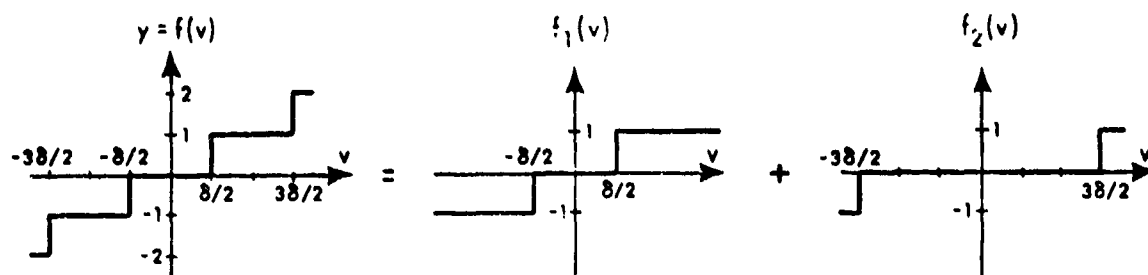
(a) Decomposition of a Five-Level Symmetric Quantizer
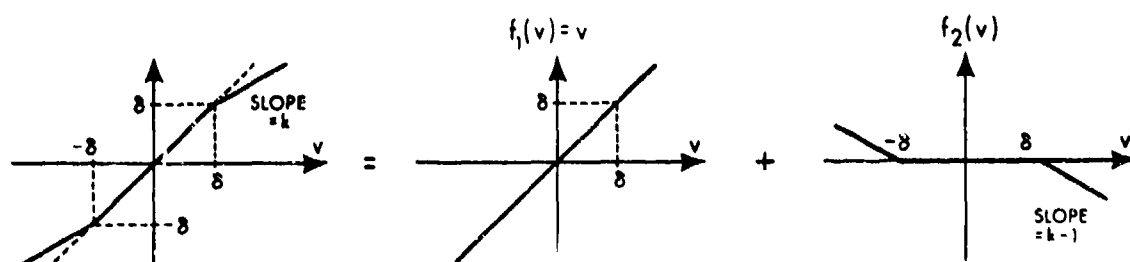
(b) Decomposition of a Gain-Changing Nonlinearity

Figure A.1-2   Decomposition of Complicated Piecewise-Linear Characteristics into Basic Components

Gain-Changing Nonlinearity (Fig. A.1-2b)

$$\hat{f} = m + (k-1)\left\{2m - \sigma\left[G\left(\frac{\delta+m}{\sigma}\right) - G\left(\frac{\delta-m}{\sigma}\right)\right]\right\}$$

$$n = 1 + (k-1)\left\{2 - PI\left(\frac{\delta+m}{\sigma}\right) - PI\left(\frac{\delta-m}{\sigma}\right)\right\}$$

(A.1-14)

The functions PF, PI and G (Eq. (A.1-7)) also occur in quasi-linearizing nonlinearities having the factor sign(v). Three common examples of this type of characteristic are

Absolute Value Function   y = v sign(v)

$$\hat{f} = 2\sigma G\left(\frac{m}{\sigma}\right) - m$$

$$n = 2PI\left(\frac{m}{\sigma}\right) - 1$$

(A.1-15)

Odd Square Law $\quad y = v^2 \text{ sign}(v)$

$$\hat{f} = 2m\sigma PF\left(\frac{m}{\sigma}\right) + (m^2 + \sigma^2)\left[2PI\left(\frac{m}{\sigma}\right) - 1\right]$$

(A.1-16)

$$n = 4\sigma PF\left(\frac{m}{\sigma}\right) + 2m\left[2PI\left(\frac{m}{\sigma}\right) - 1\right]$$

Exponential Saturation $\quad y = \left[1 - e^{-\alpha|v|}\right]\text{sign}(v)$

$$\hat{f} = 2PI\left(\frac{m}{\sigma}\right) + e^{\frac{1}{2}\alpha^2 p}\left\{e^{\alpha m}\left[1 - PI\left(\alpha\sigma + \frac{m}{\sigma}\right)\right] - e^{-\alpha m}\left[1 - PI\left(\alpha\sigma - \frac{m}{\sigma}\right)\right]\right\} - 1$$

$$n = \frac{2}{\sigma}PF\left(\frac{m}{\sigma}\right) + \alpha e^{\frac{1}{2}\alpha^2 p}\left\{e^{\alpha m}\left[1 - PI\left(\alpha\sigma + \frac{m}{\sigma}\right) - \frac{1}{\alpha\sigma}PF\left(\alpha\sigma + \frac{m}{\sigma}\right)\right]\right.$$

$$\left. + e^{-\alpha m}\left[1 - PI\left(\alpha\sigma - \frac{m}{\sigma}\right) - \frac{1}{\alpha\sigma}PF\left(\alpha\sigma - \frac{m}{\sigma}\right)\right]\right\}$$

(A.1-17)

These results complete the catalog of ridf's for single-input nonlinearities.

A.2 RIDF'S FOR TWO-INPUT NONLINEARITIES

General case: $\quad y = f(v_1, v_2), \quad E\left[v_i\right] = m_i, \quad r_i = v_i - m_i$

$$E\left[\underline{r}\ \underline{r}^T\right] = \begin{bmatrix} p_{11} & p_{12} \\ p_{12} & p_{22} \end{bmatrix} = \begin{bmatrix} \sigma_1^2 & \rho\sigma_1\sigma_2 \\ \rho\sigma_1\sigma_2 & \sigma_2^2 \end{bmatrix}$$

Quasi-linear representation: $\quad y = \hat{f} + \underline{n}^T\underline{r}$

$$= \hat{f} + n_1 r_1 + n_2 r_2$$

<u>Definition of ridf's:</u>

$$\hat{f} = E\left[f(v_1,v_2)\right] = \frac{1}{2\pi\sigma_1\sigma_2(1-\rho^2)^{\frac{1}{2}}} \int_{-\infty}^{\infty} \int_{-\infty}^{\infty} f(v_1,v_2)\exp\left\{-\frac{1}{2(1-\rho^2)}\right.$$

$$\left. \left[\left(\frac{r_1}{\sigma_1}\right)^2 - 2\rho\,\frac{r_1 r_2}{\sigma_1\sigma_2} + \left(\frac{r_2}{\sigma_2}\right)^2\right]\right\} dv_1 dv_2$$

$$n_1 = \frac{\partial\hat{f}}{\partial m_1}$$

$$n_2 = \frac{\partial\hat{f}}{\partial m_2}$$

A.2.1   Simple Analytic Nonlinearities

Most of the results of Eqs. (A.2-1) to (A.2-8) were reported in Ref. 3.

<u>$y = v_1 v_2$</u>

$$\hat{f} = m_1 m_2 + p_{12}$$

$$n_1 = m_2 \tag{A.2-1}$$

$$n_2 = m_1$$

<u>$y = v_1 v_2^2$</u>

$$\hat{f} = m_1(m_2^2 + p_{22}) + 2m_2 p_{12}$$

$$n_1 = (m_2^2 + p_{22}) \tag{A.2-2}$$

$$n_2 = 2(m_1 m_2 + p_{12})$$

$\underline{y = v_1 v_2^3}$

$$\hat{f} = m_1 m_2 (m_2^2 + 3p_{22}) + 3p_{12}(m_2^2 + p_{22})$$

$$n_1 = m_2(m_2^2 + 3p_{22}) \tag{A.2-3}$$

$$n_2 = 3m_1(m_2^2 + p_{22}) + 6m_2 p_{12}$$

$\underline{y = v_1^2 v_2^2}$

$$\hat{f} = (m_1^2 + p_{11})(m_2^2 + p_{22}) + 2p_{12}(2m_1 m_2 + p_{12})$$

$$n_1 = 2m_1(m_2^2 + p_{22}) + 4m_2 p_{12} \tag{A.2-4}$$

$$n_2 = 2m_2(m_1^2 + p_{11}) + 4m_1 p_{12}$$

$\underline{y = v_1 \cos v_2}$

$$\hat{f} = e^{-\frac{1}{2}p_{22}}(m_1 \cos m_2 - p_{12} \sin m_2)$$

$$n_1 = e^{-\frac{1}{2}p_{22}} \cos m_2 \tag{A.2-5}$$

$$n_2 = -e^{-\frac{1}{2}p_{22}}(m_1 \sin m_2 + p_{12} \cos m_2)$$

$\underline{y = v_1 \sin v_2}$

$$\hat{f} = e^{-\frac{1}{2}p_{22}}(m_1 \sin m_2 + p_{12} \cos m_2)$$

$$n_1 = e^{-\frac{1}{2}p_{22}} \sin m_2 \tag{A.2-6}$$

$$n_2 = e^{-\frac{1}{2}p_{22}}(m_1 \cos m_2 - p_{12} \sin m_2)$$

$v_1^2 \cos v_2$

$$\hat{f} = e^{-\frac{1}{2}p_{22}} \left[\left(m_1^2 + p_{11} - p_{12} \right) \cos m_2 - 2m_1 p_{12} \sin m_2 \right]$$

$$n_1 = e^{-\frac{1}{2}p_{22}} \left(2m_1 \cos m_2 - 2p_{12} \sin m_2 \right) \tag{A.2-7}$$

$$n_2 = -e^{-\frac{1}{2}p_{22}} \left[\left(m_1^2 + p_{11} - p_{12} \right) \sin m_2 + 2m_1 p_{12} \cos m_2 \right]$$

$v_1^2 \sin v_2$

$$\hat{f} = e^{-\frac{1}{2}p_{22}} \left[2m_1 p_{12} \cos m_2 + \left(m_1^2 + p_{11} - p_{12} \right) \sin m_2 \right]$$

$$n_1 = e^{-\frac{1}{2}p_{22}} \left[2p_{12} \cos m_2 + 2m_1 \sin m_2 \right] \tag{A.2-8}$$

$$n_2 = e^{-\frac{1}{2}p_{22}} \left[-2m_1 p_{12} \sin m_2 + \left(m_1^2 + p_{11} - p_{12} \right) \cos m_2 \right]$$

Results for nonlinearities involving higher powers of input variables can be obtained directly using the relations of Case 2 of Section 4.3. For powers or products of trigonometric functions, e.g., $v_1 \sin^2 v_2$, the use of trigonometric identities, as

$$\sin^2 v_2 = \frac{1}{2} (1 - \cos 2v_2)$$

permit the direct use of results given in Eqs. (A.2-5) to (A.2-8).

A.2.2 Analytic Nonlinearities Without Closed-Form Gaussian ridf's

The quasi-linearization of the range,

$$r = \sqrt{m_x^2 + y^2}$$

is treated in detail in Section 4.5. Note that it was assumed that $x \approx m_x$, i.e., the down-range component of the missile-target separation is essentially deterministic, as is true for head-on intercepts (Fig. 3.5-1). In this case, the range is a function of one random variable, y. We further noted that the most effective approximate ridf for this nonlinearity was obtained by using the triangular distribution for y (Table C.2-1); this result is given in Eq. (4.5-10).

In the seeker noise model, Section 3.6-1, related nonlinearities arise in the range-dependent components of the noise. Thus approximate ridf's for the following two nonlinearities were obtained in Ref. 4, based on the triangular distribution for y:

Range Proportional Noise $y = v_1 \sqrt{m_x^2 + v_2^2}$

$$\hat{f} \approx \frac{m_1}{v} \operatorname{sign}(m_x) \left[\sqrt{1+v^2} + v^2 \log\left(\frac{1+\sqrt{1+v^2}}{v}\right) + \frac{4}{\sqrt{6}}\left(v^3 - (1+v^2)^{3/2}\right)\right]$$

$$n_1 = \frac{\hat{f}}{m_1} \tag{A.2-9}$$

$$n_2 \approx \sqrt{\frac{2}{3}} \, p_{12} \left[(1+4v^2)\sqrt{1+v^2} - 4v^3 - 3v^2 \log\left(\frac{1+\sqrt{1+v^2}}{v}\right)\right]$$

where v is an auxiliary parameter given by

$$v \triangleq \frac{|m_x|}{\sqrt{6}\,\sigma_2} \tag{A.2-10}$$

Inverse Range Proportional Noise $\quad y = \dfrac{v_1}{\sqrt{m_x^2 + v_2^2}}$

$$\hat{f} \cong \sqrt{\frac{2}{3}} \ \frac{m_1}{\sigma_2} \left[\log \left(\frac{1 + \sqrt{1+v^2}}{v} \right) + v - \sqrt{1+v^2} \right]$$

$$n_1 = \frac{\hat{f}}{m_1} \tag{A.2-11}$$

$$n_2 \cong - \sqrt{\frac{2}{3}} \ \frac{p_{12}}{\sigma_2^3} \left[\log \left(\frac{1 + \sqrt{1+v^2}}{v} \right) + 2 \left(v - \sqrt{1+v^2} \right) \right]$$

where v is given in Eq. (A.2-10).

A third nonlinearity that is not tractable for gaussian random variables is the inverse tangent function, which is required in obtaining the line-of-sight angle from the cartesian coordinate representation of the missile-target separation, viz.

$$\theta = f(v_1, v_2) = \tan^{-1} \left(\frac{v_1}{v_2} \right) \tag{A.2-12}$$

The approximate ridf's for this nonlinearity were also derived in Ref. 4, using the truncated expansion technique demonstrated in Section 4.4, as follows:

Inverse Tangent $\quad y = \tan^{-1}(v_1/v_2)$

$$\hat{f} \cong \tan^{-1} \left(\frac{m_1}{m_2} \right) + \frac{1}{\left(m_1^2 + m_2^2 \right)^2} \left[m_1 m_2 (p_{22} - p_{11}) + \left(m_1^2 - m_2^2 \right) p_{12} \right]$$

$$n_1 \cong \frac{m_2}{m_1^2 + m_2^2} \tag{A.2-13}$$

$$n_2 \cong \frac{-m_1}{m_1^2 + m_2^2}$$

These results conclude the presentation of ridf's for two-input nonlinearities.

A.3   RIDF'S FOR SELECTED THREE-INPUT NONLINEARITIES

The following results are useful for nonlinear airframe models as described in Section 3.4; many of these ridf's were first reported in Ref. 3.

$$\underline{y = v_1 v_2 v_3}$$

$$\hat{f} = m_1 m_2 m_3 + m_1 p_{23} + m_2 p_{13} + m_3 p_{12}$$

$$n_1 = m_2 m_3 + p_{23}$$

$$n_2 = m_1 m_3 + p_{13} \tag{A.3-1}$$

$$n_3 = m_1 m_2 + p_{12}$$

$$\underline{y = v_1 v_2 v_3^2}$$

$$\hat{f} = (m_3^2 + p_{33})(m_1 m_2 - p_{12}) + 2m_3(m_1 p_{23} + m_2 p_{13}) + 2p_{13}p_{23}$$

$$n_1 = m_2(m_3^2 + p_{33}) + 2m_3 p_{23}$$

$$n_2 = m_1(m_3^2 + p_{33}) + 2m_3 p_{13} \tag{A.3-2}$$

$$n_3 = 2(m_1 m_2 + p_{12})m_3 + 2(m_1 p_{23} + m_2 p_{13})$$

$$\underline{y = v_1 v_2 v_3^3}$$

$$\hat{f} = m_3(m_3^2 + p_{33})(m_1 m_2 + p_{12}) + 3(m_3^2 + p_{33})(m_1 p_{23} + m_2 p_{13}) + 6m_3 p_{13}p_{23}$$

$$n_1 = m_2 m_3(m_3^2 + 3p_{33}) + 3p_{23}(m_3^2 + p_{33}) \tag{A.3-3}$$

$$n_2 = m_1 m_3 (m_3^2 + 3p_{33}) + 3p_{13}(m_3^2 + p_{33})$$

$$n_3 = 3(m_3^2 + p_{33})(m_1 m_2 + p_{12}) + 6(m_1 m_3 p_{23} + m_2 m_3 p_{13} + p_{13} p_{23})$$

(A.3-3)(Cont.)

$\underline{y = v_1 v_2^2 v_3^2}$

$$\hat{f} = \left[m_1(m_2^2 + p_{22}) + 2m_2 p_{12} \right] (m_3^2 + p_{33}) + 2m_3 p_{13}(m_2^2 + p_{22})$$

$$+ 2m_1 p_{23}(2m_2 m_3 + p_{23}) + 4p_{23}(m_2 p_{13} + m_3 p_{12})$$

$$n_1 = (m_2^2 + p_{22})(m_3^2 + p_{33}) + 2p_{23}(2m_2 m_3 + p_{23})$$

(A.3-4)

$$n_2 = 2(m_1 m_2 + p_{12})(m_3^2 + p_{33}) + 4(m_2 m_3 p_{13} + m_1 m_3 p_{23} + p_{13} p_{23})$$

$$n_3 = 2(m_1 m_3 + p_{13})(m_2^2 + p_{22}) + 4(m_2 m_3 p_{12} + m_1 m_2 p_{23} + p_{12} p_{23})$$

Expressions for still higher powers of v_1, v_2 and v_3 can be obtained by extending the techniques given in Section 4.3.

The following nonlinearities are required for 3-dimensional coordinate transformations:

$\underline{y = v_1 \sin v_2 \sin v_3}$

$$\hat{f} = \frac{1}{2} e^{-\frac{1}{2}(p_{22} + p_{33})} \left[e^{p_{23}} \left\{ m_1 \cos(m_2 - m_3) - (p_{12} - p_{13})\sin(m_2 - m_3) \right\} \right.$$

$$\left. - e^{-p_{23}} \left\{ m_1 \cos(m_2 + m_3) - (p_{12} + p_{13})\sin(m_2 + m_3) \right\} \right]$$

$$n_1 = \frac{1}{2} e^{-\frac{1}{2}(p_{22} + p_{33})} \left[e^{p_{23}} \cos(m_2 - m_3) - e^{-p_{23}} \cos(m_3 + m_3) \right]$$

(A.3-5)

A-14

$$n_2 = -\frac{1}{2} e^{-\frac{1}{2}(p_{22}+p_{33})}\left[e^{p_{23}}\Big\{m_1\sin(m_2-m_3)+(p_{12}-p_{13})\cos(m_2-m_3)\Big\}\right.$$

$$\left. -e^{-p_{23}}\Big\{m_1\sin(m_2+m_3)+(p_{12}+p_{13})\cos(m_2+m_3)\Big\}\right]$$

$$n_3 = \frac{1}{2} e^{-\frac{1}{2}(p_{22}+p_{33})}\left[e^{p_{23}}\Big\{m_1\sin(m_2-m_3)+(p_{12}-p_{13})\cos(m_2-m_3)\Big\}\right.$$

$$\left. +e^{-p_{23}}\Big\{m_1\sin(m_2+m_3)+(p_{12}+p_{13})\cos(m_2+m_3)\Big\}\right]$$

$$(A.3-5)(Cont.)$$

$$\underline{y = v_1 \cos v_2 \cos v_3}$$

$$\hat{f} = \frac{1}{2} e^{-\frac{1}{2}(p_{22}+p_{33})}\left[e^{p_{23}}\Big\{m_1\cos(m_2-m_3)-(p_{12}-p_{13})\sin(m_2-m_3)\Big\}\right.$$

$$\left. +e^{-p_{23}}\Big\{m_1\cos(m_2+m_3)-(p_{12}+p_{13})\sin(m_2+m_3)\Big\}\right]$$

$$n_1 = \frac{1}{2} e^{-\frac{1}{2}(p_{22}+p_{33})}\left[e^{p_{23}}\cos(m_2-m_3)+e^{-p_{23}}\cos(m_2+m_3)\right]$$

$$n_2 = -\frac{1}{2} e^{-\frac{1}{2}(p_{22}+p_{33})}\left[e^{p_{23}}\Big\{m_1\sin(m_2-m_3)+(p_{12}-p_{13})\cos(m_2-m_3)\Big\}\right.$$

$$\left. +e^{-p_{23}}\Big\{m_1\sin(m_2+m_3)+(p_{12}+p_{13})\cos(m_2+m_3)\Big\}\right]$$

$$n_3 = \frac{1}{2} e^{-\frac{1}{2}(p_{22}+p_{33})}\left[e^{p_{23}}\Big\{m_1\sin(m_2-m_3)+(p_{12}-p_{13})\cos(m_2-m_3)\Big\}\right.$$

$$\left. -e^{-p_{23}}\Big\{m_1\sin(m_2+m_3)+(p_{12}+p_{13})\cos(m_2+m_3)\Big\}\right]$$

$$(A.3-6)$$

A-15

$$\underline{y = v_1 \sin v_2 \cos v_3}$$

$$\hat{f} = \frac{1}{2} e^{-\frac{1}{2}(p_{22}+p_{33})} \left[e^{p_{23}} \left\{ m_1 \sin(m_2-m_3) + (p_{12}-p_{13})\cos(m_2-m_3) \right\} \right.$$

$$\left. + e^{-p_{23}} \left\{ m_1 \sin(m_2+m_3) + (p_{12}+p_{13})\cos(m_2+m_3) \right\} \right]$$

$$n_1 = \frac{1}{2} e^{-\frac{1}{2}(p_{22}+p_{33})} \left[e^{p_{23}} \sin(m_2-m_3) + e^{-p_{23}} \sin(m_2+m_3) \right]$$

$$n_2 = \frac{1}{2} e^{-\frac{1}{2}(p_{22}+p_{33})} \left[e^{p_{23}} \left\{ m_1 \cos(m_2-m_3) - (p_{12}-p_{13})\sin(m_2-m_3) \right\} \right.$$

$$\left. + e^{-p_{23}} \left\{ m_1 \cos(m_2+m_3) - (p_{12}+p_{13})\sin(m_2+m_3) \right\} \right]$$

$$n_3 = \frac{1}{2} e^{-\frac{1}{2}(p_{22}+p_{33})} \left[e^{p_{23}} \left\{ -m_1 \cos(m_2-m_3) + (p_{12}-p_{13})\sin(m_2-m_3) \right\} \right.$$

$$\left. + e^{-p_{23}} \left\{ m_1 \cos(m_2+m_3) - (p_{12}+p_{13})\sin(m_2+m_3) \right\} \right]$$

$$(A \ 3-7)$$

The last result is obtained in Example 6 of Section 4.3; the first two nonlinearities may be quasi-linearized by the same technique illustrated in that example.

A.4 RIDF'S FOR GUIDANCE LAW NONLINEARITIES

A.4.1 Proportional Guidance

Referring to Eqs. (3.5-6) and (3.5-8), the acceleration command is the output of a limiter whose input is a highly

nonlinear function of six system variables, viz.

$$a_c = f(a_1\phi_1 + a_2\phi_2 + a_3v_1) \triangleq f(\phi') \qquad (A.4-1)$$

where the components ϕ_1 and ϕ_2 are given by

$$\phi_1 = v_1 v_6$$

$$\phi_2 = v_1 \frac{\cos(v_2+\theta)}{\cos(v_3-\theta)} \qquad (A.4-2)$$

The latter equation can be expressed in terms of system state variables by substituting the LOS angle relation,

$$\theta = \tan^{-1} \frac{v_4}{v_5}$$

to obtain

$$\phi_2 = v_1 \frac{v_5\cos(v_2)-v_4\sin(v_2)}{v_5\cos(v_3)+v_4\sin(v_3)} \qquad (A.4-3)$$

Assuming that the input to the limiter, ϕ' in Eq.(A.4-1), is nearly gaussian, we quasi-linearize the acceleration command using Eq. (A.1-9),

$$a_c \cong \hat{f} + nr \qquad (A.4-4)$$

where r is the random component of ϕ', and

$$\hat{f} = 2m - \sigma \left[G\left(\frac{a_{max}+m}{\sigma}\right) - G\left(\frac{a_{max}-m}{\sigma}\right) \right] \qquad (A.4-5)$$

$$n = 2 - PI\left(\frac{a_{max}+m}{\sigma}\right) - PI\left(\frac{a_{max}-m}{\sigma}\right)$$

where m and σ are the mean and standard deviation of ϕ', respectively.

A-17

Next, we must obtain the statistics of ϕ', i.e., m and σ, for use in Eq. (A.4-5); to do this, consider the three constituents given in Eq. (A.4-1): The third term is linear, thus presenting no problem, and for the product of variables, ϕ_1 of Eq. (A.4-2), we use Eq. (A.2-1) to obtain

$$\hat{\phi}_1 = m_1 m_6 + p_{16}$$

$$n_1^{(1)} = m_6 \qquad\qquad\qquad\qquad\qquad \text{(A.4-6)}$$

$$n_6^{(1)} = m_1$$

The second term, ϕ_2 in Eq. (A.4-2), is impossible to quasi-linearize exactly in closed form under the gaussian assumption; thus we use a generalization of the truncated series expansion approach discussed in Section 4.5 (Eq. (4.5-3)):

$$\hat{\phi}_2 = \phi_2(m_1, m_2, \ldots, m_5) + \frac{1}{2} \sum_{i=1}^{5} \sum_{j=1}^{5} \frac{\partial^2 \phi_2}{\partial m_i \partial m_j} \; p_{ij} \quad \text{(A.4-7)}$$

$$n_i^{(2)} = \frac{\partial \phi_2(m_1, m_2, \ldots, m_5)}{\partial m_i}, \qquad i = 1, 2, \ldots, 5 \quad \text{(A.4-8)}$$

Listing the partial derivatives called for in Eq. (A.4-8) requires the introduction of some auxiliary notation:

$$\psi_1 = m_5 \cos m_2 - m_1 \sin m_2$$

$$\psi_2 = m_5 \cos m_3 + m_4 \sin m_3$$

$$\qquad\qquad\qquad\qquad\qquad\qquad\qquad \text{(A.4-9)}$$

$$\psi_3 = -m_5 \sin m_2 - m_4 \cos m_2$$

$$\psi_4 = -m_5 \sin m_3 + m_4 \cos m_3$$

In terms of these expressions, the quantities required to evaluate Eq. (A.4-8) can be shown to be

$$\phi_2(m_1, m_2, \ldots, m_5) = m_1 \frac{\psi_1}{\psi_2}$$

$$\frac{\partial \phi_2}{\partial m_1} = \frac{\psi_1}{\psi_2} \cong n_1^{(2)}$$

$$\frac{\partial \phi_2}{\partial m_2} = \frac{\psi_3}{\psi_2} m_1 \cong n_2^{(2)}$$

$$\frac{\partial \phi_2}{\partial m_3} = -\frac{\psi_1 \psi_4}{\psi_2^2} m_1 \cong n_3^{(2)}$$

$$\frac{\partial \phi_2}{\partial m_4} = -\frac{m_1 m_5}{\psi_2^2} \sin(m_2 + m_3) \cong n_4^{(2)}$$

$$\frac{\partial \phi_2}{\partial m_5} = \frac{m_1 m_4}{\psi_2^2} \sin(m_2 + m_3) \cong n_5^{(2)} \qquad\qquad (A.4\text{-}10)$$

$$\frac{\partial^2 \phi_2}{\partial m_1^2} = 0$$

$$\frac{\partial^2 \phi_2}{\partial m_1 \partial m_2} = \frac{\psi_3}{\psi_2}$$

$$\frac{\partial^2 \phi_2}{\partial m_1 \partial m_3} = -\frac{\psi_1 \psi_4}{\psi_2^2}$$

$$\frac{\partial^2 \phi_2}{\partial m_1 \partial m_4} = -\frac{m_5}{\psi_2^2} \sin(m_2 + m_3)$$

$$\frac{\partial^2 \phi_2}{\partial m_1 \partial m_5} = \frac{m_4}{\psi_2^2} \sin(m_2 + m_3)$$

$$\frac{\partial^2 \phi_2}{\partial m_2^2} = -\frac{\psi_1}{\psi_2} m_1$$

$$\frac{\partial^2 \phi_2}{\partial m_2 \partial m_3} = -\frac{\psi_3 \psi_4}{\psi_2^2} m_1$$

$$\frac{\partial^2 \phi_2}{\partial m_2 \partial m_4} = -\frac{m_1 m_5}{\psi_2^2} \cos(m_2 + m_3)$$

$$\frac{\partial^2 \phi_2}{\partial m_2 \partial m_5} = \frac{m_1 m_4}{\psi_2^2} \cos(m_2 + m_3)$$

$$\frac{\partial^2 \phi_2}{\partial m_3^2} = \frac{\psi_1 m_1}{\psi_2^3} \left(\psi_2^2 + 2\psi_4^2\right)$$

(A.4-10)(Cont.)

$$\frac{\partial^2 \phi_2}{\partial m_3 \partial m_4} = \frac{m_1 m_5}{\psi_2^3} \left(\psi_4 \sin(m_2 + m_3) - \psi_1\right)$$

$$\frac{\partial^2 \phi_2}{\partial m_3 \partial m_5} = \frac{m_1 m_4}{\psi_2^3} \left(\psi_4 \sin(m_2 + m_3) - \psi_1\right)$$

$$\frac{\partial^2 \phi_2}{\partial m_4^2} = 2 \frac{m_1 m_5}{\psi_2^3} \sin(m_3) \sin(m_2 + m_3)$$

$$\frac{\partial^2 \phi_2}{\partial m_4 \partial m_5} = -\frac{m_1}{\psi_2^3} \left(\psi_2 - 2m_5 \cos(m_3)\right) \sin(m_2 + m_3)$$

$$\frac{\partial^2 \phi_2}{\partial m_5^2} = -\frac{2m_1 m_4}{\psi_2^3} \cos(m_3) \sin(m_2 + m_3)$$

Returning to Eq. (A.4-1), we have

$$m = a_1\hat{\phi}_1 + a_2\hat{\phi}_2 + a_3 m_1 \qquad\text{(A.4-11)}$$

where $\hat{\phi}_1$ and $\hat{\phi}_2$ are given in Eqs. (A.4-7) and (A.4-8). The random component of ϕ' can be expressed in terms of the quasi-linear gains in the same equations to be

$$r = \begin{bmatrix} r_1 & r_2 & \cdots r_6 \end{bmatrix} \begin{bmatrix} a_1 n_1^{(1)} + a_2 n_1^{(2)} + a_3 \\[6pt] a_2 n_2^{(2)} \\[6pt] a_2 n_3^{(2)} \\[6pt] a_2 n_4^{(2)} \\[6pt] a_2 n_5^{(2)} \\[6pt] a_1 n_6^{(1)} \end{bmatrix}$$

$$\triangleq \underline{r}^T \underline{b} \qquad\text{(A.4-12)}$$

Since r is a quasi-linear combination of the random components of the six variables v_i, the variance is approximately

$$\sigma^2 = E\left[r^2\right] \approx E\left[\underline{b}^T \underline{r}\, \underline{r}^T \underline{b}\right]$$

$$= \underline{b}^T P \underline{b} \qquad\text{(A.4-13)}$$

Given the statistics m and σ required in Eq. (A.4-5), the quasi-linearization of Eq. (A.4-1) is completed as follows: We express a_c as a mean $\hat{f}$ plus the inner product of a vector of ridf's with the random vector,

$$a_c = \hat{f} + \underline{n}_a^T\, \underline{r} \qquad\text{(A.4-14)}$$

The quantity $\hat{f}$ is specified in Eqs. (A.4-6) and (A.4-11) to (A.4-13), and by inspection

$$\underline{n}_a = n\underline{b} \qquad\qquad (A.4-15)$$

where n is given in Eq. (A.4-6). The foregoing describing function development was originally performed and verified in Ref. 4; a more complete discussion of its basis is given in that work.

The approach outlined above in Eqs. (A.4-1) to (A.4-15) considers a nonlinearity of the form

$$a_c = f\left(\phi'(v_1, v_2, \ldots, v_6)\right)$$

i.e., a nonlinear function of a nonlinearity. Because it is essentially impossible to quasi-linearize this relation as a whole, we have first quasi-linearized ϕ' to obtain the statistics m and σ necessary to calculate the ridf's for $f(\phi')$, Eq. (A.4-6), then "cascaded the ridf's" for the random part in arriving at Eq. (A.4-14). While this is not a completely rigorous procedure, we must rely on a priori knowledge that in the guidance law, ϕ' can reasonably be assumed to be nearly gaussian. In this situation, the above technique adequately represents the guidance law nonlinear effects.

A.4.2 Digital Guidance

A major source of nonlinearity in the estimation algorithm of the guidance module is embodied in the range dependence of the Kalman filter gain vector. Referring to the development of Section 3.5.2, we combine Eqs. (3.5-15), (3.5-16), (3.5-18) and (3.5-22) to arrive at the nonlinear difference equation

$$\underline{\hat{x}}_f(t_k^+) = \underline{\hat{x}}_f(t_k) + \underline{p}\ \psi(r) \left[z(t_k) - \frac{x_{f_1}(t_k)}{r} \right] \qquad (A.4-16)$$

The time-varying vector $\underline{p}$ is comprised of the first column of the filter covariance matrix P_f (Eqs. (3.5-19) and (3.5-23)), ψ is given by

$$\psi(r) = \frac{r}{\left(p_{f_{11}}+\sigma_1^2\right) + \sigma_3^2 r^2 + \sigma_2^2 r^4} \tag{A.4-17}$$

with $p_{f_{11}}$ the first diagonal element of P_f and $\sigma_1, \sigma_2, \sigma_3$ specifying the rms seeker noise levels, and r is the present range,

$$r = \sqrt{x^2(t_k) + y^2(t_k)} \tag{A.4-18}$$

Thus from Eq. (A.4-16) we see that the first nonlinearity which must be quasi-linearized in order to study the nonlinear implementation of the filtering algorithm is of the form

$$f(v_1, v_2, v_3) = v_1\psi(r) = \frac{v_1\sqrt{v_2^2+v_3^2}}{\alpha_1 + \alpha_2(v_2^2+v_3^2) + \alpha_3(v_2^2+v_3^2)^2} \tag{A.4-19}$$

where v_1 represents the measurement z (which is typically a linear combination of system state variables; cf. Fig. 3.5-5), v_2 and v_3 correspond to x and y, and the parameters α_i correspond to the coefficients in the denominator of ψ (Eq.(A.4-17)) in the obvious way.

As in the preceeding case (the proportional guidance law, Eq. (A.4-1)), the nonlinearity in Eq. (A.4-19) is too complicated to permit the derivation of exact ridf's. We thus again resort to the truncated series expansion technique derived in Section 4.5:

$$\hat{f} \approx f(\underline{m}) + \frac{1}{2}\sum_{j=1}^{3}\sum_{k=1}^{3}\frac{\partial^2 f(\underline{m})}{\partial m_j \partial m_k}p_{jk}$$

$$n_j \cong \frac{\partial f(\underline{m})}{\partial m_j} , \qquad j = 1,2,3 \tag{A.4-20}$$

The details required to complete the quasi-linearization of f are the partial derivatives indicated in Eq. (A.4-20):

$$f = \frac{m_1\sqrt{m_2^2+m_3^2}}{\alpha_1+\alpha_2(m_2^2+m_3^2)+\alpha_3(m_2^2+m_3^2)^2} \triangleq \frac{m_1 m_r}{d(m_r)} \qquad (A.4\text{-}21)$$

$$n_1 \approx \frac{m_r}{d(m_r)}$$

$$n_2 \approx \frac{m_1 m_2 (\alpha_1 - \alpha_2 m_r^2 - 3\alpha_3 m_r^4)}{m_r d^2(m_r)} \qquad (A.4\text{-}22)$$

$$n_3 \approx \frac{m_1 m_3 (\alpha_1 - \alpha_2 m_r^2 - 3\alpha_3 m_r^4)}{m_r d^2(m_r)}$$

$$\frac{\partial^2 f}{\partial m_1^2} = 0$$

$$\frac{\partial^2 f}{\partial m_1 \partial m_2} = \frac{m_2 (\alpha_1 - \alpha_2 m_r^2 - 3\alpha_3 m_r^4)}{m_r d^2(m_r)}$$

$$\frac{\partial^2 f}{\partial m_1 \partial m_3} = \frac{m_3 (\alpha_1 - \alpha_2 m_r^2 - 3\alpha_3 m_r^4)}{m_r d^2(m_r)} \qquad (A.4\text{-}23)$$

$$\frac{\partial^2 f}{\partial m_2^2} = \frac{m_1 (\alpha_1 - \alpha_2 m_r^2 - 3\alpha_3 m_r^4)}{m_r d^2(m_r)} - \frac{m_1 m_2^2}{m_r^3 d^3(m_r)}$$

$$\left[\alpha_1^2 + 6\alpha_1 \alpha_2 m_r^2 + 3(6\alpha_1 \alpha_3 - \alpha_2^2) m_r^4 - 10\alpha_2 \alpha_3 m_r^6 - 15\alpha_3^2 m_r^8 \right]$$

$$\frac{\partial^2 f}{\partial m_2 \partial m_3} = -\frac{m_1 m_2 m_3}{m_r^3 d^3(m_r)} \left[\alpha_1^2 + 6\alpha_1 \alpha_2 m_r^2 + 3(6\alpha_1 \alpha_3 - \alpha_2^2) m_r^4 \right.$$

$$\left. -10\alpha_2 \alpha_3 m_r^6 - 15\alpha_3^2 m_r^8 \right]$$

$$\frac{\partial^2 f}{\partial m_3^2} = \frac{m_1 (\alpha_1 - \alpha_2 m_r^2 - 3\alpha_3 m_r^4)}{m_r d^2(m_r)} - \frac{m_1 m_3^2}{m_r^3 d^3(m_r)}$$

$$\left[\alpha_1^2 + 6\alpha_1 \alpha_2 m_r^2 + 3(6\alpha_1 \alpha_3 - \alpha_2^2) m_r^4 - 10\alpha_2 \alpha_3 m_r^6 - 15\alpha_3^2 m_r^8 \right]$$

These relations complete the quasi-linearization of Eq. (A.4-19) according to Eq. (A.4-20).

The second nonlinearity in Eq. (A.4-16) is of the form

$$f(v_1,v_2,v_3) = v_1 \frac{\psi(r)}{r} = \frac{v_1}{\alpha_1+\alpha_2(v_2^2+v_3^2)+\alpha_3(v_2^2+v_3^2)^2} \qquad (A.4-24)$$

where v_1 now represents the first filter state, x_{f_1}. As above,

$$f = \frac{m_1}{\alpha_1+\alpha_2 m_r^2+\alpha_3 m_r^4} = \frac{m_1}{d(m_r)} \qquad (A.4-25)$$

$$n_1 \approx \frac{1}{d(m_r)}$$

$$n_2 \cong - \frac{2m_1 m_2(\alpha_2+2\alpha_3 m_r^2)}{d^2(m_r)} \qquad (A.4-26)$$

$$n_3 \cong - \frac{2m_1 m_3(\alpha_2+2\alpha_3 m_r^2)}{d^2(m_r)}$$

$$\frac{\partial^2 f}{\partial m_1^2} = 0$$

$$\frac{\partial^2 f}{\partial m_1 \partial m_2} = - \frac{2m_2(\alpha_2+2\alpha_3 m_r^2)}{d^2(m_r)}$$

$$\frac{\partial^2 f}{\partial m_1 \partial m_3} = - \frac{2m_3(\alpha_2+2\alpha_3 m_r^2)}{d^2(m_r)} \qquad (A.4-27)$$

$$\frac{\partial^2 f}{\partial m_2^2} = - \frac{2m_1(\alpha_2+2\alpha_3 m_r^2)}{d^2(m_r)} + \frac{8m_1 m_2^2}{d^3(m_r)} \left[(\alpha_2^2-\alpha_1\alpha_3)+3\alpha_3 m_r^2(\alpha_2+\alpha_3 m_r^2) \right]$$

$$\frac{\partial^2 f}{\partial m_2 \partial m_3} = \frac{8m_1 m_2 m_3}{d^3(m_r)} \left[(\alpha_2^2 - \alpha_1 \alpha_3) + 3\alpha_3 m_r^2 (\alpha_2 + \alpha_3 m_r^2) \right]$$

$$\frac{\partial^2 f}{\partial m_3^2} = - \frac{2m_1(\alpha_2 + 2\alpha_3 m_r^2)}{d^2(m_r)} + \frac{8m_1 m_3^2}{d^3(m_r)} \qquad \text{(A.4-27)(Cont.)}$$

$$\left[(\alpha_2^2 - \alpha_1 \alpha_3) + 3\alpha_3 m_r^2 (\alpha_2 + \alpha_3 m_r^2) \right]$$

complete the requirements for a quasi-linear representation of the second basic Kalman filter nonlinearity specified in Eq. (A.4-24), in accordance with Eq. (A.4-20).

A second important source of nonlinearity in the digital guidance module is the t_{go}-dependence of the optimal control gains, and the acceleration command limiter. The latter is of the same form as indicated in Eq. (A.4-1),

$$a_c = f(c_1 v_1 + c_2 v_2 + c_3 v_3) \triangleq f(\phi') \qquad \text{(A.4-28)}$$

where v_1, v_2 and v_3 represent the Kalman filter estimates of missile-target lateral separation, y, lateral separation rate, $\dot{y}$, and missile acceleration, a_t, as discussed in Section 3.5.2. The gains c_i considered here are those given in Eqs. (3.5-27) to (3.5-30), under the assumptions that the missile dynamics are neglected (by permitting ω_m to approach infinity) and that the control effort weighting, γ, in the performance index, Eq.(3.5-24), is zero:

$$c_1 = \frac{3}{t_{go}^2}$$

$$c_2 = \frac{3}{t_{go}} \qquad \text{(A.4-29)}$$

$$c_3 = \frac{3}{(\omega_t t_{go})^2} \left[e^{-\omega_t t_{go}} + \omega_t t_{go} - 1 \right]$$

The gain c_3 can reasonably be simplified by taking the first 5 terms of the expansion of $e^{-\omega_t t_{go}}$, i.e.,

$$c_3 \approx 3 \left[\frac{1}{2} - \frac{1}{6} \omega_t t_{go} + \frac{1}{24} (\omega_t t_{go})^2 \right] \qquad (A.4\text{-}30)$$

is a good approximation until the last fraction of a second of an engagement and is more readily implemented in the guidance module.

In order to estimate t_{go}, the digital system may hold the range from the previous measurement, r_{k-1}, and difference it with the present value, as indicated in Eq. (3.5-32), viz.

$$t_{go} = \frac{\tau_s \sqrt{v_4^2 + v_5^2}}{v_6 - \sqrt{v_4^2 + v_5^2}} \qquad (A.4\text{-}31)$$

where v_6 represents the digital state holding r_{k-1}, and $\sqrt{v_4^2 + v_5^2}$ is the present range in cartesian coordinates in the state vector formulation.

Combining Eqs. (A.4-27) to (A.4-30) yields the complete nonlinear representation of the acceleration command limiter input:

$$\phi' = \frac{3v_1 \left[v_6 - \sqrt{v_4^2 + v_5^2} \right]^2}{\tau_s^2 (v_4^2 + v_5^2)} + \frac{3v_2 \left[v_6 - \sqrt{v_4^2 + v_5^2} \right]}{\tau_s \sqrt{v_4^2 + v_5^2}}$$

$$+ 3v_3 \left\{ \frac{1}{2} - \frac{\alpha_4}{6} \frac{\sqrt{v_4^2 + v_5^2}}{v_6 - \sqrt{v_4^2 + v_5^2}} + \frac{\alpha_4^2}{24} \frac{v_4^2 + v_5^2}{\left[v_6 - \sqrt{v_4^2 + v_5^2} \right]^2} \right\}$$

$$(A.4\text{-}32)$$

where

$$\alpha_4 \overset{\Delta}{=} \omega_t \tau_s \qquad\qquad (A.4\text{-}33)$$

Since the basic form given in Eqs. (A.4-28) and (A.4-32) is exactly analogous to that treated in the proportional guidance law, Section A.4-1, we can abbreviate the previous presentation as follows: First, the variance of ϕ' is given approximately by Eq. (A.4-13),

$$\sigma^2 \cong \underline{b}^T \, P\underline{b}$$

where $\underline{b}$ is the vector of first partial derivatives of $\phi'(\underline{m})$, viz.

$$b_1 = \frac{\partial \phi'(\underline{m})}{\partial m_1} = -\frac{3\left[m_6 - \sqrt{m_4^2 + m_5^2}\right]^2}{\tau_s^2 (m_4^2 + m_5^2)} \overset{\Delta}{=} \frac{3(m_6 - m_r)^2}{(\tau_s m_r)^2}$$

$$b_2 = \frac{\partial \phi'}{\partial m_2} = \frac{3(m_6 - m_r)}{\tau_s m_r}$$

$$b_3 = \frac{\partial \phi'}{\partial m_3} = 3\left[\frac{1}{2} - \frac{\alpha_4}{6}\frac{m_r}{m_6 - m_r} + \frac{\alpha_4^2}{24}\frac{m_r^2}{(m_6 - m_r)^2}\right]$$

$$\qquad\qquad (A.4\text{-}34)$$

$$b_4 = \frac{\partial \phi'}{\partial m_4} = m_4\left[\frac{6m_1 m_6(m_r - m_6)}{\left[\tau_s m_r^2\right]^2} - \frac{3m_2 m_6}{\tau_s m_r^3}\right.$$

$$\left. - \frac{\alpha_4 m_3 m_6}{2m_r(m_6 - m_r)^2} + \frac{\alpha_4^2 m_3 m_6}{4(m_6 - m_r)^3}\right]$$

$$b_5 = \frac{\partial \phi'}{\partial m_5} = \frac{m_5 b_4}{m_4}$$

$$b_6 = \frac{\partial \phi'}{\partial m_6} = \frac{6m_1(m_6 - m_r)}{(\tau_s m_r)^2} + \frac{3m_2}{\tau_s m_r}$$

$$+ \frac{\alpha_4 m_3}{2} \left[\frac{m_r}{(m_6 - m_r)^2} - \frac{\alpha_4}{2} \frac{m_r^2}{(m_6 - m_r)^3} \right] \quad \text{(A.4-34)(Cont.)}$$

Then we evaluate m using the approximation of Eq. (A.4-7), for which we require the following second partial derivatives:

$$\frac{\partial^2 \phi'}{\partial m_1^2} = 0$$

$$\frac{\partial^2 \phi'}{\partial m_1 \partial m_2} = 0$$

$$\frac{\partial^2 \phi'}{\partial m_1 \partial m_3} = 0$$

$$\frac{\partial^2 \phi'}{\partial m_1 \partial m_4} = \frac{6m_4 m_6 (m_r - m_6)}{(\tau_s m_r^2)^2}$$

$$\frac{\partial^2 \phi'}{\partial m_1 \partial m_5} = \frac{6m_5 m_6 (m_r - m_6)}{(\tau_s m_r^2)^2} \qquad \text{(A.4-35)}$$

$$\frac{\partial^2 \phi'}{\partial m_1 \partial m_6} = \frac{6(m_6 - m_r)}{(\tau_s m_r)^2}$$

$$\frac{\partial^2 \phi'}{\partial m_2^2} = 0$$

$$\frac{\partial^2 \phi'}{\partial m_2 \partial m_3} = 0$$

$$\frac{\partial^2 \phi'}{\partial m_2 \partial m_4} = - \frac{3m_4 m_6}{\tau_s m_r^3}$$

$$\frac{\partial^2 \phi'}{\partial m_2 \partial m_5} = -\frac{3 m_5 m_6}{\tau_s m_r^3}$$

$$\frac{\partial^2 \phi'}{\partial m_2 \partial m_6} = \frac{3}{\tau_s m_r}$$

$$\frac{\partial^2 \phi'}{\partial m_3^2} = 0$$

$$\frac{\partial^2 \phi'}{\partial m_3 \partial m_4} = -\frac{\alpha_4 m_4 m_6}{2 m_r (m_6 - m_r)^3} \left[\left(1 + \frac{\alpha_4}{2} \right) m_r - m_6 \right]$$

$$\frac{\partial^2 \phi'}{\partial m_3 \partial m_5} = \frac{\alpha_4 m_5 m_6}{2 m_r (m_6 - m_r)^3} \left[\left(1 + \frac{\alpha_4}{2} \right) m_r - m_6 \right]$$

$$\frac{\partial^2 \phi'}{\partial m_3 \partial m_6} = \frac{\alpha_4 m_r}{2 (m_6 - m_r)^3} \left[m_6 - \left(1 + \frac{\alpha_4}{2} \right) m_r \right]$$

(A.4-35)(Cont.)

$$\frac{\partial^2 \phi'}{\partial m_4^2} = \frac{b_4}{m_4} + \frac{m_4}{m_5} \frac{\partial^2 \phi'}{\partial m_4 \partial m_5}$$

$$\frac{\partial^2 \phi'}{\partial m_4 \partial m_5} = m_4 m_5 \left[\frac{6 m_1 m_6 (4 m_6 - 3 m_r)}{(\tau_s m_r^3)^2} + \frac{9 m_2 m_6}{\tau_s m_r^5} - \frac{\alpha_4 m_3 m_6}{2 (m_6 - m_r)^3} \right.$$
$$\left. \left\{ \frac{3 m_r - m_6}{m_r^2} - \frac{3 \alpha_4}{2 (m_6 - m_r)} \right\} \right]$$

$$\frac{\partial^2 \phi'}{\partial m_4 \partial m_6} = m_4 \left[\frac{6 m_1 (m_r - 2 m_6)}{(\tau_s m_r^2)^2} - \frac{3 m_2}{\tau_s m_r^3} + \frac{\alpha_4 m_3 (m_6 + m_r)}{2 m_r (m_6 - m_r)^3} \right.$$
$$\left. - \frac{\alpha_4^2 m_3 (2 m_6 + m_r)}{4 (m_6 - m_r)^4} \right]$$

A-30

$$\frac{\partial^2 \phi'}{\partial m_5^2} = \frac{b_4}{m_4} + \frac{m_5}{m_4} \frac{\partial^2 \phi'}{\partial m_4 \partial m_5}$$

$$\frac{\partial^2 \phi'}{\partial m_5 \partial m_6} = \frac{m_5}{m_4} \frac{\partial^2 \phi'}{\partial m_4 \partial m_6} \qquad\qquad (A.4\text{-}35)(\text{Cont.})$$

$$\frac{\partial^2 \phi}{\partial m_6^2} = \frac{6m_1}{(\tau_s m_r)^2} + \frac{\alpha_4 m_3 m_r}{(m_6 - m_r)^4} \left[m_r\left(1 + \frac{3\alpha_4}{4}\right) - m_6 \right]$$

With these results, we have the vector , required to evaluate σ^2 (Eq. (A.4-13)) and the second partial derivatives needed to obtain m according to

$$m = \phi'(\underline{m}) + \frac{1}{2} \sum_{i=1}^{6} \sum_{j=1}^{6} \frac{\partial^2 \phi'}{\partial m_i \partial m_j} P_{ij} \qquad\qquad (A.4\text{-}36)$$

These statistics permit the calculation of the limiter ridf's, Eq. (A.4-6); $\hat{f}$ is then the required mean component of the limited digital acceleration command and the random component ridf vector is simply

$$\underline{n}_a = n\underline{b} \qquad\qquad (A.4\text{-}37)$$

as before (Eq. (A.4-15)). This completes the quasi-linear representation of the Kalman filter gains and optimal control gains in the digital guidance module.

The random input describing functions catalogued in this appendix should be sufficiently inclusive to permit the direct quasi-linearization of a quite broad variety of system models representing the missile-target intercept problem. The examples and new results given in Chapter 4 (especially Cases 1 to 3 of Section 4.3) allow ridf's to be calculated for a number of other nonlinearities with a relatively modest analytic effort. A majority of the nonlinearities treated in this handbook are also

of common occurrence in other nonlinear system models, so it is our hope that Chapter 4 and this appendix will facilitate the use of CADET in other applications as well.

APPENDIX B

EXTENSIONS OF CADET

B.1 INTRODUCTION

We have indicated that there are situations in which the basic CADET methodology is inadequate. As discussed in Section 4.2, the most common difficulty that arises is that the random component of a nonlinearity input, v_i, has zero correlation with the output, $z = f(v_i)$. For example,

$$z = \cos v_1, \qquad E\left[v_1\right] = m_1 = 0$$

$$z = v_1 v_2, \qquad E\left[v_i\right] = m_i = 0, \qquad i = 1,2$$

are cases for which

$$E\left[z\ v_i\right] \equiv 0$$

where v_i is a gaussian random variable. In this event, the random input describing functions (ridf's) for the random component -- which by definition only capture the nonlinearity input-output relations for the correlated components of the output -- are identically zero. If this problem occurs in a primary transmission path of the system model, a statistical analysis using the basic CADET approach may be significantly in error.

A practical resolution of the difficulty described above has been proposed in Ref. 20. It is based on the selective

relaxation of the assumption that all of the state variables are jointly normal; in this way it is possible to propagate the first- and second-order statistics, $\underline{m}$ and P, accurately using modified CADET methodology if some of the higher-order moments (corresponding to the states that are not assumed to be gaussian) are propagated as well.[*]

We present the essentials of Modified CADET via treatment of a simple low-order example. This material is directly based on the research documented in Ref. 20.

B.2 BASIC CADET FAILURE

In this section, we analyze an example using both the basic CADET approach and a direct solution technique (which is too cumbersome to use in all but the simplest situations) to demonstrate the need for extension of CADET in some circumstances. Consider the nonlinear system depicted in Fig. B.2-1, which has an output that is the integral of a simple product nonlinearity driven by two random biases. We assume that the corresponding state vector differential equation and initial conditions are given by

$$\underline{x} = \underline{f}(\underline{x}) = \begin{bmatrix} 0 \\ 0 \\ x_1 x_2 \end{bmatrix} \tag{B.2-1}$$

$$E\left[\underline{x}(0)\right] \triangleq \underline{m}_0 = \begin{bmatrix} m_{1_0} \\ m_{2_0} \\ m_{3_0} \end{bmatrix} \tag{B.2-2}$$

---

[*]If all state variables are jointly normal, then m and P completely characterize the statistical properties of the system variables and higher-order moments are redundant.

R-16226
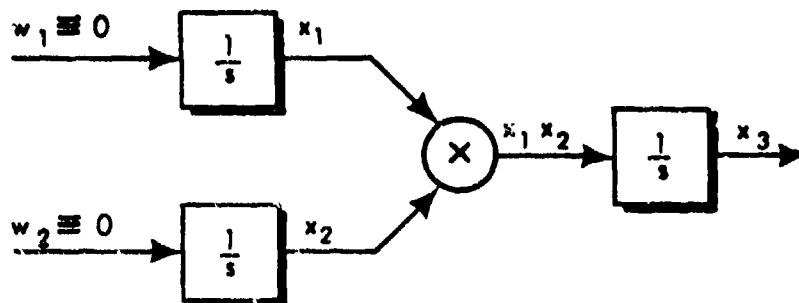
Figure B.2-1   A Product Nonlinearity Driven
                    by Random Biases

$$E\left[(\underline{x}(0)-\underline{m}_0)(\underline{x}(0)-\underline{m}_0)^T\right] \triangleq P_0 = \begin{bmatrix} p_{11_0} & p_{12_0} & 0 \\ p_{12_0} & p_{22_0} & 0 \\ 0 & 0 & p_{33_0} \end{bmatrix} \qquad (B.2-3)$$

Equation (B.2-3) indicates that the initial condition on x_3 is independent of those on the first two states. Since there are no random inputs ($\underline{w} = 0$), the evolution of the state variables is completely determined by the random initial conditions.

First, we indicate the exact solution, which can be obtained by direct integration. For any initial conditions x_{1_0} and x_{2_0}, the first two states remain constant, by Eq. (B.2-1). The solution for the third state is then given by

$$x_3(t) = x_{3_0} + x_{1_0}x_{2_0}t \qquad (B.2-4)$$

Taking the mean and variance of this solution, using the statistics specified in Eqs. (B.2-2) and (B.2-3), we obtain

$$m_3(t) = m_{3_0} + (m_{1_0}m_{2_0}+p_{12_0})t$$

$$p_{33}(t) = p_{33_0} + \left[m_{1_0}(m_{1_0}p_{22_0}+m_{2_0}p_{12_0}) \qquad (B.2-5)\right.$$

$$\left. +m_{2_0}(m_{2_0}p_{11_0}+m_{1_0}p_{12_0})+p_{11_0}p_{22_0}+p_{12_0}^2\right]t^2$$

In applying basic CADET, Eqs. (1.2-6) and (1.2-7), we require the ridf's given by

$$\hat{f} = \begin{bmatrix} 0 \\ 0 \\ E[x_1 x_2] \end{bmatrix} = \begin{bmatrix} 0 \\ 0 \\ m_1 m_2 + p_{12} \end{bmatrix}$$

$$NP = E\left[\underline{f}(\underline{x})\underline{r}^T\right] = \begin{bmatrix} 0 & 0 & 0 \\ 0 & 0 & 0 \\ E[x_1 x_2 r_1] & E[x_1 x_2 r_2] & E[x_1 x_2 r_3] \end{bmatrix} \tag{B.2-6}$$

$$= \begin{bmatrix} 0 & 0 & 0 \\ 0 & 0 & 0 \\ m_1 p_{12} + m_2 p_{11} + E\left[r_1^2 r_2\right] & m_1 p_{22} + m_2 p_{12} + E\left[r_1 r_2^2\right] & m_1 p_{23} + m_2 p_{13} + E\left[r_1 r_2 r_3\right] \end{bmatrix}$$

Under the assumption that all of the states are jointly normal, the expected values of the form $E[r_1 r_2 r_j]$, $j = 1,2,3$, given in the third row of NP in Eq. (B.2-6) are all zero. We can then evaluate the time derivatives of $m_3(t)$ and $p_{33}(t)$ using Eq. (1.2-7), and integrate directly to obtain

$$m_3(t) = m_{3_0} + (m_{1_0} m_{2_0} + p_{12_0})t$$

$$p_{33}(t) = p_{33_0} + \left[m_{1_0}(m_{1_0} p_{22_0} + m_{2_0} p_{12_0}) + m_{2_0}(m_{2_0} p_{11_0} + m_{1_0} p_{12_0})\right] t^2 \tag{B.2-7}$$

On comparing Eqs. (B.2-5) and (B.2-7) we observe that the mean is propagated correctly by basic CADET in the above example. In the variance equation, however, we note that the terms $p_{11_0} p_{22_0} t^2$ and $(p_{12_0} t)^2$ are absent in the CADET result. If m_{1_0} and m_{2_0} are zero, CADET indicates that $p_{33}(t)$ is identically equal to its initial value p_{33_0}, while the exact result increases with time,

$$p_{33}(t)\Big|_{m_1 = m_2 = 0} = p_{33_0} + \left(p_{12_0}^2 + p_{11_0}p_{22_0}\right)t^2 \quad (B.2-8)$$

In the general case (nonzero means and correlated states driving the product nonlinearity), then, CADET will do relatively well in estimating the variance of x_3 if

$$2m_{1_0}m_{2_0}p_{12_0} + m_{2_0}^2 p_{11_0} + m_{1_0}^2 p_{22_0} \gg p_{11_0}p_{22_0} + p_{12_0}^2 \quad (B.2-9)$$

This is a quite restrictive condition.

As demonstrated in Section 1.2, CADET will propagate the mean and covariance of the nonlinear system exactly if the expected values appearing in Eq. (B.2-6) are correctly evaluated. Basic CADET does not evaluate these expectations appropriately for the product nonlinearity just considered, because the probability density function of the product of two gaussian random variables is clearly nongaussian. Thus x_3 cannot be assumed to be jointly normal with x_1 and x_2 without causing CADET accuracy deterioration, except in cases that satisfy Eq. (B.2-9). An approach for modifying CADET, which tends to eliminate this source of error, is introduced and explained in the next section.

B.3   TWO GENERALIZATIONS OF CADET

B.3.1   Exact Solutions via Higher Moment Propagation

Having motivated the need for generalizing basic CADET by demonstrating its breakdown for a system having a product non-linearity, a technique for extending CADET is introduced using the same example. Consider the problem originally posed in Section B.2 -- the nonlinear system of Fig. B.2-1 driven by two random

bias states. Since x_3 is not jointly gaussian with x_1 and x_2, no assumptions are made regarding the density function of x_3. The states driving the nonlinearity are still given to be jointly normal. Referring to Eq. (B.2-6), lack of knowledge of the joint density $p(x_1,x_2,x_3)$ implies that the term $E\left[r_1 r_2 r_3\right]$ cannot be immediately evaluated. In order to obtain this otherwise unknown higher-order moment, consider its propagation in time, in the same sense that basic CADET considers the propagation of the mean and covariance. Making use of the chain rule and the commutativity of differentiation and expectation, we obtain the following expression for the derivation of the higher-order moment:

$$\dot{p}_{123} \triangleq \frac{d}{dt} E\left[r_1 r_2 r_3\right] = E\left[\dot{r}_1 r_2 r_3\right] + E\left[r_1 \dot{r}_2 r_3\right] + E\left[r_1 r_2 \dot{r}_3\right]$$

The first two terms are zero since r_1 and r_2 are constant; the last term is evaluated using

$$\dot{r}_3 = \dot{x}_3 - \dot{m}_3 = x_{1_0} x_{2_0} - \left(m_{1_0} m_{2_0} + p_{12_0}\right)$$

to be

$$\dot{p}_{123} = p_{11_0} p_{22_0} + p_{12_0}^2 \tag{B.3-1}$$

Integrating Eq. (B.3-1), and substituting into Eq. (B.2-6), we have

$$NP = \begin{bmatrix} 0 & 0 & 0 \\ 0 & 0 & 0 \\ \left\{m_{1_0} p_{12_0} + m_{2_0} p_{11_0}\right\} & \left\{m_{1_0} p_{22_0} + m_{2_0} p_{12_0}\right\} & \left\{m_{1_0} p_{23} + m_{2_0} p_{13} + \left(p_{11_0} p_{22_0} + p_{12_0}^2\right)t\right\} \end{bmatrix}$$

$$\tag{B.3-2}$$

Evaluating $\dot{P}$ according to Eq. (1.2-7) and integrating, we obtain the result given in Eq. (B.2-5) which is the exact solution to the problem.

To summarize this methodology, the lack of knowledge about the joint probability density function of the system states is compensated by introducing additional differential equations that govern the propagation of selected higher-order moments of the state variables. Initially, the components of the state vector may be assumed to be jointly gaussian in distribution; this establishes the initial values of the higher-order moments. As these moments propagate, however, the normal relation between $\underline{m}$, P and the higher-order moments disappears, due to the evolving nongaussian nature of the system states caused by the existence of the nonlinearity in the system.

B.3.2 A Further Application of Exact Higher Moment Propagation

A more complicated dynamic system containing the product nonlinearity is shown in Fig. B.3-1. The two nonlinearity input states are assumed to be band-limited gaussian processes with correlation determined by the parameter α, and the output of the multiplier is passed through two stages of low-pass linear dynamics. The state vector differential equation formulation of this system model is given by

$$\underline{\dot{x}} = \begin{bmatrix} -1 & 0 & 0 & 0 \\ 0 & -1 & 0 & 0 \\ 0 & 0 & -0.1 & 0 \\ 0 & 0 & 0.1 & -0.1 \end{bmatrix} \underline{x} + \begin{bmatrix} 0 \\ 0 \\ 0.1\ x_1 x_2 \\ 0 \end{bmatrix} + \begin{bmatrix} 1 & 0 \\ \alpha & 1 \\ 0 & 0 \\ 0 & 0 \end{bmatrix} \underline{w} \quad (B.3-3)$$

where $\underline{x}$ and $\underline{w}$ are the state vector and the input vector of gaussian white noise processes, respectively. Note that the correlation between x_1 and x_2 is given by

16227
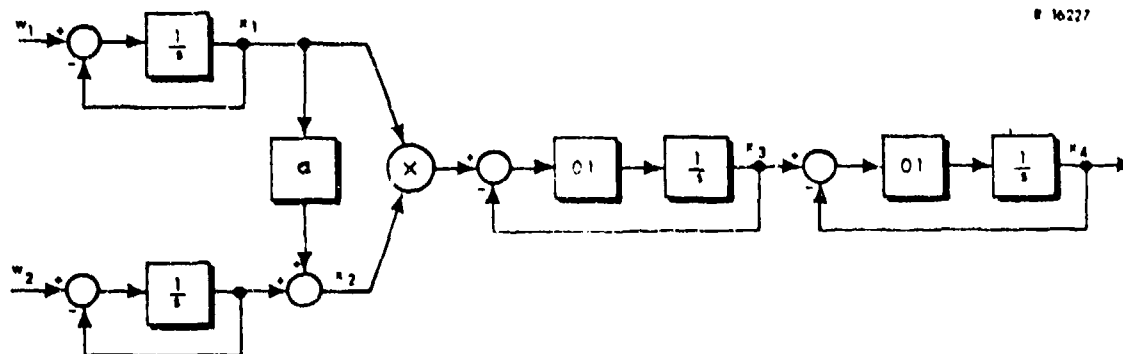
Figure B.3-1   Dynamic System With a Product-
of-States Nonlinearity

$$p_{12} = \alpha \sigma_1^2 \tag{B.3-4}$$

so the degree of correlation is directly proportional to α. The
state variable initial conditions were chosen to be zero; then
given the constant input means, b_i, and spectral densities, q_i
(refer to Eq. (1.1-2)), the statistics of the states driving the
multiplier can be directly obtained to be

$$m_1 = b_1(1 - e^{-t})$$

$$p_{11} = q_1(1 - e^{-2t})$$

$$m_2 = (b_2 + \alpha b_1)(1 - e^{-t}) \tag{B.3-5}$$

$$p_{22} = (q_2 + \alpha q_1)(1 - e^{-2t})$$

The statistical analysis of the system depicted in Fig.
B.3-1 was carried out in Ref. 20 by applying basic CADET, exact
higher moment propagation (hereafter designated HMP), and the
monte carlo method (200 trials). In the cases presented here,

α is taken to be 0.1, and the input white noise processes were chosen to have means and spectral densities given by $b_i = 0.01$, $q_i = 1.0$ respectively. Consequently, from Eq. (B.3-5) we observe that the means are much less than the rms values, so, as indicated in Eq. (B.2-9), it would be anticipated that CADET would be quite inaccurate in this circumstance. The results are portrayed in Fig. B.3-2; since the driving states, x_1 and x_2, are jointly gaussian, we confine our attention to the evolution of σ_3 and σ_4 with time. Observe that the HMP result is exact, as verified by the monte carlo data, while the basic CADET analysis is completely inadequate in its projection of σ_3 and σ_4 versus time.

For the above example the HMP analysis only entailed the propagation of two higher-order moments, $E\left[r_1 r_2 r_3\right]$ and $E\left[r_1 r_2 r_4\right]$. The computer time expenditure was thus nearly identical with that of basic CADET; the monte carlo analysis required 26 times the CADET computational expense.

A question of some importance regarding the general practicality of HMP concerns the impact of increasing the complexity of the system before and after the nonlinearity. As demonstrated in Ref. 20, simply introducing coupling between states 1 and 2, e.g. replacing the first two state variable differential equations in Eq. (B.3-3) with

$$\dot{x}_1 = a_{11} x_1 + a_{12} x_2 + w_1$$

$$\dot{x}_2 = a_{22} x_2 + w_2$$

increases the number of higher order moments that must be propagated from 2 to 4. A similar increase in computational complexity occurs when the system is made more complicated following the non-linearity. Thus the analysis of high-order closed-loop systems via HMP may be impractical.

R-16300
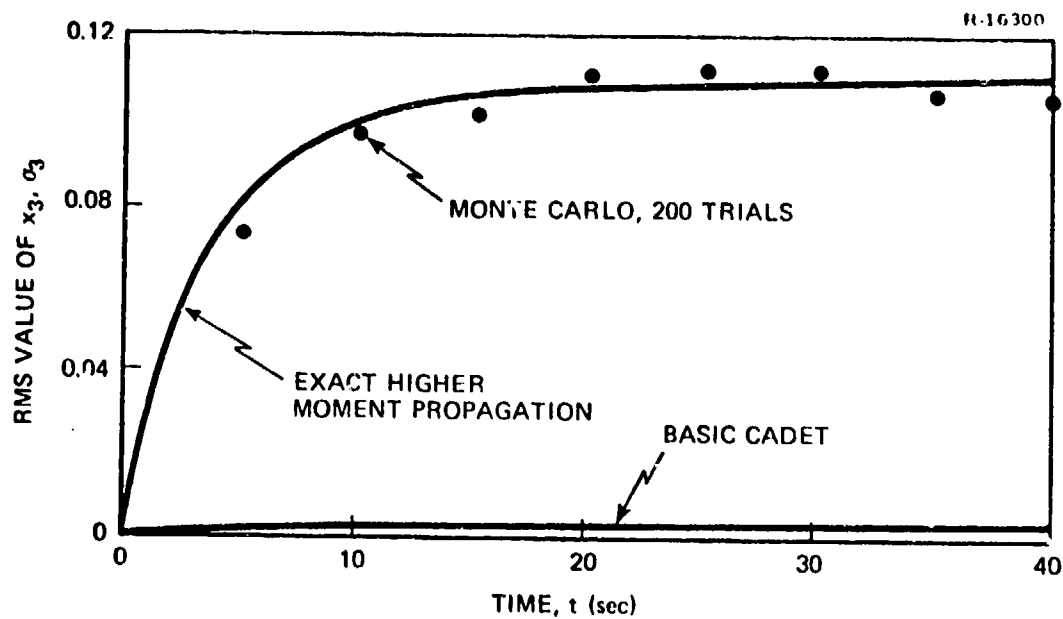
(a) The rms Value of x_3
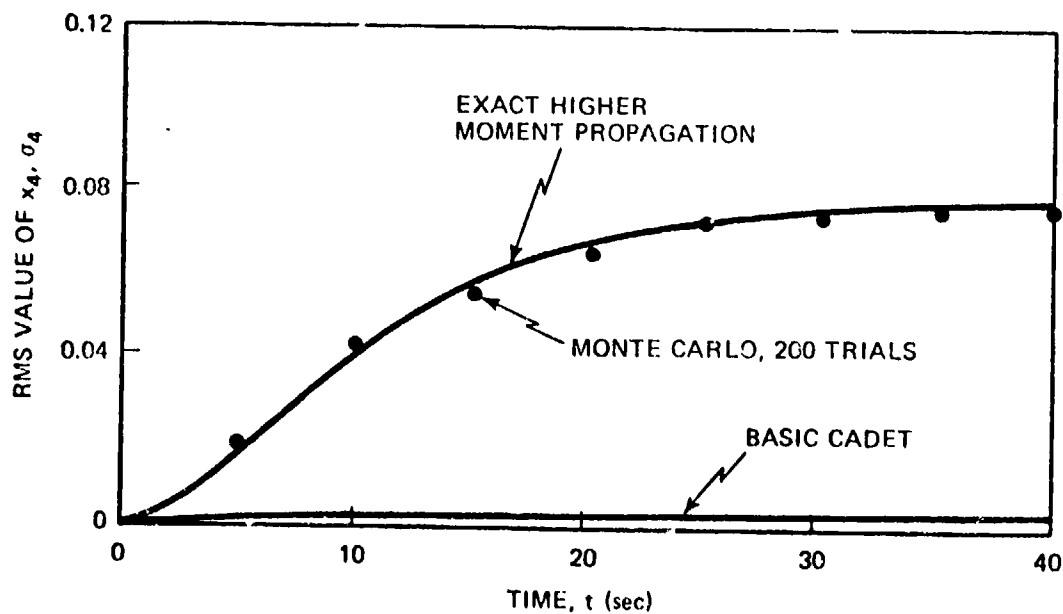
(b) The rms Value of x_4

Figure B.3-2   Simulation Results for a System Containing
                 a Product-of-States Nonlinearity

B.3.3 Modified CADET

The Modified CADET methodology suggested in Ref. 20 serves the purpose of providing a significant increase in the accuracy of CADET without the great increase in computational burden that may be necessitated in using HMP to treat high-order systems, especially those in a closed-loop configuration where all or nearly all of the system state variables may be nongaussian.

The application of Modified CADET to the simple system treated in the preceding section (Fig. b.3-1), containing a product nonlinearity followed by two stages of linear dynamics, is summarized by the following basic steps:

- Relax the gaussian assumption _only on that component of the state vector "nearest" the output of the nonlinearity_ (i.e., x_3 in Fig. B.3-1); _retain the assumption of joint normality on all other states_.

- Develop expressions for the derivatives of all resulting unknown higher-order moments appearing in the evaluation of the expected values in $\bar{f}$ and NP, Eq. (1.2-6) (as in Eq. (B.2-6)).

- Integrate these derivatives along with the derivatives of the system mean and covariance from assumed initial values.

The rationale behind this _selective_ assumption of joint normality is that in general, states more than a few integrations from the nonlinearity (e.g., x_4 in Fig. B.3-1) can be assumed to be jointly normal with respect to other gaussian states (e.g., x_1 and x_2 in the same figure), for reasons discussed in Section 1.2.

To demonstrate the usefulness of Modified CADET, we treat the same example as above (Figs. B.3-1 and B.3-2) under the assumption that x_4 is gaussian. Then $E\left[r_1 r_2 r_4\right]$ is identically zero, and only one higher-order moment is propagated. The corresponding time

history of σ_4 is compared with the HMP result in Fig. B.3-3; clearly it provides a close approximation to the exact solution.

R-16299
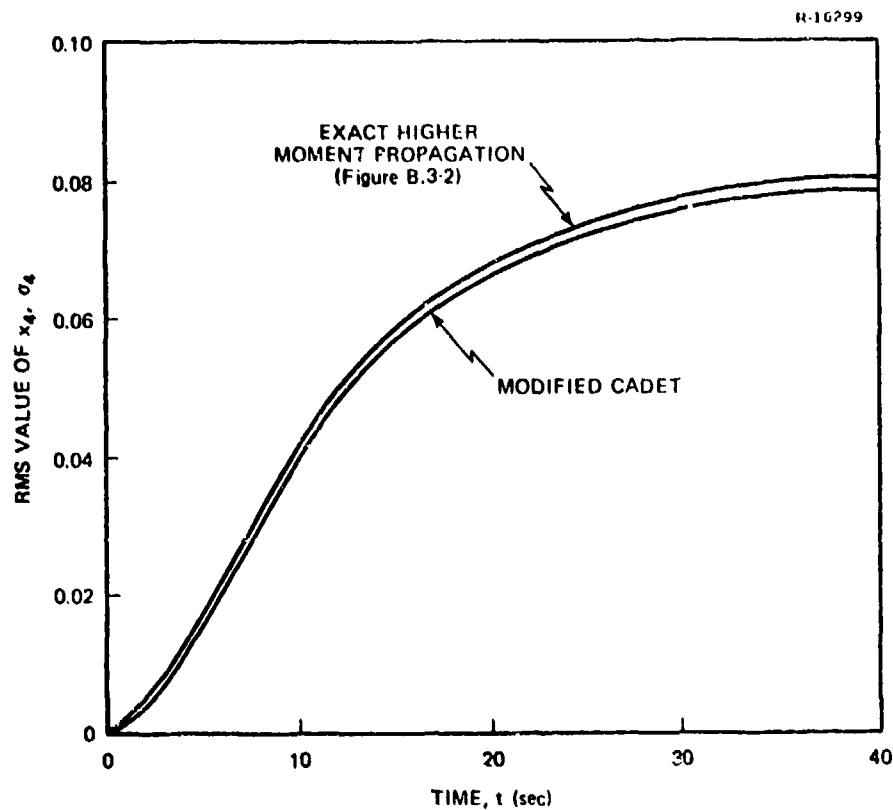
Figure B.3-3   Modified CADET Solution For the System Shown in Fig. B.3-1 With Only One State Assumed Nongaussian

Modified CADET represents a methodology which potentially broadens the usefulness of the CADET concept, permitting its applicability to a wider class of nonlinear systems. For the low-order examples presented in this appendix, Modified CADET has clear-cut advantages, and we anticipate that it will be a useful method for improving the accuracy of statistical analyses for more complex systems.

APPENDIX C

THE MONTE CARLO METHOD: APPLICATION AND RELIABILITY

C.1 DESCRIPTION OF THE TECHNIQUE

The monte carlo method provides an approach for the statistical analysis of the performance of a nonlinear system with random inputs, based on direct simulation. It entails determining the system response to a finite number of "typical" initial conditions and noise input functions which are generated according to their specified statistics. Thus, the information required for monte carlo analysis includes the system model, initial condition statistics, and random input statistics.

The system model can be given in the form of a state vector differential equation,

$$\dot{\underline{x}} = \underline{f}(\underline{x}, \underline{y}, t) \qquad (C.1-1)$$

where $\underline{x}$ is the vector of system states, $\underline{y}$ is a vector of random inputs, and $\underline{f}(\underline{x}, \underline{y}, t)$ represents the nonlinear time-varying dynamic relationships in the system. We assume at the outset that the elements of $\underline{y}$ are correlated random processes with deterministic components that may be nonzero; in this case, a system model of the form

$$\dot{\underline{x}} = \underline{f}(\underline{x}, t) + G(t) \underline{w}(t) \qquad (C.1-2)$$

where $\underline{w}$ is the sum of a vector of white noise processes and a deterministic vector can generally be obtained that is equivalent to Eq. (C.1-1), as discussed in Section 1.2. Henceforth,

we treat Eq. (C.1-2) as the basic system model; it is portrayed in block diagram notation in Fig. C.1-1.

R-11802
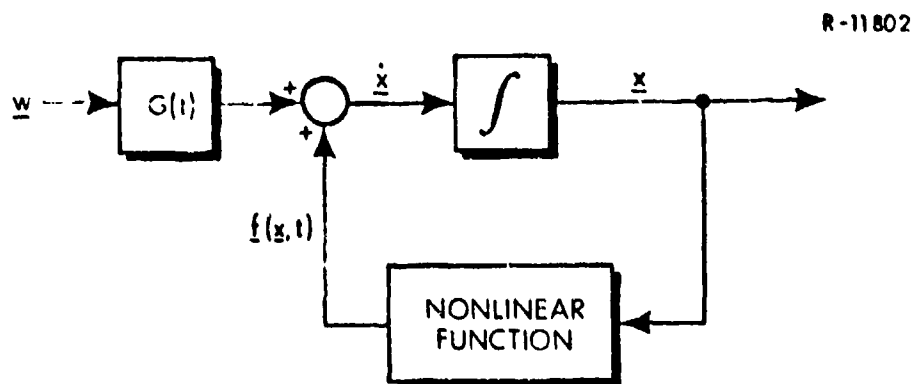
Figure C.1-1   Nonlinear System Model

The initial condition of the state vector is specified by assuming that the state variables are jointly normal. Thus, given an initial mean vector and covariance matrix*,

$$E\left[\underline{x}(0)\right] = \underline{m}_0$$

$$(C.1-3)$$

$$E\left[(\underline{x}(0) - \underline{m}_0)(\underline{x}(0) - \underline{m}_0)^T\right] = P_0$$

the initial condition specification is complete. As stated above, the input vector $\underline{w}$ is assumed to be composed of elements that are white noise processes, plus an additive deterministic component or mean; thus

$$E\left[\underline{w}(t)\right] = \underline{b}(t)$$

$$(C.1-4)$$

$$E\left[(\underline{w}(t)-\underline{b}(t))\,(\underline{w}(\tau)-b(\tau))^T\right] = Q(t)\;\delta(t-\tau)$$

---

*$E\begin{bmatrix} \ \end{bmatrix}$ denotes the expected value of the bracketed variable.

where Q(t) is the input spectral density matrix and the impulse function $\delta(t-\tau)$ indicates that the input vector random components have zero autocorrelation for $t \neq \tau$; i.e., the quantity $\underline{u}(t) = \underline{w}(t)-\underline{b}(t)$ is "white noise", as stated.

Given the above information, monte carlo analysis requires a large number, say q, of representative simulations of the system response, viz., the q-fold repetition of the following procedure: First, an initial condition vector is chosen according to the statistics indicated above; i.e., a random number generator calculates the elements of a random vector $\underline{x}(0)$ based on Eq. (C.1-3). Then a random initial input vector, $\underline{w}(0)$, is generated, using the statistics given in Eq. (C.1-4)*. These vectors provide the data for evaluation of $\underline{\dot{x}}(0)$ in Eq.(C.1-2) which in turn is used to propagate the solution from $t=0$ to $t=h$ according to any standard technique for the digital integration of a state vector differential equation. Then, given $\underline{x}(h)$, simulation continues by the generation of a new value of the input noise vector $\underline{w}(h)$, evaluation of $\underline{\dot{x}}(h)$, numerical integration to obtain $x(2h)$ and so on, to the specified terminal time t_f.

---

*We simulate white noise with spectral density matrix Q(t) by using a random number generator to obtain an independent sequence of random vectors $\underline{u}(kh)$, $k=0,1,2,\ldots$ satisfying

$$E\left[\underline{u}(kh)\right] = \underline{0}$$

$$E\left[\underline{u}(kh)\underline{u}^T(kh)\right] = \frac{1}{h} Q(kh)$$

Then we define $\underline{u}(t)$ by

$$\underline{u}(t) = \underline{u}(kh), \quad kh \leq t < (k+1)h$$

where h is a small time increment. For h small (1/h much larger than the bandwidth of the system in question), $\underline{u}(t)$ is an accurate approximation to a white noise process.

Performing q independent simulations yields an ensemble of state trajectories, each denoted $\underline{x}^{(i)}(t:\underline{x}^{(i)}(0), \underline{w}^{(i)}(t))$ to stress the dependence of the trajectory on the random initial condition and noise input sample function:

$$
\left.
\begin{array}{l}
\underline{x}^{(1)}(t; \; \underline{x}^{(1)}(0), \; \underline{w}^{(1)}(t)) \\[2ex]
\underline{x}^{(2)}(t; \; \underline{x}^{(2)}(0), \; \underline{w}^{(2)}(t)) \\[1ex]
\vdots \\[1ex]
\underline{x}^{(q)}(t; \; \underline{x}^{(q)}(0), \; \underline{w}^{(q)}(t))
\end{array}
\right\} ; \; 0 \leq t \leq t_f \qquad \text{(C.1-5)}
$$

Each satisfies the state vector differential equation (Eq. (C.1-2)) to within the accuracy of the numerical integration method used, and the ensembles of initial conditions, $\underline{x}^{(i)}(0)$, and random inputs, $\underline{w}^{(i)}(t)$, obey the statistical conditions given in Eqs. (C.1-3) and (C.1-4), subject to the limitations of the random number generator employed. The mean $\underline{m}(t)$ and covariance $P(t)$ of the state vector are estimated by averaging over the ensemble of trajectories using the relations

$$
\hat{\underline{m}}(t) \triangleq \frac{1}{q} \sum_{i=1}^{q} \underline{x}^{(i)}(t) \doteq \underline{m}(t)
$$

$$
\hat{P}(t) \triangleq \frac{1}{q-1} \sum_{i=1}^{q} (\underline{x}^{(i)}(t) - \hat{\underline{m}}(t))(\underline{x}^{(i)}(t) - \hat{\underline{m}}(t))^T \doteq P(t)
$$

$$\text{(C.1-6)}$$

where $\hat{\underline{m}}(t)$ and $\hat{P}(t)$ denote the estimated values[*]. The essence of the monte carlo technique is illustrated in Fig. C.1-2.

---

[*]In estimating P, we observe that it is necessary to divide by $(q-1)$, since the sample variance,

$$
P_s \triangleq \frac{1}{q} \sum_{i=1}^{q} (\underline{x}^{(i)} - \hat{\underline{m}})(\underline{x}^{(i)} - \hat{\underline{m}})^T
$$

is biased (Ref. 8), i.e.,

$$
E\left[P_s\right] = \frac{q-1}{q} P
$$
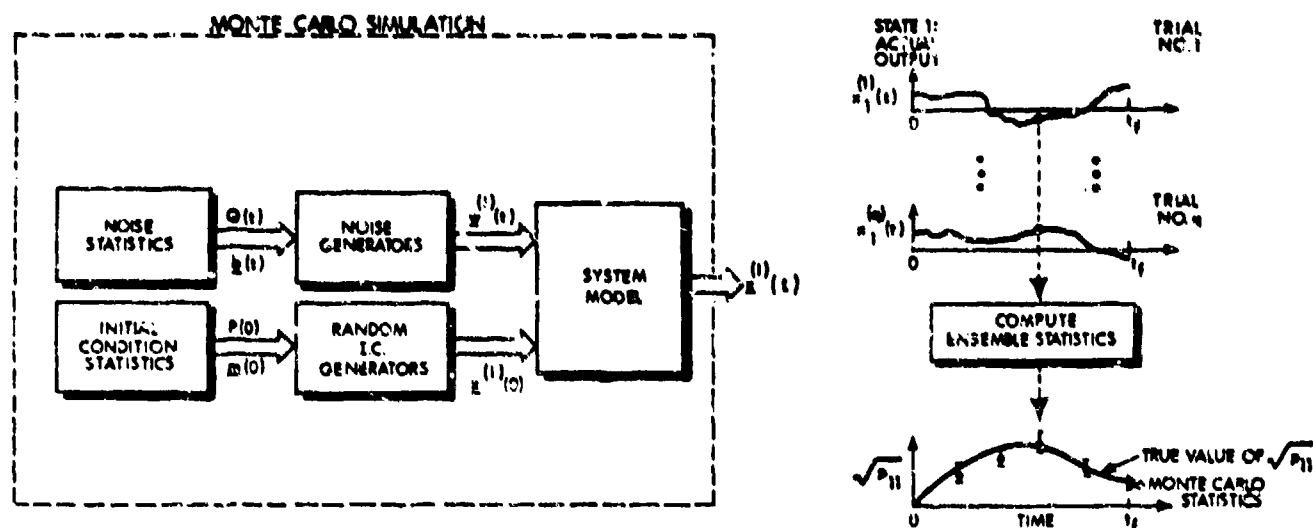
Figure C.1-2   Schematic Characterization of the
Monte Carlo Technique

C.2   ASSESSMENT OF ACCURACY -- CONFIDENCE INTERVALS

In order to assess the accuracy of the approximate sta-
tistics given in Eq. (C.1-6), it is necessary to consider the
statistical properties of the estimates $\hat{\underline{m}}(t)$ and $\hat{P}(t)$. To sim-
plify the notation, consider a scalar random variable y (e.g.,
the value of some system state variable at some time of interest),
and let m and p represent the true values of the mean and vari-
ance of y,

$$m = E\left[y\right]$$

$$p = E\left[(y - m)^2\right]$$

(C.2-1)

By performing one set of q monte carlo trials, we obtain a single
estimate of m and p, which we denote $\hat{m}$ and $\hat{p}$. These estimates
are also random variables; that is, if another set of q monte

carlo trials were performed independently of the first set, but
with the same statistics for the initial conditions and noise
inputs, then a different ensemble of simulations results, and
different estimates for the mean and variance would be obtained.
If q is sufficiently large, then we can invoke the central limit
theorem to justify the assumption that the random variables $\hat{m}$
and $\hat{p}$ are gaussian*, a..d thus that their distributions are
asymptotically specified by the following statistics for large
q (Ref. 21):

$$E[\hat{m}] = m$$

$$E[\hat{p}] = p$$

$$\sigma_{\hat{m}}^2 \triangleq E[(\hat{m} - m)^2] = \frac{p}{q}$$

$$\sigma_{\hat{p}}^2 \triangleq E[(\hat{p} - p)^2] = \frac{\mu_4 - p^2}{q}$$

(C.2-2)

where μ_4 is the fourth central moment,

$$\mu_4 = E[(y - m)^4]$$

(C.2-3)

For many common probability density functions (pdf's), a con-
stant λ exists such that
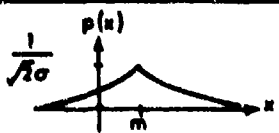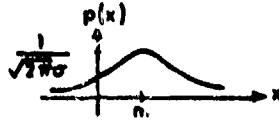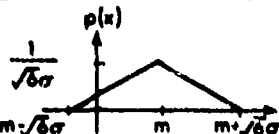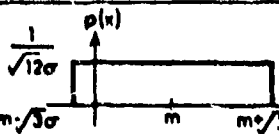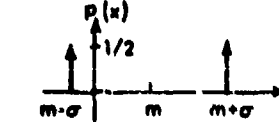
$$\mu_4 = \lambda p^2$$

(C.2-4)

Table C.2-1 gives a summary of values of λ, known as the kurto-
sis or excess of the density, for some common pdf's. For pdf's

---

*For q<20, it is necessary to assume that $\hat{p}$ has the chi square
distribution if y is a gaussian variable (Ref. 22); if y is
significantly nongaussian, the validity of the gaussian as-
sumption for $\hat{m}$ and $\hat{p}$ may require considerably more than twenty
trials.

TABLE C.2-1

SOME COMMON PROBABILITY DENSITY FUNCTIONS

R-11798

DESIGNATION	FUNCTIONAL REPRESENTATION*	GRAPHICAL REPRESENTATION	λ
EXPONENTIAL	$\frac{1}{\sqrt{2}\sigma}\ \exp\left(-\frac{\sqrt{2}}{\sigma}|x-m|\right),$ $-\infty < x < +\infty$		6
NORMAL	$\frac{1}{\sqrt{2\pi}\sigma}\ \exp\left(-\frac{1}{2}\left(\frac{x-m}{\sigma}\right)^2\right),$ $-\infty < x < +\infty$		3
TRIANGULAR	$\frac{1}{\sqrt{6}\sigma}\left(1-\frac{|x-m|}{\sqrt{6}\sigma}\right),$ $m-\sqrt{6}\sigma \le x \le m+\sqrt{6}\sigma$		2.4
UNIFORM	$\frac{1}{\sqrt{12}\sigma},$ $m-\sqrt{3}\sigma \le x \le m+\sqrt{3}\sigma$		1.8
BIPOLAR (Discrete)	$\frac{1}{2}\delta(x-m-\sigma)$ $+\frac{1}{2}\delta(x-m+\sigma)$		1.0

*Formulated to have mean m and standard deviation σ

of this type, we can express both of the standard deviations of the estimated statistics given in Eq. (C.2-2) in terms of the true variance, p, to obtain

$$\sigma_{\hat{m}} = \sqrt{\frac{p}{q}}$$

$$\sigma_{\hat{p}} = \sqrt{\frac{\lambda - 1}{q}}\ p$$

(C.2-5)

The above discussion of the statistics of the gaussian random variable $\hat{p}$ provides the basis for determining a range in the vicinity of $\hat{p}$ such that the true value of p is guaranteed to

lie within that range with a specified probability, ψ. This is done by determining the number, n_σ, of standard deviations, $\sigma_{\hat{p}}$, such that

$$\text{Prob}\left[0 \le |p - \hat{p}| \le n_\sigma \sigma_{\hat{p}}\right] = \psi \qquad (C.2\text{-}6)$$

Since $\hat{p}$ is approximately gaussian, n_σ is the solution to

$$\frac{1}{\sqrt{2\pi}} \int_{-n_\sigma}^{n_\sigma} \exp\left(-\frac{1}{2}\zeta^2\right)d\zeta = \psi \qquad (C.2\text{-}7)$$

For example, if the desired probability is 0.95, Eq. (C.2-7) yields $n_\sigma = 1.96$. Other values of n_σ corresponding to different values of ψ can be obtained from probability integral tables (Ref. 18); several representative values are given in Table C.2-2.

TABLE C.2-2

CUMULATIVE PROBABILITY WITHIN n_σ
STANDARD DEVIATIONS OF THE MEAN
FOR A GAUSSIAN RANDOM VARIABLE

n_σ	ψ
1.0	0.6827
1.645	0.9000
1.960	0.9500
2.576	0.9900

To reformulate Eq. (C.2-6) into an inequality for p, we substitute for $\hat{\sigma}_p$ from Eq (C.2-5) into Eq. (C.2-6) to obtain

$$\text{Prob}\left[\underline{p} \triangleq \frac{\hat{p}}{1 + n_\sigma \sqrt{\frac{\lambda - 1}{q}}} \le p \le \frac{\hat{p}}{1 - n_\sigma \sqrt{\frac{\lambda - 1}{q}}} \triangleq \bar{p} \right] = \psi$$

$$(C.2\text{-}8)$$

that is, the true value of p lies between the values $\underline{p}$ and $\overline{p}$ indicated in Eq. (C.2-8) with probability ψ. Alternatively, in terms of the estimated rms value of the variable, $\hat{\sigma}$, we have the comparable result

$$\text{Prob}\left[\underline{\sigma} \leq \sigma \leq \overline{\sigma}\right] = \psi$$

where $\underline{\sigma}$ and $\overline{\sigma}$ are given by

$$\underline{\sigma} \triangleq \sqrt{\underline{p}} = \frac{\hat{\sigma}}{\sqrt{1 + n_\sigma \sqrt{\frac{\lambda - 1}{q}}}} \triangleq \underline{p}\,\hat{\sigma}$$

$$\overline{\sigma} \triangleq \sqrt{\overline{p}} = \frac{\hat{\sigma}}{\sqrt{1 - n_\sigma \sqrt{\frac{\lambda - 1}{q}}}} \triangleq \overline{p}\,\hat{\sigma}$$

(C.2-9)

The quantities $\underline{\sigma}$ and $\overline{\sigma}$ are referred to as <u>lower and upper confidence limits</u>; the value of ψ expressed as a percent is the <u>degree of confidence</u>. Equation (C.2-9) demonstrates that the standard deviation confidence limits can be obtained from $\hat{\sigma}$ simply by using the multipliers $\underline{p}$ and $\overline{p}$. The latter are functions only of the kurtosis, λ, the number of monte carlo trials, q, and the number of standard deviations, n_σ, required to achieve the desired degree of confidence.

The problem of making a reasonable choice of λ, which depends upon the statistics of the random variable y, must be faced before the confidence limit multipliers can be calculated. One option is to determine an approximate value of λ by estimating the fourth central moment using the q sample values of the variable y, and calculating

$$\lambda \cong \hat{u}_4/\hat{p}^2 \triangleq \hat{\lambda}$$

The value of λ need not be known exactly, since the confidence limits $\underline{\sigma}$ and $\overline{\sigma}$ are not extremely sensitive to errors in this parameter. Unfortunately, as we note in a subsequent example, a meaningful estimate of λ can often require several hundred trials. In the absence of reliable information about the higher central moments, it is frequently assumed that y is gaussian; i.e., that $\lambda = 3$. However, if there is any reason to believe that the pdf for y has abnormally heavily weighted tails -- as in the case of the exponential distribution in Table C.2-1, for example -- then a larger value of λ may be required in order to arrive at a realistic assessment of the accuracy of an estimated rms value obtained via the monte carlo technique.

Values of $\underline{\rho}$ and $\overline{\rho}$ for $\lambda = 3$ are indicated as functions of the number of monte carlo trials in Fig C.2-1, for two typical values of confidence. As an example of the significance of the confidence interval, if we desire to have 99% certainty that σ is within 10% of the estimated value, $\hat{\sigma}$; i.e.,

$$\text{Prob}\left[0.90\,\hat{\sigma} \le \sigma \le 1.1\,\hat{\sigma}\right] = 0.99 \qquad (C.2\text{-}10)$$

then Fig. C.2-1 demonstrates that it is necessary to perform 440 trials; 256 trials suffice for 95% confidence.*

Figure C.2-2 shows the deterioration that occurs in the accuracy of the monte carlo estimated standard deviation, for a given level of confidence, if the kurtosis of the random variable is greater than 3 due to y being nongaussian. We discuss an instance where $\lambda \cong 15$ in Section C.3; in this case, even for 256 trials, the upper 95% confidence limit is 36% greater than the estimated value of σ.

---

*Note that the bounds, $\underline{\rho}$ and $\overline{\rho}$, are not symmetric with respect to one; thus the point at which $\overline{\rho}$ crosses 1.1 determines the value of η for which Eq. (C.2-10) is satisfied.
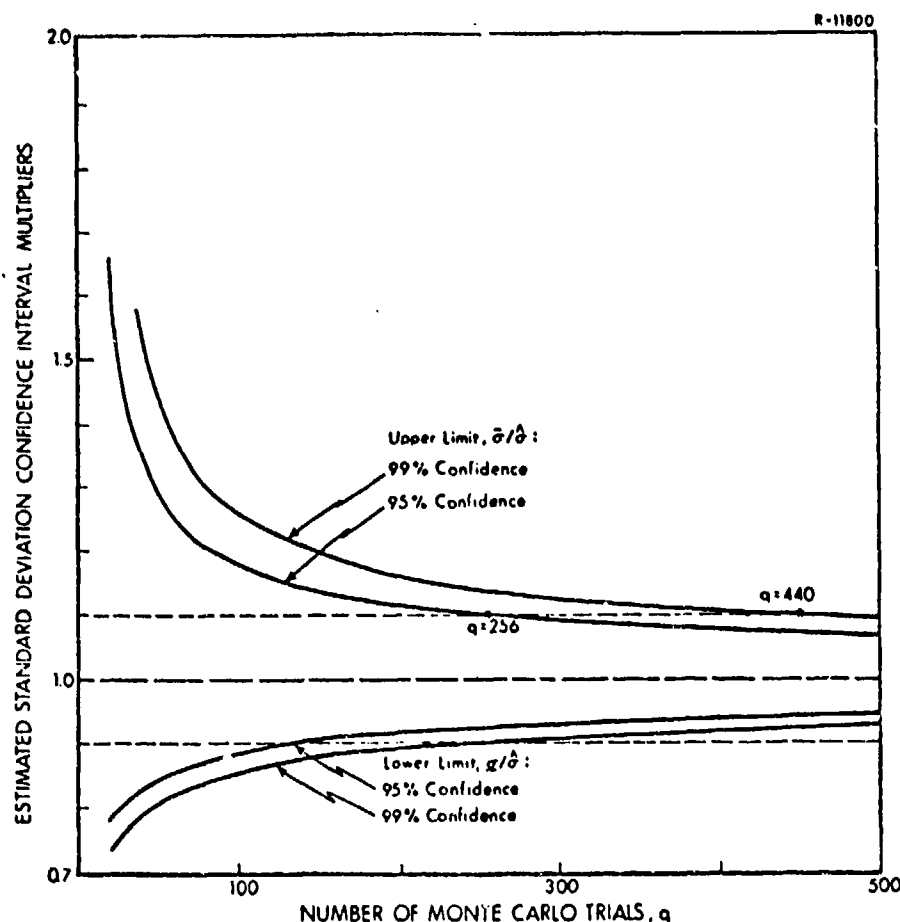
Figure C.2-1   Typical Confidence Interval Multipliers
for the Estimated Standard Deviation of
a Gaussian Random Variable ($\lambda = 3$)

     The confidence interval calculation for the estimated
mean is quite direct, since $\sigma_{\hat{m}}$ (Eq. (C.2-5)) is not a function of
the mean. The same value of n_σ is obtained for the desired de-
gree of confidence (e.g., from Eq. (C.2-7), $n_\sigma = 1.96$ for $\psi =$
0.95 corresponding to 95% confidence), and the value[*] of $\bar{p}$ given
in Eq. (C.2-8) is used in deriving the result that for $\underline{m}$ and
$\bar{m}$ given by

---

[*]While $\sigma_{\hat{m}}$ is given by $\sqrt{p/q}$ in Eq. (C.2-5), the true value of p
is unknown. Thus a conservative (large) value of $\sigma_{\hat{m}}$ is ob-
tained by using $\bar{p}$.
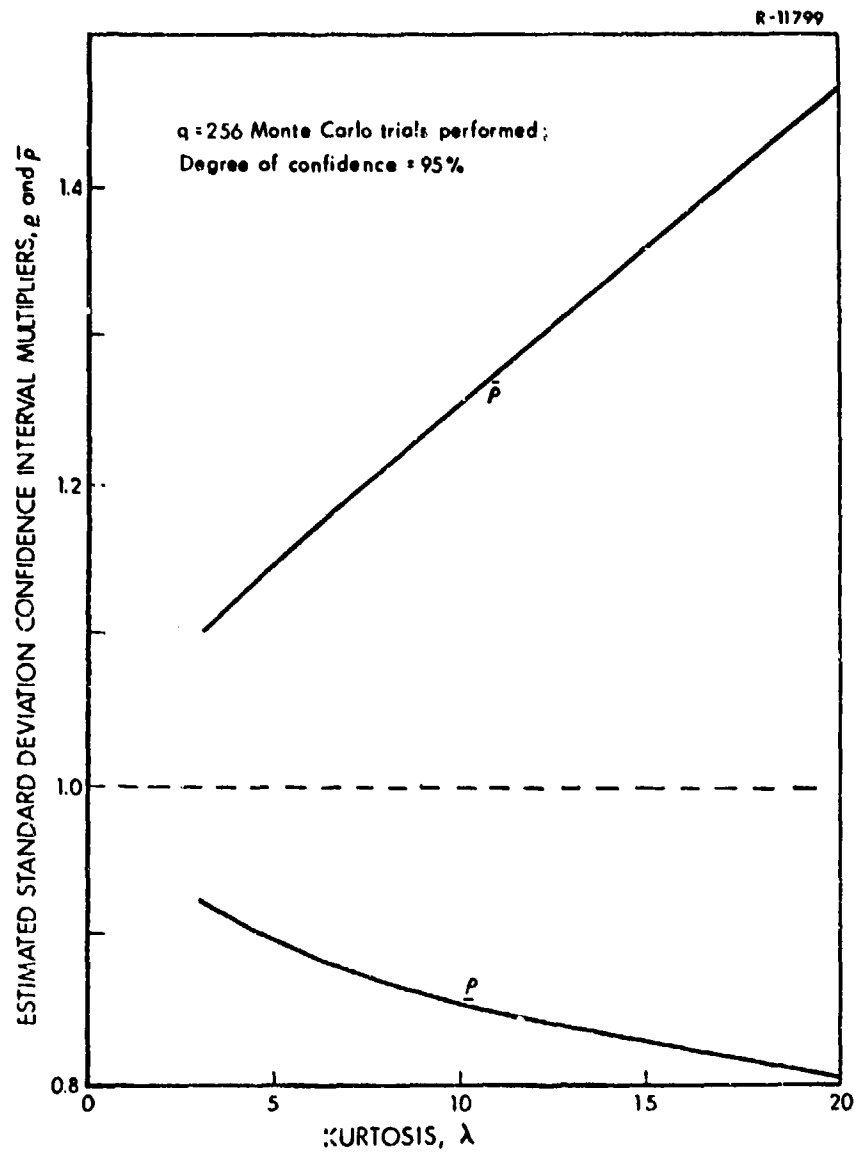
Figure C.2-2   Effect of Kurtosis on Confidence
                Interval Limits

$$\underline{m} = \hat{m} - n_\sigma \sqrt{\dfrac{\underline{p}}{q}}$$

$$\overline{m} = \hat{m} + n_\sigma \sqrt{\dfrac{\overline{p}}{q}}$$

(C.2-11)

one can assert that

$$\text{Prob } \left[\underline{m} \leq m \leq \overline{m} \right] = \psi \qquad (C.2\text{-}12)$$

Here, we see that $\underline{m}$ and $\overline{m}$ cannot be readily expressed in terms of a multiple of $\hat{m}$.

The confidence limit concept developed above provides a statistical measure of the accuracy of the estimated mean and standard deviation of a random variable obtained by using the monte carlo method. It is only possible to assess the accuracy of such estimates in a probabilistic sense; e.g., for 256 trials, we can assert, for example, that an estimated standard deviation (rms value) of a gaussian random variable is within 10% of the true value, with probability 0.95 (with 95% confidence). We note below that even this assessment may be open to question if kurtosis is not known at least approximately, however.

C.3   ILLUSTRATIVE EXAMPLES

Considerable practical experience has been gained in applying the monte carlo method in studies undertaken to validate the use of CADET to provide accurate and efficient performance evaluations for tactical missile guidance systems (Refs. 1, 2 and 4). The significance of the confidence interval concept and the important role played by kurtosis have been graphically demonstrated by the results obtained, as the following example shows (Ref.4).

A variable of particular interest in the planar missile-target intercept problem during the terminal homing phase is the cross-range (lateral) separation between the missile and target, denoted y (refer to Fig. 3.2-1). In a typical analysis, y (and all other system variables) is assumed to be gaussian at the initiation of the terminal homing phase, and y remains quite

C-13
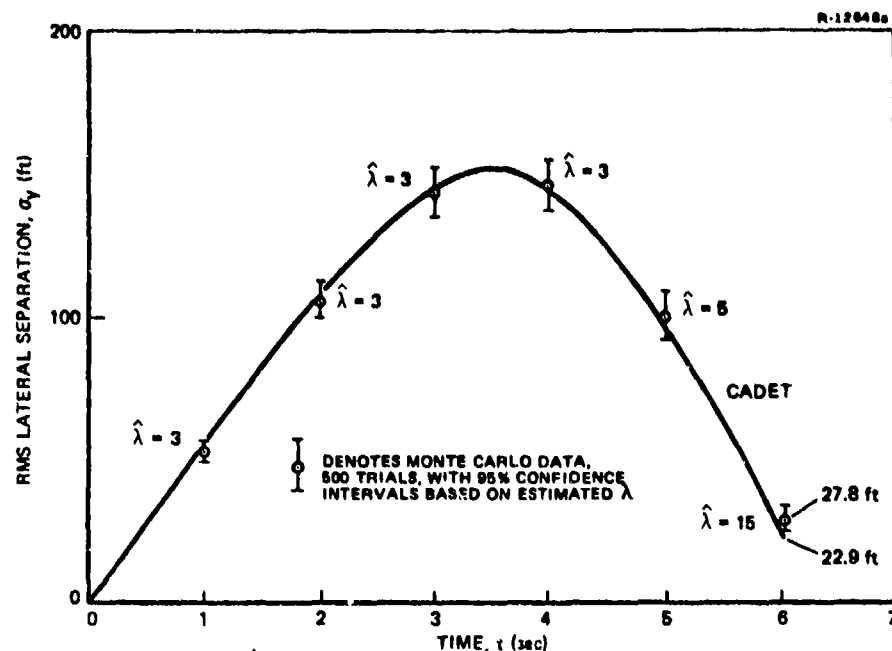
Figure C.3-1   Time History of rms Missile-Target
Lateral Separation

gaussian until the last few seconds of the engagement. Fig. C.3-1
shows the variation of σ_y with time during a six-second engage-
ment, where a quite highly nonlinear system model of the type
developed in Chapter 3 with 17 state variables, 9 nonlinearities
and 5 random inputs has been used for simulation purposes. The
solid curve is obtained by CADET, and the results of a 500-trial
monte carlo study are indicated with circled data points to indi-
cate $\hat{\sigma}_y$ and vertical I-bars to indicate the 95% confidence inter-
val. The estimated value of kurtosis is also indicated near each
data point; as observed above, $\hat{\lambda}$ is nearly 3 until the last second,
while at the final time, t=6 sec, $\hat{\lambda}$ is 15, which is indicative of
the quite highly nongaussian character of the final lateral separ-
ation (miss distance).

Figure C.3-2 gives a more detailed view of the CADET and
monte carlo analysis depicted in Fig. C.3-1; for two values of
time the estimated σ_y is shown as a function of the number of trials
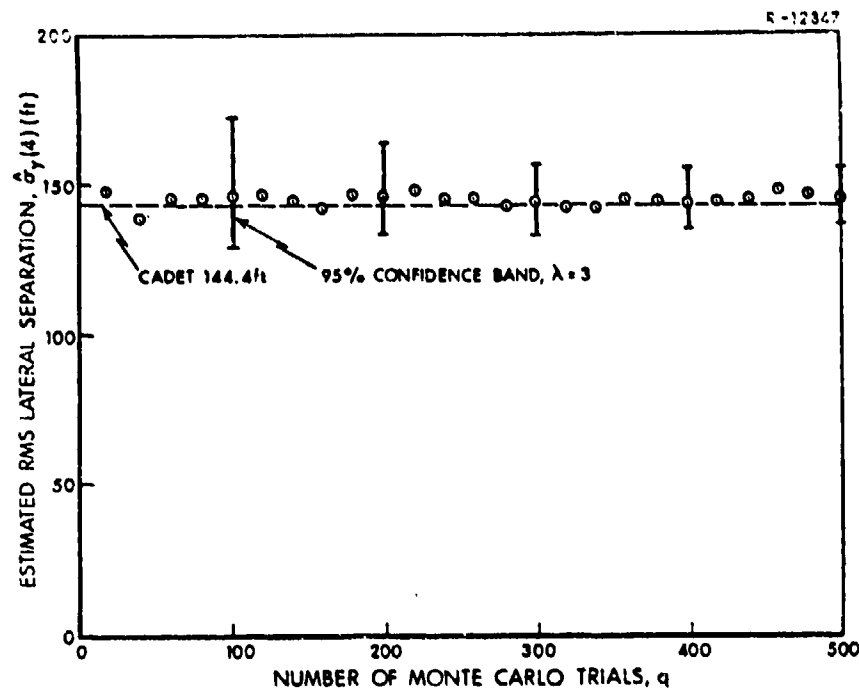
(a) t = 4 sec
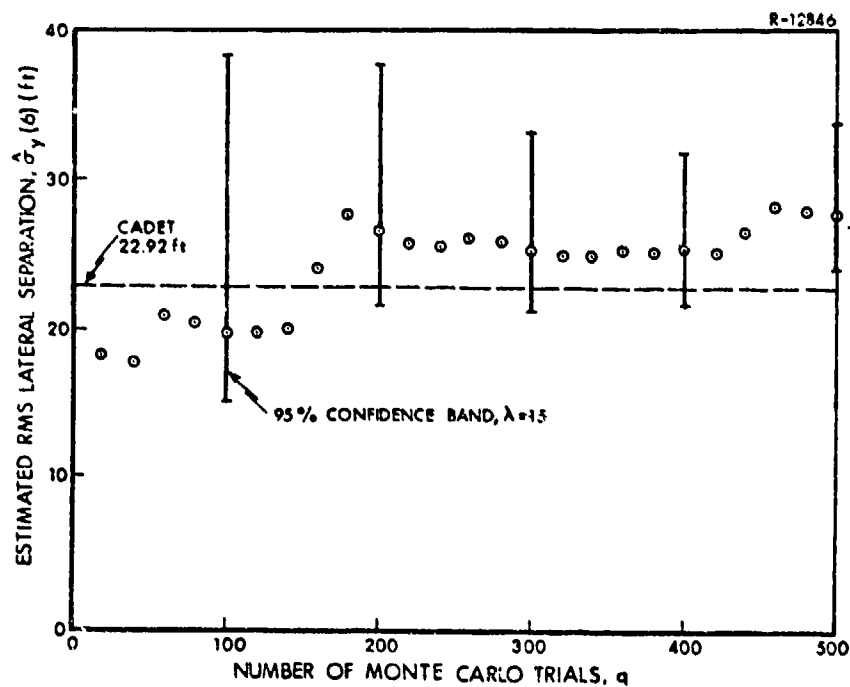
(b) t = 6 sec

Figure C.3-2   Comparison of CADET and Monte Carlo
rms Lateral Separation

performed, q. We note in Fig. C.3-2a that the estimated value of σ_y at t=4 appears to "settle" to about 145 ft after a few hundred trials; after 500 trials we have the result that

$$\text{Prob}\left[138 \text{ ft} \leq \sigma_y(4) \leq 156 \text{ ft}\right] = 0.95 \qquad (C.3-1)$$

which indicates that the monte carlo estimate of σ_y has nearly converged to its true value with high probability. The situation at six seconds is quite different, as demonstrated in Fig. C.3-2b. For $\hat{\lambda} = 15$ the result of 500 trials is

$$\text{Prob}\left[24.7 \leq \sigma_y(6) \leq 33.9 \text{ ft}\right] = 0.95 \qquad (C.3-2)$$

which indicate a considerable margin for error in the monte carlo estimate of σ_y, on a percentage basis.

A synopsis of a part of the data portrayed in Fig. C.3-2b is provided in Table C.3-1, broken down into five sets of 100 trials (set 1 corresponding to the first 100 trials, set 2 including trials 101 to 200, etc.). The data demonstrates that in this case the result of 100 trials is highly random -- with $\hat{\sigma}_y(6)$ varying between 19.72 ft and 35.88 ft; the variation exhibited by $\hat{\lambda}$ is even more dramatic. We also observe that there exists a clear relation between $\hat{\lambda}$ and $\hat{\sigma}_y$; $\hat{\sigma}_y$ is small if $\hat{\lambda}$ is small and $\hat{\sigma}_y$ is large if $\hat{\lambda}$ is large. This phenomenon is a direct result of the basic significance of kurtosis· if λ is appreciably larger than 3, then the "tails" of the density function are abnormally heavily weighted -- implying that there is an unusually high probability of the occurrence of very large values of the random variable in comparison with a gaussian random variable having the same standard deviation. (To cite an example, given two random variables with unity variance, y_1 normally distributed and y_2 exponentially distributed ($\lambda = 6$; Table C.2-1), the probability that $|y_1| \geq 3$ is only 0.0027, compared with the probability of 0.0144 that $|y_2| \geq 3$.) Thus the

TABLE C.3-1

ESTIMATED STANDARD DEVIATION AND KURTOSIS
FOR LATERAL SEPARATION, t = 6 sec

100-Trial Set Number	$\hat{\sigma}_y$ (ft)	$\hat{\lambda}$
1	19.72	4
2	32.08	15
3	22.25	6
4	25.67	4
5	35.88	23
Aggregate* (500 Trials)	27.78	15

*To obtain aggregated values for $\hat{\sigma}_y$ and $\hat{\lambda}$,
it is necessary to average the corresponding
values of variance and fourth central moment
(Eqs. (C.2-2) and (C.2-3)).

incidence of several large values of $|y|$ in the space of a few
trials results in a sudden jump in the estimated σ_y, as evident in
the vicinity of 160 and 440 trials in Fig. C.3-2b, while it is
probable that the "settling" observed during the third and fourth
sets of trials is due to the untypically benign character of these
trials (an abnormally small number of trials occurred in which
$|y|$ is large). Table C.3-1 thus demonstrates a fundamental pro-
blem with the monte carlo method applied to nonlinear systems:
Analysis based on a modest but seemingly reasonable number of
trials (say 100) may be quite inconclusive unless the value of
λ is known quite accurately in advance. Thus the analyst should
be extremely cautious in assessing the reliability of monte carlo
estimated statistics, even if the estimated kurtosis is monitored.
In the preceding example, the importance of a few large values of
miss distance that occur in a set of trials in characterizing the
tails of the pdf, and thus in determining the kurtosis of a non-
gaussian random variable, also demonstrates that the common

practice of "discarding the pathological trials" can lead to very misleading results.

C.4   CONFIDENCE INTERVAL LIMIT TABLES

The confidence interval limits of an estimated standard deviation $\hat{\sigma}$ can be expressed as multiples of $\hat{\sigma}$, viz.,

$$\underline{\sigma} = \underline{\rho}\ \hat{\sigma}$$
$$\overline{\sigma} = \overline{\rho}\ \hat{\sigma} \qquad\qquad (C.4\text{-}1)$$

where $\underline{\rho}$ and $\overline{\rho}$ are determined only by the desired degree of confidence, the kurtosis of the random variable, λ, and the number of trials performed, q.   These multiples, $\underline{\rho}$ and $\overline{\rho}$, have the form

$$\underline{\rho} = \frac{1}{\left[1 + n_\sigma \sqrt{\frac{\lambda - 1}{q}}\right]^{\frac{1}{2}}}$$

$$\qquad\qquad (C.4\text{-}2)$$

$$\overline{\rho} = \frac{1}{\left[1 - n_\sigma \sqrt{\frac{\lambda - 1}{q}}\right]^{\frac{1}{2}}}$$

where n_σ is determined by the confidence ψ expressed as a decimal fraction,

$$\frac{1}{\sqrt{2\pi}} \int_{-n_\sigma}^{n_\sigma} \exp\left(-\frac{1}{2}\zeta^2\right)d\zeta = \psi \qquad\qquad (C.4\text{-}3)$$

This formulation, Eq. (C.4-1), makes it particularly convenient to present the confidence interval multipliers in tabular form. Thus we include Tables C.4-1 to C.4-3 for easy reference, giving

confidence interval multipliers $\underline{\rho}$ and $\overline{\rho}$ for 90% confidence (ψ = 0.90), 95% confidence and 99% confidence. This data is directly applicable to gaussian variables, or any other case where λ = 3; for other values of kurtosis, the confidence interval multipliers can be determined by use of the **gaussian equivalent number of trials**, derived as follows: for a specified degree of confidence (or, equivalently, a given value of n_σ) the multipliers $\underline{\rho}$ and $\overline{\rho}$ (Eq. (C.4-2)) are determined solely by the ratio $(\lambda - 1)/q$. Thus given a set of monte carlo trials typified by the parameters (q, λ), the confidence interval multipliers are identical to those for (q_{eq}, 3) where q_{eq} is chosen to satisfy

$$\frac{3 - 1}{q_{eq}} = \frac{\lambda - 1}{q} \qquad \text{(C.4-4)}$$

or

$$q_{eq} = \frac{2q}{\lambda - 1} \qquad \text{(C.4-5)}$$

The desired multipliers $\underline{\rho}$ and $\overline{\rho}$ may then be obtained from the appropriate table of confidence interval multipliers for gaussian random variables under q_{eq}.

Example: In the preceding section we discussed a study of 500 trials where λ = 15; to obtain $\underline{\rho}$ and $\overline{\rho}$ use

$$q_{eq} = \frac{1000}{14} = 70$$

as given in Eq. (C.4-5). From Table C.4-2, under the entry for 70 trials, we see that the 95% confidence interval limit multipliers are $\underline{\rho}$ = 0.866, $\overline{\rho}$ = 1.225.

TABLE C.4-1

90 PERCENT CONFIDENCE INTERVAL LIMITS,
GAUSSIAN RANDOM VARIABLES, q TRIALS
$(n_\sigma = 1.645)$

q	$\underline{\rho}$	$\bar{\rho}$	q	$\underline{\rho}$	$\bar{\rho}$
20	0.807487	1.464364	200	0.926523	1.094265
22	0.814433	1.425104	210	0.928115	1.091676
24	0.820599	1.393521	220	0.929604	1.089268
26	0.826126	1.367472	230	0.931001	1.087032
28	0.831122	1.345555	240	0.932315	1.084951
30	0.835670	1.326515	250	0.933555	1.083007
32	0.839834	1.310573	260	0.934726	1.081186
34	0.843669	1.296336	270	0.935835	1.079476
36	0.847216	1.283735	280	0.936888	1.077867
38	0.850511	1.272468	290	0.937889	1.076348
40	0.853584	1.262375	300	0.938843	1.074912
42	0.856458	1.253223	320	0.940621	1.072261
44	0.859157	1.244893	340	0.942248	1.069865
46	0.861696	1.237273	360	0.943745	1.067686
48	0.864092	1.230269	380	0.945127	1.065693
50	0.866358	1.223806	400	0.946410	1.063865
55	0.871527	1.209615	420	0.947605	1.062173
60	0.876101	1.197662	440	0.948721	1.060607
65	0.880183	1.187427	460	0.949767	1.059151
70	0.883970	1.178543	480	0.950750	1.057793
75	0.887213	1.170742	500	0.951676	1.056522
80	0.890265	1.163826	520	0.952550	1.055329
85	0.893068	1.157642	540	0.953378	1.054207
90	0.895655	1.152072	560	0.954163	1.053149
95	0.898053	1.147023	580	0.954908	1.052149
100	0.900284	1.142420	600	0.955617	1.051203
105	0.902367	1.138202	650	0.957251	1.049040
110	0.904318	1.134320	700	0.958713	1.047126
115	0.906150	1.130731	750	0.960032	1.045415
120	0.907876	1.127402	800	0.961230	1.043874
125	0.909506	1.124303	850	0.962324	1.042478
130	0.911048	1.121409	900	0.963329	1.041205
135	0.912509	1.118699	950	0.964257	1.040038
140	0.913898	1.116154	1000	0.965116	1.038963
145	0.915220	1.113760	1100	0.966660	1.037046
150	0.916480	1.111501	1200	0.968013	1.035382
160	0.918833	1.107343	1300	0.969212	1.033922
170	0.920990	1.103600	1400	0.970283	1.032626
180	0.922977	1.100208	1500	0.971248	1.031466
190	0.924815	1.097117	2000	0.974959	1.027075

TABLE C.4-2

95 PERCENT CONFIDENCE INTERVAL LIMITS, GAUSSIAN RANDOM VARIABLES, q TRIALS
$(n_\sigma = 1.960)$

q	$\underline{p}$	$\overline{p}$	q	$\underline{p}$	$\overline{p}$
20	0.781848	1.657247	200	0.914210	1.115388
22	0.789372	1.573320	210	0.916033	1.112299
24	0.794071	1.539303	220	0.917740	1.109265
26	0.802092	1.497989	230	0.919332	1.106453
28	0.807546	1.464009	240	0.920850	1.103840
30	0.812522	1.435490	250	0.922274	1.101402
32	0.817087	1.411156	260	0.923620	1.099121
34	0.821299	1.390109	270	0.924896	1.096982
36	0.825201	1.371693	280	0.926107	1.094970
38	0.828832	1.355420	290	0.927259	1.093074
40	0.832223	1.340917	300	0.928358	1.091283
42	0.835400	1.327895	320	0.930407	1.087980
44	0.838386	1.316127	340	0.932284	1.084999
46	0.841199	1.305430	360	0.934012	1.082293
48	0.843856	1.295656	380	0.935610	1.079822
50	0.846373	1.286683	400	0.937094	1.077554
55	0.852123	1.267138	420	0.938476	1.075463
60	0.857222	1.250839	440	0.939769	1.073527
65	0.861789	1.236999	460	0.940980	1.071729
70	0.865911	1.225069	480	0.942120	1.070053
75	0.869659	1.214659	500	0.943193	1.068485
80	0.873087	1.205478	520	0.944208	1.067016
85	0.876240	1.197308	540	0.945169	1.065634
90	0.879153	1.189980	560	0.946080	1.064333
95	0.881857	1.183362	580	0.946946	1.063104
100	0.884375	1.177348	600	0.947770	1.061940
105	0.886729	1.171856	650	0.949670	1.059286
110	0.888936	1.166813	700	0.951372	1.056938
115	0.891011	1.162165	750	0.952908	1.054843
120	0.892967	1.157863	800	0.954305	1.052958
125	0.894815	1.153867	850	0.955581	1.051251
130	0.896566	1.150143	900	0.956754	1.049696
135	0.898227	1.146662	950	0.957837	1.048271
140	0.899806	1.143400	1000	0.958840	1.046960
145	0.901309	1.140335	1100	0.960646	1.044624
150	0.902744	1.137448	1200	0.962229	1.042600
160	0.905425	1.132145	1300	0.963632	1.040823
170	0.907885	1.127385	1400	0.964887	1.039248
180	0.910154	1.123083	1500	0.966018	1.037840
190	0.912256	1.119167	2000	0.970373	1.032517

TABLE C.4-3

99 PERCENT CONFIDENCE INTERVAL LIMITS, GAUSSIAN RANDOM VARIABLES, q TRIALS
$(n_\sigma = 2.576)$

q	$\underline{\rho}$	$\overline{\rho}$	q	$\underline{\rho}$	$\overline{\rho}$
20	0.738071	2.467137	200	0.891497	1.161088
22	0.746410	2.208189	210	0.893721	1.156225
24	0.753870	2.039417	220	0.895306	1.151753
26	0.760604	1.919349	230	0.897765	1.147621
28	0.766728	1.829951	240	0.899613	1.143796
30	0.772334	1.758031	250	0.901358	1.140236
32	0.777496	1.700693	260	0.903010	1.136915
34	0.782271	1.653232	270	0.904578	1.133807
36	0.786709	1.613199	280	0.906068	1.130891
38	0.790849	1.578906	290	0.907487	1.128149
40	0.794725	1.549151	300	0.908840	1.125563
42	0.798365	1.523048	320	0.911370	1.120609
44	0.801794	1.499936	340	0.913690	1.116533
46	0.805031	1.479303	360	0.915830	1.112663
48	0.808095	1.460754	380	0.917811	1.109139
50	0.811001	1.443971	400	0.919653	1.105912
55	0.817664	1.408197	420	0.921371	1.102945
60	0.823597	1.379144	440	0.922979	1.100204
65	0.828928	1.355002	460	0.924488	1.097662
70	0.833757	1.334565	480	0.925909	1.095298
75	0.838160	1.317003	500	0.927249	1.093091
80	0.842199	1.301717	520	0.928517	1.091024
85	0.845922	1.288269	540	0.929718	1.089085
90	0.849371	1.276330	560	0.930858	1.087260
95	0.852579	1.265644	580	0.931942	1.085539
100	0.855572	1.256012	600	0.932976	1.083913
105	0.858376	1.247278	650	0.935359	1.080208
110	0.861009	1.239313	700	0.937498	1.076940
115	0.863489	1.232014	750	0.939431	1.074030
120	0.865831	1.225295	800	0.941191	1.071418
125	0.868047	1.219087	850	0.942801	1.069057
130	0.870148	1.213328	900	0.944282	1.066909
135	0.872145	1.207969	950	0.945651	1.064945
140	0.874046	1.202966	1000	0.946920	1.063139
145	0.875858	1.198283	1100	0.949208	1.059929
150	0.877589	1.193888	1200	0.951216	1.057152
160	0.880830	1.185856	1300	0.952999	1.054720
170	0.883810	1.178686	1400	0.954595	1.052569
180	0.886563	1.172238	1500	0.956035	1.050647
190	0.889118	1.166402	2000	0.961594	1.043409

REFERENCES

1. Gelb, A. and Warren, R.S., "Direct Statistical Analysis of Nonlinear Systems: CADET," AIAA Journal, Vol. 11, No. 5, May 1973, pp.689-694.

2. Price, C.F. and Warren, R.S., "Performance Evaluation of Homing Guidance Laws for Tactical Missiles," The Analytic Sciences Corp., Report No. TR-170-4, January 1973.

3. Warren, R.S. and Siegel, J., "Missile Performance Analysis Using CADET," The Analytic Sciences Corp., Report No. TR-286-2, August 1973.

4. Taylor, J.H. and Price, C.F., "Direct Statistical Analysis of Missile Guidance Systems via CADET^{TM}," The Analytic Sciences Corp., Report No. TR-385-3, to be published.

5. Jazwinski, A.H., Stochastic Processes and Filtering Theory, Academic Press Inc., New York, 1970.

6. Gelb, A. and Vander Velde, W.E., Multiple-Input Describing Functions and Nonlinear System Design, McGraw-Hill Book Co., New York, 1968.

7. Phaneuf, R.J., "Approximate Nonlinear Estimation," Ph.D. Thesis, Dept. of Aeronautics and Astronautics, M.I.T., Cambridge, Mass., May 1968.

8. Papoulis, A., Probability, Random Variables, and Stochastic Processes, McGraw-Hill Book Co., New York, 1965.

9. Price, C.F., "Optimal Stochastic Guidance Laws for Tactical Missiles," The Analytic Sciences Corp., Report No. TR-170-2, September 1.

10. Price, C.F., "Adaptive Control and Guidance for Tactical Missiles," The Analytic Sciences Corp., Report No. TR-170-1, Vol. II, June 1970.

11. Gelb, A. (Ed.), Applied Optimal Estimation, The MIT Press, Cambridge, Mass., 1974.

12. Bryson, A.E., Jr. and Ho, Y.C., Applied Optimal Control, Blaisdell Publishing Co., Waltham, Mass., 1969.

13.   Willems, G., "Optimal Controllers for Homing Missiles,"
        Report No. RE-TR-68-15, U.S. Army Missile Command,
        Redstone Arsenal, Huntsville, Alabama, September 1968.

14.   Skolnik, M.I., Introduction to Radar Systems, McGraw-Hill
        Book Co., New York, 1962.

15.   Gibson, J.E., Nonlinear Automatic Control, McGraw-Hill
        Book Co., New York, 1963.

16.   Goldstein, H., Classical Mechanics, Addison-Wesley
        Publishing Co., Reading, Mass., 1950.

17.   Gradshteyn, I.S. and Ryzhik, I.M., Table of Integrals,
        Series, and Products, Academic Press Inc., New York, 1965.

18.   Abramowitz, M. and Stegun, I.A. (Eds.), Handbook of
        Mathematical Functions with Formulas, Graphs, and Mathe-
        matical Tables, No. 55 in National Bureau of Standards
        Applied Mathematics Series, U.S. Department of Commerce,
        Washington, D.C., 1964.

19.   Peirce, B.O. and Foster, R.M., A Short Table of Integrals
        (Fourth Ed.), Oxford University Press, London, 1956.

20.   Geier, J,G., "Approximate Direct Statistical Analysis of
        Nonlinear Systems," Master's Thesis, Dept. of Aeronautics
        and Astronautics, M.I.T., Cambridge, Mass., June 1973.

21.   Bucy, R.S., Hecht, C. and Senne, K.D., "An Engineer's
        Guide to Building Nonlinear Filters," Seiler Research
        Lab. Report No SRL-TR-72-0004 (USAF Systems Command),
        May 1972.

22.   Bowker, A.H. and Lieberman, G.J., Engineering Statistics,
        Prentice-Hall, Inc., Englewood Cliffs, N.J., 1959.

23.   Siegel, J., "Missile Performance Analysis Using CADET,"
        The Analytic Sciences Corp., Report No. TR-449-1, to
        be published.